TSRR

IFAC-TSRR vol. 4 (2012) 241-388

ESSenCe Analysis of Campaign Data
ESA-ESTEC Contract 4000101374/NL/10/CT-CCN2

Ugo Cortesi [(1)], Samuele Del Bianco [(1)], Marco Gai [(1)],
Bianca Maria Dinelli [(2)], Elisa Castelli [(2)], Bärbel Vogel [(3)],
Roland Ruhnke [(4)], Björn-Martin Sinnhuber [(4)]

([1]) Istituto Fisica Applicata "Nello Carrara" del CNR (IFAC-CNR)
([2]) Istituto di Scienze dell'Atmosfera e del Clima, ISAC-CNR
([3]) Institut für Energie und Klimaforschung Stratosphäre, Forschungzentrum Jülich, IEK-7, FZJ
([4]) Karlsruhe Institute of Technology, KIT, IMK-AFS

 ISSN 2035-5831

1 Introduction

The present document is the Final Report of the extension of the PACD (Premier Analysis of Campaign Data) project, aimed at the analysis of limb measurements acquired by the MARSCHALS instrument during the two flights of the ESSenCe (ESA Sounder Campaign 2011) campaign conducted in December 2011 from Kiruna, Sweden (Lat. $67.8\,^{\circ}$N, Lon. $20.4\,^{\circ}$E). It contains the description of the research activities carried out by the project team in the period from the Kick-off (30.05.2012) to the Final Meeting (13.09.2012).

These include the analysis of MARSCHALS measurements during the two flights of the ESSenCe campaign and the validation of the retrieval products, along with an assessment of the impact of clouds on the outcomes of the measurements and of the inversion process. The final section of the report describes the activities conducted for the comparison of MARSCHALS retrieved profiles and simulations from the atmospheric chemistry and transport models CLaMS (Chemical Lagrangian Model of the Stratosphere) and EMAC (ECHAM/MESSy Atmospheric Chemistry). Consolidated results for ESSenCe Flight 1 and Flight 2 and conclusions are presented.

2 New characterization data and code verification

MARSCHALS (Millimetre wave Airborne Receivers for Spectroscopic) Level 2 (L2) data analysis is performed using the L2 software suite developed in the context of the previous study supported by ESA: "*The Scientific Analysis of Limb Sounding Observations of the Upper Troposphere*", Contract N. ESTEC/Contract 16530/02/NL/MM. The software suite is mainly composed by two modules:

1. **SAMM** (**S**upervising **A**nalyzer of **M**ARSCHALS **M**easurements)
   This module is a tool dedicated to perform a first selection of the MARSCHALS measurements, to convert the data contained in the L1 files in a format readable by the MARC code, and to generate a preliminary overview and diagnostics of the flight data.

2. **MARC** (**MA**RSCHALS **R**etrieval **C**ode)
   This module contains the core part of the code devoted to the retrieval of vertical profiles of atmospheric targets, as well as instrumental scalar quantities to assess the quality of the measurements. The retrieval is performed by processing a set of measured (or simulated) spectral data.

More details about the MARC and SAMM modules can be found in the L2 ADD [38] and in the L2 User Manual [39]. In this section we recall the main features of the pre-processor code (SAMM) useful for the subsequent discussion and we report the new functionalities of SAMM and MARC codes implemented for the handling and for the analysis of the data acquired during the ESSenCe (ESA Sounder Campaign 2011) campaign. A more detailed description of the pre-processor and of the retrieval code can be found in the SCOUT O3 analysis report [40].

2.1 The main features of the pre-processor

The main features of the pre-processor were developed for SCOUT O3 analysis, in order to allow the L1 data processing by using MARC retrieval module.

- *Rearrangement of the Lines Of Sight (LOS)*
  in the L1B data file, the LOSs are not monotonically sorted with decreasing (or increasing) pointing angle; the pre-processor rearranges the LOS in increasing order;

- *Rearrangement on the spectral data*
  in L1B data file the spectral data, as well as the spectral error and all related quantities are not sorted with increasing frequency; the pre-processor rearranges the spectral channels with frequencies in increasing order;

- *Rearrangement on the filter spectral response*
  spectral response is provided for each filter as a function of low frequency; the pre-processor translates this data in the Band B, C, and D frequency using the local oscillator frequency;

- *Implementation of manual selection of the LOS*
  the user can exclude one or more LOS from the file of observations; this manual selection has been added to exclude LOS having large values of χ^2-test.

- *Computation of the average spectral error*
  for each LOS, the pre-processor computes an average (root mean square (rms)) value for the spectral error; the user can decide to use the original error or the averaged one in the retrieval.

- *Treatment of spectra containing unrealistic values*
  some spectra in band B contain channels having unrealistic values (null or very large values) in spectral data and/or in spectral data errors; when the file of the observations to be analysed is produced, these channels can be replaced with values selected by the user. This feature of the pre-processor enables the exclusion of the unrealistic values from the analysis by introducing a large value in the spectral error. The channels marked as unrealistic are not taken into account, when the average spectral error is computed.

- *Overview of Level 1B data*
  the SAMM pre-processor produces a set of output files used to characterize the data acquired during the flight. Among these, the *flight overview* contains general data related to the measurement campaign. Along with the flight overview, the pre-processor generates a *scan overview* file containing auxiliary data related to a specific selected scan: the geo-location of the instrument (altitude, latitude, longitude); the pointing angle; the geo-location of the refracted tangent point (altitude, latitude, longitude); the values of the spectral quantifiers computed by the pre-processor (continuum, noise and contrast levels).

- *Sweep selection criteria*
  for each measured scan, the pre-processor enables either an automatic selection or a manual selection of the sweeps which are going to be analysed. The main automatic selection criteria are:

  – *Altitude range selection*: only sweeps having tangent altitude included in a selected range are extracted;

  – *Noise selection*: only sweeps having noise less than a noise threshold are extracted;

  – *Contrast level selection*: only sweeps having a contrast level greater than a threshold value are extracted;

  – *Tangent altitude behaviour*: if two consecutive sweeps have increasing pointing angles, but not decreasing tangent altitudes, the lower-most is automatically excluded.

  The automatic selection of the sweeps can be manually modified by editing a LOG file automatically produced by SAMM. The file, along with the scan diagnostics, contains a flag that is automatically set to 1 if the sweep has been included in the data to be analysed, or to zero if the sweep has been discarded. Changing manually the flag the automatic selection is overwritten in the subsequent run of the SAMM code.

2.2 New features of the pre-processor

During the PREMIER Analysis of Campaign Data (PACD) project, some additional features were included in the pre-processor to better characterize the actual data [6].

- *Spectrum contrast level*
  this quantifier can be used to identify and/or filter the observations having a low contrast in the spectral lines. In the SCOUT O3 version of SAMM the contrast level was defined as the ratio between the mean spectral intensity in two frequency intervals of each band. In the new version of SAMM the contrast level related to a given spectrum is defined as the difference between two reference intensities.

- *Averaged Brightness Temperature of each spectrum*
  this quantifier can be used to identify and/or filter the observations having anomalous behaviour due to either pointing problems or cloud contamination. The averaged Brightness Temperature (BT_{av}) quantifier is computed by averaging the spectral intensity over the whole spectral range of the band.

- *New format for some auxiliary files*
  new reading routines have been developed, in order to manage the new format of some auxiliary files (Instrumental Line Shape (ILS) and Field Of View (FOV)).

- *Mean spectrum and standard deviation*
  a new significant feature implemented in the pre-processor is the computation of the mean spectrum and of the associated standard deviation. The mean spectrum is computed by averaging all the observations acquired at the same nominal pointing angle.

- *Observations dataset*
  by using the new developed feature, the pre-processor is able to create different configurations of the observation dataset resulting from different definitions of the observed spectrum and of the measurement error.

In the context of ESSenCe campaign data analysis, two additional features have been included in the pre-processor, in order to skip the 'bad' channels (corresponding to anomalous values of the spectrum or/and of the associated error) identified in the L1 files.

- *Channel mask*
  a channel dependent mask has been introduced in the pre-processor. All the values of the spectrum of the masked channels are not modified, while the associated error is replaced with a large value (10^6 Kelvin).

- *Spectrum and error check and replacement*
  a check of the values of the spectrum and of its error is introduced in the pre-processor. In particular, the channel is flagged if:

  – the value of the spectrum is equal to val_1
  – the value of the error is equal to val_2
  – the value of the spectrum is less than or equal to val_3
  – the value of the spectrum is greater than or equal to val_4
  – the value of the spectrum is less than or equal to val_5 times the error

  where val_1, val_2, val_3, val_4, and val_5 values are indicated in the settings file. The value of the spectrum of the flagged channel and its associated error are replaced with user-dependent values indicated in the settings file.

2.3 New features of the MARC code

During the PREMIER Analysis of Campaign Data (PACD) project, some additional features were included in the MARC code [6]. In particular, in the following we describe the implementation of the frequency shift retrieval and of the exportation of the inputs required for the data fusion analysis.

- *Implementation of frequency shift retrieval*
  in order to reduce the systematic errors due to the instrumental characterisation and to produce a feedback to the L1 team on the quality of the spectral calibration, the possibility to retrieve the frequency shift has been implemented in the MARC code. This parameter is a band dependent parameter, so if we analyse a measurement performed on 3 bands, 3 different values of the frequency shift are provided by the code. This parameter is not geometry dependent, because we assume that the frequency shift is due to the instrumental characterisation.

- *Implementation of the exportation of the MSS input products*
  MARC has been modified, in order to export at the last retrieval iteration all the information to calculate the Measurement Space Solution (MSS) [4]. In particular, MARC exports:

  – the vector $(S_y^{-1/2} * (y - F(x_0))$, where S_y in the total (random and systematic) Variance Covariance Matrix (VCM) of the observation, y are the observations and $F(x_0)$ are the simulations at the last retrieval iteration;
  – the matrix $S_y^{-1/2} * K$, where K is the Jacobian matrix;
  – the vector x_0 that is the state vector at the last retrieval iteration.

  A stand alone software has been implemented, in order to compute the MSS related to MARSCHALS and MIPAS-STR (Michelson Interferometer for Passive Atmospheric Sounding - STRatospheric aircraft) data and to perform the data fusion.

In the context of ESSenCe campaign data analysis, some additional features have been included in the MARC retrieval code:

- *Partition function upgrade*
  in the MARC code, we have upgraded the partition function subroutine according to the last version produced by R. R. Gamache (*tips_2009.for*). In this version, there are better values for PH_3 and better high temperature CH_4 partition sums (for CH_4 see [73]). These changes have no effects on the MARSCHALS retrieval, since these molecules do not contribute to the measured spectra, however we have updated the routine in order to be consistent with the latest version of the Gamache subroutine.

Tab. 1: List of the Flight 1 and Flight 2 L1B data files.

Flight Name	L1B Data File Name
Flight 1	mar_20111211_201201111529_00111b.dat
Flight 2	mar_20111216_201204101745_00111b.dat

Tab. 2: Band definition for SCOUT O3 and ESSenCe.

	SCOUT O3			PremierEx and ESSenCe		
Band	Initial Frequency GHz	Number of Points	Frequency Sampling MHz	Initial Frequency GHz	Number of Points	Frequency Sampling MHz
B	294.16	58	200	296.76	44	200
C	316.58	45	200	317.78	39	200
D	342.30	33	200	341.90	32	200

- *High resolution Averaging Kernel matrix*
  MARC has been modified in order to export the high resolution Averaging Kernel (AK) matrix. This matrix is computed by MARC on the specie dependent retrieval grid with respect to the finer species independent vertical grid. This AK matrix can be used to evaluate the species dependent vertical resolution of the MARSCHALS measurements and to compare the MARSCHALS products with the atmospheric profiles obtain by atmposheric models.

- *Bad channels selection*
  a sweep and scan dependent channel mask has been included in MARC in order to manually skip the bad channels. The code now reads an auxiliary file named filter.dat for each scan containing for each spectrum the list of channels that have to be masked. The masking is performed artificially setting the noise to 1.0E6. If the file is not present, the analysis retains all the channels as in the previous analyses.

- *Radiometric Noise Formula*
  the formula agreed for the SCOUT O3 and PACD campaigns (see formula 5.6 pag. 32 of MARSCHALS Level 1 ATBD, file l1atbd_v2p2.pdf), has been changed and the L1B data field named SPECTRAL_DATA_ERROR is representing the total measurement error that has to be used in the retrieval without adding any other terms to it (information provided by RAL).

3 Level 1B data and auxiliary information

Two successful flights have been performed: one on December 11, 2011 and one on December 16, 2011. Both the flights were performed during the ESSenCe (ESA Sounder Campaign 2011) scientific campaign in the Arctic region (Kiruna Sweden, Lat. $67.8\,^{\circ}\mathrm{N}$, Lon. $20.4\,^{\circ}\mathrm{E}$) and will be called the Flight 1 and Flight 2. The L1B datasets delivered by RAL for the Flight 1 and Flight 2 are reported in table 1.

The ILS characterization and the band definitions used in the ESSenCe campaign data analysis were provided by RAL on July 2010 and are the same used for the PREMIER-EX Scientific Flight data analysis [6]. The band definitions are reported in Table 2 and compared to the ones used in the SCOUT O3 analysis.

The FOV characterization for each band used in the ESSenCe campaign are the same used for the PREMIER-EX Scientific Flight data analysis [6], and were provided by RAL on November 2010. The FOV functions are reported in blue in Fig. 1 and compared to the FOV used in SCOUT O3 data analysis (red).

3.1 Channel selection

During the ESSenCe campaign not all the channels of MARSCHALS spectrometer were working properly. The strategy adopted by the RAL team was to shift the malfunctioning channels to spectral regions where there are no spectral features of the molecules of interest, and flag those channels so that they were not included in the analysis. The percentage of flagged channels is 7% for band C, 4.5% for band B and 3.5% for band D.

However, after running a preliminary analysis, we noticed that some of the unflagged channels have been working properly only for some spectra. In particular, we found that these channels had values that were not consistent with the simulated spectra, with differences well above the corresponding noise level. In the following we will call these channels 'bad channels'. The bad channels were not the same for all the spectra, but each

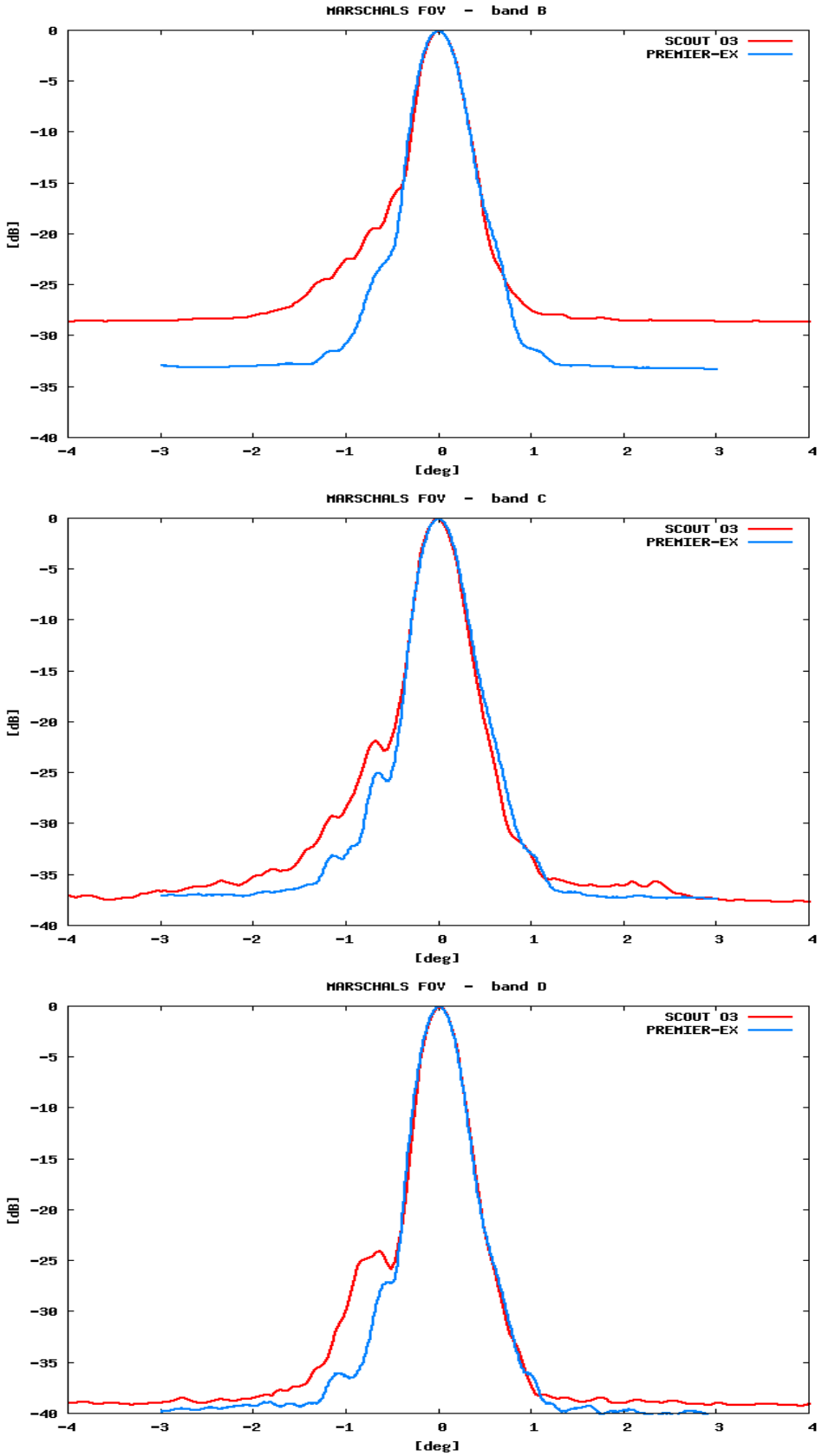

Fig. 1: FOV for each MARSCHALS band used in the SCOUT O3 campaign data analysis (red) and in PREMIER-EX and ESSenCe campaign data analysis (blue).

measured spectrum had a different set of them. Masking each bad channel for the whole flight would significantly reduce the number of useful spectral points during the retrieval, and therefore affect the quality of the retrieval products. In fact we have run two analyses: one retaining all the bad channels and one excluding all of them from the whole flight. The first test produced very high chi-test values and unrealistic results (as expected). However the second test highlighted that the total exclusion of these channels could compromise the quality of the retrievals, since for some scans the spectra for which these channels assumed unrealistic values were just a minor fraction.

Therefore we have implemented in MARC the option to use a scan and spectra dependent spectral mask to remove from the analysis only the 'real' bad channels. However, because the identification of the bad channels was very tricky and to develop an automatic procedure for filtering them was going to be very time consuming, we decided to check each spectrum and flag manually the bad channels using as reference the difference between the spectra simulated at the final step of the second analysis and the noise level. For the identified bad channels we have artificially enhanced the noise level to a very high value (1.0E6 K) so that their weight in the retrieval was negligible. Despite the fact that the choice of bad channels is somehow arbitrary, this method produced very good results. The number of bad channels was not constant from scan to scan, but on average they were the 1.33% for Flight 1 and the 0.83% for Flight 2.

3.2 Initial Guess Atmosphere and a priori errors

A preliminary step for the analysis of MARSCHALS observations is the definition of the status of the atmosphere that is used also as a priori information for the retrieved targets. Therefore the initial status of the atmosphere has to be as close as possible to the true status of the atmosphere, in order to minimise the impact of interfering species whose VMRs are not a retrieval target and to have a good a priori estimate of the profiles that are the retrieval targets. The initial guess atmosphere used for the analysis of both flights is a combination of the ECMWF data, that can be obtained for the dates of the flights and personalised for each scan, and climatological data.

Temperature, pressure, water and ozone can be extracted from the ECMWF (European Center for Medium range Weather Forecasting) database. ECMWF data were extracted from the MARS Archive (Meteorological Archival and Retrieval System), where data for Temperature (K), Specific Humidity (Q) (kg/kg) and Ozone Mass Mixing Ratio (MMR) (kg/kg) can be retrieved on a chosen latitude-longitude grid and on model levels. Data for the geopotential (m^2/s^2) and for the pressure (hPa) at the surface can also be extracted on the same latitude-longitude grid. There are different version of the atmospheric datasets reported over different numbers of model levels: 16, 19, 31, 40, 50, 60, 62, 91 each relative to different pressure ranges. The value of the pressure at each model level can be calculated through a given formula using the value of the pressure at the surface [1]. The data of the MARS archive are available at four different times for each day: 00:00, 06:00, 12:00 and 18:00 (UTC). Since for MARSCHALS data analysis the atmospheric status has to be reported on an altitude grid, the pressure-dependent profiles are converted into altitude-dependent ones using the geopotential altitude at the surface and the hydrostatic equilibrium.

In our study we decided to use the 91 model levels data to obtain vertical profiles of Temperature, pressure, O_3 and H_2O on a high resolution vertical grid that extends up to 70-78 km.

For the other gases included in the analysis and for all the interfering species, the initial atmospheric status was extracted from the IG2 database, developed by J. Remedios for MIPAS/ENVISAT analyses [51]. The IG2 database contains one average profile valid over a wide latitude band, along with the 1-sigma variability relative to that latitude band. IG2 profiles were used as initial guess for the target species N_2O, HNO_3 and CO. The data used for the analysis of both ESSenCe flights were the ones relative to the polar latitudinal band in winter.

Since in the MARC code we use Optimal Estimation to retrieve the atmospheric data, we need to define the error associated to the initial guess profiles that, in our analysis, are also used as a priori information. This error is very important because it defines the strength of the constraint imposed during the retrieval procedure. Moreover it is also used to characterize the quality of the retrieved data, through the use of the individual information gain quantifier.

The a priori errors used in the analysis of both flights were the climatological 1 sigma variability obtained from the IG2 database for all the target species but for Temperature, where a 3 K constant error was used . When the 1-sigma variability was lower than a certain threshold value of the a priori profile, its value was artificially enhanced to match this threshold. The threshold value has been tuned through test retrievals, and was finally set to 200% of the a priori profile for both the flights.

4 Analysis of MARSCHALS Flight 1 measurements

In this section, we report the results of the analysis carried out on the MARSCHALS L1 data acquired during the Flight 1 on 11.12.2011.

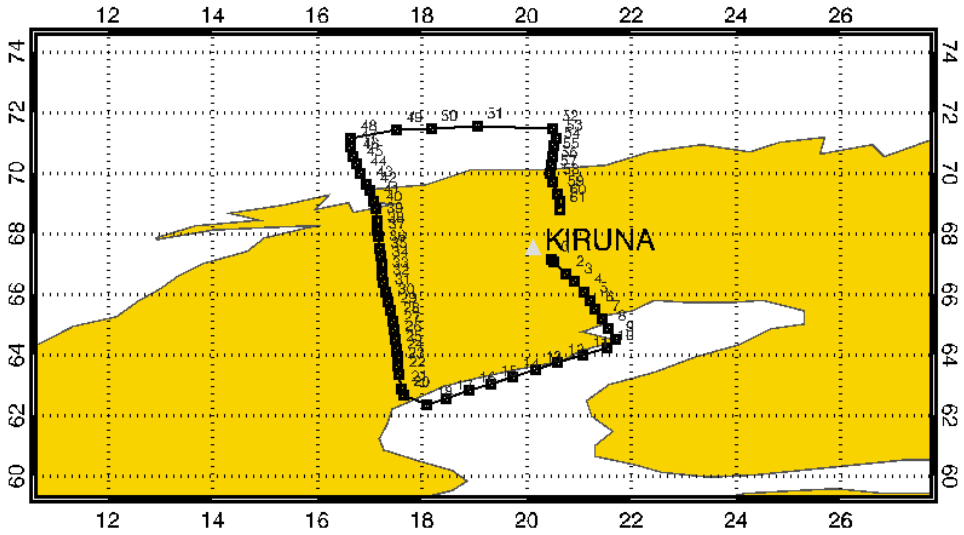

Fig. 2: The Flight 1 track plotted versus latitude and longitude. The black dots show the average position of each scan.

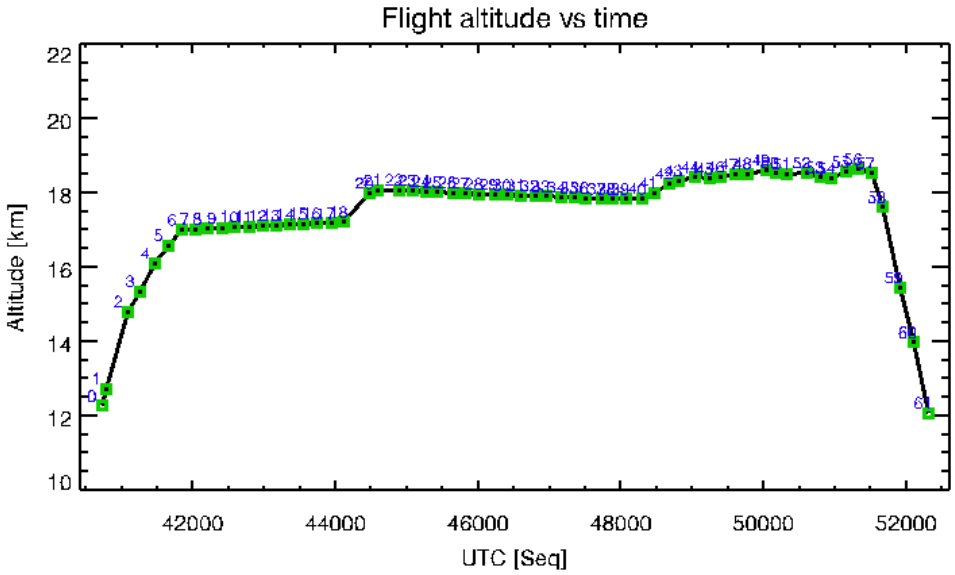

Fig. 3: The GPS flight altitude and the analysed scans position plotted versus the Universal Time Coordinate (UTC).

4.1 Geophysical Scenario

4.1.1 Flight overview

The flight track of MARSCHALS Flight 1 is shown in Fig. 2, while Fig. 3 reports the altitude of the M-55 aircraft during the flight plotted versus time (UTC).

As can be seen in Fig. 2 the M-55 made a rectangular flight path. The portion of atmosphere sampled during the flight is highlighted in the three panels of Fig. 4, that show the position of the tangent points of the scans of band B (top panel), C (central panel) and D (bottom panel) during the flight.

In the three panels of Fig. 5 we report the barometric altitude of the aircraft along with the tangent altitudes of the observations of bands B (top panel), C (central panel), and D (bottom panel) extracted from the level 1 files. Even if the GPS and the barometric altitudes differ, we use these plots to evaluate the variation of the vertical coverage of the measurements during the flight. The tangent point altitudes along the whole flight calculted by the MARC code using the GPS altitude for the final set of analysed data is reported in Fig. 7.

Fig. 5 shows that some scans as 10, 19, 49, 52, in band B; 21 and 51 in band C and 29, 32, 53 in band D may not be good for the analysis because of the reduced altitude coverage and or because acquired during changes of direction of the aircraft.

At the end of this flight, the Level 1 team discovered a bug in the way the UCSE roll-angle record was handled:

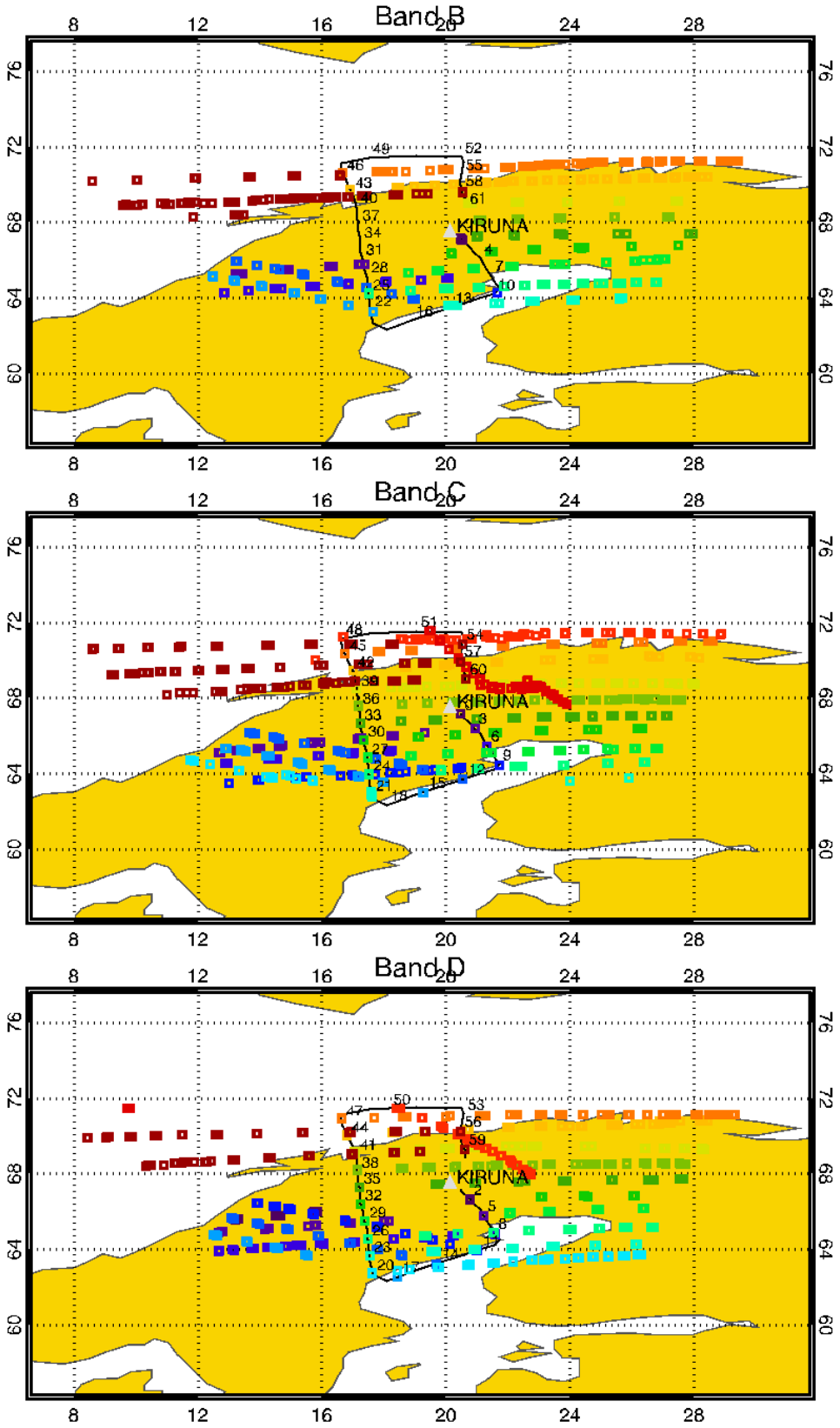

Fig. 4: The flight track with the Geo-location of Band B (top) Band C (middle) and Band D (bottom) tangent points plotted versus latitude and longitude. Different colours are used to identify each scan.

a constant offset was handled by the pointing system of the instrument with the wrong sign, causing a +0.5 degree offset when the aircraft was at level attitude and a periodic roll-angle oscillations in the flight sections that were following a constant longitude. This resulted in a costant offset of 0.5 degrees between the commanded and the real pointing. The correct pointing was determined a-posteriori by the level 1 team. However, the vertical sampling of MARSCHALS scans in the upper atmosphere resulted less dense than what was nominally intended. This problem was not present in Flight 2, therefore we decided to perform the analysis of Flight 1 after the analysis of Flight 2.

Fig. 3 shows that the aircraft altitude was nearly constant in three parts of the flight (from scan 6 to 18, from scan 21 to 40, and from 43 to 57). This is a requirement for having the MARC code working at its best. We therefore expect to have the best data for the analysis for these scans.

4.1.2 Initial Guess Atmosphere: Scan dependent ECMWF profiles

As reported in Sec. 3.2, ECMWF data can be extracted on a personalized latitude and longitude grid. For the 11.12.2011 flight we selected the following latitude-longitude grid:

- Latitude grid from 60 deg to 76 deg with a step of 1.125 deg
- Longitude grid from 5 deg to 30 deg with a step of 1.125 deg

According to the fact that the flight was performed approximately from 11:00 to 14:00 UTC, we downloaded the ECMWF datasets for 06:00 UTC, 12:00 UTC and 18:00 UTC of 11 December 2011. The selected ECMWF profiles were interpolated in latitude, longitude and time in order to obtain the profiles at the time and at the average geo-locations of MARSCHALS instrument during the flight. This process was applied to Temperature, pressure, Q and O_3 MMR altitude profiles.

In order to obtain H_2O and O_3 VMR profiles the data for Q and Ozone MMR needed to be converted. For the conversion of Q into H_2O VMR we have used the same expression reported in Equation 5-1 of [3], while for the conversion of O_3 MMR into O_3 VMR we have used the expression reported in Equation 5-2 of the same technical note. The result of this procedure were altitude profiles from 0.5 to about 77 km for Temperature, pressure, O_3 and H_2O VMR. The profiles have been extrapolated up to 120 km using the same strategy adopted in the SCOUT O3 analysis, that is using the shape of the IG2 profiles.

4.2 Analysis

In this section we report the results of the analysis of the measurements acquired during the first flight.

4.2.1 Analysed dataset and preliminary analysis

As already said, the analysis of the first flight was performed after the analysis of the second flight. Therefore the retrieval strategy and the vertical grids of the preliminary analysis were set to the ones already used in Flight 2 (see sec. 5.2.1). The preliminary analysis was first performed filtering only the bad channels identified by the level 1 team for all the spectra.

We used the procedure described in sect. 3.1 to mask the unmasked 'bad channels', therefore reducing the number of used spectral points for each scan. The preliminary analysis used to identify the bad channels also showed that, probably due to the pointing problems that were reported by the RAL team, some spectra were affected by an error in the assigned pointing (and thus their tangent altitude was wrong). These spectra were then removed from the analysis. Figure 6 reports the total number of spectral points of all the used spectra of each scan, with superimposed in blue the number of spectral points masked by the level 1 team and in red the number of spectral points masked after the preliminary level 2 analysis. The green bars represent the number of spectral points really used in the analysis.

The χ-test values obtained in the preliminary analysis showed that in general the chi square values assumed values below 2.5 and above 1, suggesting that the noise level reported into the level1 files was correct. Moreover the ozone and HNO_3 retrieved profiles at 15 km in the first part of the flight were lower than the ones retrieved in the following part of the flight. Since the ozone a-priori profile was showing the same feature we performed two tests one with constant a-priori profile and one with the O_3 profiles (and all the other ECMWF data) interpolated at the average geolocation of the tangent points. Both analyses showed the same structure, confirming the independence of the obtained results from the a-priori.

After masking the bad channels and removing the spectra affected by pointing problems, we had significant improvements in the analysis (e.g. reduction in the χ-test of scan 15, good results for scans 6, 7 ,8 that we thought should be discarded after the preliminary analysis). All the subsequent tests were then performed using the "cleaned" set of L1B data. The position of the tangent altitudes (calculated by MARC using the GPS aircraft

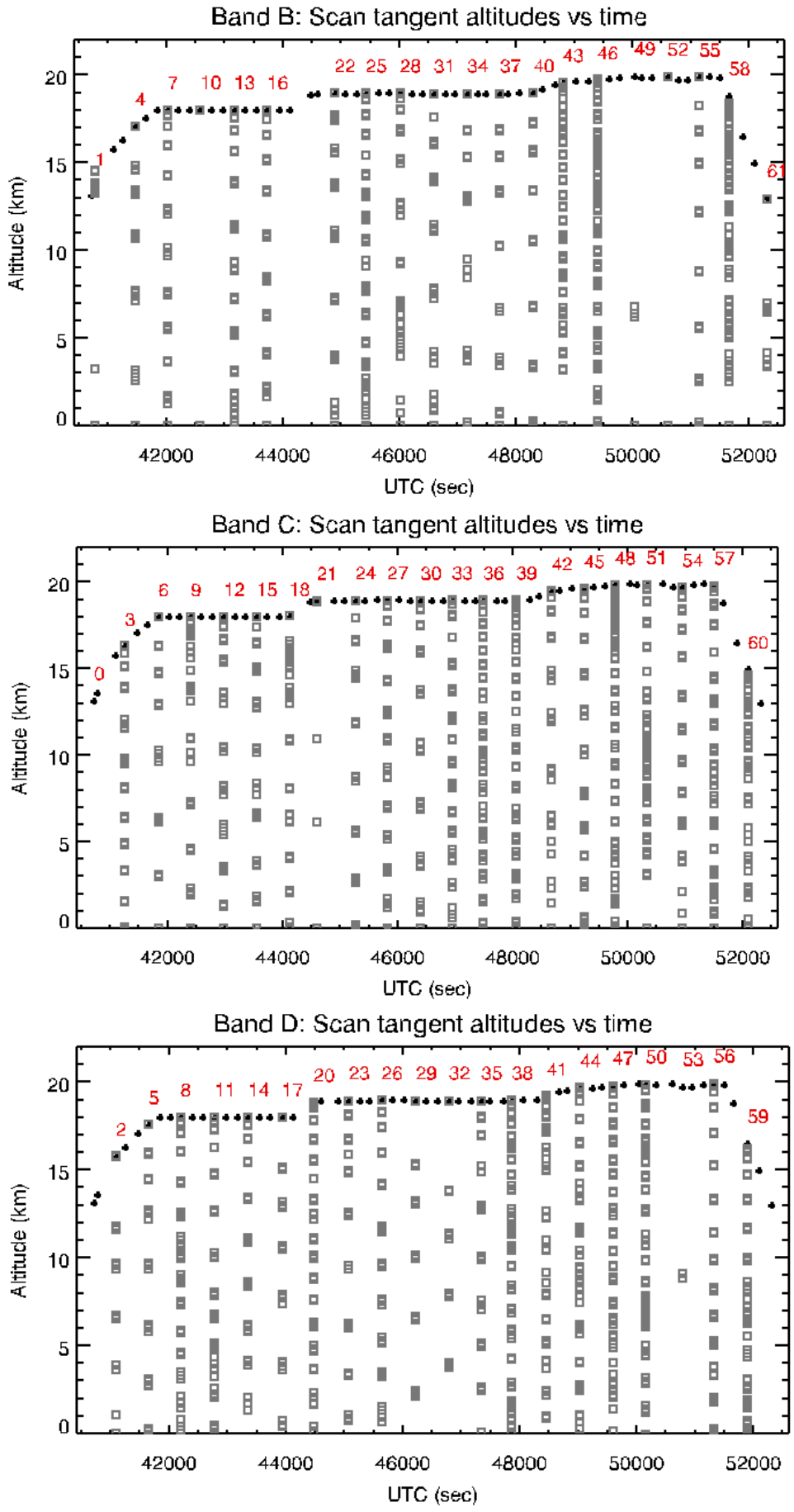

Fig. 5: The flight altitude and the analysed scans tangent altitudes position plotted versus the UTC. Top panel: band B, central panel: band C, bottom panel: band D.

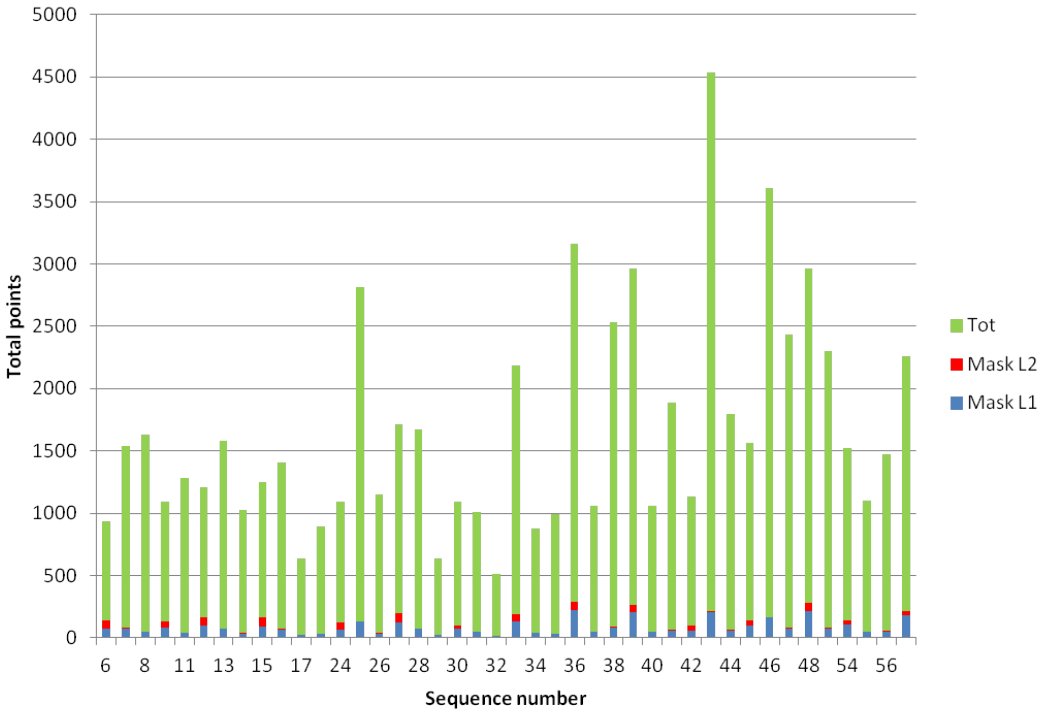

Fig. 6: Bar plot of the total number of spectral points (green), number of spectral points masked by the level 1 team (blue) and number of spectral points masked after the preliminary level 2 analysis (red)

altitude) of the ”cleaned” L1B dataset with respect to the acquisition time are reported in Fig. 7. In the figure we report only the tangent points of the scan used in the final analysis.

Further tests were performed in order to evaluate if it was possible for this flight to set the threshold for the a priori error to 200%, as we did in the Flight 2 data analysis. The same tests reported for the Flight 2 were then repeated also for Flight 1. Even if some more oscillations are present in the retrieved N_2O profiles for the Flight 1 with respect to the Flight 2 we decided to keep the threshold of 200% for both the flights.

4.2.2 Final Analysis

The retrieval features used in the final analysis of the Flight 1 are similar to the the features used for Flight 2 analysis and can be summarised as follows:

Retrieval strategy:

- Band C: T, H_2O, O_3, HNO_3, Pointing, gain, Offset, Continuum, Frequency Shift

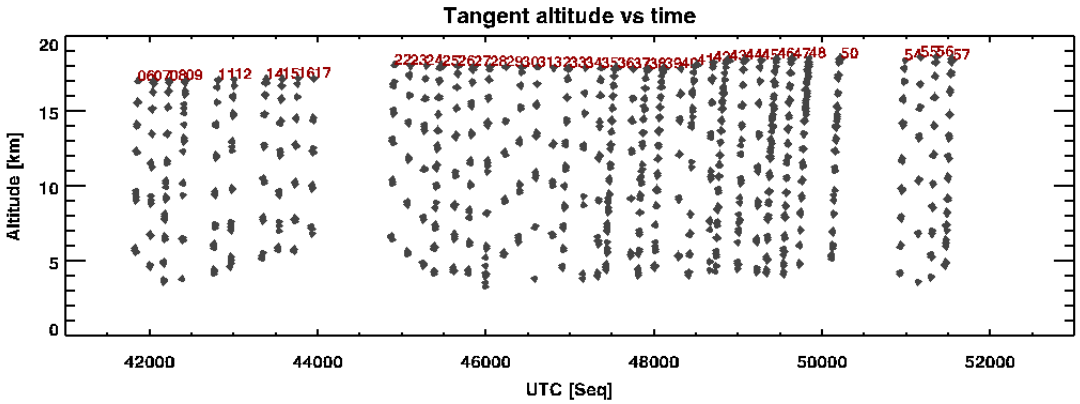

Fig. 7: Tangent altitudes calculated by MARC using the GPS aircraft altitude for the ”cleaned” L1B dataset used for the Flight 1 data analysis versus time (UTC).

- Band B: H_2O, O_3, HNO_3, N_2O, Pointing, gain, Offset, Continuum,Frequency Shift(T from Band C previous scan, H_2O initial guess and error from band C)
- Band D: H_2O, O_3, HNO_3, CO, Pointing, gain, Offset, Continuum, Frequency Shift (T from Band C previous scan, H_2O initial guess and error from band C)

Observations used down to 4 km and top of the atmosphere at about 65 km.
Used retrieval grids:

- T 24,20,18,17,15,13,11,9,7,5
- H_2O 24,21,18,17,16,15,14,13,12,11,10,9,8,7,6,5
- O_3 24,21,18,17,16,15,14,13,12,11,8,5
- HNO_3 23,20,17,16,14,12,9,6
- N_2O 20,16,14,12,10,8
- CO 21,17,13,7
- Continuum 18,17,16,15,14,13,12,11,10,9,8,7,6

A priori profiles: T, H_2O, O_3 from ECMWF archive (from 0 to approximately 72-78km). Others from IG2 Polar winter atmosphere

A priori errors: 3K for T, 1-sigma variability or 200% (if 1-sigma variability is lower) for O_3 and H_2O,1-sigma variability or 200% (if 1-sigma variability is lower) for HNO_3, CO, N_2O

We used the spectral database specifically developed for the MASTER study [27].

4.2.3 Retrieval results

The results obtained during the analysis of the Flight 1 are reported in this section. After running the analysis we found that scans 18 and 20 produced high χ-test values and anomalous gain values probably because they have wrong tangent altitudes because they were acquired immediately before and after the turning point of scan 19 (as shown in figure 4). These scans have therefore been discarded.

Figure 8 reports the chi square values obtained in the final analysis of Flight 1. In general the chi square values are below 2 and above 1, apart from scan 46.

The values of the trace of the Averaging Kernel matrix and of the information content for each scan are reported in Fig. 9. Despite the uneven altitude coverage of this flight, in band C the value of the trace and the information content are fairly constant over the whole flight. In band B there are a few scans (namely scans 34,37,40 and 55) that have lower trace values with respect to other scans in the same band. The same happens in band D, where some scans (17, 29 and 32) have lower values of the AK trace and information content with respect to the others. In general, the values of the AK trace and information content obtained during Flight 1 are much more variable during the flight than the ones obtained during the Flight 2 (see Fig. 49 for comparison). This is due to the pointing problems arisen during the flight that prevented an homogeneous vertical coverage during the flight.

The retrieved scalar quantities (namely the frequency shift (in MHz), the pointing bias (in deg), the offset (in K) and the gain) are shown in Figs. 10, 11, 12, and 13. The values of the frequency shift is on average 8 MHz in band B, 12 MHz in band C and 14 MHz in band D with values that are almost constant over the flight for band B and C while for band D they are more variable, expecially in scans 29 and 32 that however have low AK trace and information content values.

The retrieved pointing bias is close to 0.0 degrees for large part of the flight highlighting that the correction applied by the RAL team to the pointing angle was, in general, correct. Few scans like scans 34 and 46 have pointing bias values that deviates from 0 showing that there could be some residual pointing problems that may affect the retrieved values. The retrieved values for the offset are similar in band C and D with average value of -1 K, while the band B offset (constant through the flight) is around 2-3 K. The same behaviour was found in Flight 2 and it is probably related to different instrumental performances for the three bands. The gain values are stable during the flight for band C with values close to 1. Also in band D the gain is quite stable and close to 1 while in band B some oscillations are present. The retrieved values of the scalar quantities are in general consistent with the ones retrieved from Flight 2 (see figures 50, 51, 52, 53 for comparison).

The retrieved values for Temperature (from band C), H_2O (from band C), O_3 (from all bands), HNO_3 (from band C and D), N_2O (from band B), and CO (from band D) are reported in figures 14 to 31, mapped as a function of altitude and UTC. White points on the maps show the position of the vertical retrieval grid while the black squares

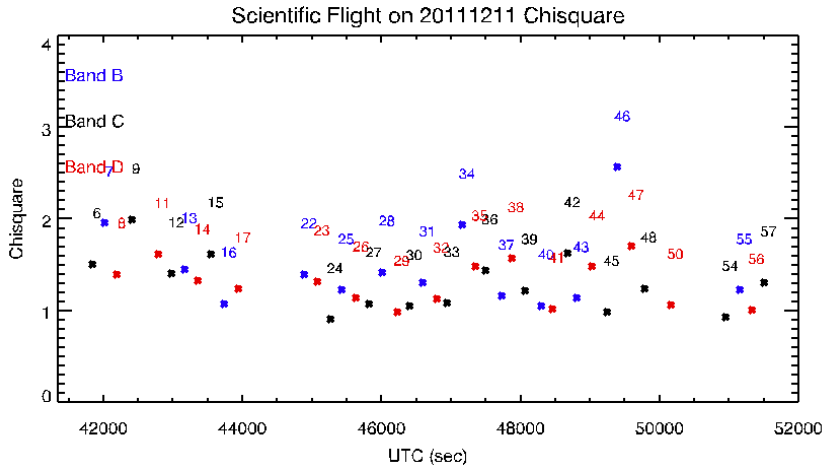

Fig. 8: Chi square for Flight 1 plotted versus the UTC (Band B in blue, Band C in black, Band D in red).

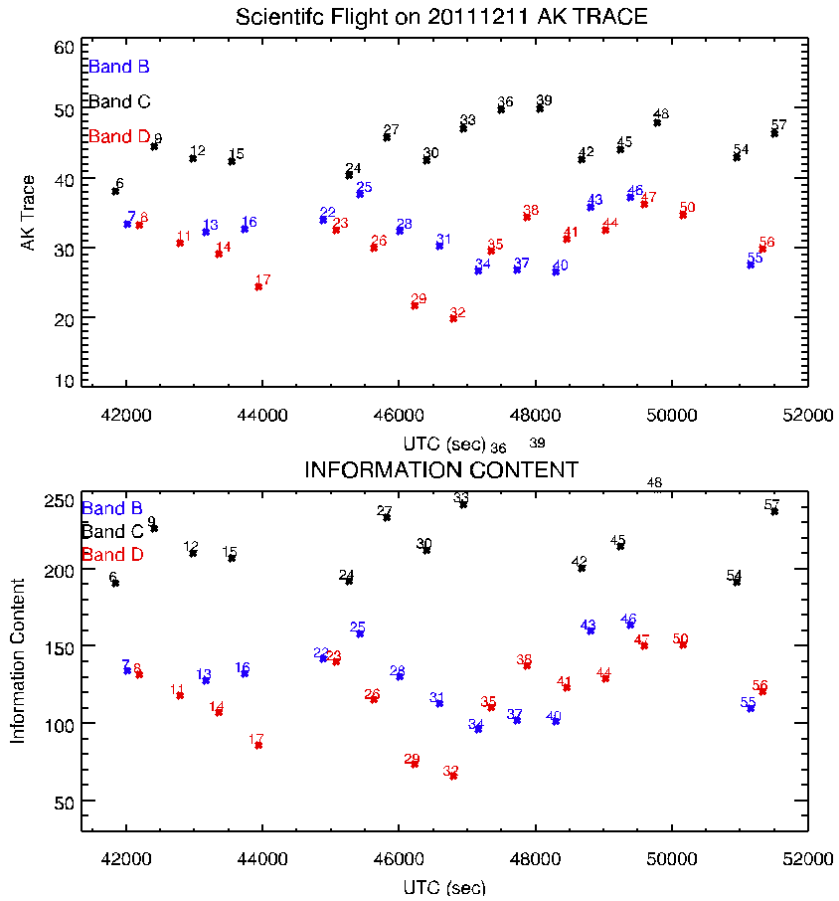

Fig. 9: Top panel: Trace of the AK matrix for Flight 1 plotted versus the UTC. Bottom panel: Information content for each scan versus the UTC (Band B in blue, Band C in black, Band D in red).

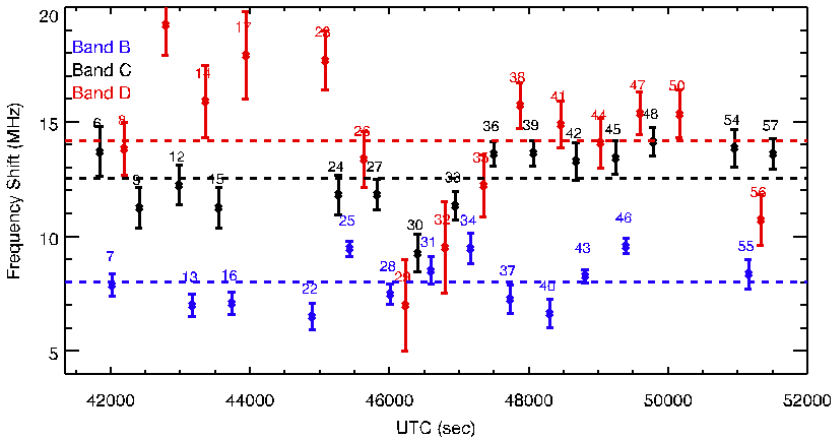

Fig. 10: Frequency shift in MHz for Flight 1 plotted versus the UTC (Band B in blue, Band C in black, Band D in red).

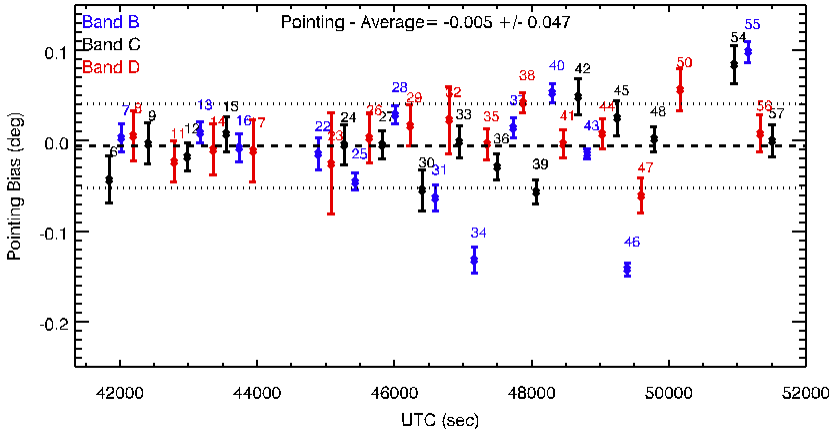

Fig. 11: Pointing Bias in deg for Flight 1 plotted versus the UTC (Band B in blue, Band C in black, Band D in red).

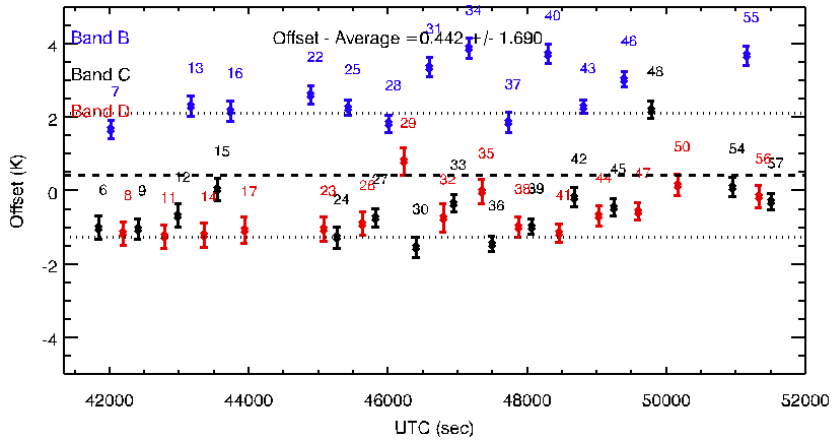

Fig. 12: Offset in K for Flight 1 plotted versus the UTC (Band B in blue, Band C in black, Band D in red).

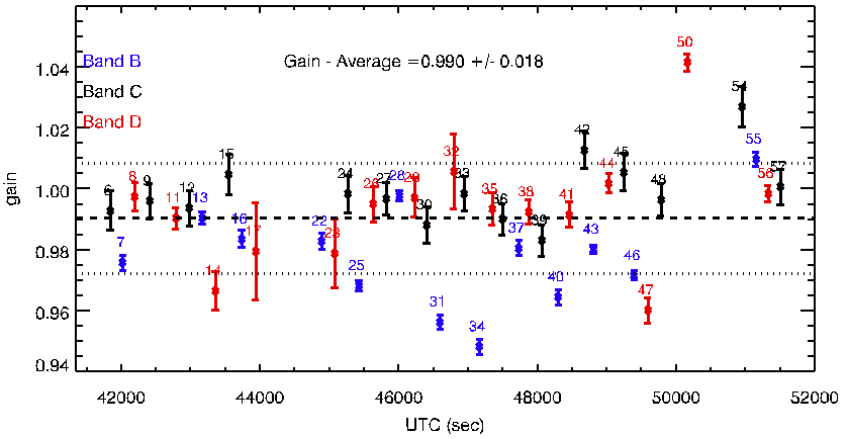

Fig. 13: Gain for Flight 1 plotted versus the UTC (Band B in blue, Band C in black, Band D in red).

show the flight altitude for each scan. For each target we plot the values of the retrieved quantities, of the biased error, of the individual information content , of the a priori profiles, of the relative biased error (in percentage) and of the FWHM of the AK matrix, that represents the vertical resolution of MARSCHALS measurenmts. The biased error is the retrieval error, that is the square root of the diagonal elements of the variance-covariance matrix of the retrieval (that is the combination of the error due to the measurement noise with the a-priori error). Definition of the individual information content can be found in [9]. The FWHM of the AK was calculated using the expression given in [53], using the absolute values of the AK terms in order to penalize the negative lobes of the averaging kernel.

Maps for temperature are reported in Fig. 14 (retrieved values and biased errors), in Fig. 15 (individual information content and a priori profile) and in Fig. 16 (relative biased error and FWHM of AK). The information content for temperature is very low (it assumes values always below 1) for the whole flight and the retrieved temperature profiles are very close to the a priori ones even if some oscillations are present (for example in scan 12 and 36); in the last part of the flight there is a hint that cold stratospheric air descended down to 15 km. The vertical resolution of the Temperature retrievals is always very low, above 4 km for almost the whole flight, confirming the low information content of the measurements.

The retrieved values of H_2O VMR (obtained from band C only) are reported in Fig. 17 (retrieved values and biased error) , in Fig. 18 (individual information content and a priori profile). and in Fig. 19 (relative biased error and FWHM of AK). Some oscillations are present in some scan (e.g. scan 54 that however has low values of the individual information content at low altitudes). In general, the individual information content is above 5 in the altitude range below 14 km for almost the whole flight. The vertical resolution shown in the lower panel of fig. 19 is homogeneous along the whole flight, it is about 1.5 km below flight altitude, and is strictly related to the vertical spacing of the retrieval grid.

Maps for O_3, that has been retrieved from the measurements of all the scans, are reported in Fig. 20 (retrieved values and bias error), in Fig. 21 (individual information content and a priori profile) and in Fig. 22 (relative biased error and FWHM of AK). The information content and the vertical resolution of ozone are oscillating along the flight, reflecting the different information contained in the three bands and the uneven vertical coverage during this flight. The vertical resolution is between 1 and 2 km in the vertical range from 10 to 17 km, while below 10 km it reaches values above 4 km. The information content is constantly about 3 at 10 km, and it assumes higher values above 15 km in the second part of the flight; this is due to the fact that the flight altitude is higher in that part of the flight, and MARSCHALS observations with tangent altitude below the flight altitude sample a region with higher content of ozone. In the first part of the flight (scan 11 to 17) the value of ozone at 15 km is lower than in the following part of the flight, as it was found during the preliminary analysis. This feacture is present also in the ECMWF data (used as initial guess) even if in the initial guess data the values are lower from scan 11 to scan 27.

A similar behaviour is also shown in the HNO_3 retrieved profiles reported in Fig. 23. Only the measurements of band C and D have enough information about HNO_3 abundance to produce good quality results when analysed independently, therefore fig.s 23, 24 and 25 report the analysis of just the two bands. In the maps of fig. 23 we see that there is a clear indication of a renitrification process at 16 km in the last part of the flight, in coincidence with the O_3 enhacement. The last part of the fligh is also the part where the individual information content is higher, therefore we can conclude that what is measured is not due to some instability in the retrieval procedure. The vertical resolution of HNO_3 retrieval is constant along the flight, a part from few scans that resent the low vertical coverage of the measurements. The HNO_3 and O_3 behaviour confirms what was reported in the ”MARSCHALS

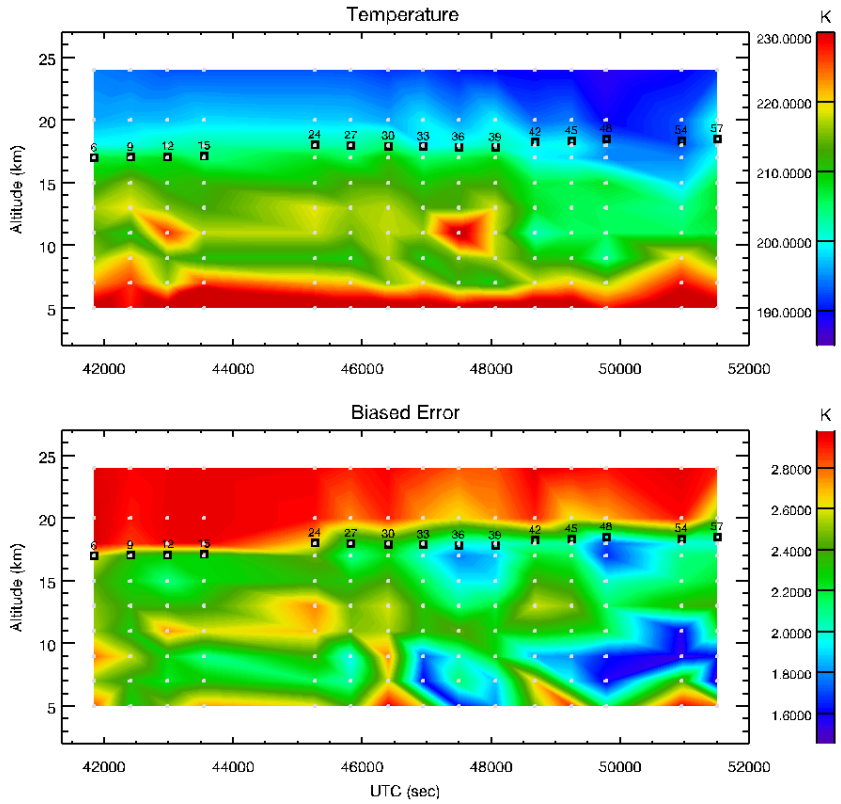

Fig. 14: Top panel: Temperature from band C for Flight 1 plotted versus the UTC and altitude. Bottom panel: Biased error plotted versus the UTC and altitude.

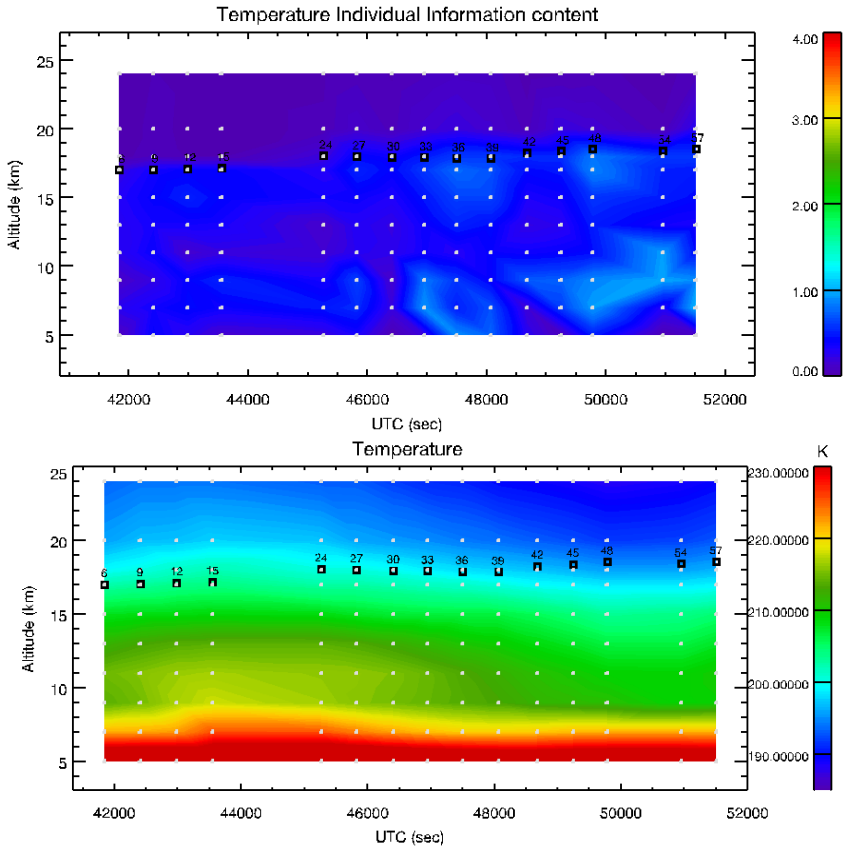

Fig. 15: Top panel: Temperature individual information content from band C for Flight 1 plotted versus the UTC and altitude. Bottom panel: Temperature initial guess from band C for Flight 1 plotted versus the UTC and altitude.

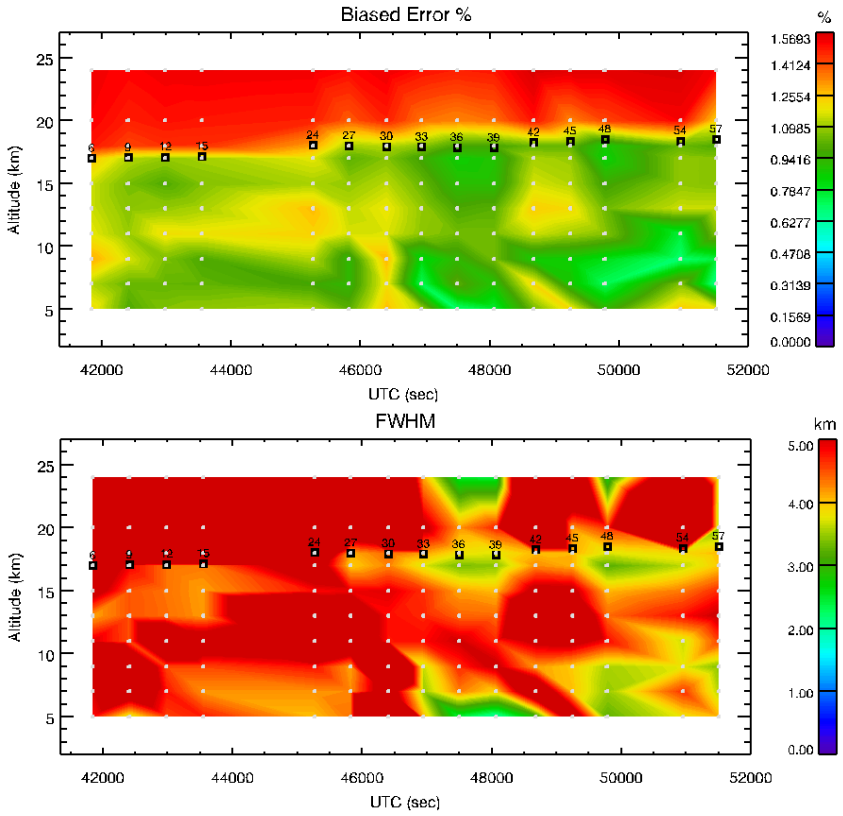

Fig. 16: Top panel: Temperature relative biased error plotted versus the UTC and altitude. Bottom panel: FWHM of Temperature AK for Flight 1 plotted versus the UTC and altitude.

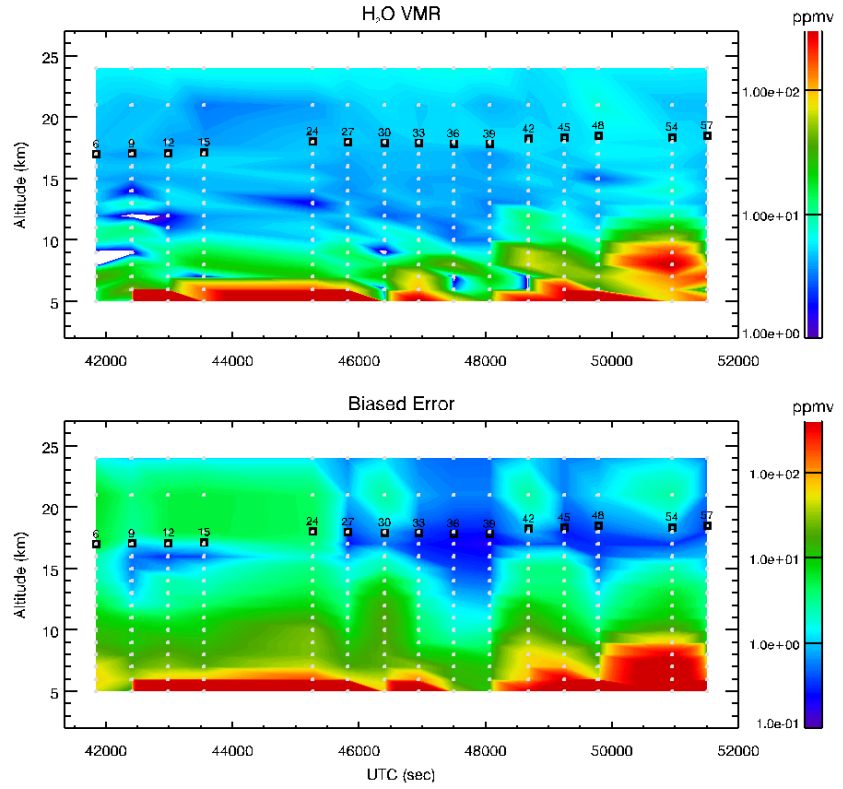

Fig. 17: Top panel: $H_2O$from band C for Flight 1 plotted versus the UTC and altitude. Bottom panel: Biased error from band C for Flight 1 plotted versus the UTC and altitude.

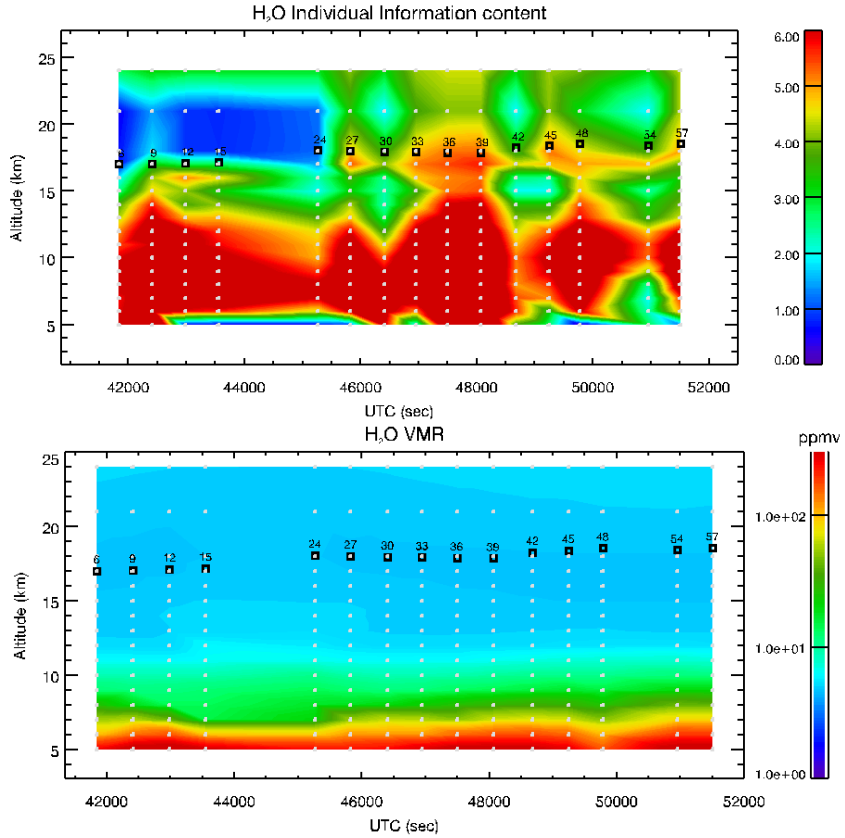

Fig. 18: Top panel: H_2O individual information content from band C for Flight 1 plotted versus the UTC and altitude. Bottom panel: H_2O initial guess from band C for Flight 1 plotted versus the UTC and altitude.

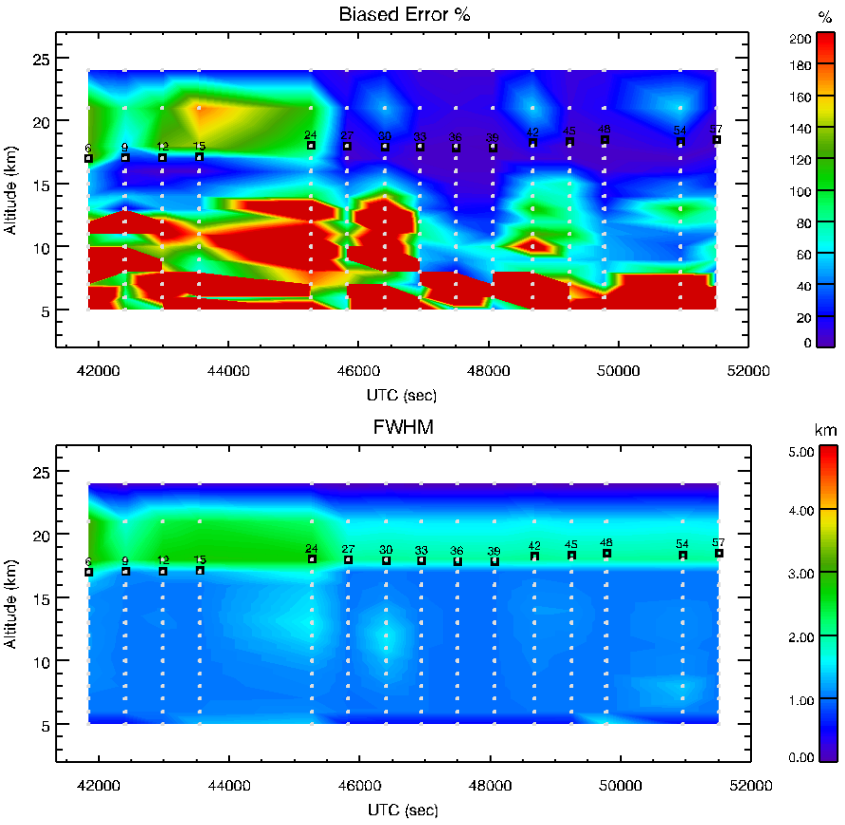

Fig. 19: Top panel: H_2O relative biased error plotted versus the UTC and altitude. Bottom panel: FWHM of H_2O AK for Flight 1 plotted versus the UTC and altitude.

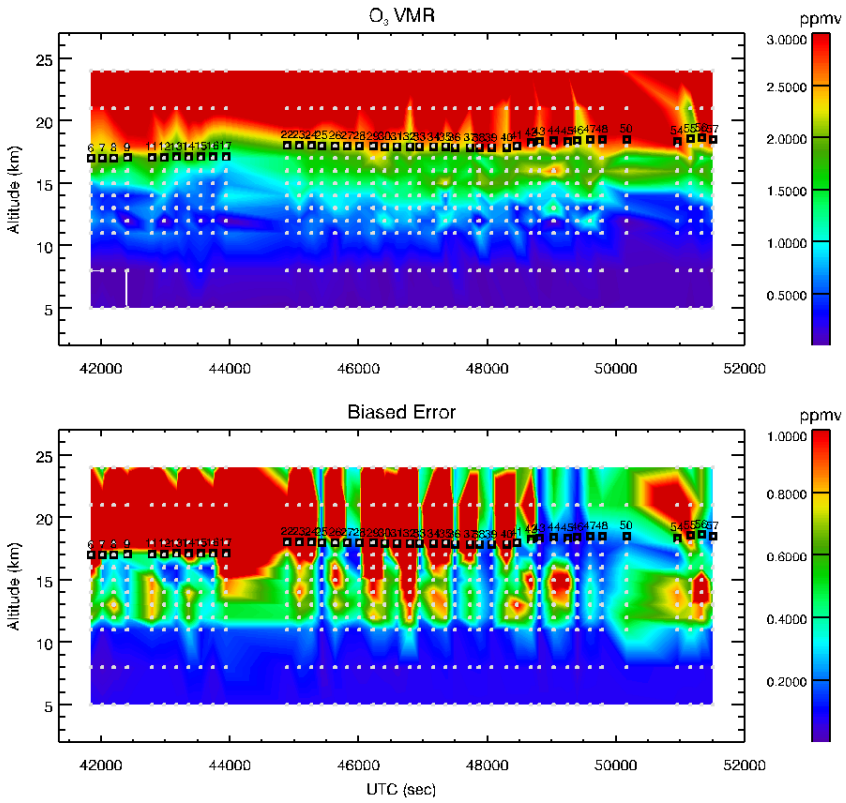

Fig. 20: Top panel: O_3 from all bands for Flight 1 plotted versus the UTC and altitude. Bottom panel: Biased error for Flight 1 plotted versus the UTC and altitude.

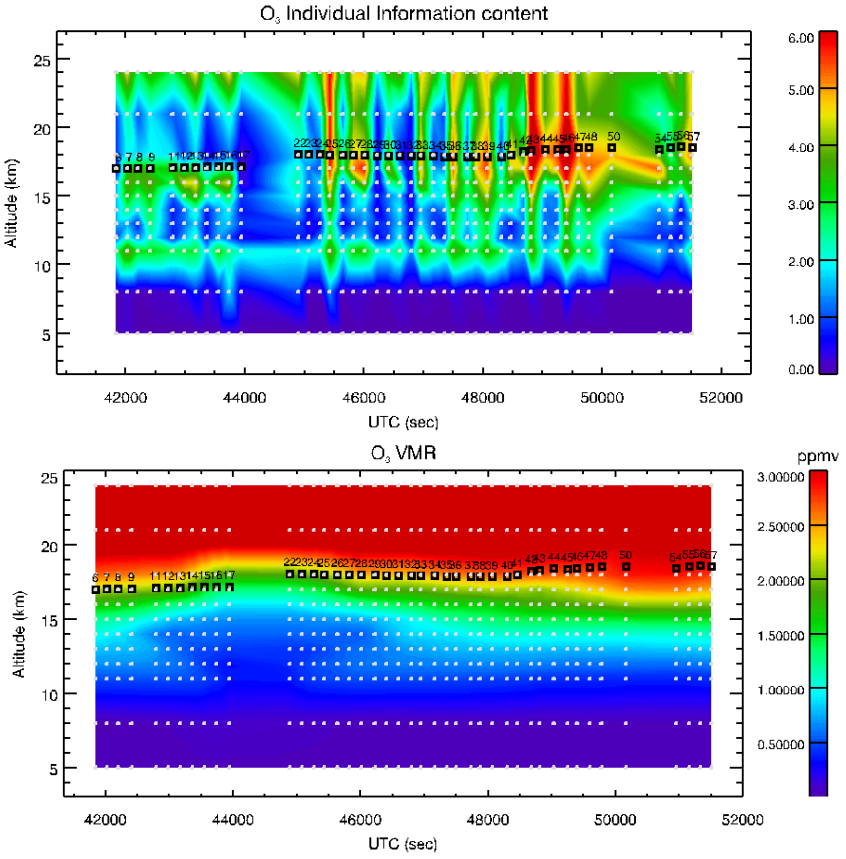

Fig. 21: Top panel: O_3 individual information content from all bands for Flight 1 plotted versus the UTC and altitude. Bottom panel: O_3 initial guess for Flight 1 plotted versus the UTC and altitude.

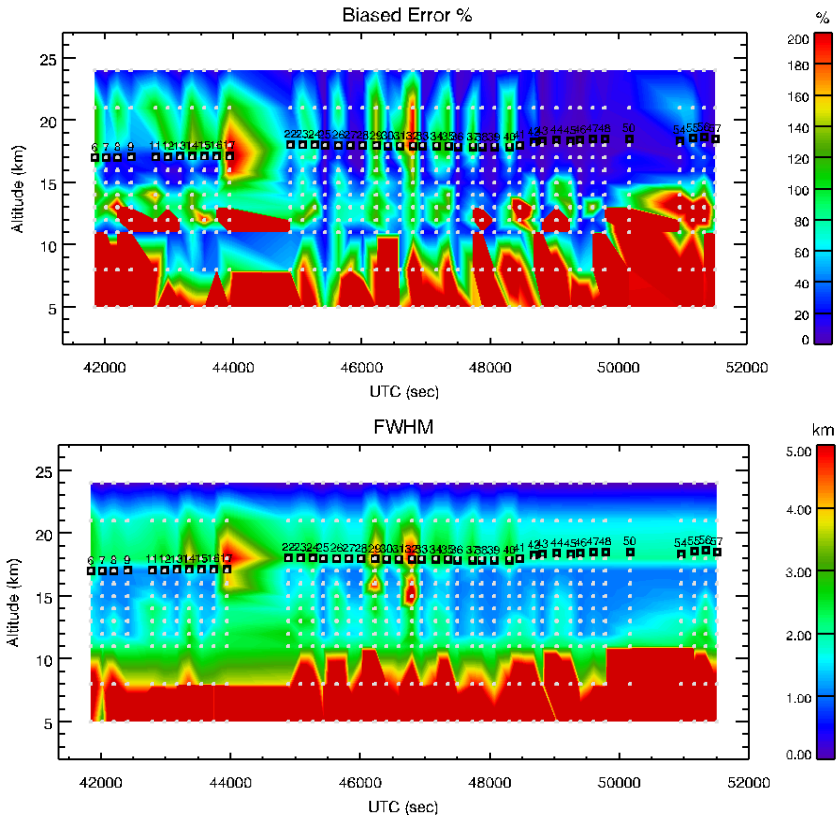

Fig. 22: Top panel: O_3relative biased error plotted versus the UTC and altitude. Bottom panel: FWHM of O_3AK for Flight 1 plotted versus the UTC and altitude.

compact data acquisition report", that is the possible presence of a tropopause folding in the first part of Flight 1.

N_2O can only be retrieved from the spectra of band B, therefore Fig.s 26, 27 and 28 report the results obtained in the analysis of band B only. The retrieved values show more oscillations with respect to the results obtained during Flight 2 (see Fig. 67). In particular strong oscillations are present at lower altitudes in those scans (from 31 to 40) for which the individual information content is lower. Despite the oscillating behaviour of the retrieval, the vertical resoltion of N_2O shown in the lower panel of fig. 28 is constant along the flight, with values around 2.5 km in the vertical range from 10 to 15 km.

The results obtained from Band D for CO retrievals are reported in Fig. 29, in Fig. 30 and in Fig. 31. Below the flight altitude the retrieved CO values are much lower (see upper panel of Fig. 29) than the a priori ones (in bottom panel of Fig. 30), while higher COvalues are found above flight altitude in the first part of the flight with respect to the second one.

The cloud coverage seen by the MARSCHALS instrument can be evaluated using the retrieved values of the external continuum, shown in Fig. 32. No opaque clouds are seen by MARSCHALS, even if in the last part of the flight the value of the external continuum is about 1 in the altitude range from 10 to about 15-14 km. However, as can be inferred from Fig. 33, the values of the individual information content is very low at these altitudes, suggesting that this value is due to retrieval artifacts more than to the presence of clouds.

4.2.4 Recursive retrievals for O_3 and HNO_3

The results obtained in the final analysis show that for almost all the targets the information content is different in each band. In particular, for targets whose spectral features are present in all bands, the accuracy of the retrieved VMR will benefit from the possibility to perform a simultaneous measurement, and therefore analysis, of the three bands. Since it is not possible with MARC to retrieve simultaneously all the band because of the different flight altitude and pointing strategy used for each scan, we have run a final analysis simulatng a multi-band retrieval using the recursive retrieval approach described below. Band C is used to retrieve Temperature and H_2O, then we have retrieved O_3 and HNO_3 in this way: the retrieval of O_3 uses the ECMWF a priori only for the scans of band B, while the analysis of band D and C uses as a priori the results of the analysis of the previous scan. The retrieval of HNO_3 uses the IG2 a priori only for the scans of band D, while the analysis of band C and B uses as a priori the results of the analysis of the previous scan. This strategy has been applied to the whole flight apart from Scan 22

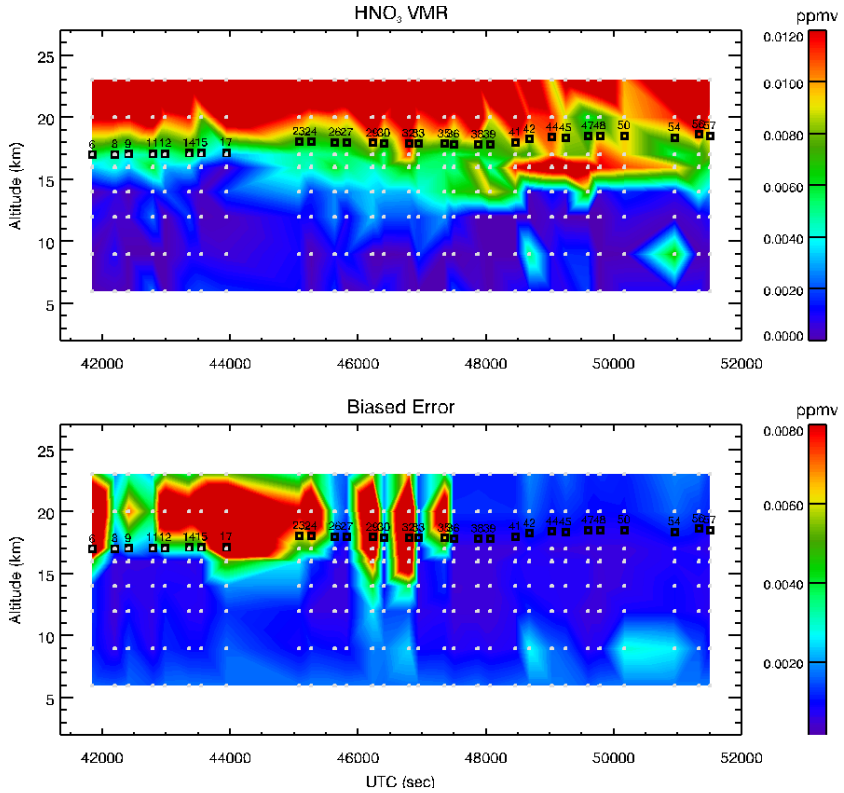

Fig. 23: Top panel: HNO_3 from band C and D for Flight 1 plotted versus the UTC and altitude. Bottom panel: Biased error from band C and D for Flight 1 plotted versus the UTC and altitude.

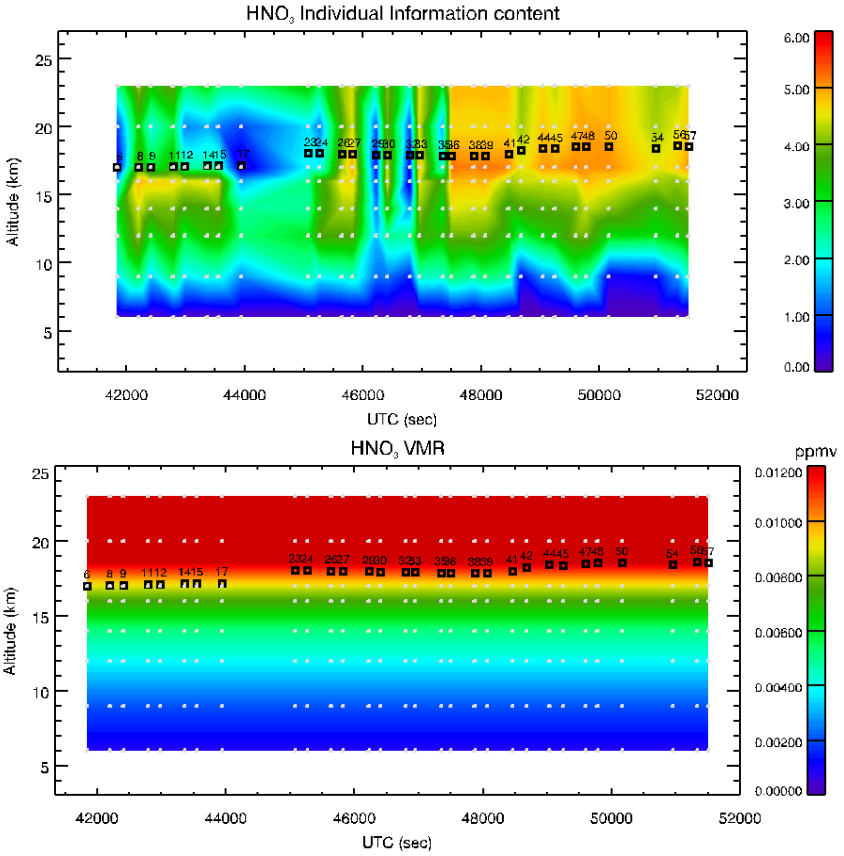

Fig. 24: Top panel: HNO_3 individual information content from band C and D for Flight 1 plotted versus the UTC and altitude. Bottom panel: HNO_3 initial guess from band C and D for Flight 1 plotted versus the UTC and altitude.

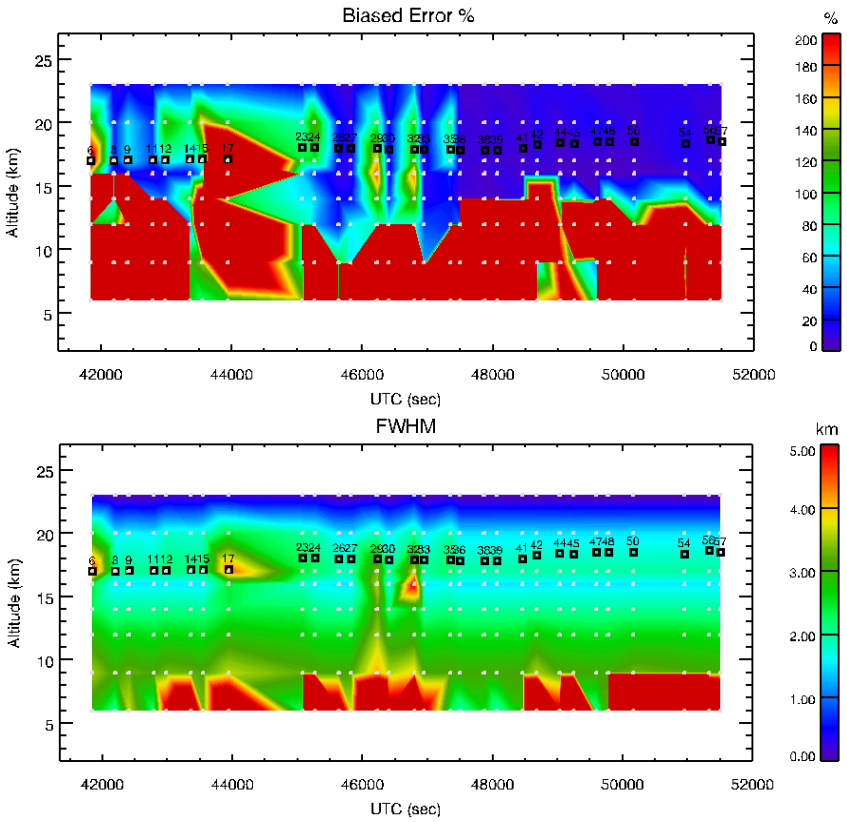

Fig. 25: Top panel: HNO_3 relative biased error plotted versus the UTC and altitude. Bottom panel: FWHM of HNO_3 AK for Flight 1 plotted versus the UTC and altitude.

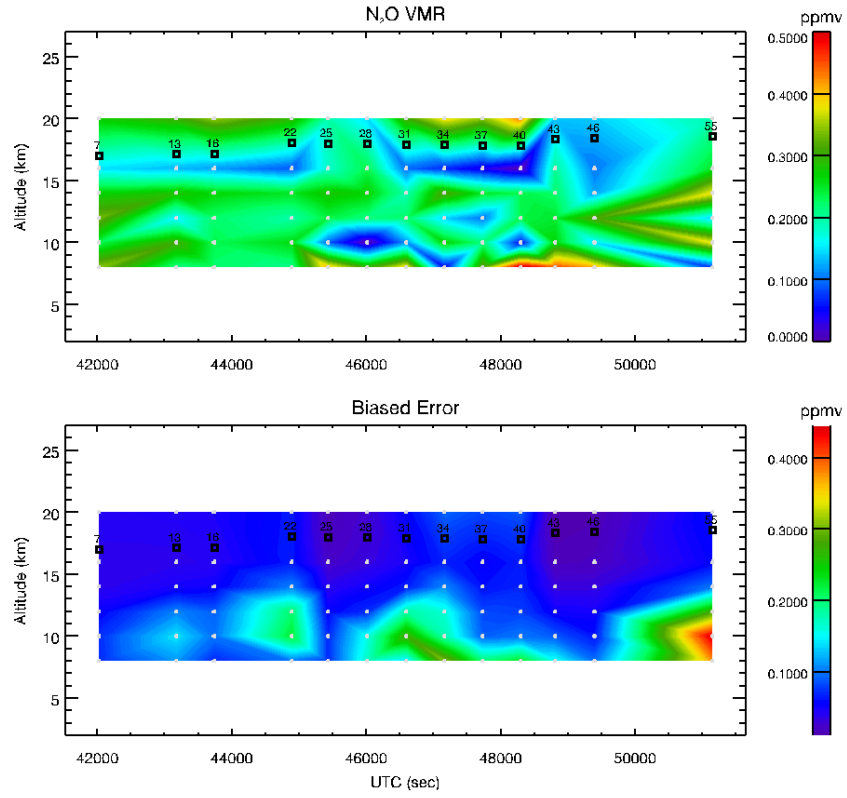

Fig. 26: Top panel: N_2O from band B for Flight 1 plotted versus the UTC and altitude. Bottom panel: Biased error from band B for Flight 1 plotted versus the UTC and altitude.

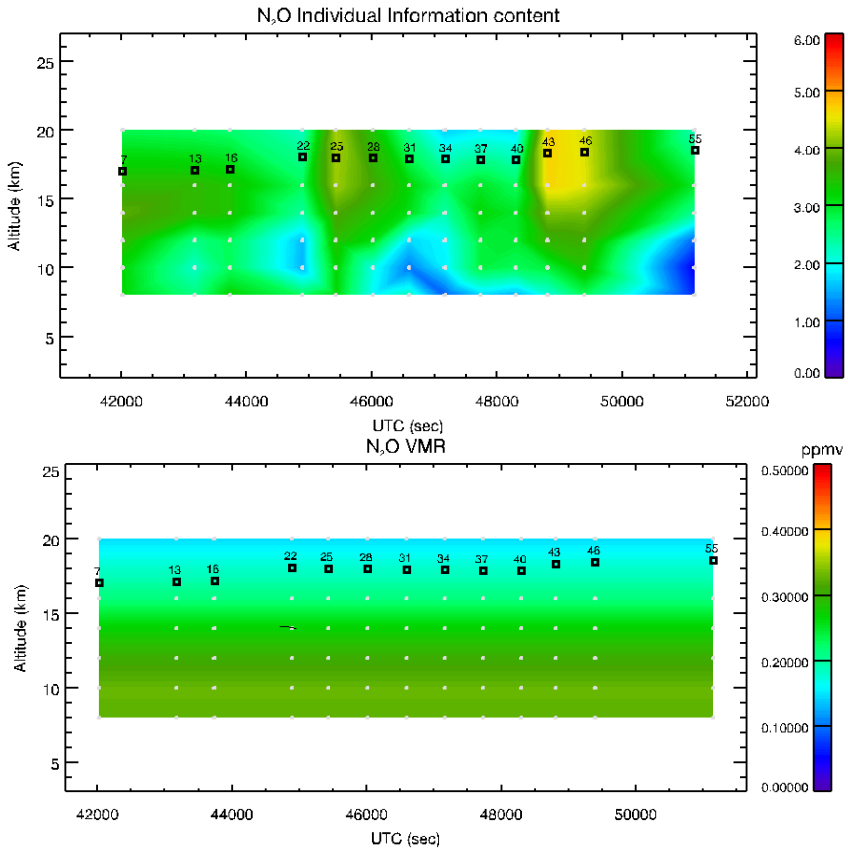

Fig. 27: Top panel: N_2O individual information content from band B for Flight 1 plotted versus the UTC and altitude. Bottom panel: N_2O initial guess from band B for Flight 1 plotted versus the UTC and altitude.

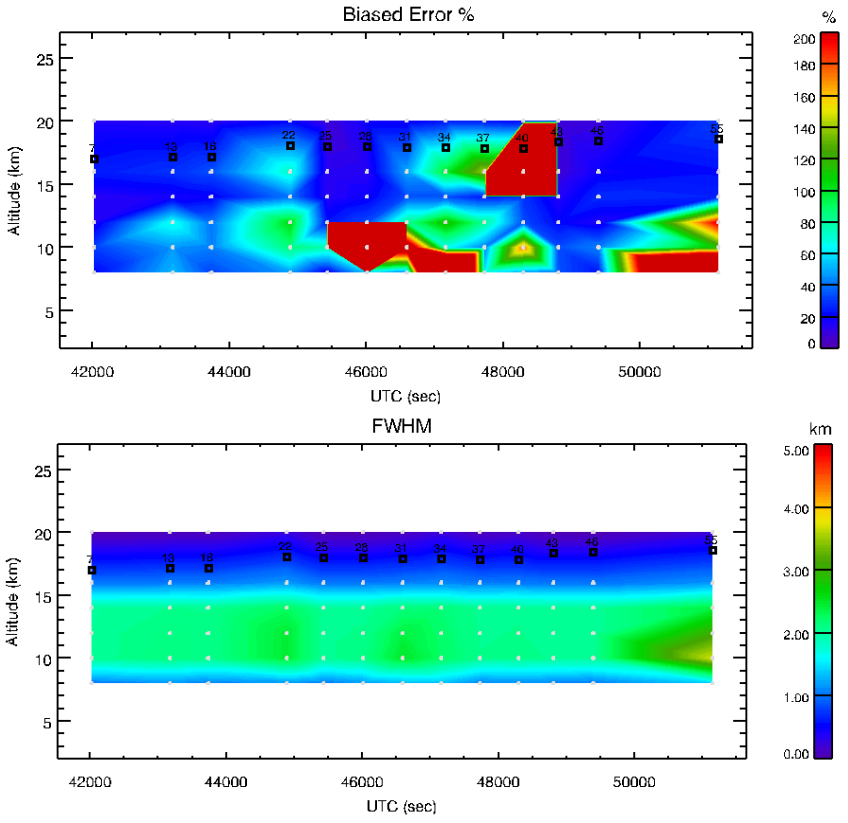

Fig. 28: Top panel: N_2O relative biased error plotted versus the UTC and altitude. Bottom panel: FWHM of N_2O AK for Flight 1 plotted versus the UTC and altitude.

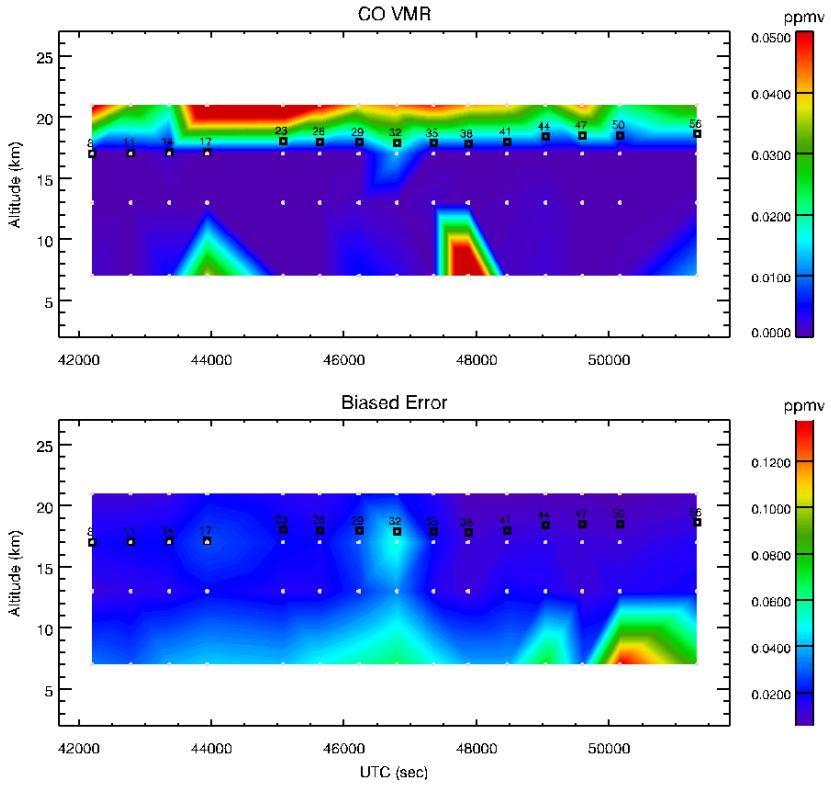

Fig. 29: Top panel: CO from band D for Flight 1 plotted versus the UTC and altitude. Bottom panel: Biased error from band D for Flight 1 plotted versus the UTC and altitude.

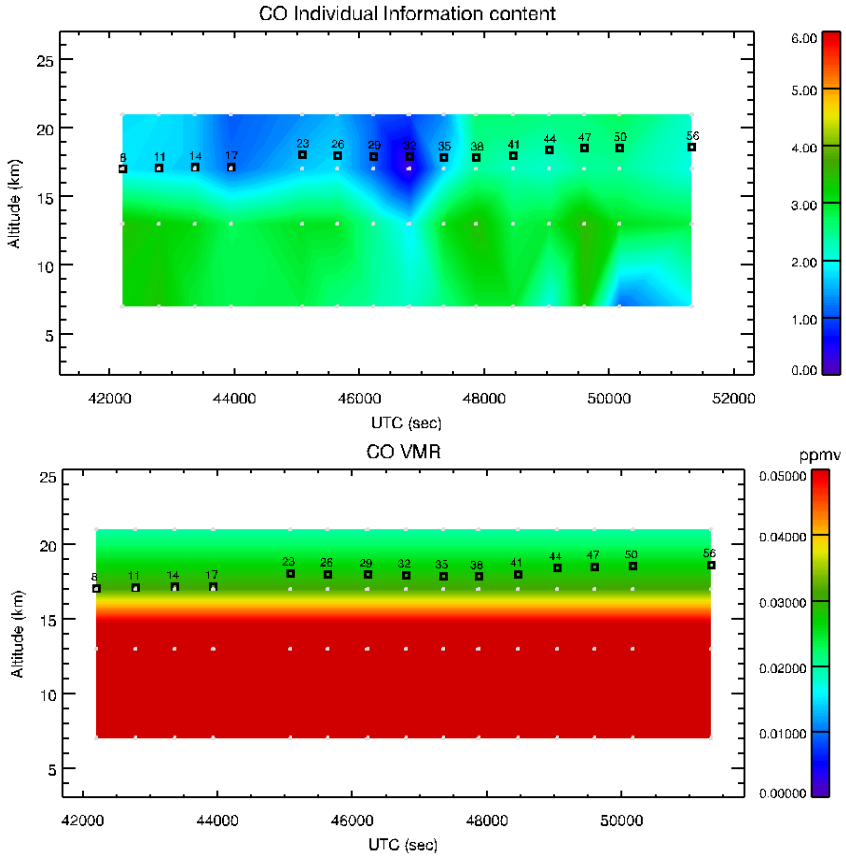

Fig. 30: Top panel: CO individual information content from band D for Flight 1 plotted versus the UTC and altitude. Bottom panel: CO initial guess for Flight 1 plotted versus the UTC and altitude.

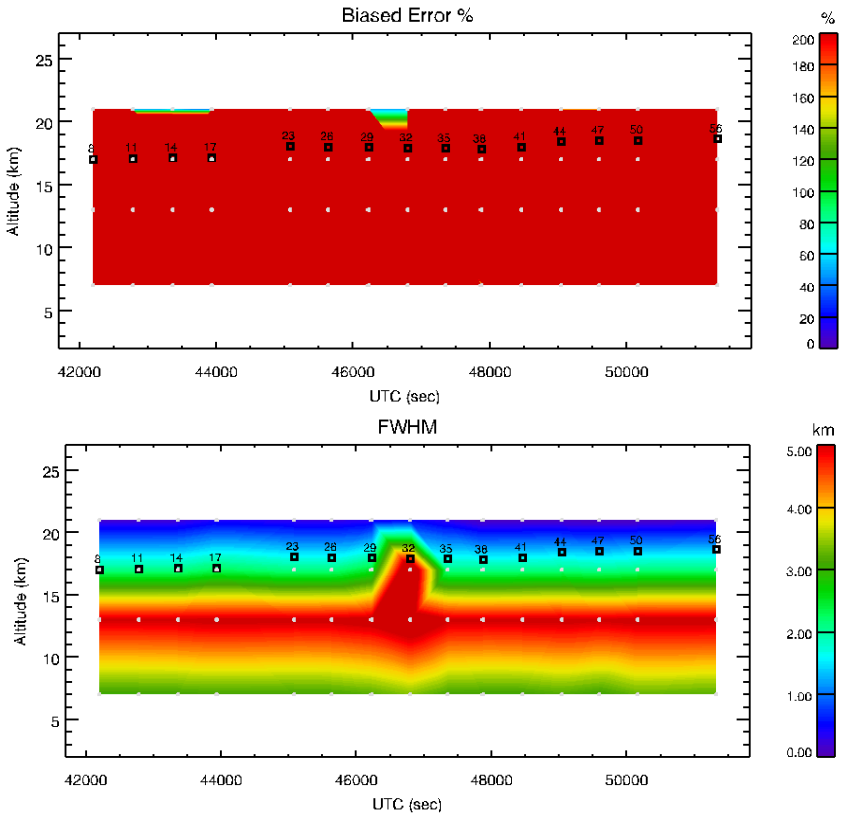

Fig. 31: Top panel: CO relative biased error plotted versus the UTC and altitude. Bottom panel: FWHM of CO AK for Flight 1 plotted versus the UTC and altitude.

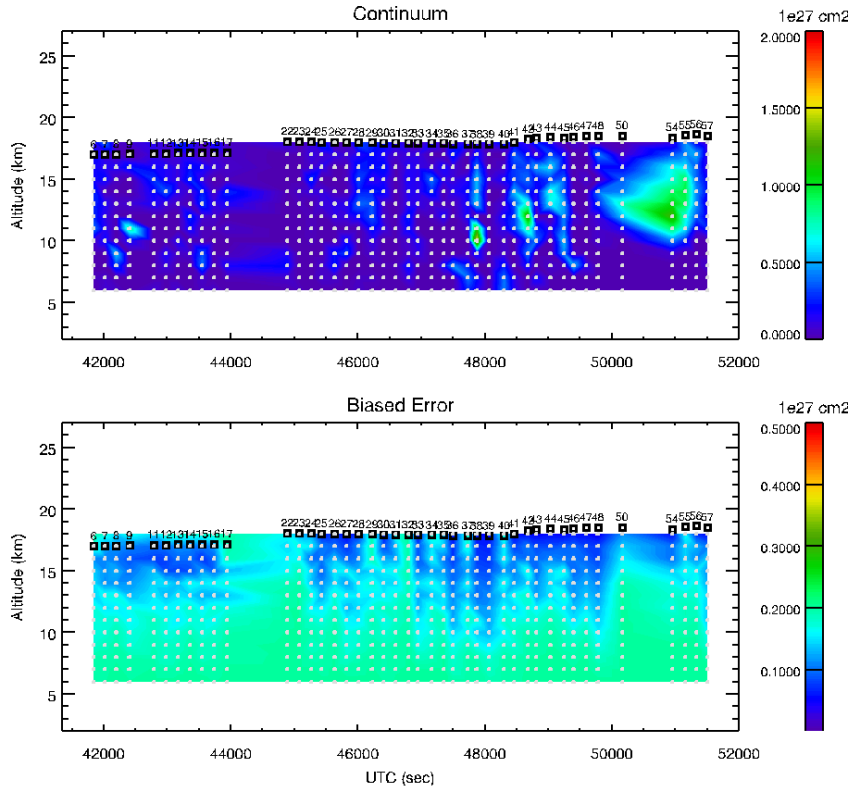

Fig. 32: Top panel: external continuum from all bands for Flight 1 plotted versus the UTC and altitude. Bottom panel: Biased error for Flight 1 plotted versus the UTC and altitude.

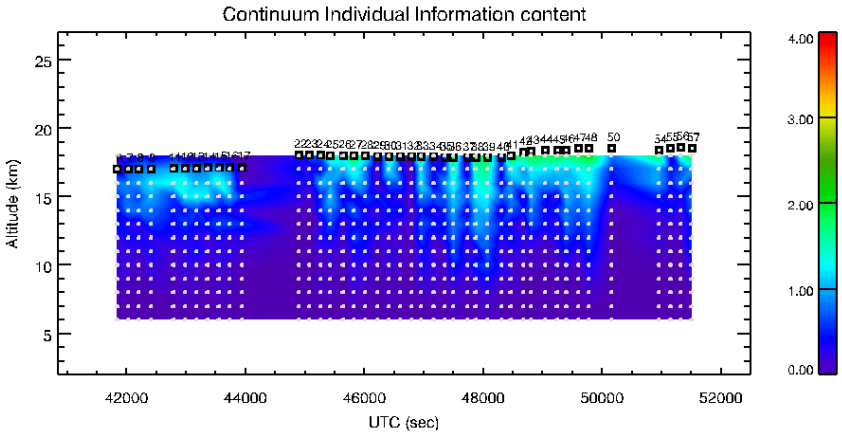

Fig. 33: external continuum individual information content for Flight 1 plotted versus the UTC and altitude.

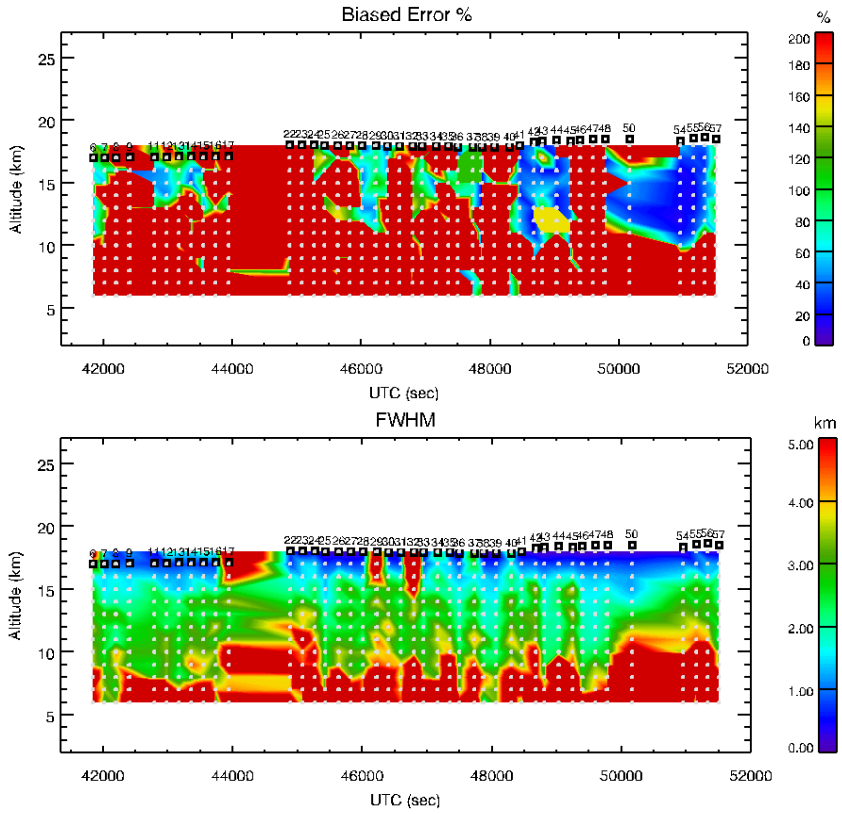

Fig. 34: Top panel: External continuum relative biased error plotted versus the UTC and altitude. Bottom panel: FWHM of external continuum AK for Flight 1 plotted versus the UTC and altitude.

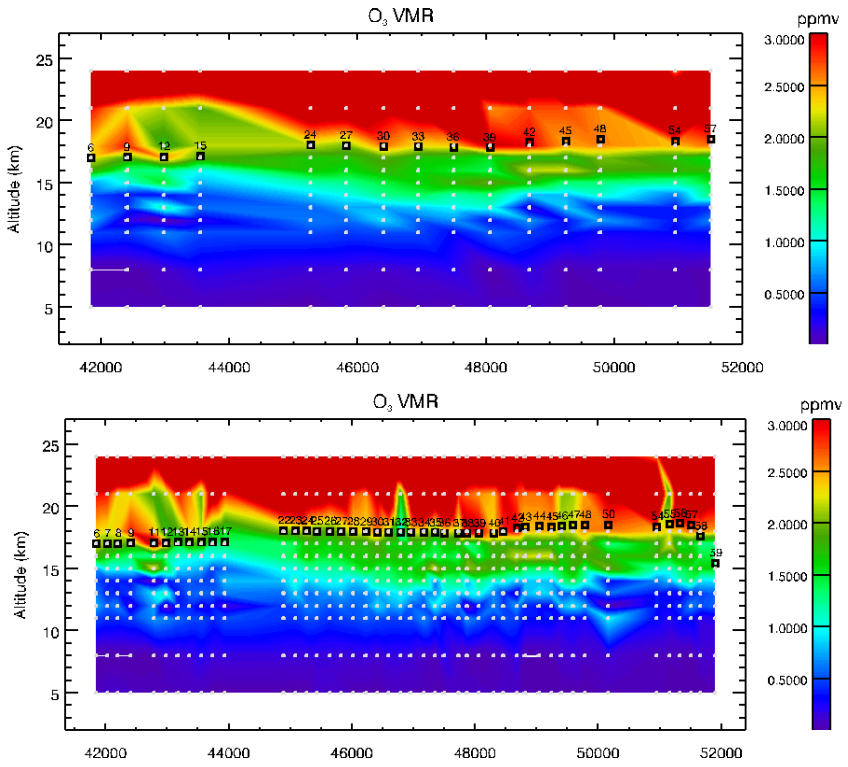

Fig. 35: Top panel: O_3 profiles retrieved using recursive retrieval strategy in band C. Bottom panel: O_3 profiles retrieved using recursive retrieval strategy in all bands.

(in band B) that has been removed from the HNO_3 retrieval since scan 21 was not good and we can not use these results for the recursive retrievals (band B alone does not provide enough information for HNO_3 retrieval).

The final results for O_3 is shown in Fig. 35, where the top panel show the map obtained using just the band C profiles and in the bottom panel the results for the full flight. The final results for HNO_3 is shown in Fig. 36, where the top panel show the map obtained using just the band B profiles and in the bottom panel the results for the full flight. In both case of O_3 and HNO_3 recursive retrievals it is clearly visible the structure already identified in the analysis, lower O_3 and HNO_3 values at about 15 km are found in the first part of the flight. Moreover, looking at the HNO_3 results in the second part of the flight we can notice a maximum in its VMR at about 16 km.

4.3 Conclusions

During Flight 1 the level 1 team discovered a constant offset of +0.5 deg between the commanded and the actual pointing angles and a periodic roll-angle oscillation in flight sections that were following a constant longitude pattern. For this reason for Flight 1 the vertical coverage of the measurements is not the nominal one but it is reduced and unevenly distributed.

The L1 spectra contain some bad channels that were not masked by the level 1 team, so we had to look at each single spectrum and flag the bad channel when their values compared to simulations and noise level were not realistic, excluding them from the analysis. Some spectra showed evidence of wrong pointing assignation and were therefore discarded from the analysis.

Following the indications of the level 1 team the noise level used in the analysis was set to the one contained in the L1 without adding any other contribution.

For the analysis we used the same retrieval strategy used in Flight 2, and after some tests, we decided to change the a priori errors and set the threshold for the 1-sigma variability for all the targets but temperature at 200%.

The results of the analysis for the first flight show that:

- *Temperature*
  Can be retrieved only from Band C and has low information content.

- *H_2O*
  Water can be retrieved from band C and in general has quite good information content.

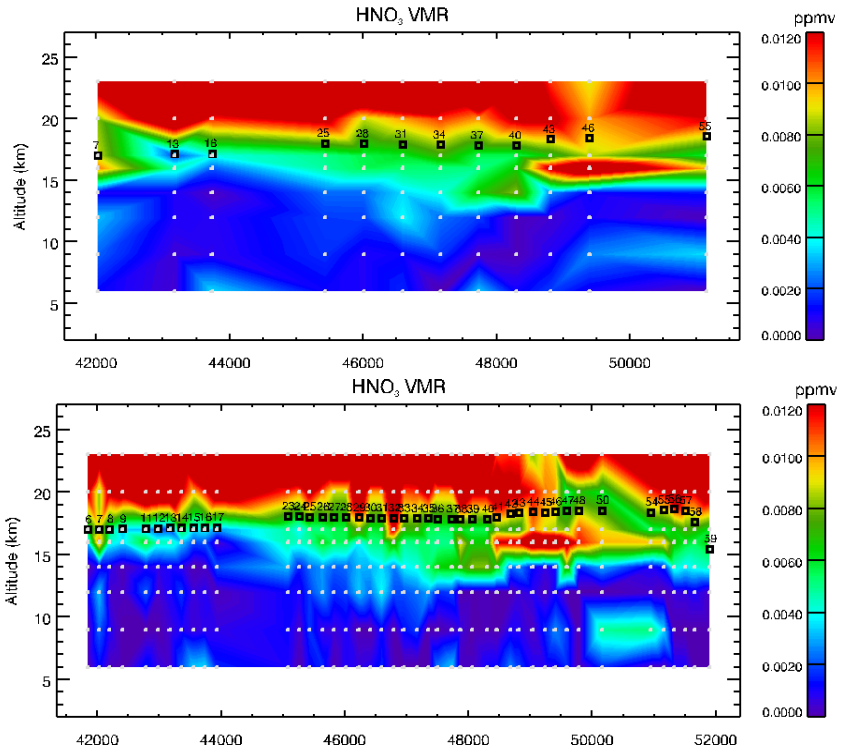

Fig. 36: Top panel: HNO_3 profiles retrieved using recursive retrieval strategy in band B. Bottom panel: HNO_3 profiles retrieved using recursive retrieval strategy in all bands.

- *O_3*
  Ozone can be retrieved from all bands. O_3 Show lower values at 15 km at the beginning of the flight.
- *HNO_3*
  Nitric acid is retrieved from bands C and D. Lower HNO_3 at 15 km are found at the beginning of the flight and higher values are found at the end. At the end of the flight we also noticed a minimum at 17 km with higher HNO_3 values above and below this altitude.
- *N_2O*
  $N_2O$is retrieved from band B. In general we found some oscillations in the profiles (more than in Flight 2 data analysis). Very strong oscillations are present in those scan with low individual information content value (reduced measurement coverage in the vertical range).
- *CO*
  co is retrieved from band D. As in Premier-ex data analysis, and in Flight 2 data analysis we obtain low CO values below flight altitude.
- *External continuum*
  External continuum can be retrieved from all bands. The external continuum has low information content below 15-14 km, and show no evidence of opaque clouds during the flight.

5 Analysis of MARSCHALS Flight 2 measurements

In this section, we report the results of the analysis carried out on the MARSCHALS L1 data acquired during the Flight 2 on 16.12.2011.

5.1 Geophysical Scenario

5.1.1 Flight overview

The flight track of MARSCHALS ESSenCe Flight 2 is shown in the top panel of Figure 37 while the bottom panel reports the altitude of the M-55 during the flight plotted with respect to the flight time (UTC). As we can see in

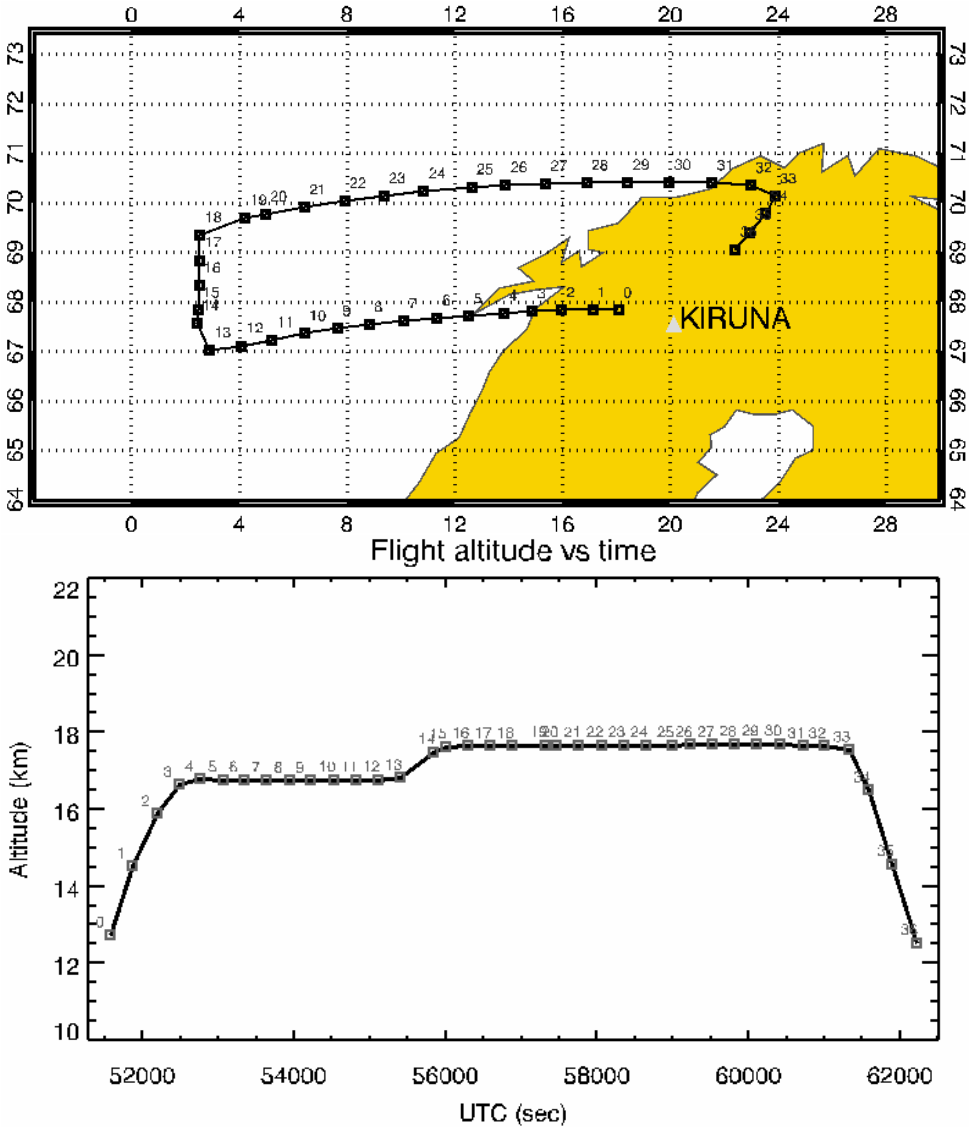

Fig. 37: Upper panel: The Flight 2 track plotted versus latitude and longitude. The black dots show the average position of each scan. Bottom panel: The GPS flight altitude and the analysed scans position plotted versus the Universal Time Coordinate (UTC)

Fig. 37 the M-55 followed a rectangular flight pattern. The portion of atmosphere sampled during the flight is highlighted in the three panels of Figure 38 that show the position of the tangent points of the scans of band B (top panel), C (central panel) and D (bottom panel) respectively during the flight.

In the "MARSCHALS Compact Data Acquisition Report" the Level 1 team reports that in Flight 2 they modified the commanded pointing angles, in order to cope with the unexpected features in the UCSE roll-angle record (Constant +0.5 degree offset when aircraft is supposed to be at i level attitude and an additional +/-1 deg sinusoidal offset in parts of the flight) that was experienced during Flight 1. Unfortunately during Flight 2 the +0.5 deg offset in the UCSE roll-angle was not present. In Fig. 38 we report the tangent point position with respect to altitude extracted from the L1B files and calculated using the baromatric aircraft altitude together with the instrument location. Even if the GPS and the barometric altitudes differ we can use these plots to evaluate the variation of the vertical coverage of the measurements during the flight. As shown in the three panels of figures 38 the altitude coverage of MARSCHALS scan was reduced due to the +0.5 deg. offset and many of the views are above horizontal so that the nominal altitude coverage is not always reached. So scans 4, 13 and 19 of Band B, scan 14 of Band D and scan 33 of Band C, may not be good for the analysis because of the reduced altitude coverage and or because acquired during changes of direction of the aircraft.

The bottom panel of Figure 37 shows that there are many parts of the flight (from scans 3 to 13 and from 14 to 33) where the aircraft altitude was nearly constant, we therefore expect to have the best data for the analysis of these scans.

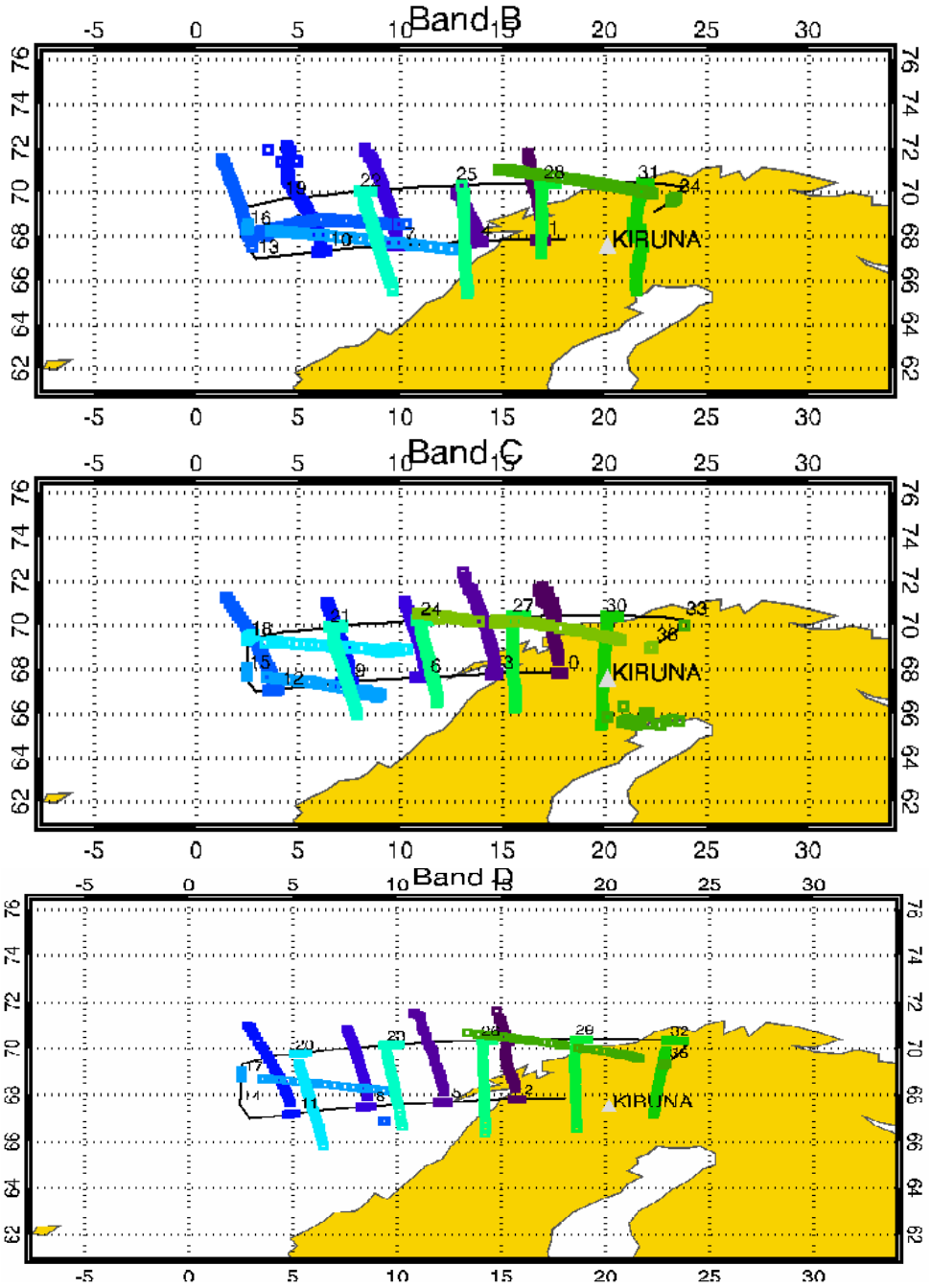

Fig. 38: The flight track with the Geo-location of Band B (top) Band C (middle) and Band D (bottom) tangent points plotted versus latitude and longitude. Different colours are used to identify each scan.

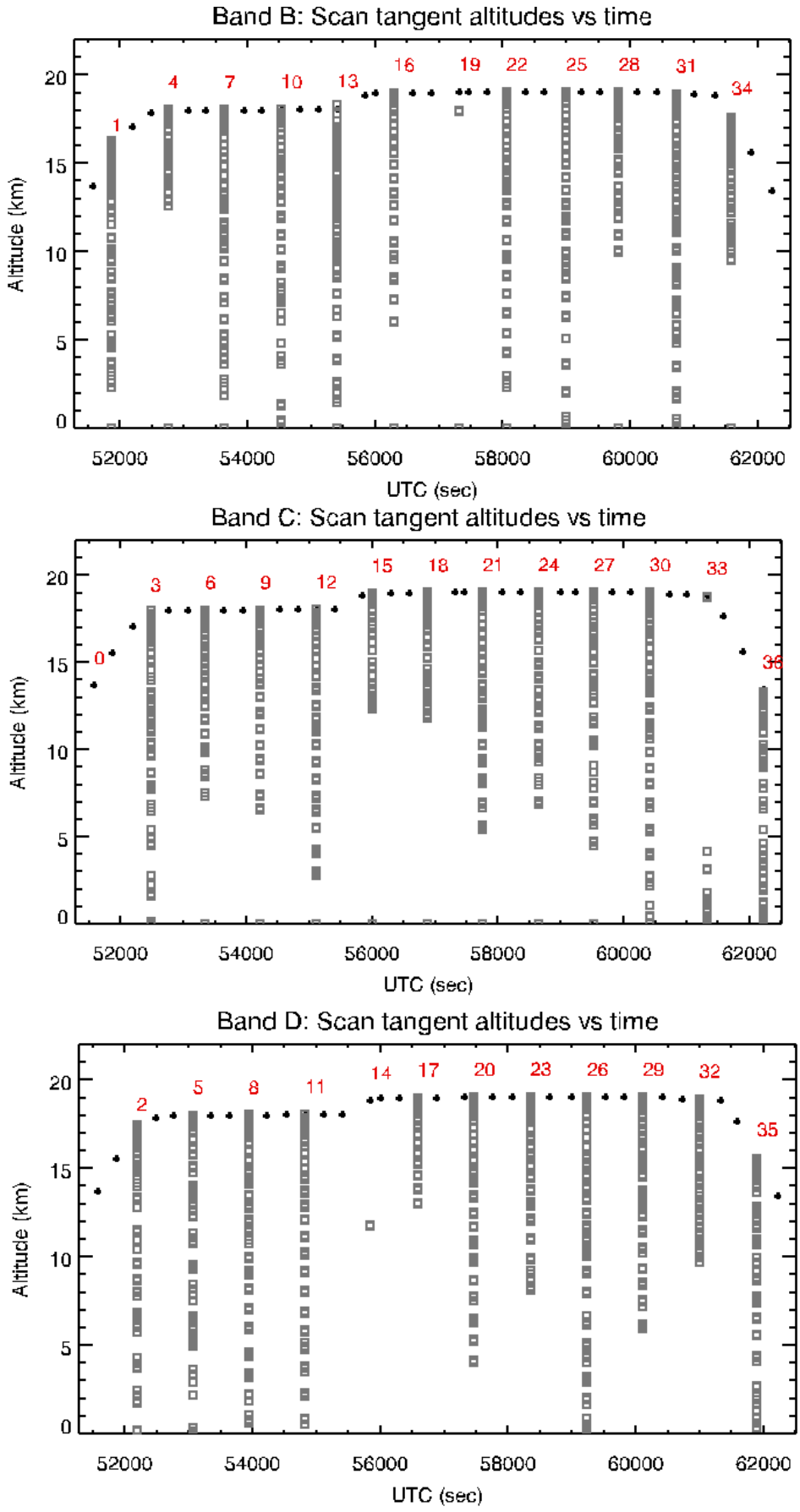

Fig. 39: The flight altitude and the analysed scans tangent altitudes position plotted versus the UTC. Top panel: band B, central panel: band C, bottom panel: band D.

5.1.2 Initial Guess Atmosphere: Scan dependent ECMWF profiles

As reported in Sec. 3.2 ECMWF data have been extracted on a personalised latitude and longitude grid that for the flight of the 16^{th} December 2011 was:

- Latitude grid from 64 deg to 74 deg with a step of 1.125 deg
- Longitude grid from 0 deg to 30 deg with a step of 1.125 deg

Since the flight was performed approximately from 14:00 to 17:00 UTC, we retrieved the ECMWF datasets at two times: 12:00 UTC and 18:00 UTC. As described in Sec. 4.1.2 the ECMWF data have been interpolated to the average latitude, longitude and time of MARSCHALS instrument during the flight. The profiles have been extrapolated up to 120 km using the same strategy adopted in the SCOUT O3 and Premier-Ex analysis, that is using the shape of the IG2 profiles.

5.2 Analysis

5.2.1 Analysed dataset and preliminary analysis

A preliminary analysis has been performed on all the scans present in the L1B files, without any screening, even if, as already said in section 5.1 and as can be seen in Fig. 39, we can expect the best performances for the scans from 6 to 33.

The same retrieval strategy used for PREMIER-EX Flights (and then applied also to the preliminary analysis of Flight 1) was used for the preliminary analysis of Flight 2:

- Band C: T, H_2O, O_3, HNO_3, Pointing, gain, Offset, Continuum, Frequency Shift
- Band B: H_2O, O_3, HNO_3, N_2O, Pointing, gain, Offset, Continuum, Frequency Shift (T from Band C previous scan, H_2O initial guess and error from band C)
- Band D: H_2O, O_3, HNO_3, CO, Pointing, gain, Offset, Continuum, Frequency Shift (T from Band C previous scan, H_2O initial guess and error from band C)
- Top of the atmosphere at about 65 km
- Observations used down to 0-1 km
- Use of Target dependent vertical retrieval grid
- Use of Optimal Estimation+Marquardt
- No hydrostatic equilibrium used during the retrieval
- Retrieval stops after 7 Gauss-Newton iterations
- a priori errors:
- 3 K for T ,1-sigma variability or 100% (if the 1-sigma variability is lower than this threshold) for O_3 and H_2O, 1-sigma variability or 50% (if 1-sigma variability is lower)for HNO_3, CO, N_2O

In the preliminary analysis we use observation down to 1 km in order to perform a first retrieval without excluding any observations above 0 km. As described above, during the analysis we stop the retrieval procedure after 7 Gauss-Newton iterations. Loooking at the results obtained in the analisys of Flight 1 and 2, usually the retrieval reaches convergence after 3-4 iterations; thus in general the threshold of 7 Gauss-Newton iterations can be considered a good stopping criterion. In few cases the retrieval stops at the 7^{th} iteration without having fullfilled the convergency criteria. For these scans we relaxed the threshold and the retrievals converged at the 8^{th} iteration with values of the χ-test very close to the ones obtained previously. During the analysis of PREMIER-EX and ESSENcE Flights we used the spectral database specifically developed for the MASTER study [27].

As reported in section 3, for all the bands some of the spectral channels were not working properly. Some of them have been already identified by the level 1 team, and had been removed from the preliminary analysis. However we found out that there were additional bad channels not identified in the level 1 data. The procedure described in sect. 3.1 was used to mask the unmasked 'bad channels', therefore reducing the number of used spectral points for each scan. The preliminary analysis used to identify the bad channels also showed that, probably due to the pointing problems that were reported by the RAL team, some spectra were affected by an error in the

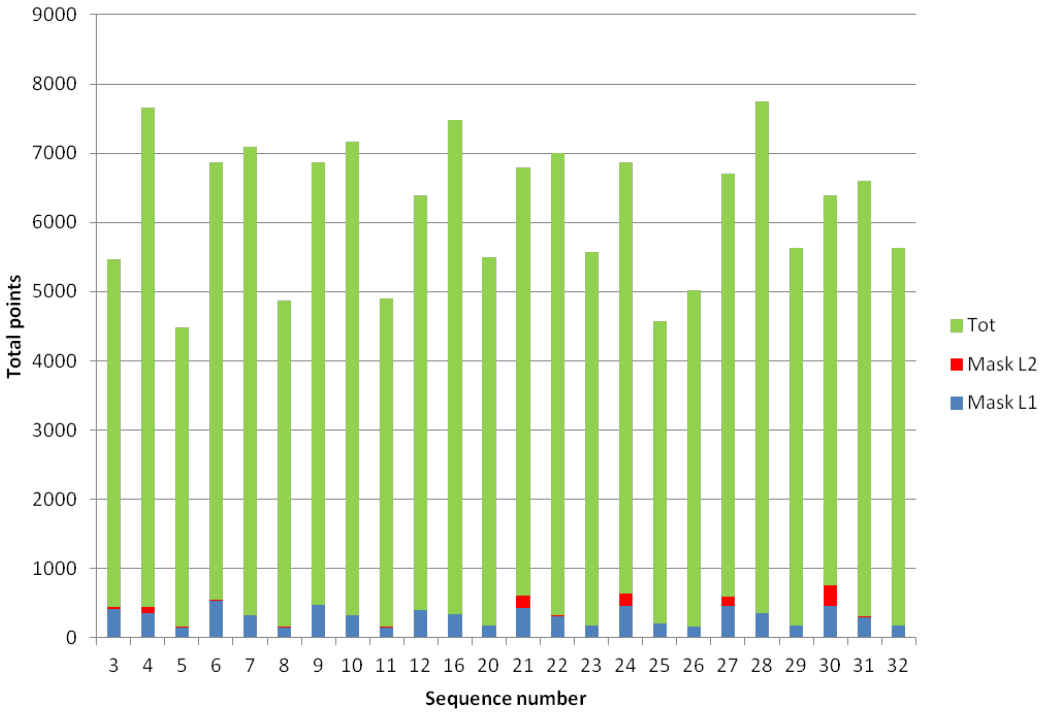

Fig. 40: Bar plot of the total number of spectral points (green), number of spectral points masked by the level 1 team (blue) and number of spectral points masked after the preliminary level 2 analysis (red)

assigned pointing (and thus their tangent altitude was wrong). These spectra were then removed from the analysis. The preliminary analysis have also been used to select the lower tangent altitude of the spectra to be included in the analysis, value that was set at 4 km.

Figure 40 reports the total number of spectral points of all the used spectra of each scan, with superimposed in blue the number of spectral points masked by the level 1 team and in red the number of spectral points masked after the preliminary level 2 analysis. The green bars represent the number of spectral points really used in the analysis.

5.2.2 Tuning the a priori errors

The strength of the constraint imposed to the retrieval results has been tuned through the tuning of the threshold value imposed to the a priori errors used in the analysis (see section 3.2). Test retrievals have been run using the following options:

- 3-K for T, threshold for the 1-sigma variability 100% for $O_3$and H_2O, threshold for the 1-sigma variability 50% for HNO_3, CO, N_2O
- 3-K for T, threshold for the 1-sigma variability 100% for O_3, H_2O, HNO_3, CO, N_2O
- 3-K for T, threshold for the 1-sigma variability 200% for O_3, H_2O, HNO_3, CO, N_2O

In Fig. 41 we report in blue the results obtained using the 50% threshold, and in red the results obtained with the 100% threshold for HNO_3 (scan 6), N_2O (scan 7) and CO (scan 8). If we compare the results obtained when the threshold for the 1-sigma variability is moved from 50% to 100% we can see negligible variations in the retrievd values.

In Fig. 42, the threshold is moved from 100% to 200% for H_2O, O_3, HNO_3(scan 6), N_2O(scan 7), and CO (scan 8). Also in this case the use of a larger constraint has almost no effects on the retrieved profiles. This means that the 100% threshold was not imposing a very strong constraint to the retrieval but also that the 200% threshold can be safely used without introducing too many oscillations in the retrieved profiles. For this reason, in order to have a more conservative approach we prefer to use 200% as threshold for the 1-sigma variability.

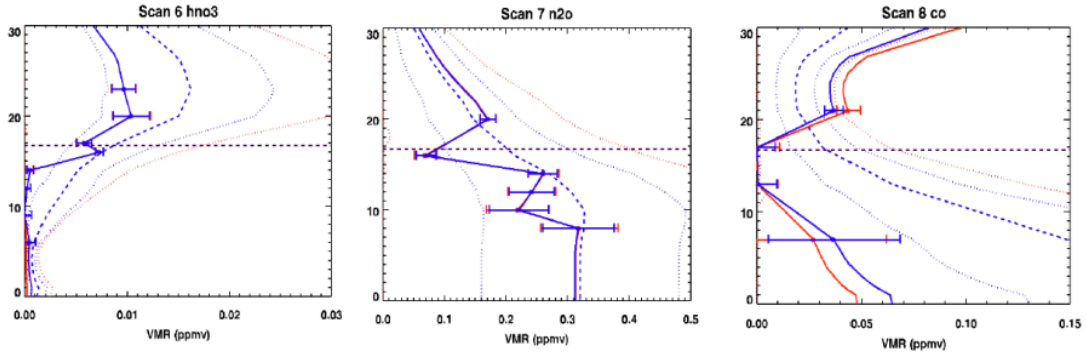

Fig. 41: Left: HNO_3 for scan 6 retrieved with 50% threshold (blue) or 100% threshold (red). Middle: N_2O for scan 7 retrieved with 50% threshold (blue) or 100% threshold (red). Right: CO for scan 8 retrieved with 50% threshold (blue) or 100% threshold (red) on 1-sigma variability

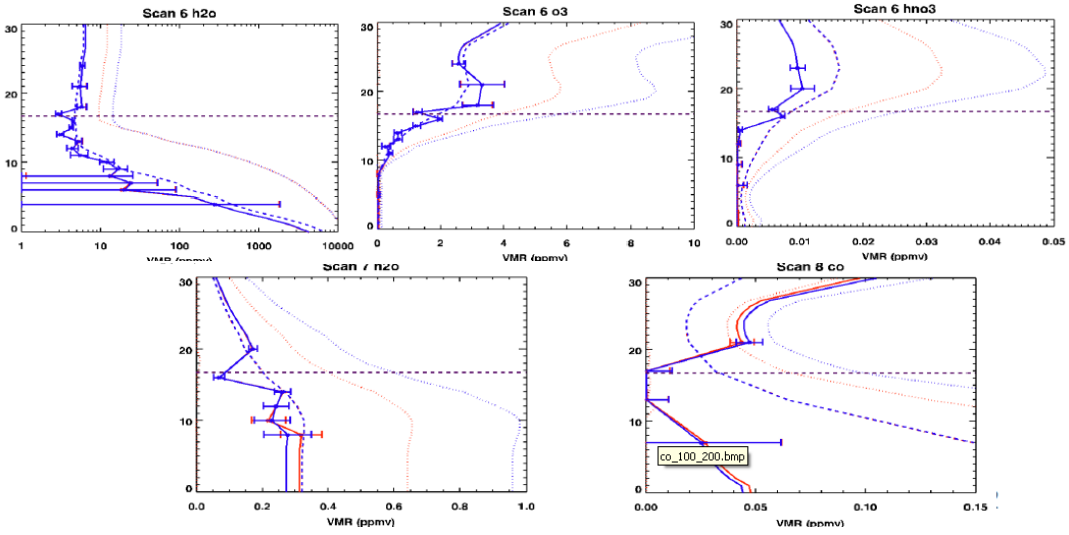

Fig. 42: Top panels: Left: H_2O Central O_3 and right HNO_3 for scan 6 retrieved with 100% threshold (red) or 200% threshold (blue). Bottom panels: Left: N_2O for scan 7 retrieved with 100% threshold (red) or 200% threshold (blue). Right: CO for scan 8 retrieved with 100% threshold (red) or 200% threshold (blue)

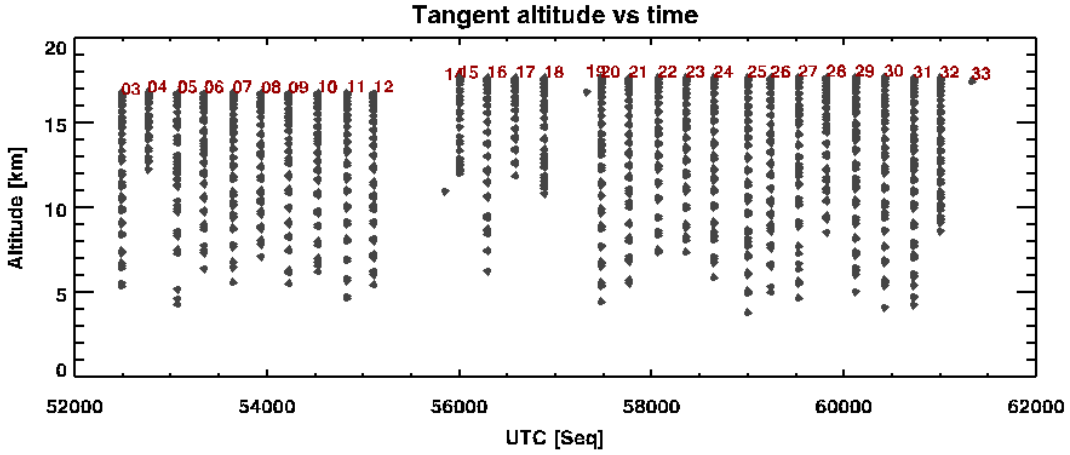

Fig. 43: Tangent altitudes calculated by MARC using the GPS aircraft altitude for each scan versus the UTC.

5.2.3 Tuning the vertical retrieval grid

Since the ESSenCe campaign was run at polar latitudes as for the scientific flight of the PREMIER-EX campaign, the preliminary analysis was run using the same target dependent retrieval grids of the Premier-Ex analyses. Since the vertical coverage of this flight was not homogeneous, as shown in Fig 43, where are reported the tangent altitudes calculated by MARC for each scan with observations down to 4 km, we have performed further tests to tune the vertical retrieval grid.

As already said we use measurements with tangent altitudes down to 4 km and for this reason the lowest point of the retrieval grids was set at 5 km. However, in the part of the flight from scan 15 to scan 20 the altitude coverage of the measurements was limited to 11-10 km. For this reason we tried to use a different approach for these scans. As first approach we tried to use retrieval grids down to 10 km for these scans. However this strategy did not produce good results. Then we run our retrievals using an priori error on H_2O set at 20% below 11 km and keep the same retrieval grid for used for all the flight. Also in this case the strategy did not produce significant improvements: in all the cases the results for scan 15 to 20 are not very good and we decided to remove those scans from the final analysis.

Different considerations can be done for scan 16 in band B that has a better altitude coverage with respect to the other scans in the range scan 15 to scan 20. Since temperature and H_2O retrieved from scan 15 are not good, the analysis of scan 16 is performed using temperature and water from ECMWF (temperature not retrieved, H_2O retrieved during the analysis).

5.2.4 CO retrievals

As in the analysis of Premier-Ex scientific flight, the retrieved values for CO for the Flight 2 are low below the flight altitude. In order to try to clarify this point we performed several tests on CO retrievals.

As starting point we evaluate the possible influence of interfering species on CO retrievals. In Fig. 44 we show a measured spectrum for scan 11 together with the initial (in green) and final (in cyan) synthetic spectra calculated by MARC. In the figure are also plotted the position of the CO line (in red) and of the HNO_3 (in yellow). Since the initial guess synthetic spectrum is produced with too much HNO_3 with respect to the final one we reduce the HNO_3 initial guess profile of a factor 100. An example of the results of this test for scan 8 is shown in the left panel of Fig. 45. As can be noticed reducing the HNO_3 initial guess profiles of a factor 100 (in red) did not produce any difference with respect to the standard profile (in blue). In the right panel of the same figure are reported the HNO_3 retrieved profiles for scan 6 using the two different a priori. As can be noticed we obtain the same HNO_3 profile starting from two very different a priori. This means that the retrieved profiles is produced by measurements more than by the a priori.

The second test that was performed on CO was to retrieve CO in sequence: For each scan in band D we first retrieved all the targets but CO. Then in a second step we retrieved CO from the same scan in band D using the profiles obtained in the first step for the other targets. All the instrumental parameters and the continuum are retrieved together with CO in this second step. An example of the results obtained with this strategy for scans 5, 8, 11 are reported in Fig. 46. The difference between CO profiles retrieved in sequence (in blue) with respect to the standard analysis (in red) are very small with slightly higher values at lower most retrieval altitude for the CO profiles retrieved in sequence.

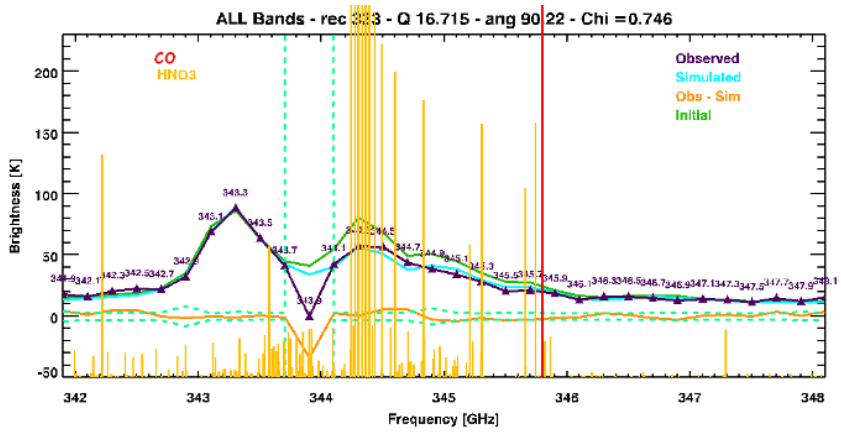

Fig. 44: Spectrum for record 333 in scan 11 together with the initial (in green) and final (in cyan) synthetic spectra calculated by MARC. In the figure are also plotted the position of the CO line (in red) and of the HNO_3 (in yellow).

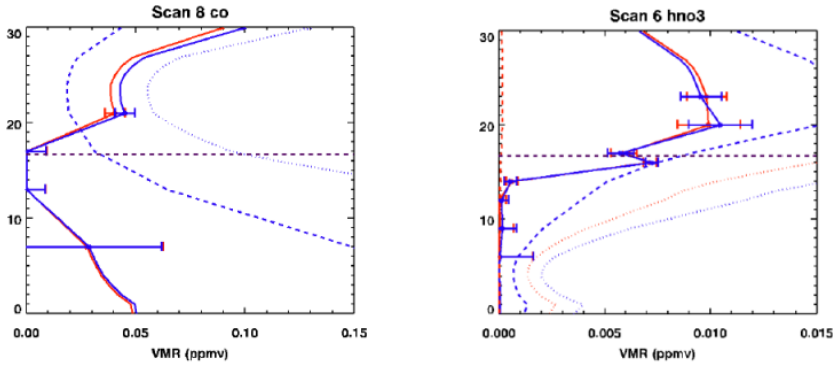

Fig. 45: Left panel: retrieved CO profile for scan 8 with HNO_3 initial guess profiles reduced by a factor 100 (in red) wrt the standard analysis (in blue). Right panel: retrieved HNO_3 profile for scan 6 with HNO_3 initial guess profiles reduced by a factor 100 (in red) wrt the standard analysis (in blue).

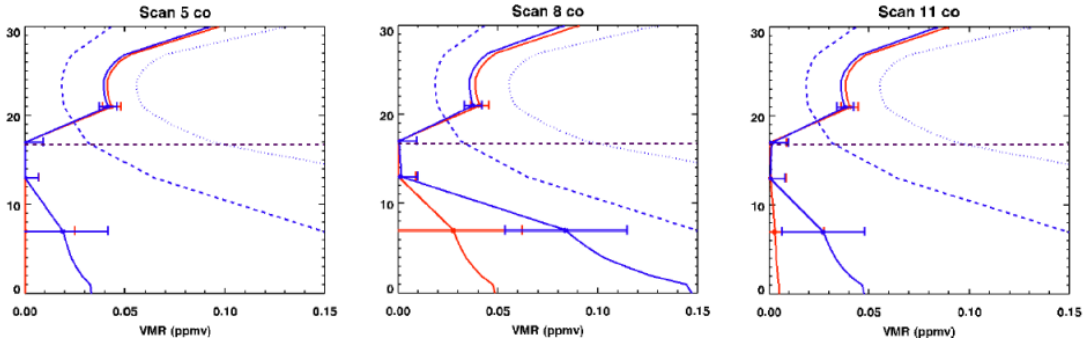

Fig. 46: Left panel: retrieved CO profile for scan 5 in standard mode (in red) or in sequence (in blue). Middle panel: CO from scan 8. Right panel: CO from scan 11.

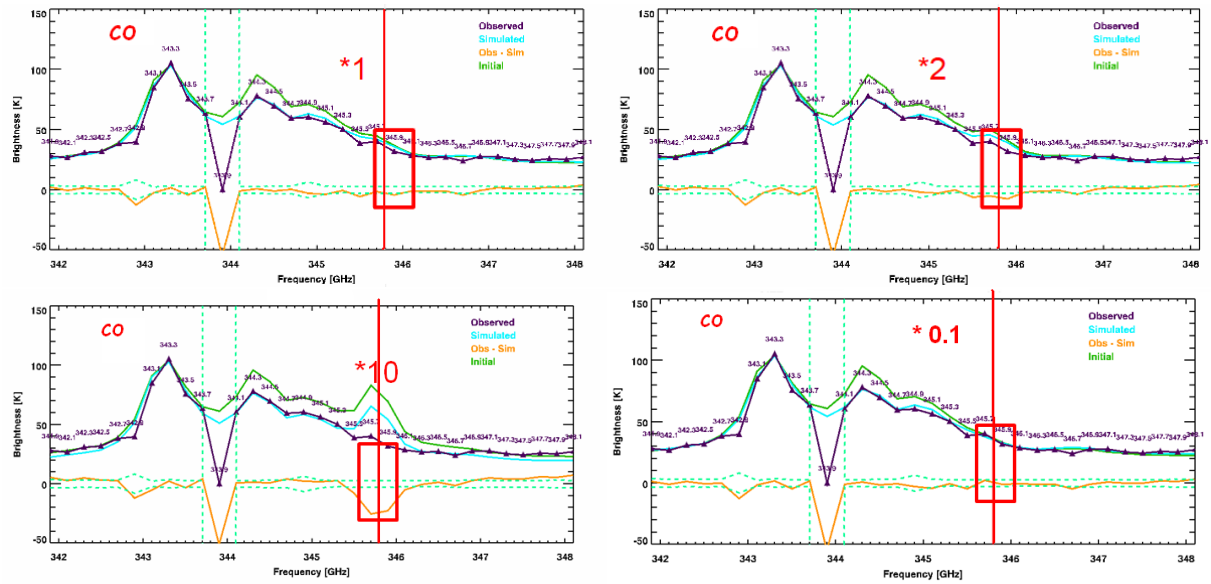

Fig. 47: Top left panel: Measured and synthetic spectra produced with standard initial guess CO profile. Top right panel: Measured and synthetic spectra produced with standard CO profile multiplied by a factor 2. Bottom left panel: Measured and synthetic spectra produced with standard CO profile multiplied by a factor 10. Bottom right panel: Measured and synthetic spectra produced with standard CO profile multiplied by a factor 0.1.

The last test that we performed on CO retrieval aimed at evaluating the sensitivity of MARSCHALS spectra to CO concentrations. We retrieve the values of all the targets but CO from band D spectra using 4 different CO profiles:

- standard CO profile from IG2 database.
- CO profile from IG2 database multiplied by a factor 2.
- CO profile from IG2 database multiplied by a factor 10.
- CO profile from IG2 database multiplied by a factor 0.1.

In Fig. 47 are reported synthetic spectra produced during the retrieval with the four different CO profiles. Since the CO is not retrieved the residual (in orange) between the simulated and the measured spectrum in the spectral region near the CO line (marked in red) reflects the sensitivity of the spectra to the amount of CO in the synthetic profiles. When we use the CO profile from the IG2 database the residual in that region is of the order of the noise (very near to the limit of the noise level, see top left panel of Fig. 47). When the CO profile is multiplied by a factor 2 the residual is above the noise level (top right panel of Fig. 47), When the CO profile is multiplied by a factor 10 the residual clearly indicates the large CO amount. As final test we multiplied the CO amount by a factor 0.1. In this case the residual is well below the noise level and very close to 0, closer to 0 than in the case of the CO profile taken from the IG2 database, indicating that we are probably in presence of a very low CO concentration that is probably not detectable (the low CO profile actually fits better the measured spectrum than the IG2 profile). These tests show that when the CO amount is significantly high MARSCHALS should be able to detect it. Further investigations are needed to understand the behaviour of the CO retrieval from MARSCHALS measurements.

5.3 Final Analysis

5.3.1 Retrieval Features

The retrieval features used in the final analysis of the Flight 2 are summarised here below:

Retrieval strategy:

Scalar quantities: Pointing bias, gain, Offset, Frequency Shift are retrieved for all bands.

Vertical profiles of:

- Band C: T, H_2O, O_3, HNO_3, External Continuum

- Band B: H_2O, O_3, HNO_3, N_2O, External Continuum, (T from Band C, H_2O initial guess and error from band C)
- Band D: H_2O, O_3, HNO_3, CO, External Continuum, (T from Band C, H_2O initial guess and error from band C)

Observations used down to 4km.
Used vertical retrieval grids:

- Temperature 24,20,18,17,15,13,11,9,7,5
- H_2O 24,21,18,17,16,15,14,13,12,11,10,9,8,7,6,5
- O_3 24,21,18,17,16,15,14,13,12,11,8,5
- HNO_3 23,20,17,16,14,12,9,6
- N_2O 20,16,14,12,10,8
- CO 21,17,13,7
- External Continuum 18,17,16,15,14,13,12,11,10,9,8,7,6

a priori profiles: T, H_2O, O_3 from ECMWF archive (from 0 to approximately 72-78 km). Others from IG2 Polar winter atmosphere

a priori errors: 3K for T, 1-sigma variability or 200% (if 1-sigma variability is lower) for O_3 and H_2O, HNO_3, CO, and N_2O

5.3.2 Results

The results of the final analysis are reported in this section. Fig. 48 shows the values of the χ-test as a function of the measurement time UTC (Band B in blue, Band C in black, Band D in red). In general the χ-test values are always above 1 (highlighting that the noise level is not overestimated) and below 2. The χ-test distribution during the flight was fairly homogenous indicating the good quality of the measurements.

The values of the trace of the Averaging Kernel matrix and of the information content for each scan are reported in Fig. 49. The value of the trace and the information content is almost constant over the flight, apart from scan 4 of band B where the AK trace is lower, due to the reduced altitude range covered by this scan. The higher values obtained for both quantifiers in band C reflects the larger number of variables retrieved from these scans.

The scalar quantities, namely the Frequency shift (in MHz), the Pointing bias (in deg), the offset (in K) and the gain are shown in the top panels of Figs. 50, 51, 52, 53. In the bottom panels of the same figures we have reported the values obtained during the analysis of the Scientific Flight of the Premier-EX campaign (10 March 2010). The values of the frequency shift is on average 9.34 MHz in band B, 13.7 MHz in band C and 14.63 MHz in band D and their values are constant over the flight in each band. Compared to the values obtained in the Scientific Flight, we see that while band B shift assumes the same values, for band C and D the values are higher. However the retrieved frequency shifts are always well below the spectral resolution of the instrument. The retrieved pointing bias is very close to 0.0 in almost all the flight (apart for some deviations for scan 7, 16, 20 and 23) highlighting that the pointing angle assignation performed by the level 1 team to the pointing angle was, in general, correct. Actually the retrieved pointing bias is more homogeneous than in the Scientific Flight, suggesting an improvement in the a-posteriori knowledge of the pointing. The retrieved values for the offset are similar in bands C and D, with average value of -1 K, while the offset of band B (constant through the flight) is around 2-3 K. In the Scientific Flight the values were similar for all bands. Again the band C and D offsets have similar values in both flights, while band B has constantly higher values in Flight 2 of the EssenCe campaign. The gain values are stable during the flight in band C with values close to 1 and the same applies to band B but with lower values. In band D the gain is more unstable expecially for scans 20 and 23 that possibly have some problems. Again we notice the different behaviour of band B in the Scientific Flight. The differences found in the band B scalar values may be due to the reduced standing wave pattern caused by the cold load upgrade performed for the EssenCe campaign.

The retrieved values for Temperature (from band C), H_2O (from band C), O_3 (from all bands), HNO_3 (from band C and D), N_2O (from band B), and CO (from band D) are reported in figures 54 to 71, mapped as a function of altitude and UTC. White points on the maps show the position of the vertical retrieval grid while the black squares show the flight altitude for each scan. For each target we plot the values of the retrieved quantities, of the biased error, of the individual information content , of the a priori profiles of the a priori profiles, of the relative biased error and of the vertical resolution computed as the FWHM of the AK matrix. The biased error is the retrieval

In general the scalar quantities are quite similar to the ones obtained for the Flight 1 (see Fig. 10, 11, 12, 13), as expected.

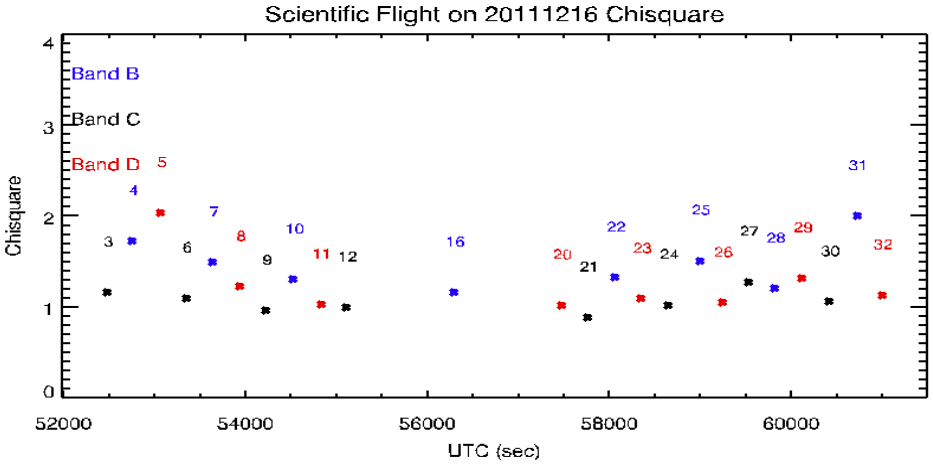

Fig. 48: Chi square for Flight 2 plotted versus the UTC (Band B in blue, Band C in black, Band D in red).

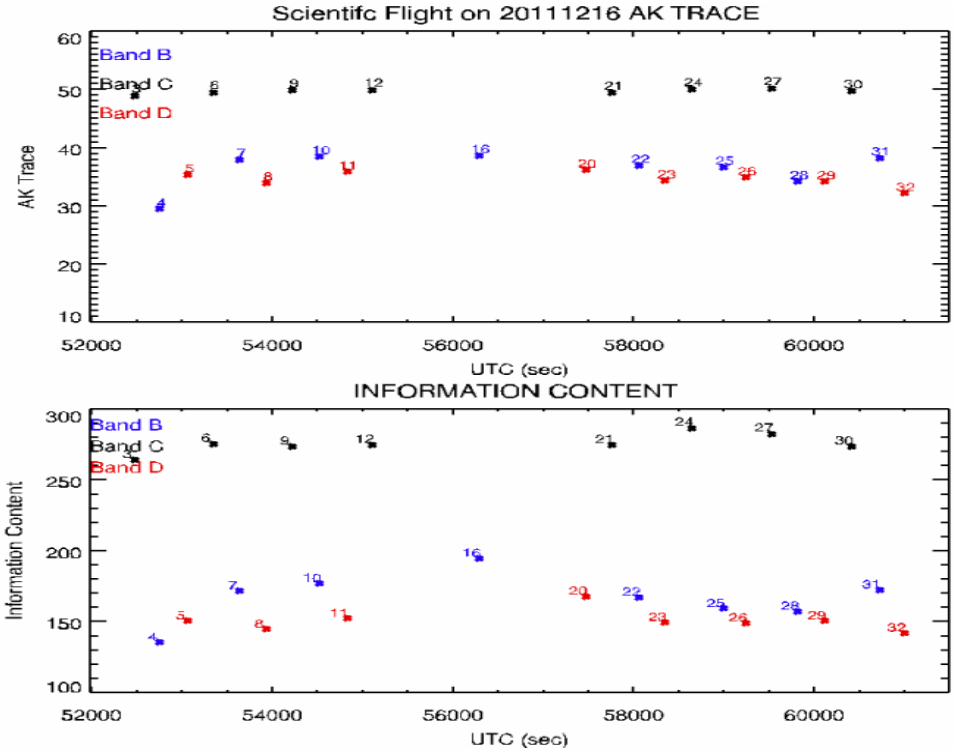

Fig. 49: Top panel: Trace of the AK matrix for Flight 2 plotted versus the UTC. Bottom panel: Information content for each scan versus the UTC (Band B in blue, Band C in black, Band D in red).

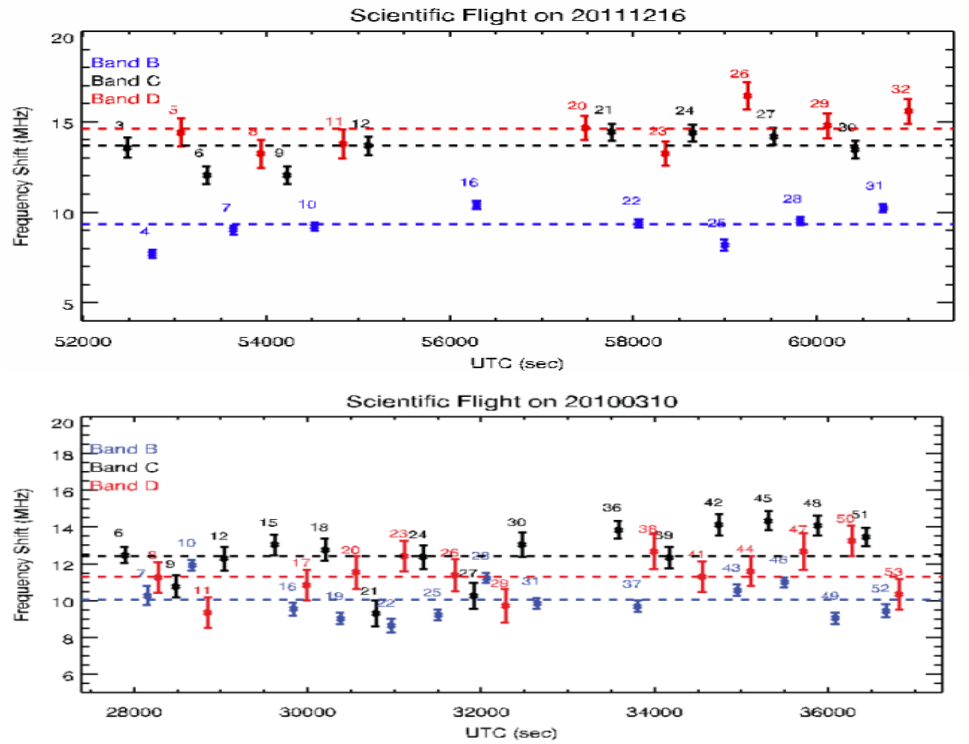

Fig. 50: Top panel: Frequency shift in MHz for Flight 2 plotted versus the UTC.(Band B in blue, Band C in black, Band D in red). Bottom panel: Frequency shift in MHz for the Premier-Ex scientific flight

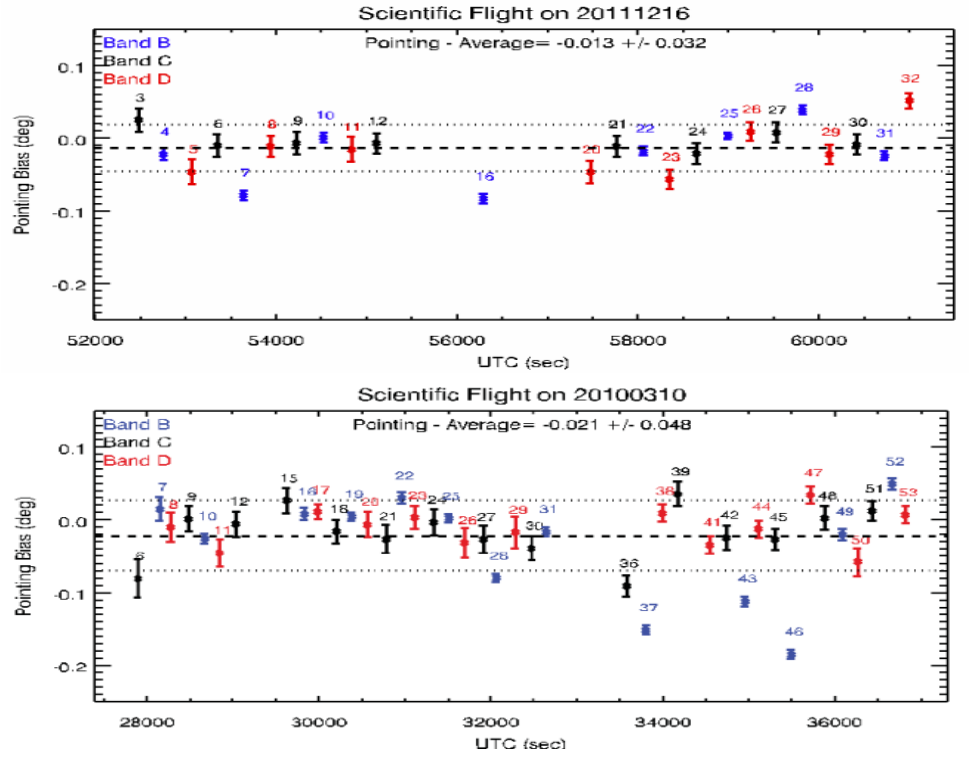

Fig. 51: Top panel: Pointing Bias in deg for Flight 2 plotted versus the UTC.(Band B in blue, Band C in black, Band D in red). Bottom panel: Pointing bias for the Premier-Ex scientific flight.

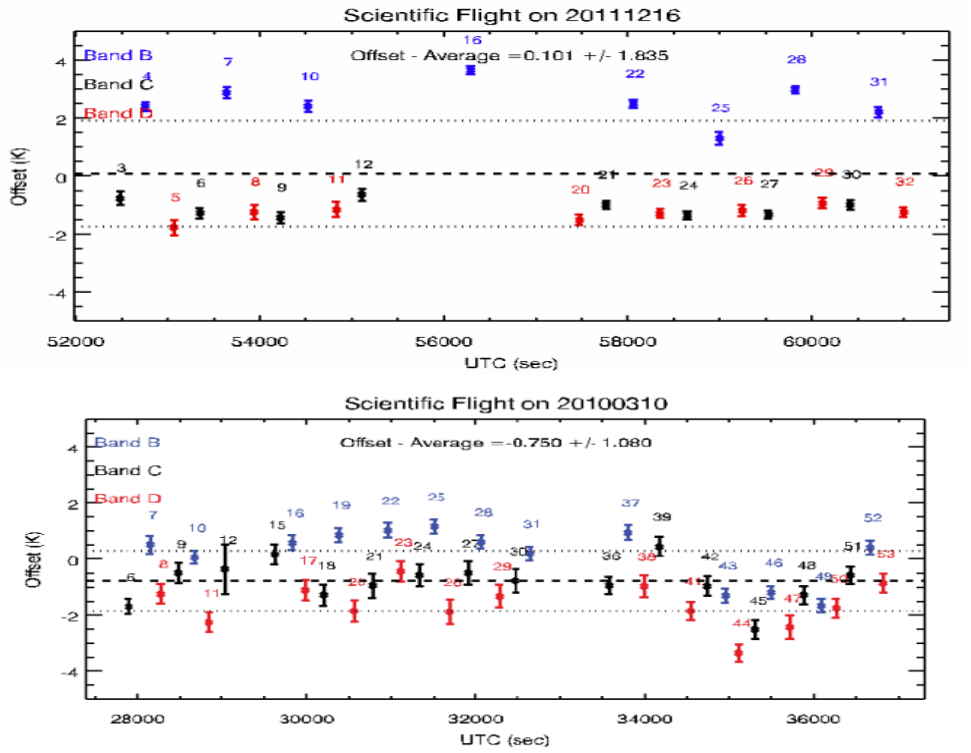

Fig. 52: Top panel: Offset in K for Flight 2 plotted versus the UTC.(Band B in blue, Band C in black, Band D in red). Bottom panel: Offset in K for the Premier-Ex scientific flight.

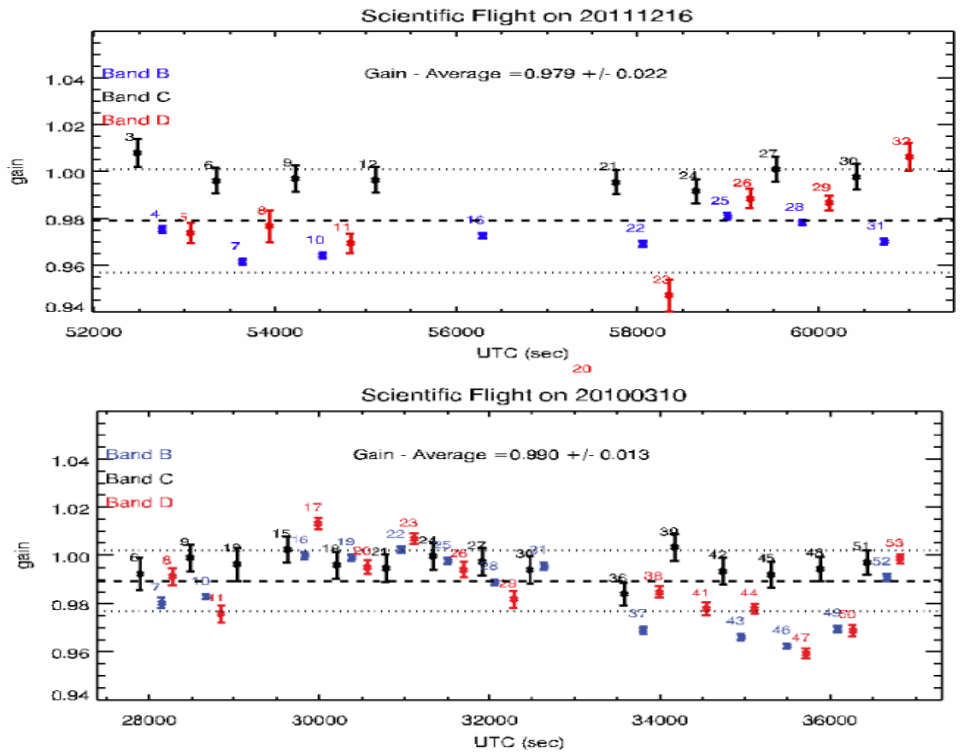

Fig. 53: Top panel: Gain for Flight 2 plotted versus the UTC.(Band B in blue, Band C in black, Band D in red). Bottom panel: Gain for the Premier-Ex scientific flight.

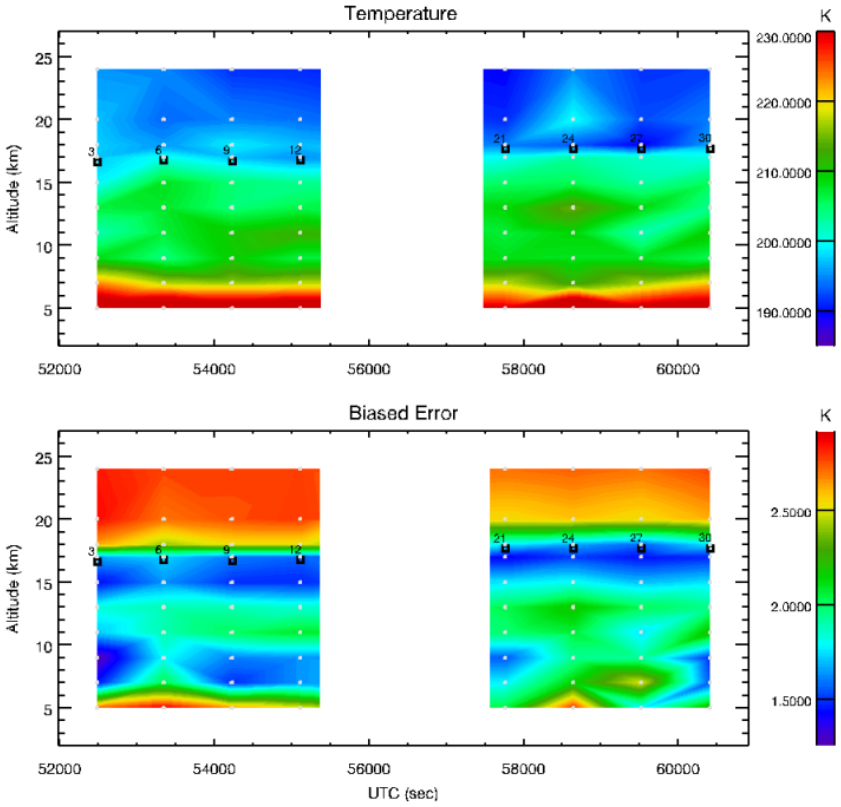

Fig. 54: Top panel: Temperature from band C for Flight 2 plotted versus the UTC and altitude. Bottom panel: Biased error from band C for Flight 2 plotted versus the UTC and altitude.

error, that is the square root of the diagonal elements of the variance-covariance matrix of the retrieval (that is the combination of the error due to the measurement noise with the a-priori error). Definition of the individual information content can be found in [9].The FWHM was calculated using the same definition used in [53] in order to penalize the negative lobes of the averaging kernel.

Maps for temperature are reported in Fig. 54 (retrieved values and biased errors), in Fig. 55 (individual information content and a priori profile) and in Fig. 56 (relative biased error and FWHM of AK). The information content for temperature is very low (it assumes values always below 1) for the whole flight and the retrieved temperature profiles are very close to the a priori ones. We can notice that the temperature profiles are constant during the whole flight. The vertical resolution of the T retrieval (shown in fig. 56) changes in the two parts of the flight; in the second part, where the aircraft was flying at higher altitudes, the vertical resolution above 17 km improves.

Similar maps for H_2O from band C are reported in Fig.s 57 (retrieved values and bias error), in Fig. 58 (individual information content and a priori profile) and in Fig. 59 (relative biased error and FWHM of AK). Retrieved H_2O is slightly lower than the a priori profile in the region between 18-11 km. The individual information content is high (around 5-6) below flight altitude and constant for the whole flight. We see an enhacement of the individual information content above flight altitude in the second part of the flight. As for temperature the H_2O retrieved profiles are constant over the whole flight. The vertical resolution for the water retrieval is driven by the vertical spacing of the retrieval grid, as for the first flight.

Maps for O_3, retrieved from all bands, are reported in Fig.s 60 (retrieved values and bias error), 61 (individual information content and a priori profile) and 62 (relative biased error and FWHM of AK). The information content of ozone is always higher than 2 above 10 km for the whole flight and is similar for the scans measured with the similar aircraft altitude. The vertical resolution of the ozone retrieval is homogeneous along the flight, with values below 1.5 km in the altitude range between 12 and 17 km. Even if in general the O_3 vertical distribution is constant over the flight, in the initial part of the flight we see a peak at about 14 km.

HNO_3 retrieved profiles reported in Fig. 63, are always much lower than the initial guess profile shown in Fig.64 and constant along the flight below flight altitude. The individual information content for HNO_3 is always higher than 2 above 8 km and its value above flight altitude is higher in the second part of the flight. The vertical resolution of HNO_3 is constant along the flight, with the best value (1.5 km) obtained at about 16 km.

N_2O retrievals results from band B scans are reported in Fig. 66, in Fig. 67 and in Fig. 68. Retrieved values are

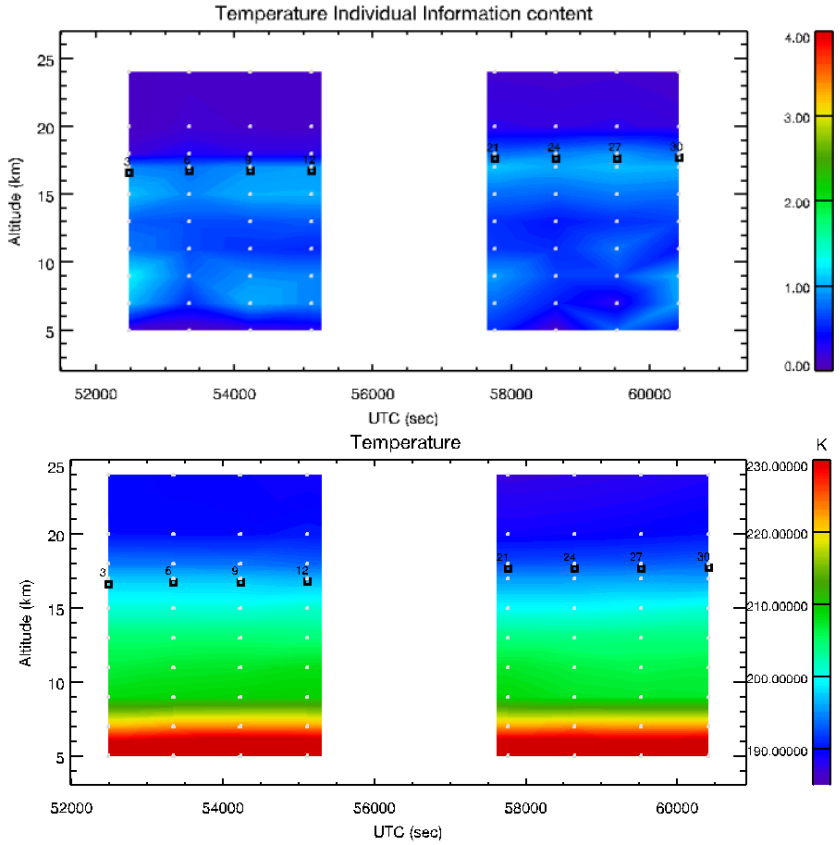

Fig. 55: Top panel: Temperature individual information content from band C for Flight 2 plotted versus the UTC and altitude. Bottom panel: Temperature initial guess from band C for Flight 2 plotted versus the UTC and altitude.

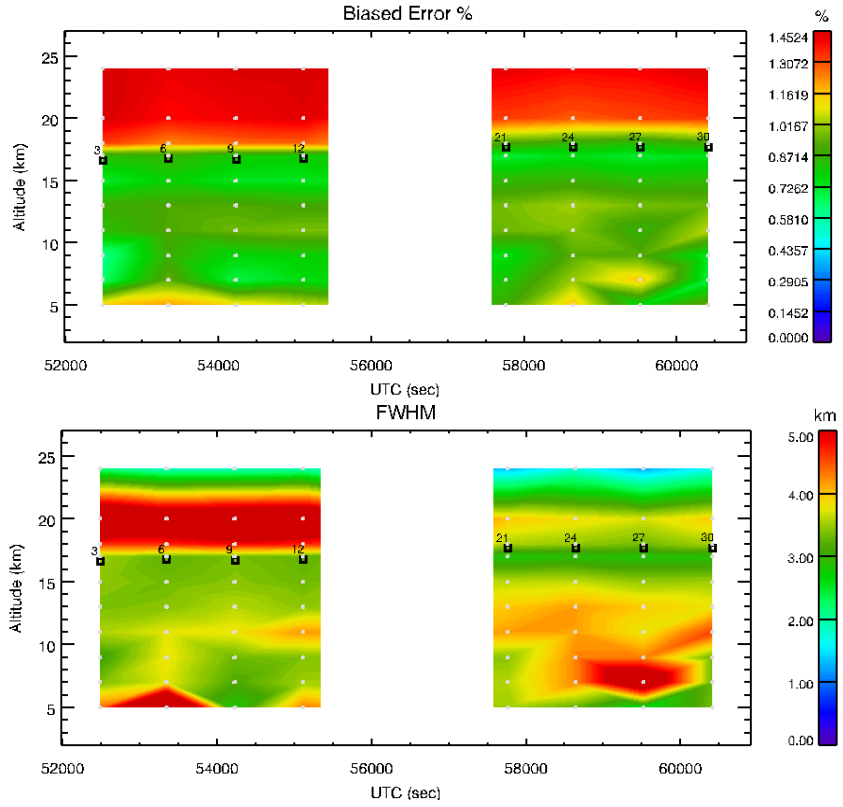

Fig. 56: Top panel: Temperature relative biased error plotted versus the UTC and altitude. Bottom panel: FWHM of Temperature AK for Flight 2 plotted versus the UTC and altitude.

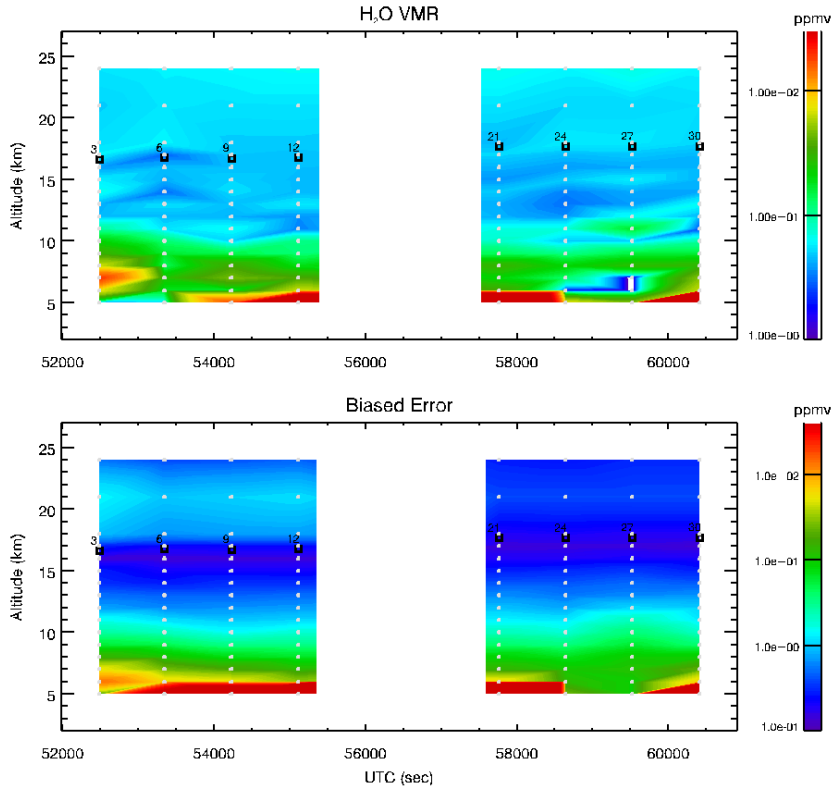

Fig. 57: Top panel: H_2O from band C for Flight 2 plotted versus the UTC and altitude. Bottom panel: Biased error from band C for Flight 2 plotted versus the UTC and altitude.

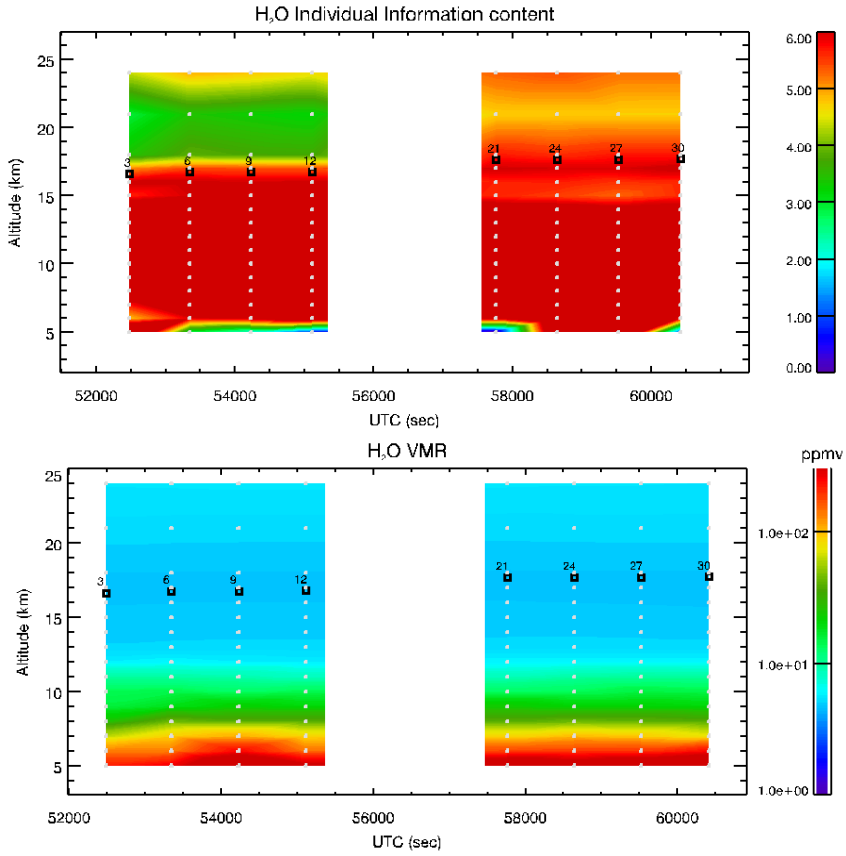

Fig. 58: Top panel: H_2O individual information content from band C for Flight 2 plotted versus the UTC and altitude. Bottom panel: H_2O initial guess from band C for Flight 2 plotted versus the UTC and altitude.

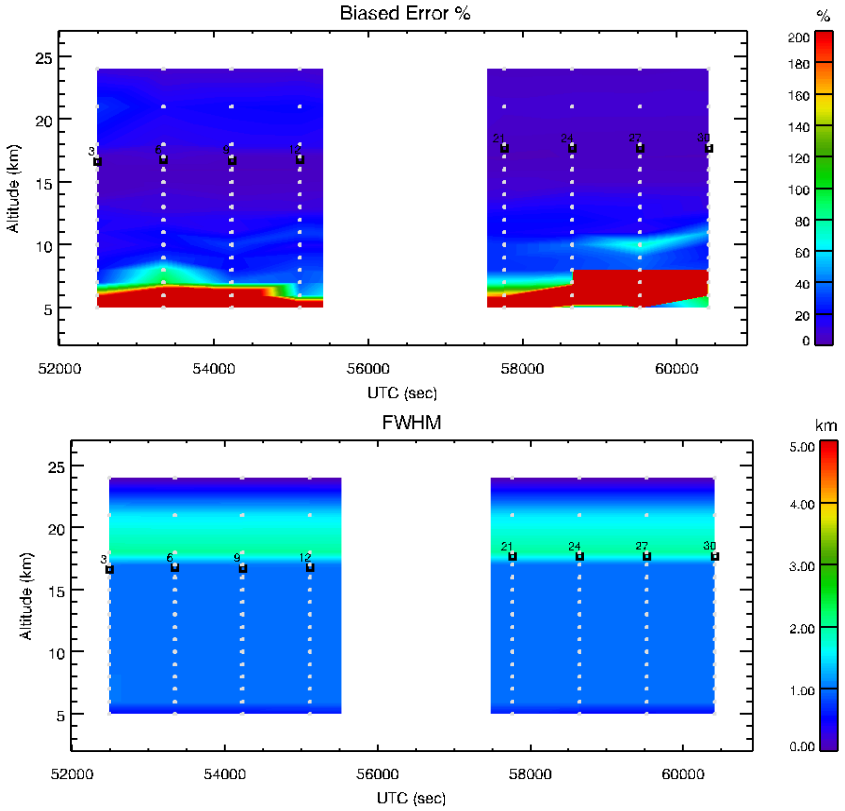

Fig. 59: Top panel: H_2O relative biased error plotted versus the UTC and altitude. Bottom panel: FWHM of H_2O AK for Flight 2 plotted versus the UTC and altitude.

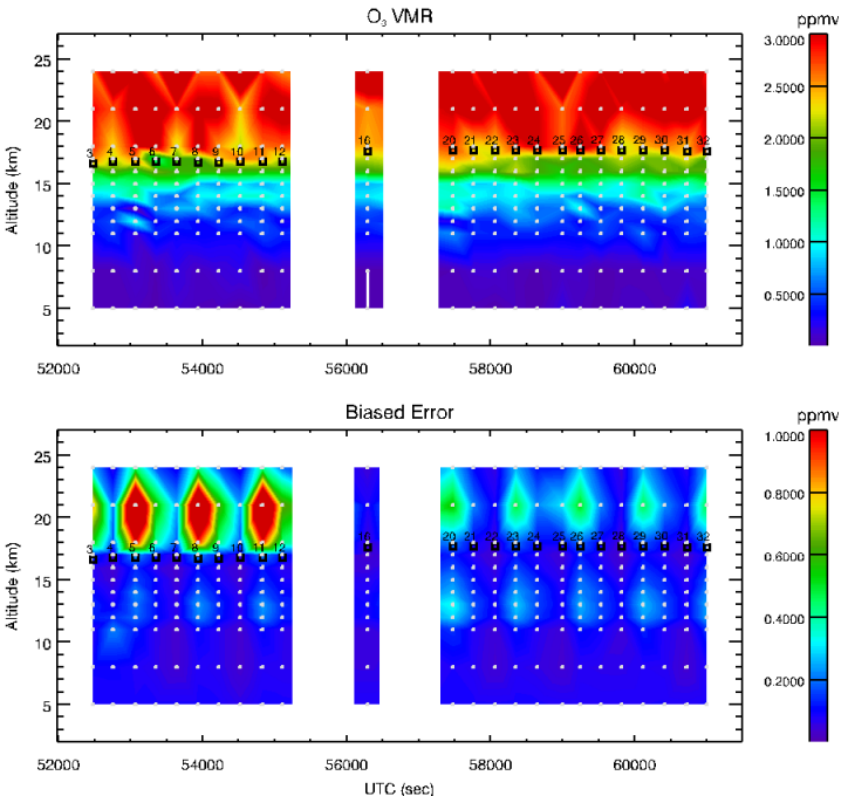

Fig. 60: Top panel: O_3 from all bands for Flight 2 plotted versus the UTC and altitude. Bottom panel: Biased error for Flight 2 plotted versus the UTC and altitude.

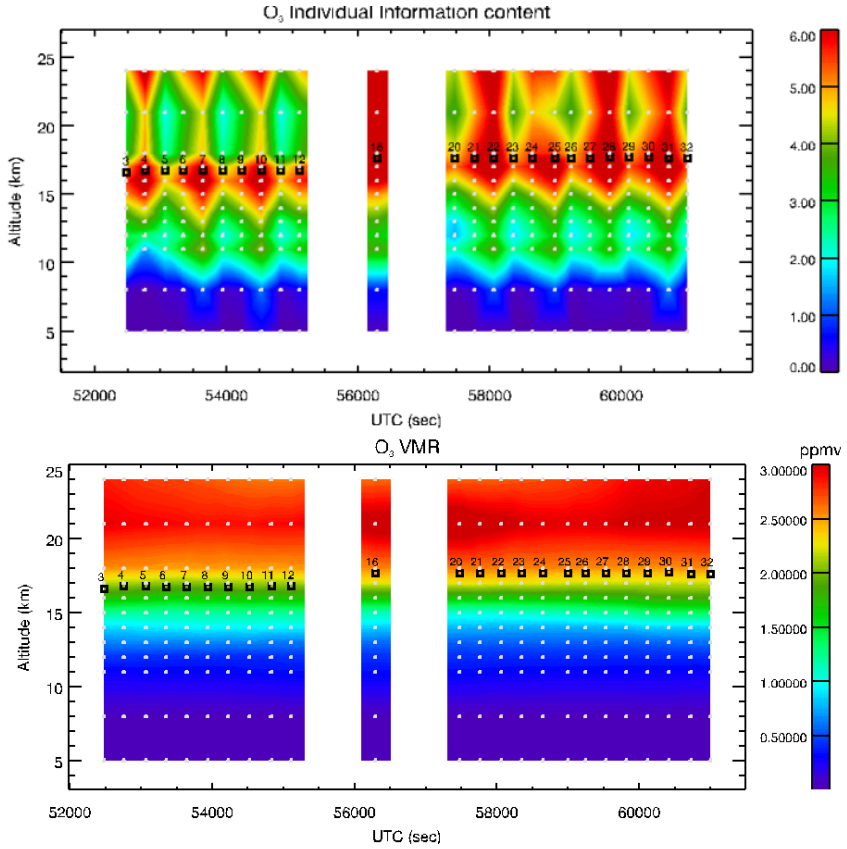

Fig. 61: Top panel: O_3 individual information content from all bands for Flight 2 plotted versus the UTC and altitude. Bottom panel: O_3 initial guess for Flight 2 plotted versus the UTC and altitude.

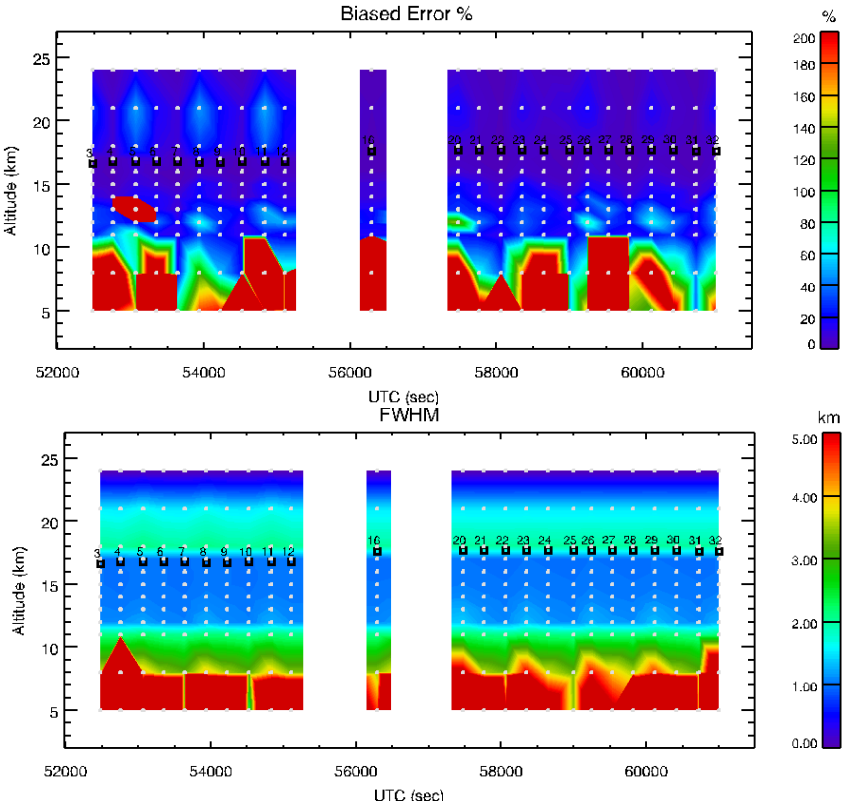

Fig. 62: Top panel: O_3 relative biased error plotted versus the UTC and altitude. Bottom panel: FWHM of O_3 AK for Flight 2 plotted versus the UTC and altitude.

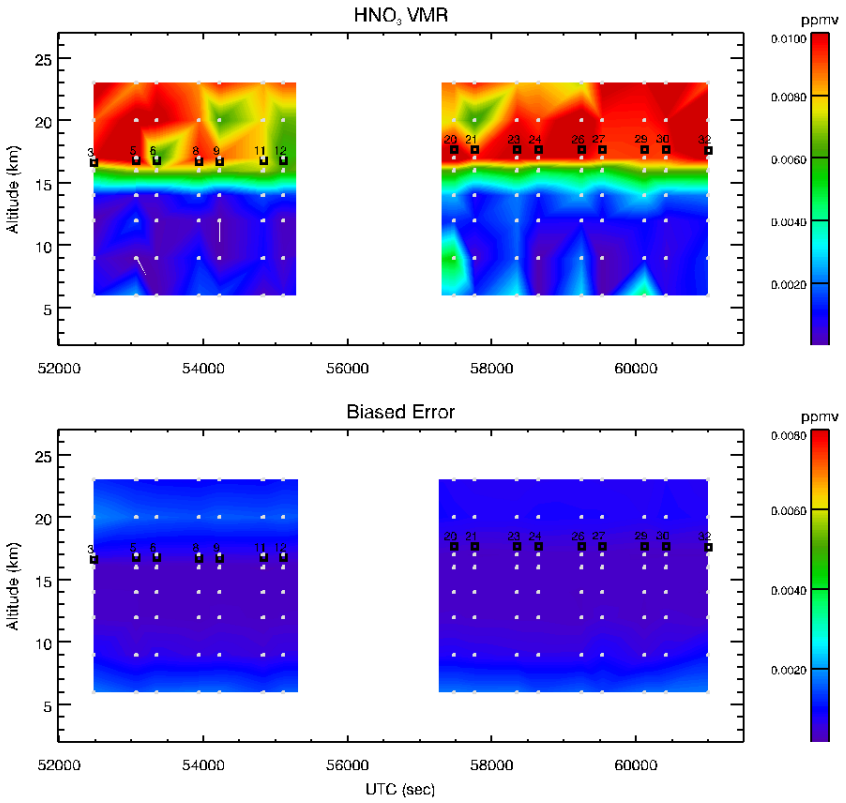

Fig. 63: Top panel: HNO_3 from band C and D for Flight 2 plotted versus the UTC and altitude. Bottom panel: Biased error from band C and D for Flight 2 plotted versus the UTC and altitude.

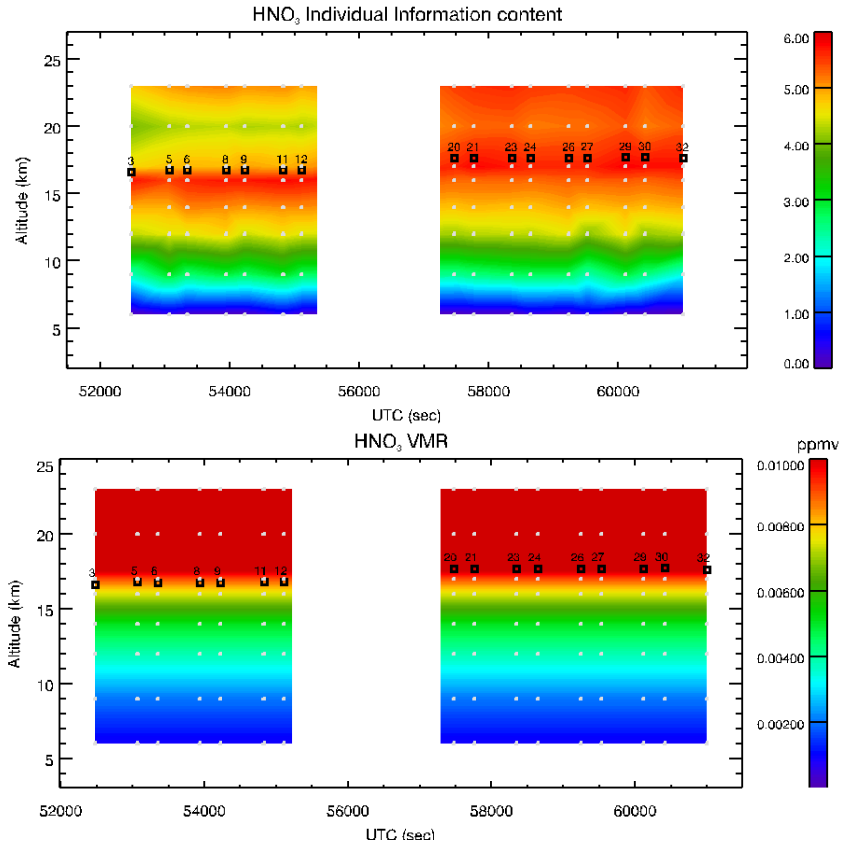

Fig. 64: Top panel: HNO_3 individual information content from band C and D for Flight 2 plotted versus the UTC and altitude. Bottom panel: HNO_3 initial guess from band C and D for Flight 2 plotted versus the UTC and altitude.

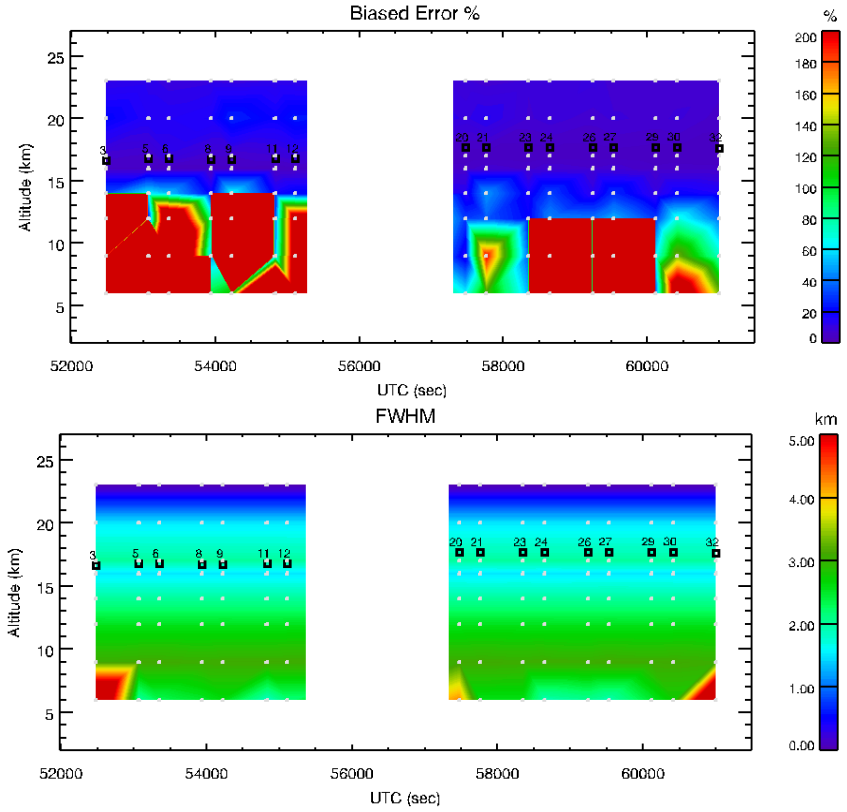

Fig. 65: Top panel: HNO_3 relative biased error plotted versus the UTC and altitude. Bottom panel: FWHM of HNO_3 AK for Flight 2 plotted versus the UTC and altitude.

constant along the flight with values lower than the a priori above 16 km. In comparison with the results obtained during the Premier-Ex campaign N_2O profiles have less oscillations despite the fact that we have increased the threshold for the 1-sigma variability to 200%.

The results obtained from Band D for CO retrievals are reported in Fig. 69, in Fig. 70 and in Fig. 71. Below the flight altitude the retrieved CO values are much lower (see upper panel of Fig. 69) than the a priori ones (in bottom panel of Fig. 70), as we have already reported.

The cloud coverage seen by the MARSCHALS instrument can be evaluated using the retrieved values of the external continuum shown in Fig. 72. As can be seen no opaque clouds are seen by MARSCHALS. Possibly some clouds are present at the beginning and at the end of the flight with CTH at about 10 km. The values of the individual information content in Fig. 73 is above 2 only above 15 km.

In order to better evaluate our results we have also mapped the retrieved O_3 and HNO_3 values versus longitude instead of time (see Fig. 75 upper panel for O_3 and lower panel for HNO_3). As can be noticed from these maps the O_3 profiles show a peak around 14 km in the region from 2.5 to 10 longitude degrees, while the HNO_3 profiles suggest denitrification above flight altitude from 4 to 9 longitude degrees.

5.4 Recursive retrievals for O_3 and HNO_3

As described for Flight 1 also for Flight 2 we performed a recursive retrievals for HNO_3 and O_3 using the same strategy described for Flight 1 in section 4.2.4. The final results for O_3 is shown in Fig. 76, where the top panel show the map obtained using just the band C profiles and in the bottom panel the results for the full flight. The final results for HNO_3 is shown in Fig. 77, where the top panel show the map obtained using just the band C profiles and in the bottom panel the results for the full flight.

Comparing these maps with the Fig. 60 we see the improvement obtained with this strategy for O_3 retrieved in band C and for the whole flight. The same conclusion can be reached for HNO_3 : the results shown in Fig. 77 compared with the Fig. 63 show the improvements achieved with the recursive strategy.

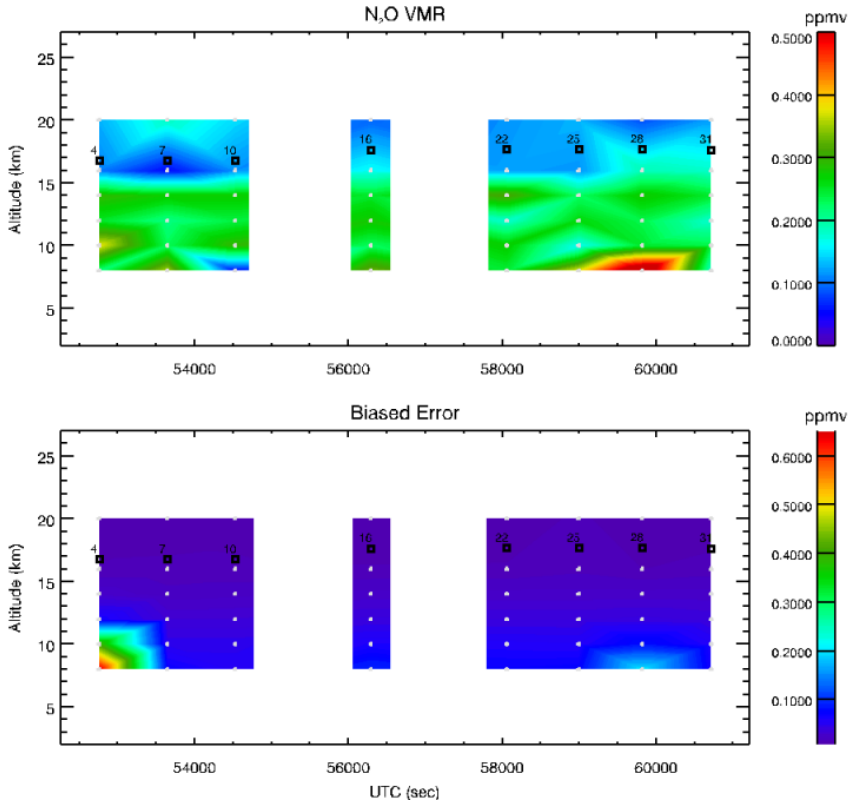

Fig. 66: Top panel: N_2O from band B for Flight 2 plotted versus the UTC and altitude. Bottom panel: Biased error from band B for Flight 2 plotted versus the UTC and altitude.

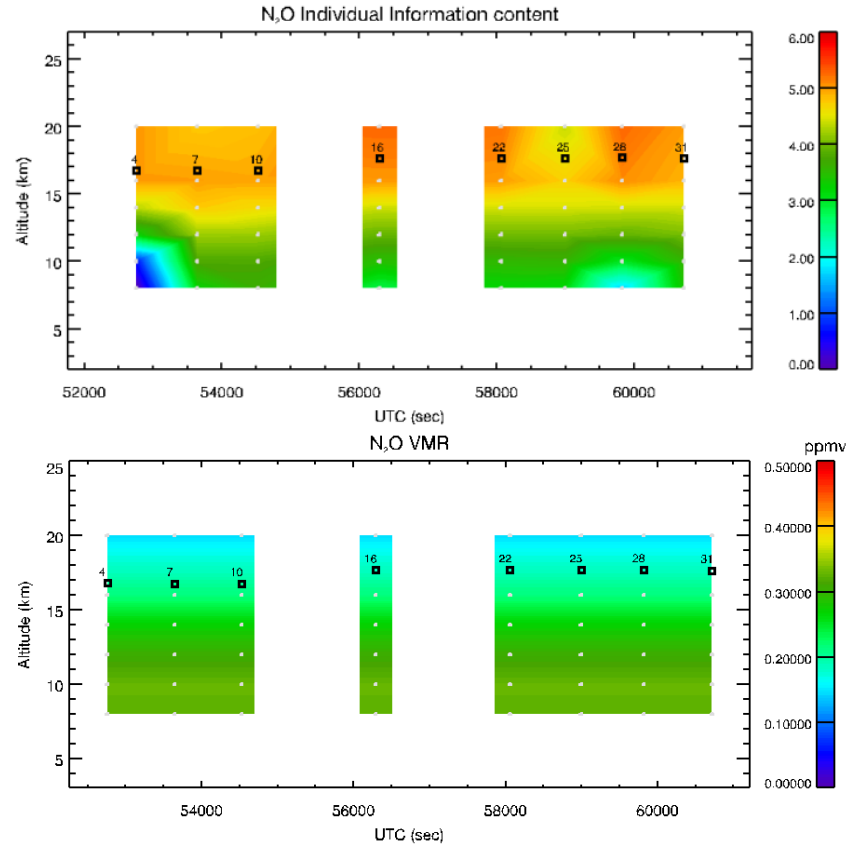

Fig. 67: Top panel: N_2O individual information content from band B for Flight 2 plotted versus the UTC and altitude. Bottom panel: N_2O initial guess from band B for Flight 2 plotted versus the UTC and altitude.

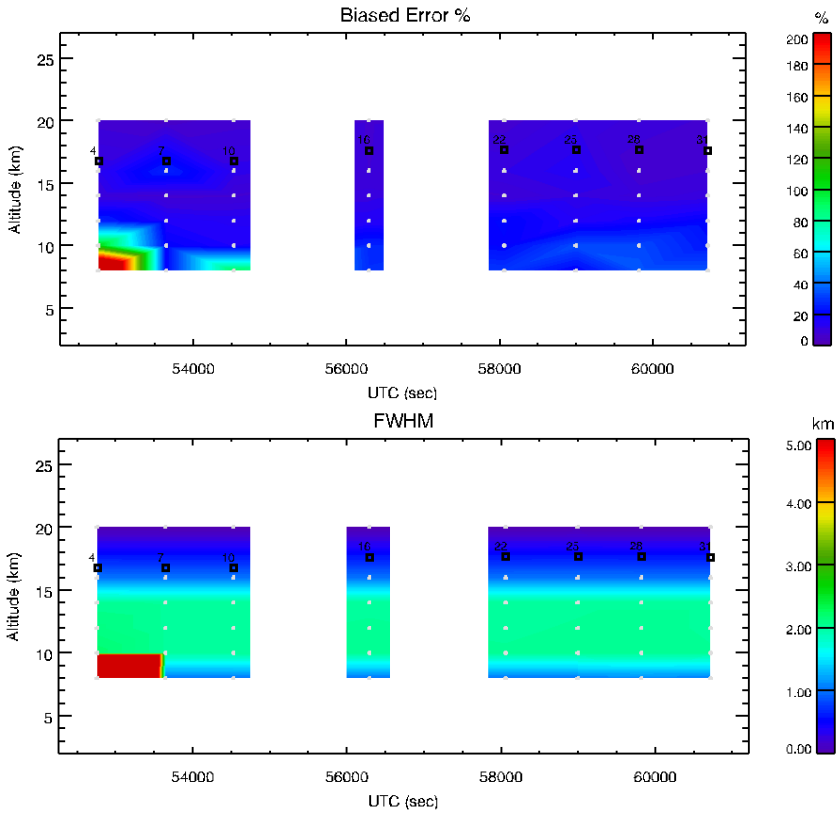

Fig. 68: Top panel: N_2O relative biased error plotted versus the UTC and altitude. Bottom panel: FWHM of N_2O AK for Flight 2 plotted versus the UTC and altitude.

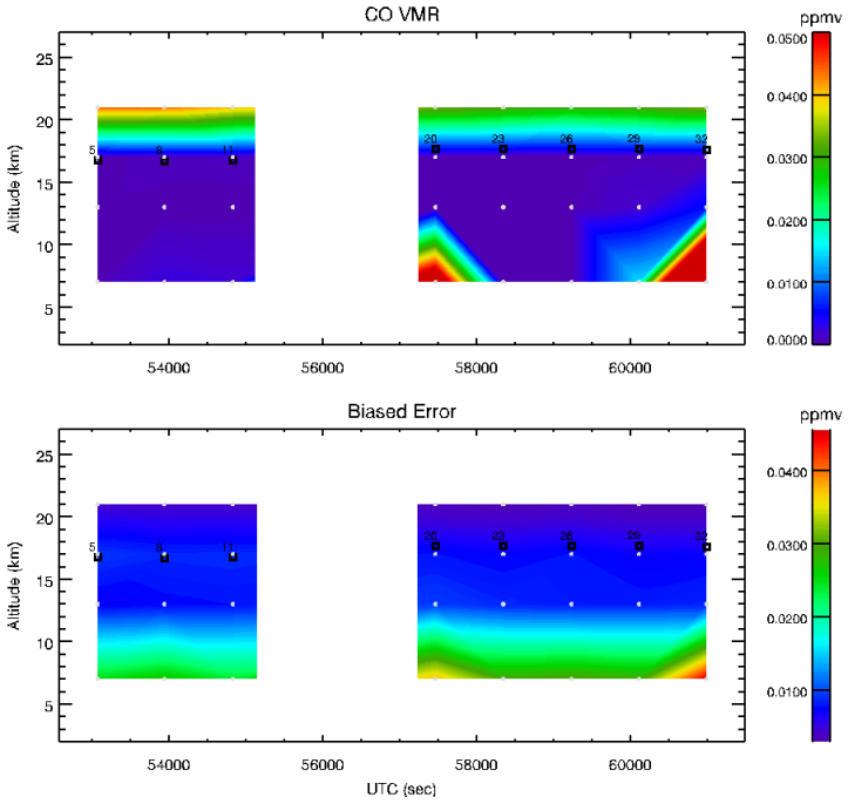

Fig. 69: Top panel: CO from band D for Flight 2 plotted versus the UTC and altitude. Bottom panel: Biased error from band D for Flight 2 plotted versus the UTC and altitude.

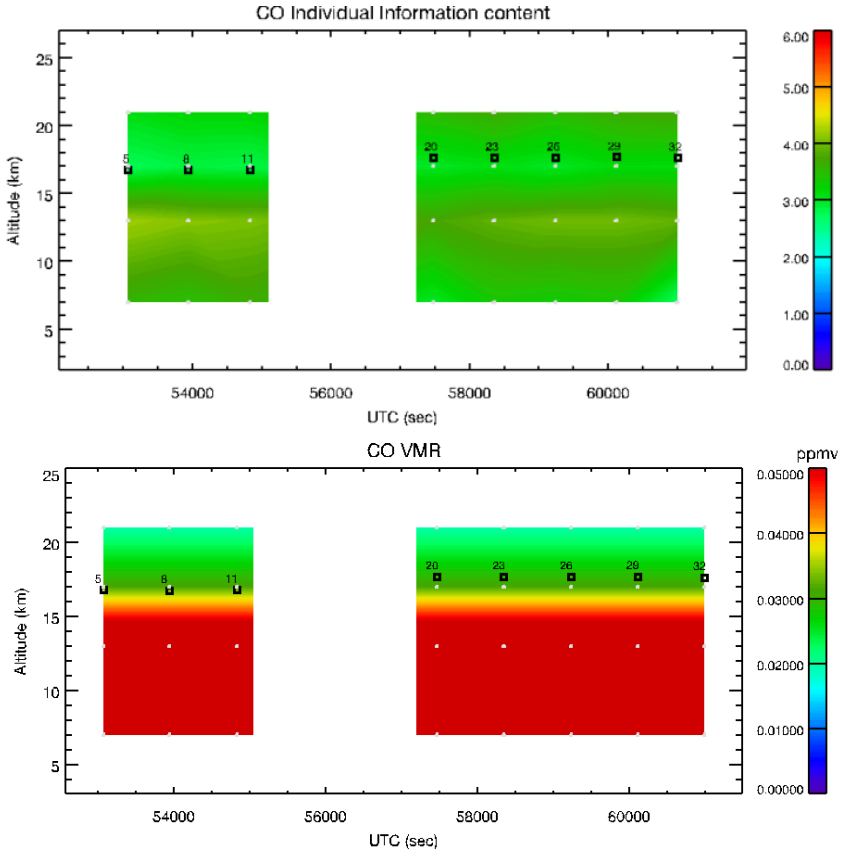

Fig. 70: Top panel: CO individual information content from band D for Flight 2 plotted versus the UTC and altitude. Bottom panel: CO initial guess for Flight 2 plotted versus the UTC and altitude.

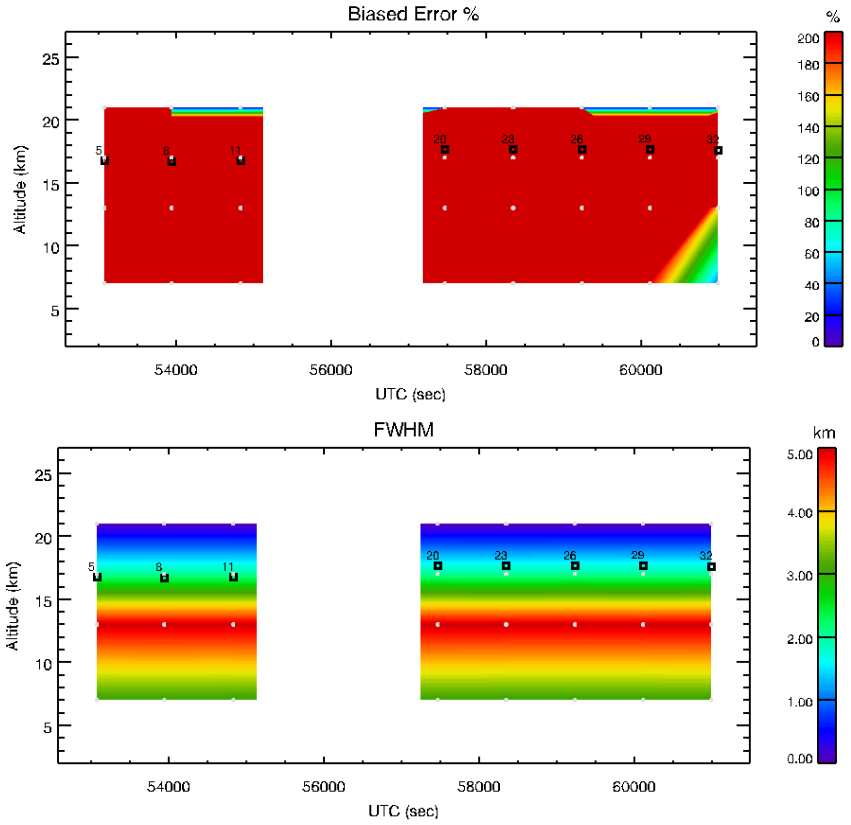

Fig. 71: Top panel: COrelative biased error plotted versus the UTC and altitude. Bottom panel: FWHM of COAK for Flight 2 plotted versus the UTC and altitude.

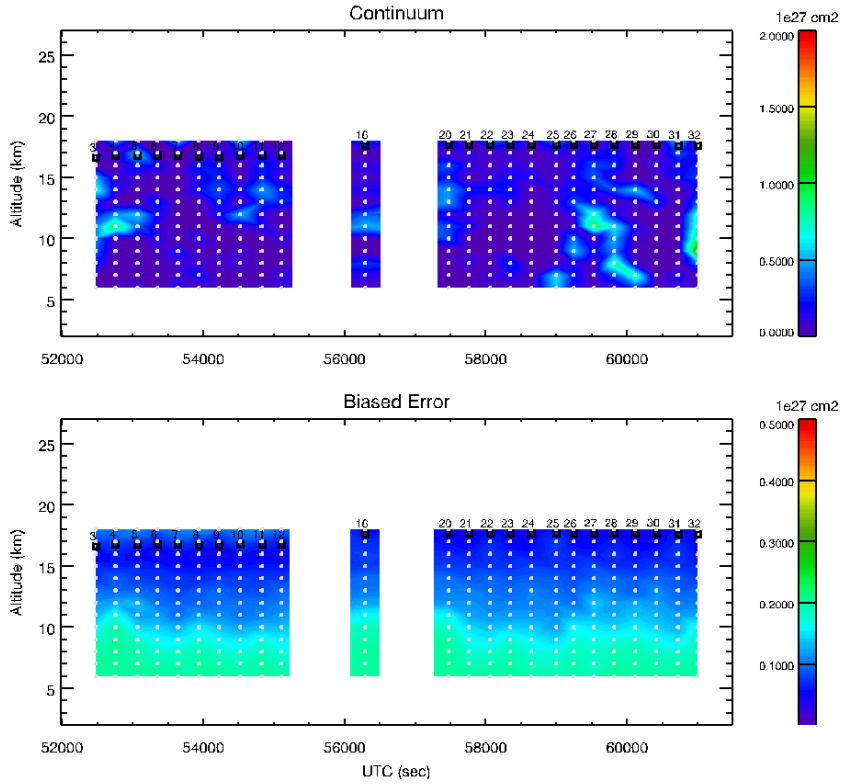

Fig. 72: Top panel: external continuum from all bands for Flight 2 plotted versus the UTC and altitude. Bottom panel: Biased error for Flight 2 plotted versus the UTC and altitude.

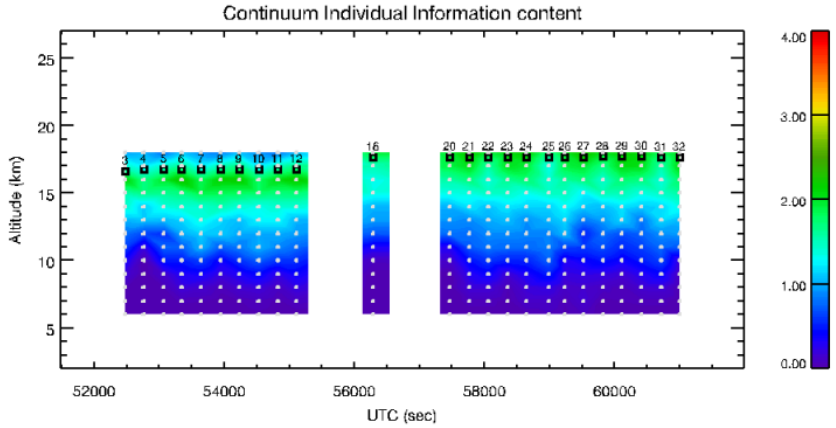

Fig. 73: external continuum individual information content for Flight 2 plotted versus the UTC and altitude.

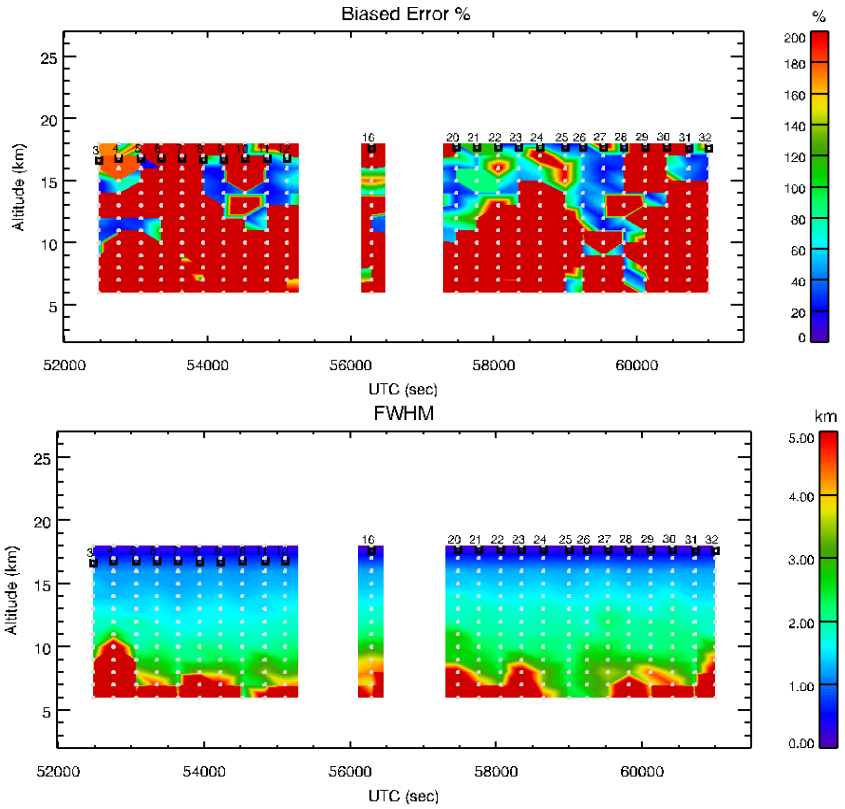

Fig. 74: Top panel: external continuum relative biased error plotted versus the UTC and altitude. Bottom panel: FWHM of external continuum AK for Flight 2 plotted versus the UTC and altitude.

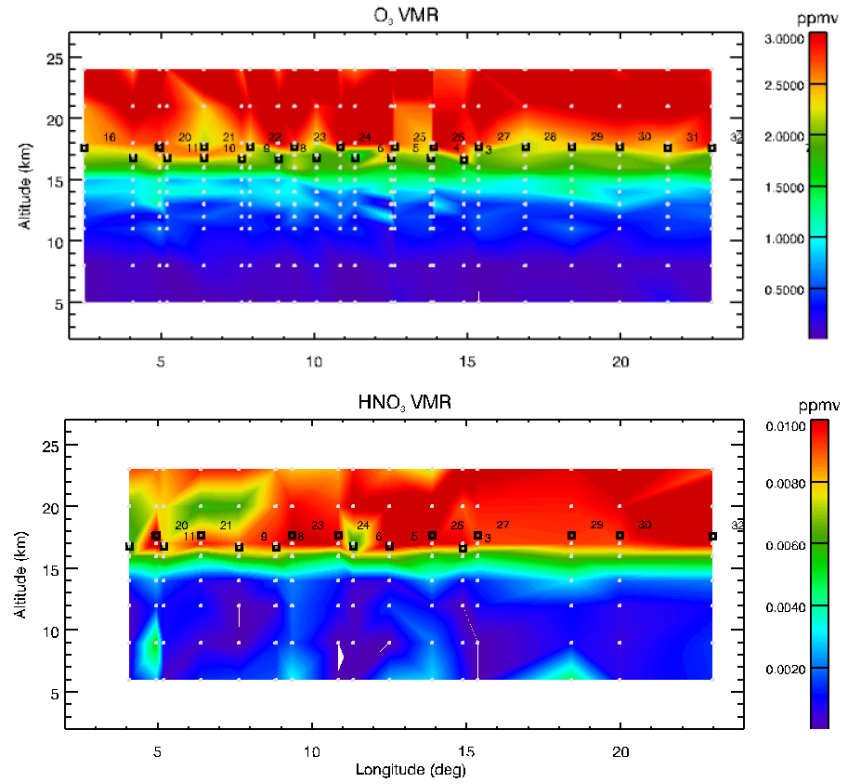

Fig. 75: Top panel: retrieved O_3 profiles as a function of longitude. Bottom panel: retrieved HNO_3 as a function of longitude.

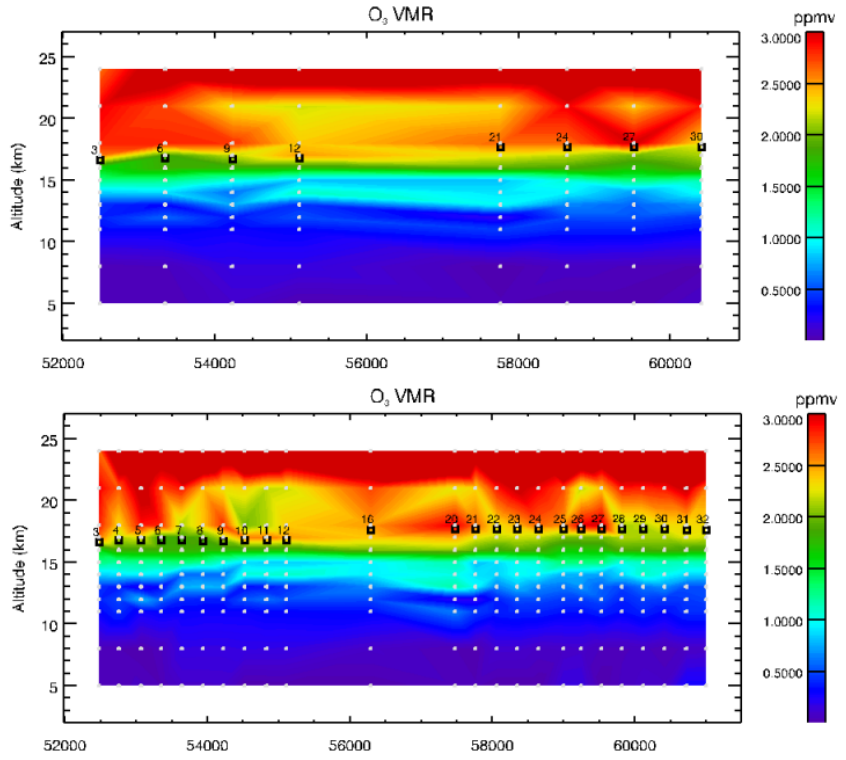

Fig. 76: Top panel: O_3 profiles retrieved using recursive retrieval strategy in band C. Bottom panel: O_3 profiles retrieved using recursive retrieval strategy in all bands.

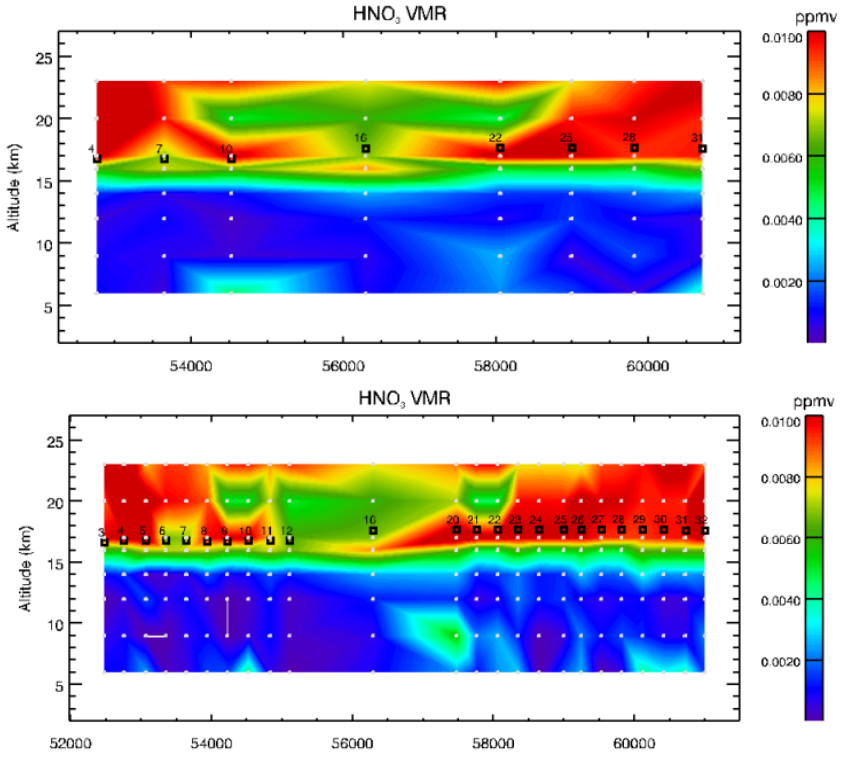

Fig. 77: Top panel: HNO_3 profiles retrieved using recursive retrieval strategy in band B. Bottom panel: HNO_3 profiles retrieved using recursive retrieval strategy in all bands.

5.5 Conclusions

During the Flight 2 the level 1 team modified the commanded pointing adding futher limb angles in order to cope with an UCSE roll angle offset of +0.5 deg. registered during the Flight 1. Since this problem did not appeared during the Flight 2 many of the limb views for Flight 2 are above horizontal and the vertical range covered by the measurements is reduced.

Also for Flight 2, as for Flight 1, the L1 spectra contain some bad channels that were not masked by RAL, so we looked at each single spectrum and flagged the bad channel when the values were not realistic (in comparison with simulations and noise level) using the same strategy used for Flight 1.

For the analysis we used the same retrieval strategy used in Premier-Ex data analysis, while after some tests we decided to change the a priori errors and set the threshold for the 1-sigma variability for all the targets but temperature at 200%.

Since the results from the CO retrievals, as in Premier-ex data analysis, show low CO values below flight altitude we performed further tests (as the investigation of possible correlation with HNO_3, sequential retrieval) but no significant improvements were obtained. Tests on the sensitivity of MARSCHALS measurements to CO concentrations show that if the CO concentration is high MARSCHALS measurements should detect it.

The results of the analysis for the second flight show that:

- *Temperature*
  Can be retrieved from Band C but has low information content. The vertical resolution changes in the two parts of the flight.

- *H_2O*
  Water can be retrieved from band C with good information content Its vertical resolution is driven by the vertical retrieval grid.

- *O_3*
  Ozone can be retrieved from all bands. O_3 profiles show a peak at 14 km for the scans acquired in the area from 2.5 to 10 deg in longitude.

- *HNO_3*
  Nitric acid can be retrieved from bands C and D. Profiles obtained using very different initial guess give consistent results. Hint of low HNO_3 values above flight altitude from 4 to 9 deg in longitude.

- *N_2O*
  N_2O is retrieved from band B only. We observe less oscillations in the profiles with respect to Premier-Ex analysis despite of the larger a priori errors used in ESSEnCe data analysis.

- *CO*
  CO is retrieved from band D scans. As in Premier-ex data analysis we obtain low CO values below flight altitude.

- *External continuum*
  External continuum can be retrieved from all bands. The external continuum has low information content below 13-14 km, and there is no evidence of opaque clouds above 10-12 km.

6 Conclusions of MARSCHALS Flight 1 and Flight 2 data analysis

During Flight 1 the level 1 team discovered a bug in the way the UCSE roll angle record was handled that caused a constant offset of +0.5 deg. For this reason in Flight 1 the vertical coverage of the measurements was not the nominal one but was anomalously distributed along the flight.

For both flights, the L1 spectra contain bad channels: some of them were identified and masked by the level 1 team, while other were not flagged. Therefore we checked every single spectrum and we flagged the bad channels when they assumed not realistic values when compared to simulations and to the noise level. Some spectra that showed evidence of wrong pointing assignation were completely discarded from the analysis.

Following the indications of the level 1 team, the noise level used in the analysis was set to the one contained in the L1 files without adding any other contribution.

The adopted retrieval strategy was the same for both flights, and was optimised for Flight 2. After some tests we decided to set the threshold value for the 1-sigma variability (used as a-priori error) to 200% for all the targets but for temperature where a constant value of 3 K was used.

Despite of the pointing problems encountered during Flight 1, quite good results were obtained during the analysis. The results of the analysis show that O_3concentration is lower at 15 km at the beginning of the flight; the same happens for HNO_3. i HNO_3 also show a minimum at 17 km towards the end of the flight and higher values above and below this altitude suggesting that we are in presence of a renitrification process. N_2Oretrieval is unstable, with strong oscillations for the scan that show low individual information content due to their reduced vertical coverage. As in the Premier-ex data analysis we obtain low CO values below flight altitude. External continuum has low information content below 15-14 km, no evidence of opaque clouds.

During Flight 2 the level 1 team modified the commanded pointing, in order to cope with the UCSE roll angle offset registered during Flight 1. Since this time the offset was null, many of the limb views of Flight 2 were above the flight altitude and the vertical range covered by the measurements was reduced.

Since the results from the CO retrievals, as in Premier-ex data analysis, showed low CO values below flight altitude we performed further tests (as the investigation of possible correlation with HNO_3or sequential retrieval) but no significant improvements were obtained. Tests on the sensitivity of MARSCHALS measurements to CO concentrations show that if the CO concentration is high MARSCHALS measurements should be able to detect it. However the reason of the low CO concentration retrieved from the measurements of both Premier-EX and ESSEnCe campaigns is not totally clear, and the results of further investigations will be reported in an appendix of the report.

The results of the analysis for Flight 2 show that O_3 has a peak at 14 km in the region from 2.5 to 10 deg in longitude, while there is an hint of low HNO_3 values above flight altitude from 4 to 9 deg. in longitude. The N_2O retrieved profiles are less oscillating than in the Premier-Ex analysis despite the larger a priori errors used in ESSEnCe data analysis. No evidence of opaque clouds can be inferred from the external continuum retrieval.

7 Validation of MARSCHALS measurements

The validation of the vertical profiles obtained during the analysis of MARSCHALS data acquired in both the ESSEnCe Flights 1 and 2 can be performed using different instruments on board the Geophysica aircraft. While remote sensing instruments are the best for the validation exercise, in situ instruments can validate the retrieved profiles only close to the take off and landing of the aircraft. During the ESSEnCe Campaign the in-situ instrument on board the Geophysica that can provide useful measurements for the comparison were Hagar (N_2O) and FISH (H_2O). Temperature can be inferred from the UCSE data. Remote sensing instrument on board the Geophysica were GLORIA and MIPAS-STR, and can provide profiles of temperature, H_2O, $O_3$and HNO_3.

Correlative data that can also be used for the validation exercise are Temperature and H_2Oprofiles from radiosondes from different stations (data at 00 and 12 UTC).

We have found data measured by three satellite instruments that can be used for the validation of MARSCHALS analysis: ENVISAT/MIPAS, ODIN/SMR and AURA/MLS. ENVISAT/MIPAS measures Temperature, H_2O, O_3, and HNO_3profiles from about 6 km (in absence of clouds) to 68 km.

ODIN/OSIRIS data are not available since OSIRIS, by its very nature, is limited to measurements in the sunlit hemisphere and when coupled to the ODIN orbit, which itself is nominally constrained to the dawn/dusk meridian, means that OSIRIS only makes useful measurements in the summer-time hemisphere.

The ENVISAT/MIPAS products used for MARSCHALS validation were the ones contained in the MIPAS2D database (see [11]) using the GMTR approach (two-dimensional (2-D) retrievals). The 2-D approach is particularly useful to model atmospheric horizontal inhomogeneities typical for instance of the polar vortex region.

AURA/MLS measures Temperature, H_2O, O_3, HNO_3, N_2O and CO and reports its data as a function of pressure. MLS data are retrieved with a 2-D approach. For this validation exercise we used the MLS data version 3.3. The main differences of this data version with the previous one are the improvements in the biases for upper tropospheric CO and HNO_3 and the extension of the vertical range for O_3 (see [34]). The errors reported for MLS retrievals are quite small. This is due to the regularization used during the retrieval procedure. Values of precision and vertical and horizontal resolution as well as the AK and FWHM can be found for each MLS retrieved specie in [34] (e.g. for O_3see table 3.17.1).

ODIN/SMR measures H_2O, O_3, HNO_3, N_2O in the 7 to 70 km altitude range. In this validation exercise we used only data with measurement response (defined as the sum of the elements of each averaging kernel) higher than 0.75 meaning that the a priori information contaminates the retrieval by less than 25% (see e.g. [52]).

7.1 Validation of the Flight 1 measurements

During the Flight 1 the M55 Geophysica did not performed any dive. For this reason vertical profiles of N_2O and H_2O are available only during the ascent and the descent of the aircraft. The geo-location and time of VMR profiles obtained from satellite instruments in coincidence with M55 Geophysica Flight 1 are shown in Fig. 78 In

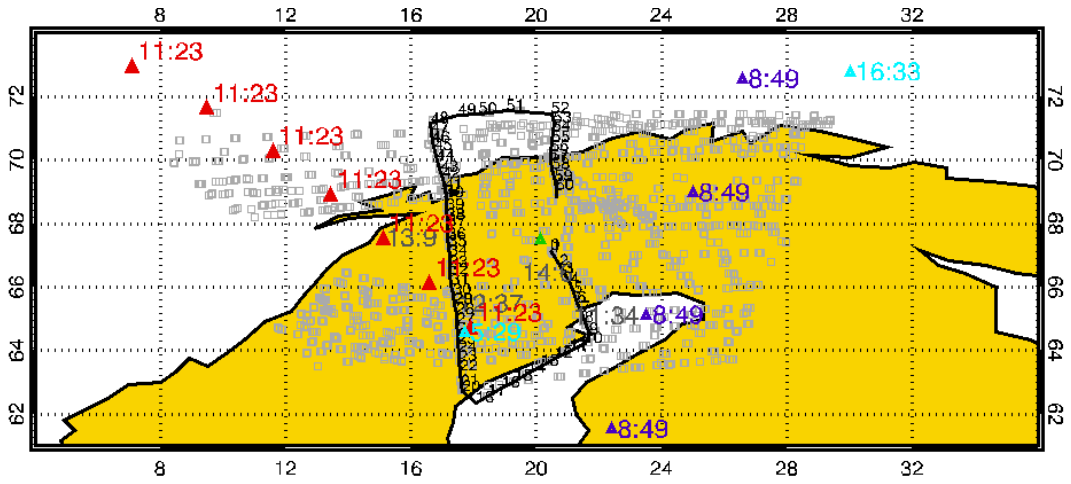

Fig. 78: MARSCHALS flight pattern and tangent points geo-location (grey) and ODIN/SMR (cyan), AURA/MLS (red) and ENVISAT/MIPAS (blue) data geo-locations.

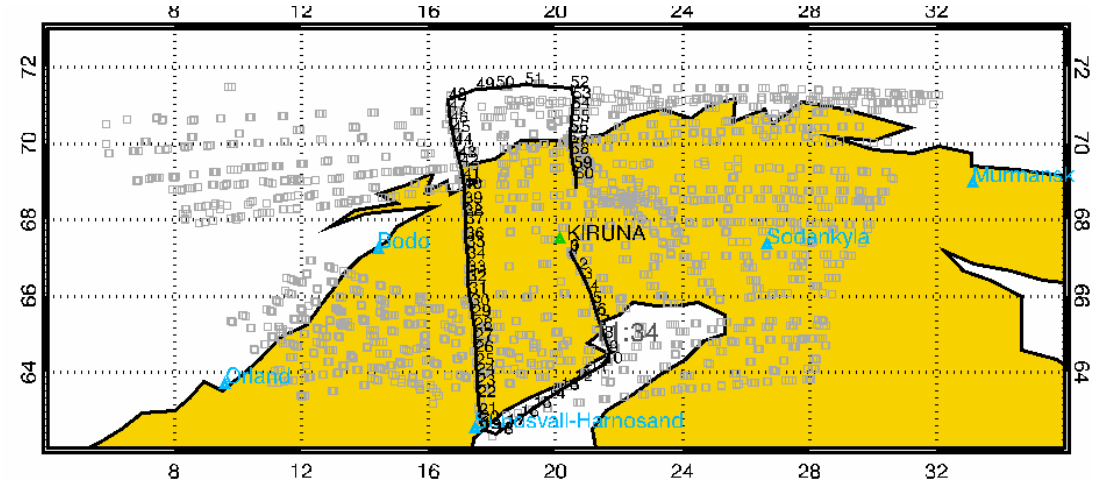

Fig. 79: MARSCHALS flight pattern and tangent points Geo-location (grey) and Radiosondes data Geo-locations.

red are reported the position and time of AURA/MLS profiles, in blue the ones for ENVISAT/MIPAS and in cyan the one for ODIN/SMR. As can be noticed we found a good temporal coincidence for AURA/MLS(20 min - 2h 50 min) and a quite good coincidence for for ENVISAT/MIPAS (2h:20 min - 5h). For the ODIN/SMR a quite bad coincidence is found in the first part of the flight (6-7 h) and a quite good coincidence in the last part of the flight (about 3 h).

The coincidence between MARSCHALS measurements and radiosondes data is shown in Fig. 79. Data from different stations (Orlando, Sodankyla, Sundsvall-Harnosand) at 12 UTC can be used to validate Temperature profiles retrieved from MARSCHALS scans.

7.1.1 Temperature validation

MARSCHALS temperature profiles can be validated using Temperature profiles from radiosondes and from satellite data (AURA/MLS, ENVISAT/MIPAS and ODIN/SMR). In Fig. 80 and in Fig. 81 are reported the temperature profiles retrieved from MARSCHALS measurements for band C scans (in grey) together with the a priori profile (dashed grey) and correlative measurements.

Data from the Sunsdsvall station are used for the coincidence with scan 9, 12 and 15, data from the Orland station for coincidence with scans 12 and 15 and Sodankyla data are used for the validation of scans 33 to 45 while Bodo data for scan 57. In figures 80 and 81 data from the stations are reported in green, while satellite data are reported as follows: AURA/MLS in red, ENVISAT/MIPAS in blue, ODIN/SMR in cyan.

Some scans like 12, 36 and 42 have a peak in MARSCHALS profiles that doesn't appear in the correlative

data, while scan 39 does not show a good agreement with the radiosonde data. For the other profiles a general good agreement can be found with both satellites (covering the higher part of the retrieval altitude range) and radiosondes data (covering the lower part of the retrieval altitude range).

7.1.2 H_2O validation

MARSCHALS H_2O profiles can be validated using FISH data during the descent, satellite data (AURA/MLS, ENVISAT/MIPAS and ODIN/SMR) and also using Station data for the lower tangent altitudes. Comparisons of retrieved H_2O profiles with correlative data are reported in Fig. 82 and in Fig. 83

As described in the previous section in case of temperature, data from the Sunsdsvall station are used for the coincidence with scan 9, 12 and 15, data from the Orland station for coincidence with scans 12 and 15 and Sodankyla data are used for the validation of scans 33 to 45 while Bodo data for scan 57. In figures 82 and 83 are also reported FISH data obtained during the descent; this data are used for the validation of MARSCHALS scans from 27 to 42 that approximately cross the air masses encountered by FISH during the descent (even if with about 50 minutes of time delay).

In the first part of the flight, from scan 6 to scan 15 MARSCHALS H_2O profiles show some oscillations with large error bars especially for pressure levels higher than 150 hPa. Above this pressure levels the retrieved profiles are in good agreement with AURA/MLS data. From scan 27 to scan 33 we have a good agreement between MARSCHALS profiles and FISH data (in particular scan 33 in Fig. 82), covering the lower part of the retrieved altitude range and also with ENVISAT/MIPAS data (covering the higher part of the retrieved altitude range). Scans from 36 to 42 show a worse agreement with the FISH data and with radiosonde data. Scan 45 is in good agreement with Sodankyla data and also with ODIN/SMR and ENVISAT/MIPAS data at high altitudes, scan 48 is in good agreement with ODIN/SMR and ENVISAT/MIPAS data at high altitudes, while scan 54 shows higher values with respect to MLS data below 100 hPa. Finally scan 57 is in very good agreement with both MLS and Bodo data. Even if there are differences among the various profiles, the MARSCHALS H_2O retrieved profiles are in good agreement with correlative measurements.

7.1.3 O_3 validation

The O_3 profiles can be validated using satellite data (AURA/MLS, ENVISAT/MIPAS and ODIN/SMR). The results obtained from the Flight 1 analysis in case of O_3 retrieval are reported in Fig. 84 for band B, in Fig. 85 for band C and in Fig. 86 for band D.

O_3 retrieved profiles from band B show a general good agreement with all the satellite used for this validation exercise, expecially below flight altitude, even if the quality of the retrieved profiles (in terms of error bars) varies from scan to scan accordingly to the vertical coverage of the measurements for each scan. The same consideration applies also to O_3 profiles retrieved from band C and band D where the influence of the measurement coverage on the retrieval results is particularly evident for scan 29 and 32. Also the results obtained from the recursive retrievals analysis, shown in Fig. 87 highlights a general good agreement with correlative measurements.

7.1.4 HNO_3 validation

As for the O_3 retrieved profiles, the HNO_3 MARSCHALS profiles can be validated using satellite data (AURA/MLS, ENVISAT/MIPAS and ODIN/SMR). The results obtained from the Flight 1 analysis in case of HNO_3 retrieval are reported in in Fig. 88 for band C and in Fig. 89 for band D.

HNO_3 profiles obtained from band C show a good agreement with ODIN/SMR data and MLS for scans 6 to 12 even if the MARSCHALS profiles show a slight negative bias with respect to MLS. HNO_3 MARSCHALS profiles are lower than Aura/MLS and ENVISAT/MIPAS data from scan 15 to 30, while the agreement improves from scan 33-36 to the end of the flight. In general, HNO_3 profiles retrieved from band D measurements show a better agreement with all the satellite data. As in case of O_3 differences in the precision of the HNO_3 retrieved profiles can be found from scan to scan, due to the measurements vertical distribution (see for example scan 29 and 32 in Fig. 89). The results of the recursive retrievals analysis for HNO_3 (see Fig. 90) show a general good agreement with satellite data even if MARSCHALS data show lower HNO_3 values below flight altitudes for scans 16, 25, 28 and 31.

7.1.5 N_2O validation

MARSCHALS N_2O profiles can be validated using HAGAR data during the descent and from satellite data (AURA/MLS, ENVISAT/MIPAS and ODIN/SMR). HAGAR data acquired during the descent are compared to

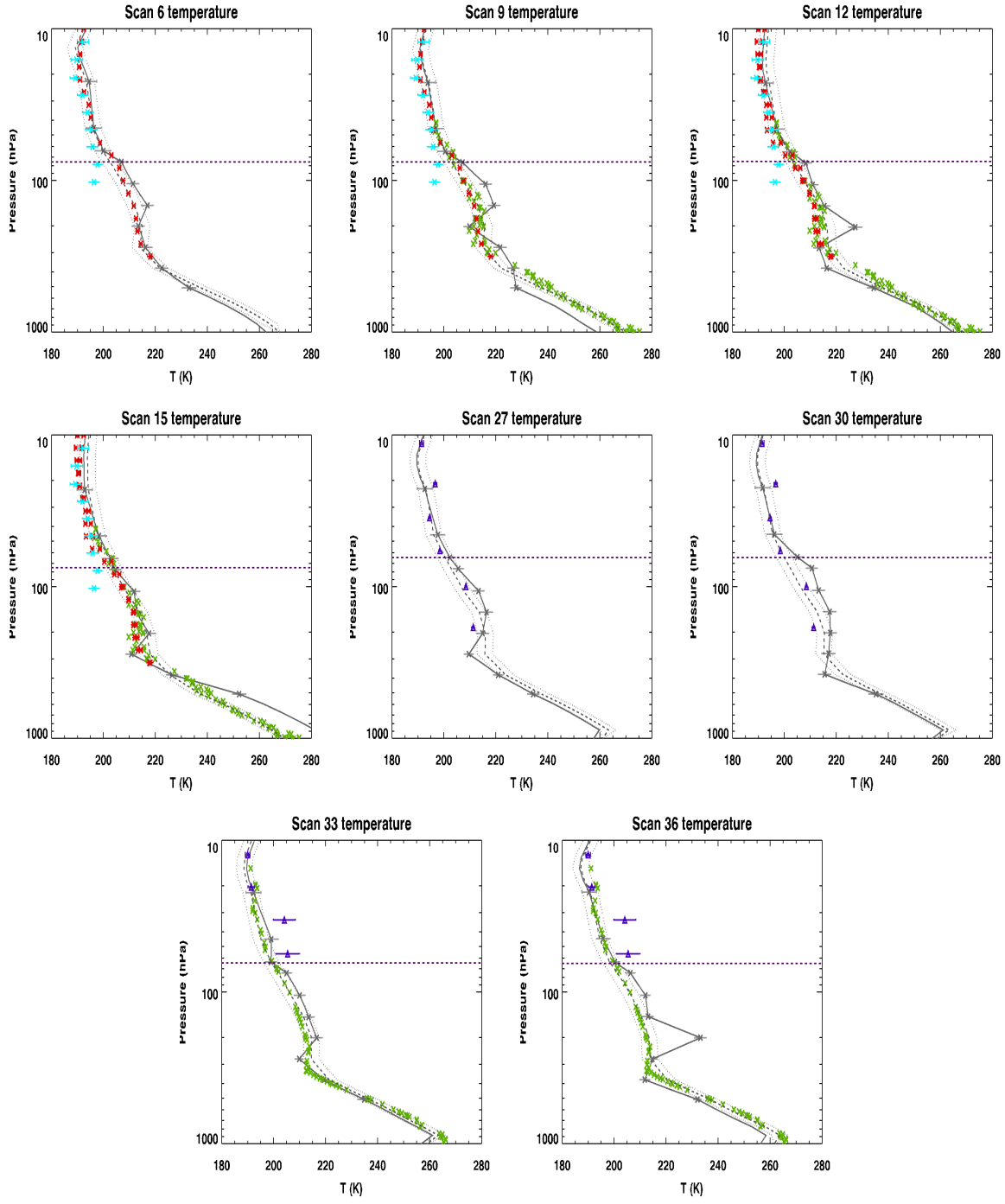

Fig. 80: MARSCHALS temperature profiles for scan 6, 9, 12, 15, 27, 30, 33,36 (in grey) together with initial guess profile (dashed) and correlative measurements: MLS in red, MIPAS in blue, SMR in cyan, radiosonde in green. Dashed purple line indicates the flight altitude level.

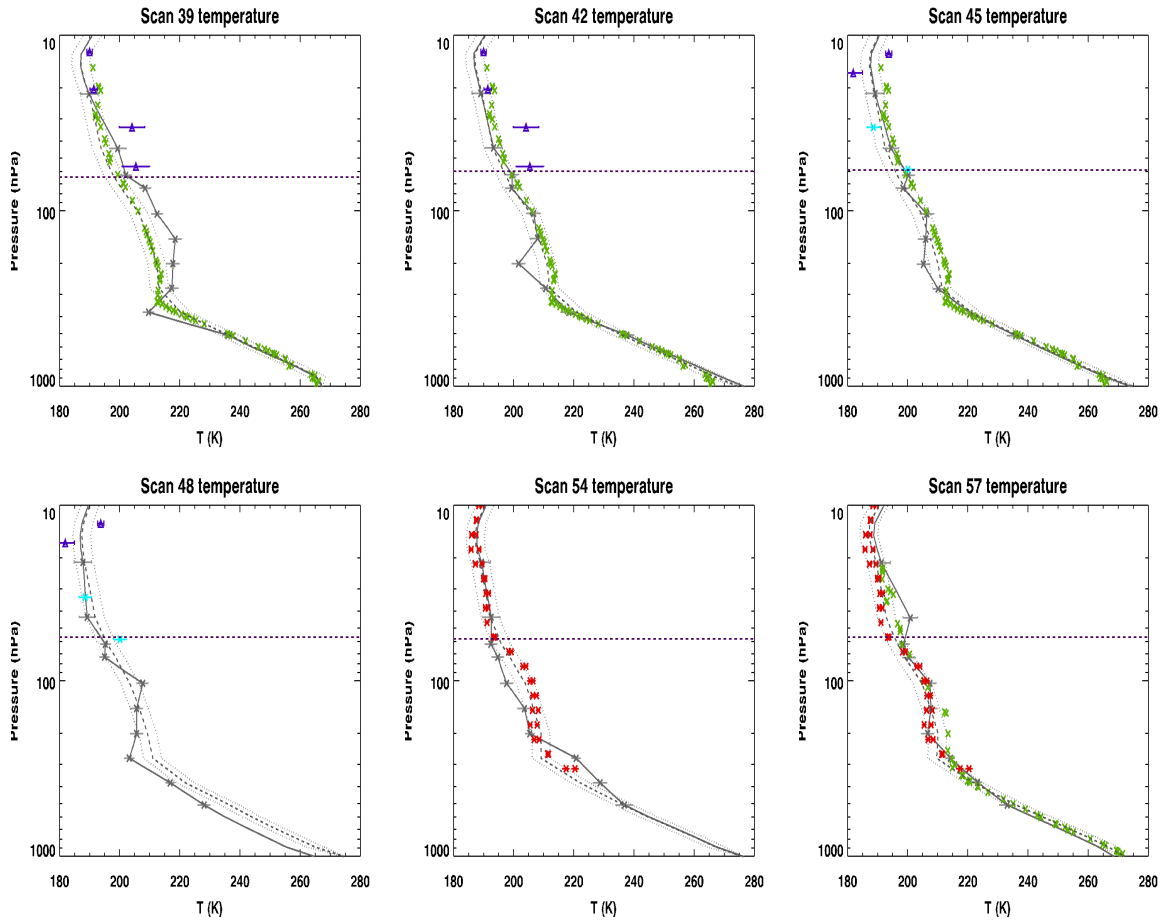

Fig. 81: MARSCHALS temperature profiles for scan 39, 42, 45, 48, 54, 57 (in grey) together with initial guess profile (dashed) and correlative measurements: MLS in red, MIPAS in blue, SMR in cyan, radiosonde in green. Dashed purple line indicates the flight altitude level.

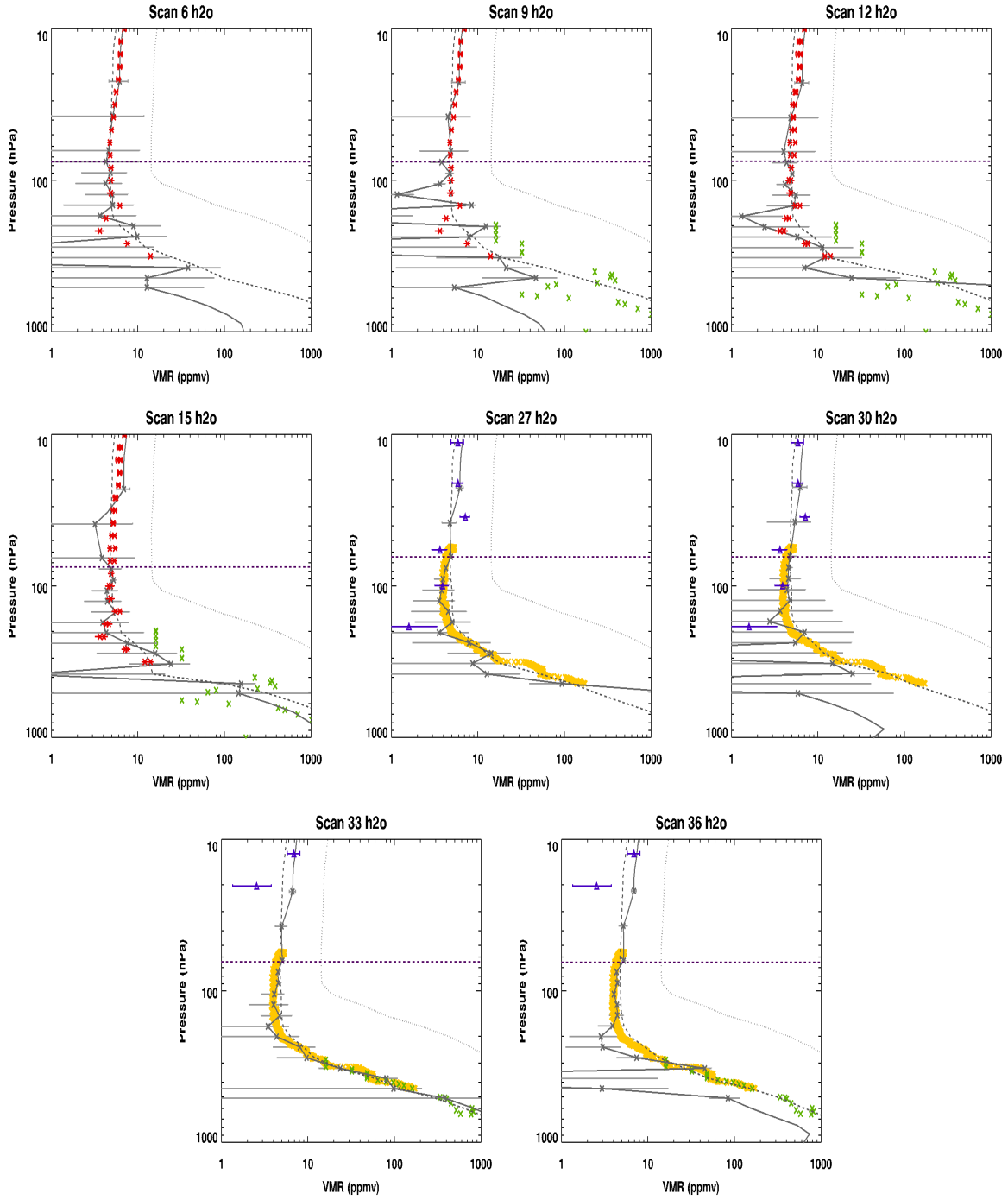

Fig. 82: MARSCHALS H_2O profiles for scan 6, 9, 12, 15, 27, 30, 33,36 (in grey) together with initial guess profile (dashed) and correlative measurements: MLS in red, MIPAS in blue, SMR in cyan, radiosonde in green and in in situ data (FISH) in yellow. Dashed purple line indicates the flight altitude level.

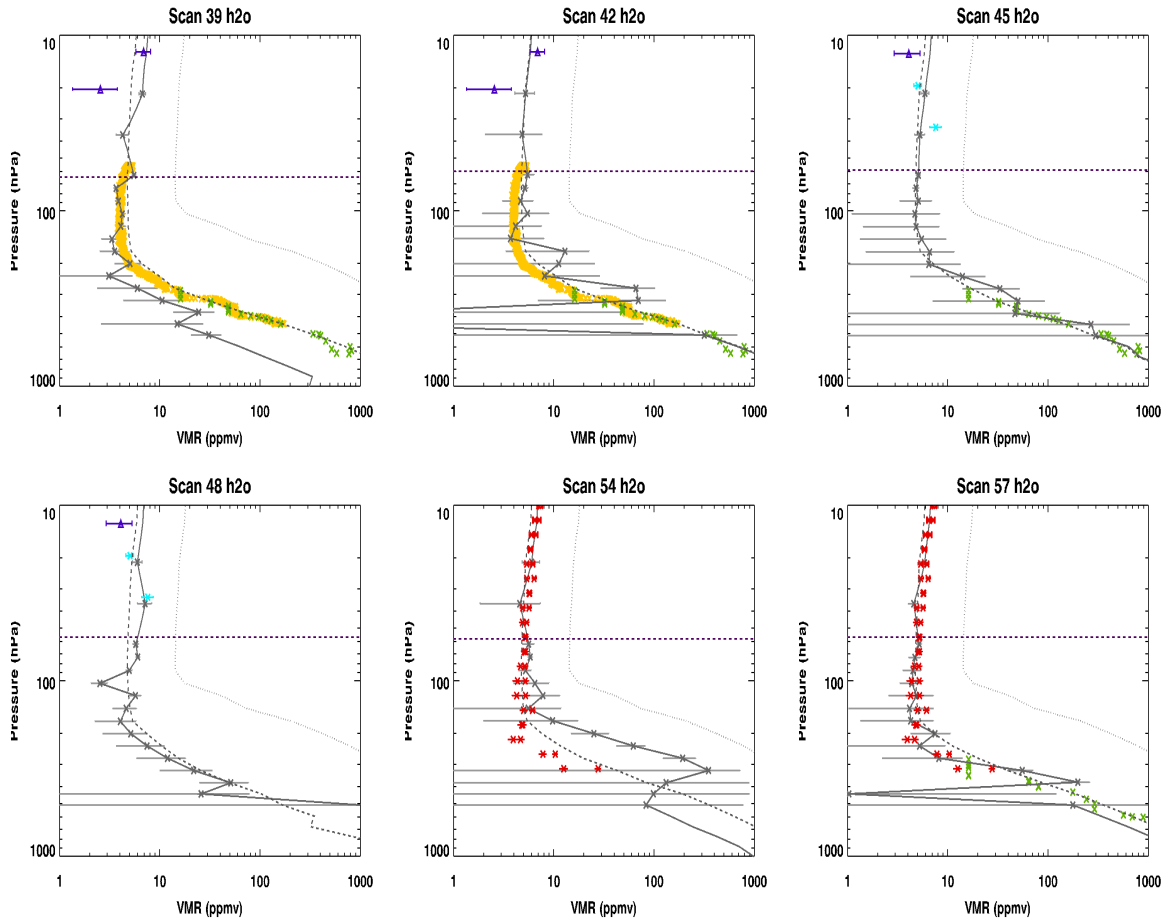

Fig. 83: MARSCHALS H_2O profiles for scan 39, 42, 45, 48, 54, 57 (in grey) together with initial guess profile (dashed) and correlative measurements: MLS in red, MIPAS in blue, SMR in cyan, radiosonde in green and in in situ data (FISH) in yellow. Dashed purple line indicates the flight altitude level.

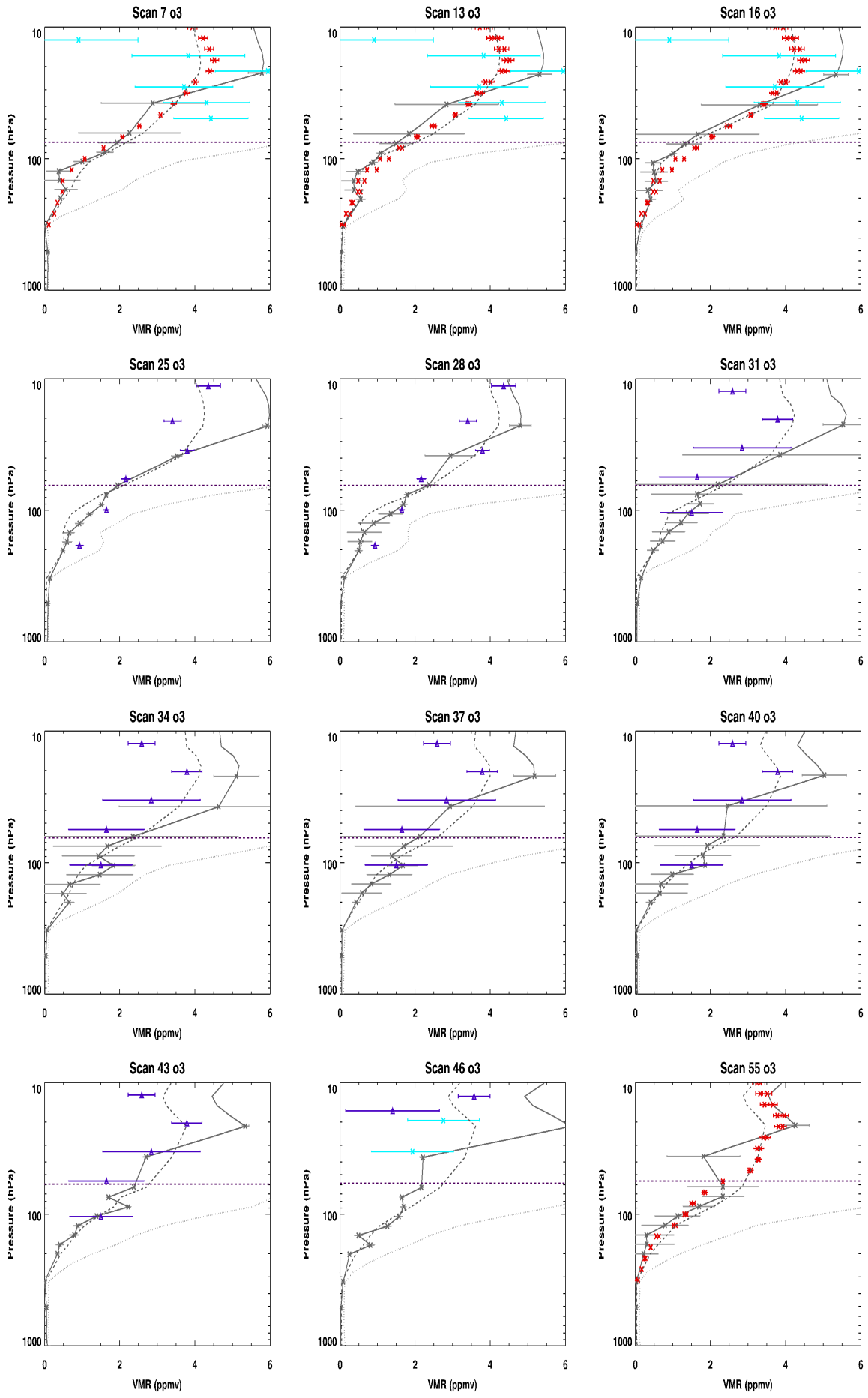

Fig. 84: MARSCHALS O_3 profiles for scan 7, 13, 16, 25, 28, 31, 34, 37, 40, 43, 46, 55 (in grey) together with initial guess profile (dashed) and correlative measurements: MLS in red, MIPAS in blue, SMR in cyan. Dashed purple line indicates the flight altitude level.

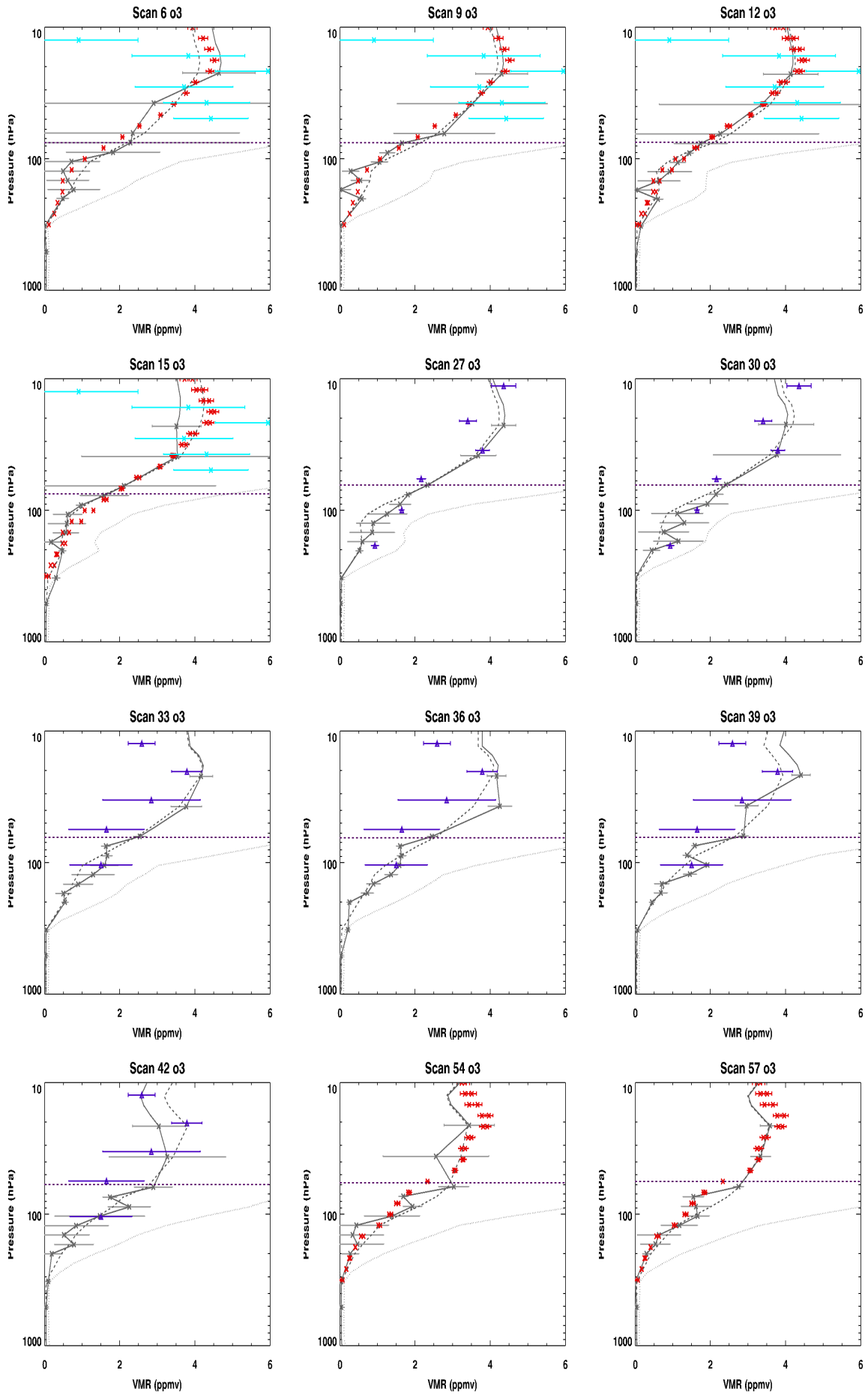

Fig. 85: MARSCHALS O_3 profiles for scan 6,9, 12, 15, 27, 30, 33,36, 39, 42, 54, 57 (in grey) together with initial guess profile (dashed) and correlative measurements: MLS in red, MIPAS in blue, SMR in cyan. Dashed purple line indicates the flight altitude level.

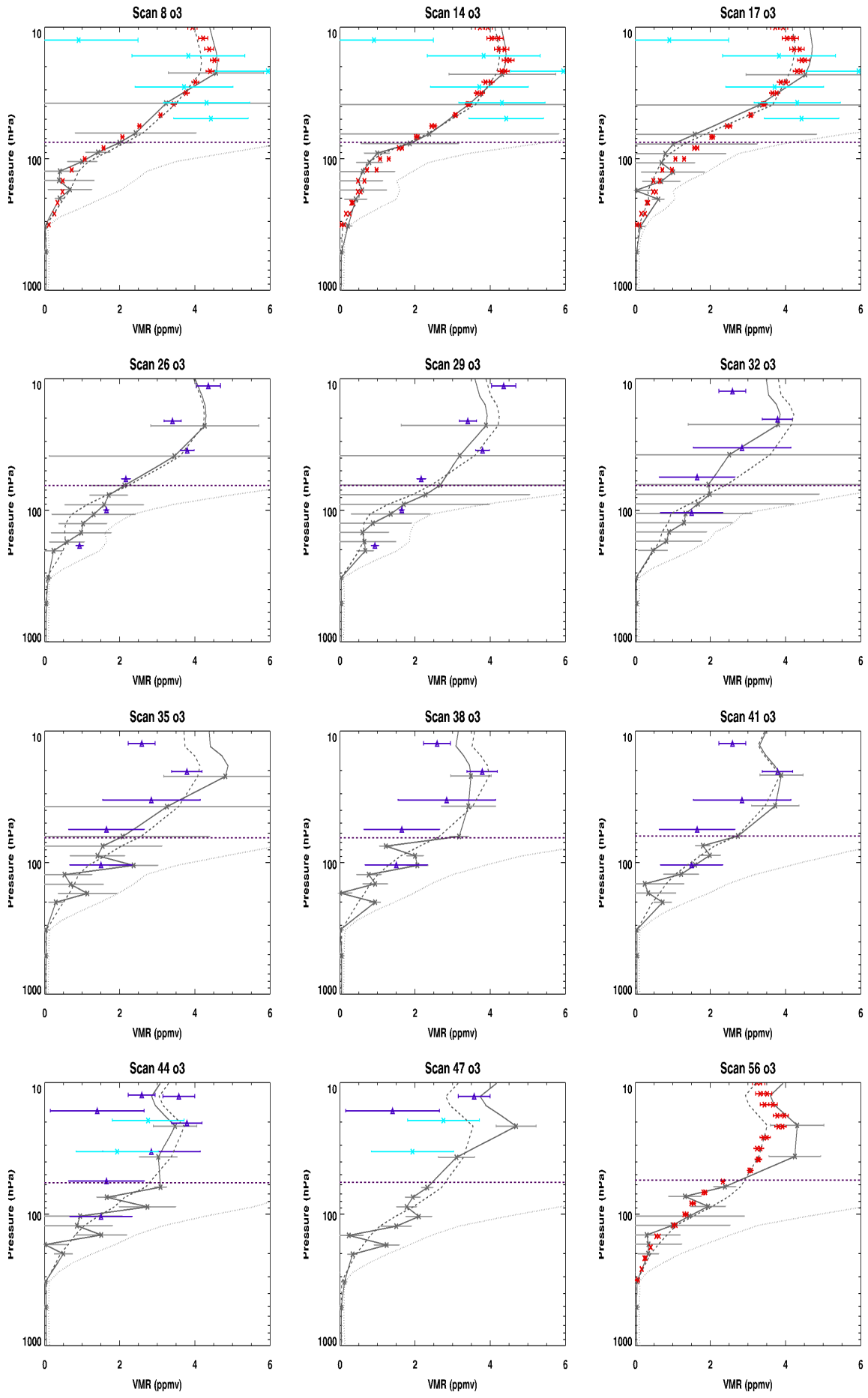

Fig. 86: MARSCHALS O_3 profiles for scan 8, 14, 17, 26, 29, 32, 35, 38, 41, 44, 47,56 (in grey) together with initial guess profile (dashed) and correlative measurements: MLS in red, MIPAS in blue, SMR in cyan. Dashed purple line indicates the flight altitude level.

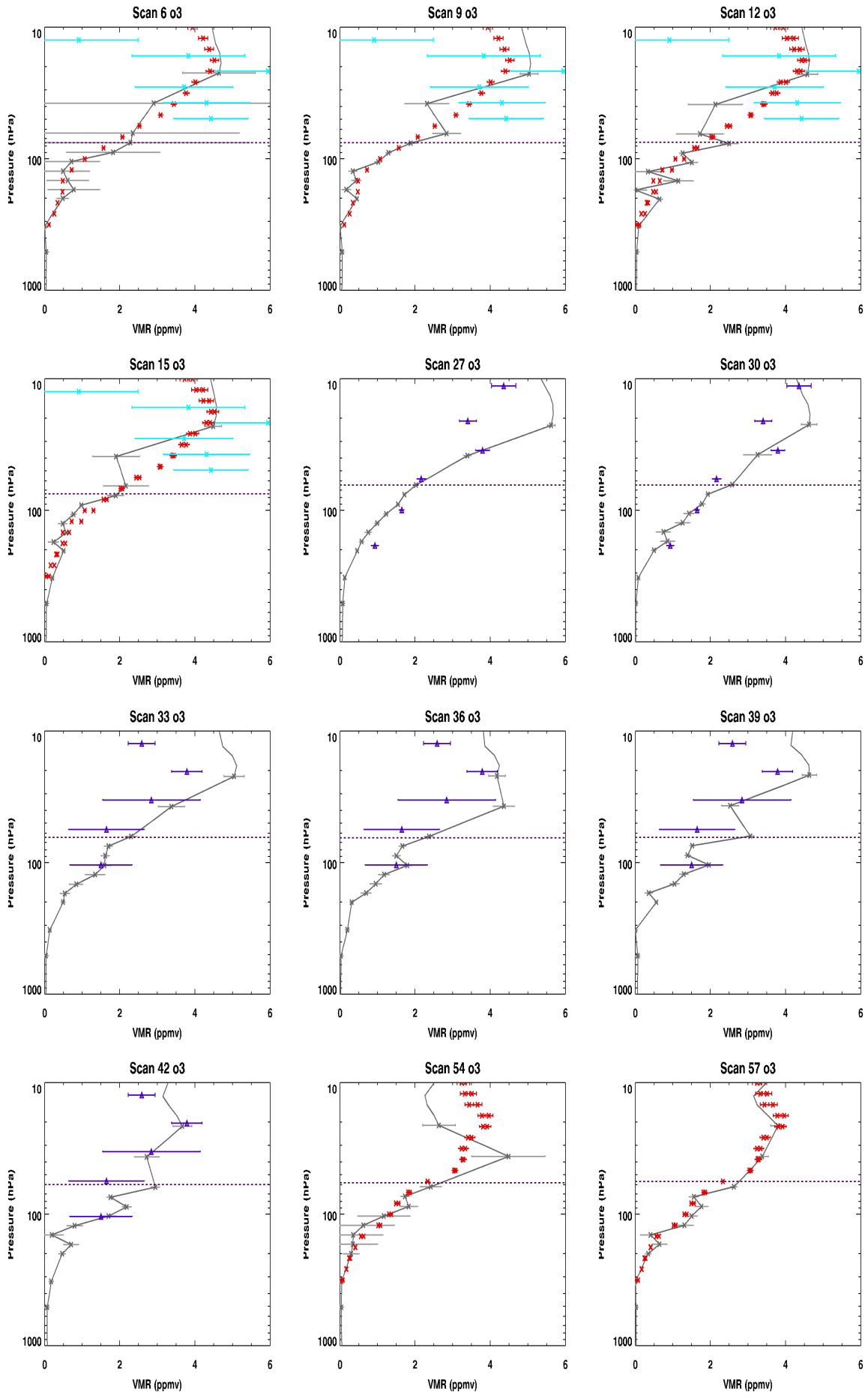

Fig. 87: MARSCHALS O_3 profiles for scan 6,9, 12, 15, 27, 30, 33,36, 39, 42, 54, 57 (in grey) obtained in the recursive retrievals analysis together with initial guess profile (dashed) and correlative measurements: MLS in red, MIPAS in blue, SMR in cyan.

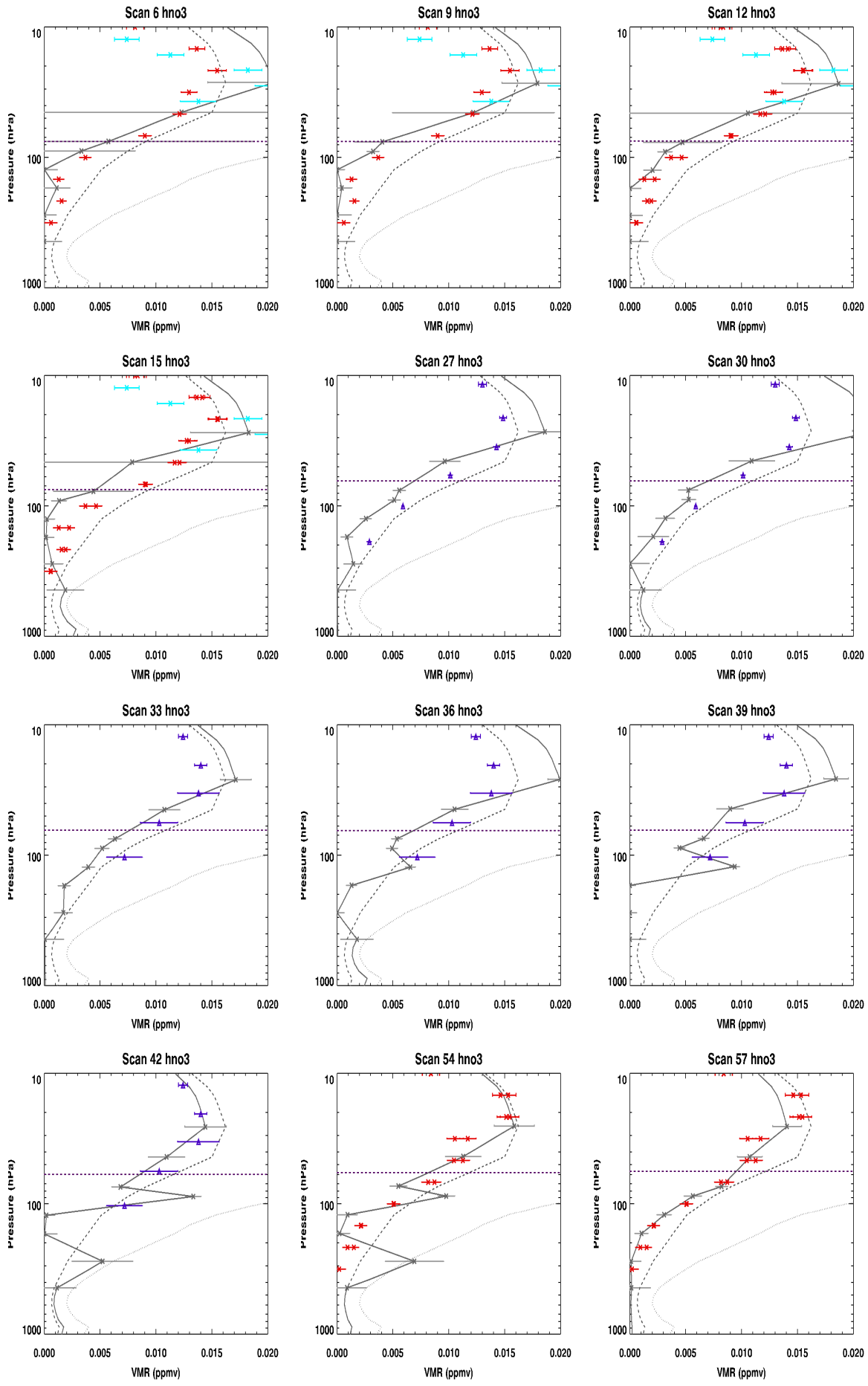

Fig. 88: MARSCHALS HNO_3 profiles for scan 6,9, 12, 15, 27, 30, 33, 36, 39, 42, 54, 57 (in grey) together with initial guess profile (dashed) and correlative measurements: MLS in red, MIPAS in blue, SMR in cyan. Dashed purple line indicates the flight altitude level.

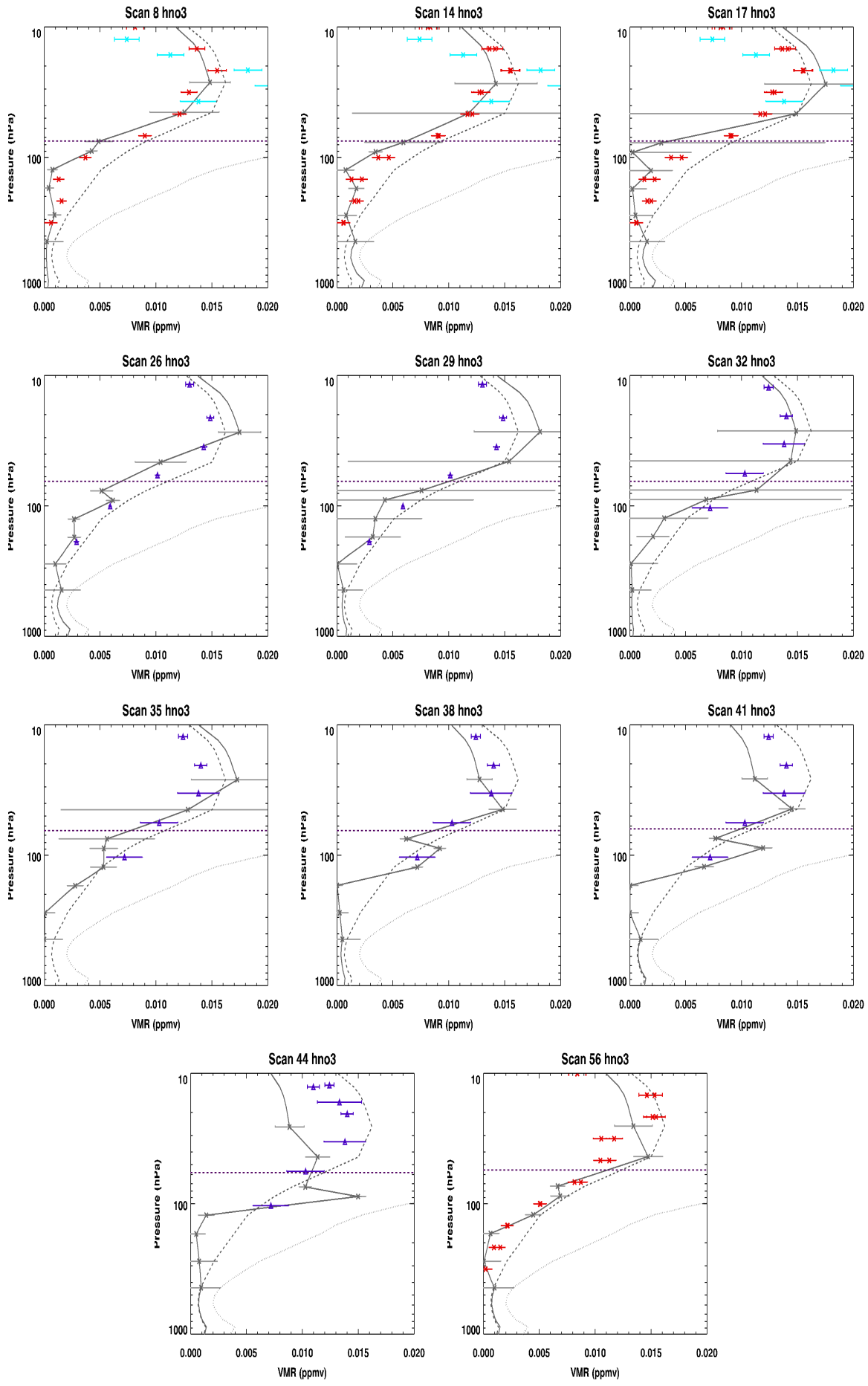

Fig. 89: MARSCHALS HNO_3 profiles for scan 8, 14, 17, 26, 29, 32,35, 38, 41, 44, 56 (in grey) together with initial guess profile (dashed) and correlative measurements: MLS in red, MIPAS in blue, SMR in cyan. Dashed purple line indicates the flight altitude level.

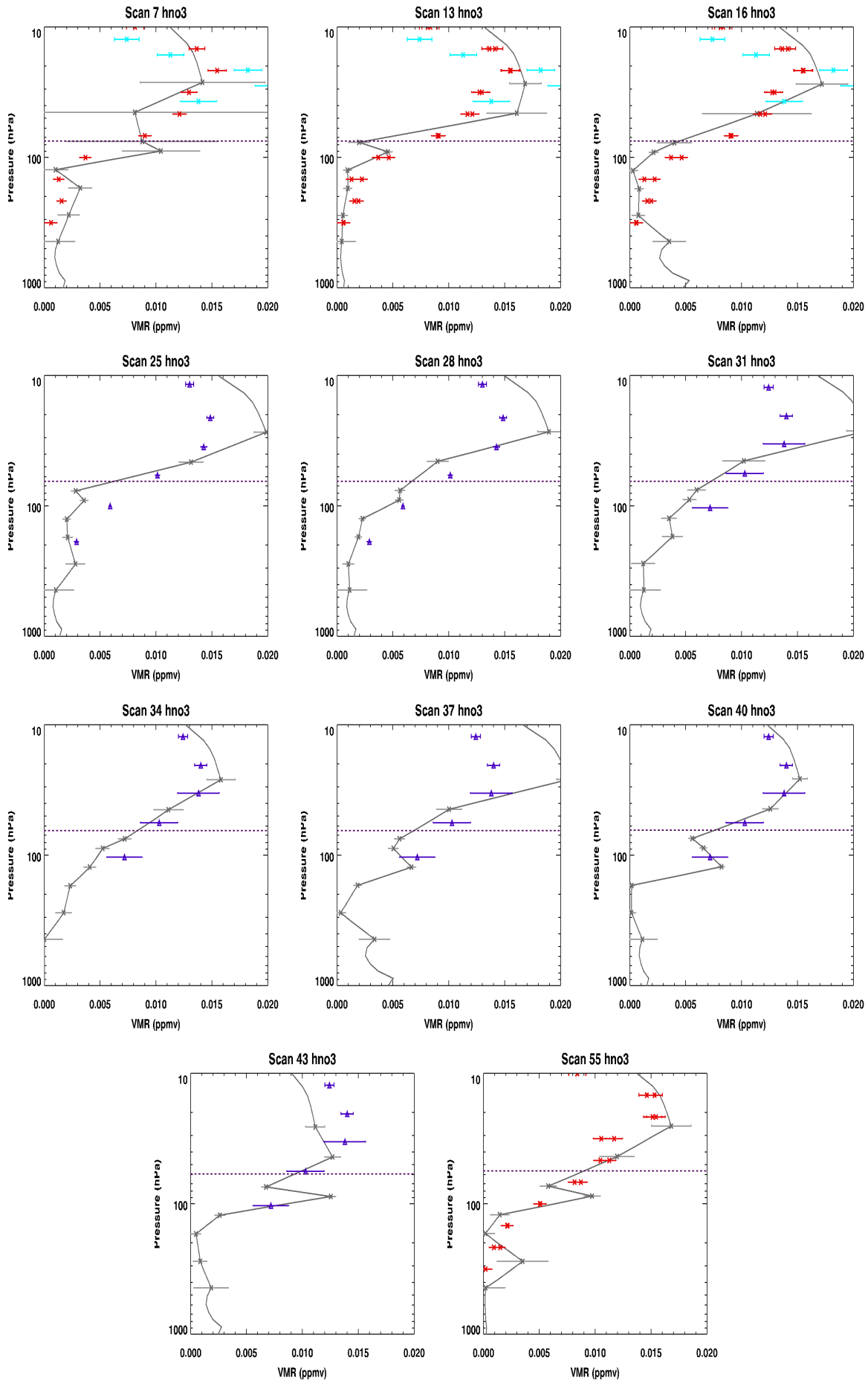

Fig. 90: MARSCHALS HNO_3 profiles for scan 7, 13, 16, 22, 25, 28, 31, 34, 37, 40, 43, 55 from recursive retrievals analysis (in grey) together with initial guess profile (dashed) and correlative measurements: MLS in red, MIPAS in blue, SMR in cyan.

N_2O results obtained from scan 22 to 43 that approximately crosses the same air masses with about 50 minutes delay.

The results of the comparisons are reported in Fig. 91. The agreement with N_2O MARSCHALS profiles and both ODIN/SMR and AURA/MLS for the first part of the flight (scan 7, 13 and 16) is good below flight altitude in the altitude range covered by the satellites data.iAbove flight altitude MARSCHALS profiles show a positive bias with respect both satellite data. The same behaviour is found for MARSCHALS profiles with respect to the ENVISAT/MIPAS profiles for scans from 25 and 28. It actually appear that the minimum found at low altitudes is confirmed by MIPAS data. The comparison with HAGAR data for the same scan is good above 200hPa. Scans 31, 34, 37 and 40 show very strong oscillations with respect to other scans and the N_2O retrieval becomes problematic. This oscillations are due to the reduced measurement coverage for these scans (low value of trace and information content). Comparison of N_2O from scan 43 and HAGAR data show lower values for MARSCHALS data. N_2O profile from scan 55 show some oscillations, even if at higher altitudes they agree with AURA/MLS data.

In general the N_2O MARSCHALS retrieved profiles oscillates, however the comparison with satellite data show a quite good agreement with all the three instruments used for this comparison below flight altitude in the altitude range covered by the satellites data. The comparison with HAGAR data show good agreement above 150-200 hPa while at lower altitudes the MARSCHALS N_2O values are lower than the HAGAR ones.

7.1.6 CO validation

The CO profiles can be validated only using Aura/MLS satellite data and the comparison are reported in Fig. 92.

The MARSCHALS retrieved CO values are lower than the MLS ones even if from MLS measurements we can see that the CO values were of the order of or also lower than our initial guess profiles. As we have seen in section 5.2.4 this profile is at the limit of the MARSCHALS sensitivity to CO.

7.1.7 Examples of comparison of MARSCHALS and AURA/MLS data using AURA/MLS Averaging Kernel

The use of the AK is quite common in the comparison of limb sounder results with other instruments. In this section we show some examples of the comparison between MARSCHALS results and AURA/MLS profiles when the AURA/MLS AK are applied to the MARSCHALS profiles for Flight 1.

The MARSCHALS retrieved profiles that MLS would observe can be calculated using:

$\mathbf{x}_M = \mathbf{x}_a + \mathbf{A}[\mathbf{x} - \mathbf{x}_a]$

where $\mathbf{A}$ is the averaging kernel matrix, $\mathbf{x}_a$ is the MLS a priori, $\mathbf{x}$ is the true profile (in our case the MARSCHALS profiles). In order to perform this calculation the MARSCHALS profiles were interpolated on the same pressure grid of MLS AK.

The MLS **n**x**n** AK are available via web and are calculated at the equator or at 70 N latitude degrees. For our analysis we used the AK calculated at 70 N latitude degrees. The AK can be obtained from the web site http://mls.jpl.nasa.gov/data/ak/ (see the MLS Version 3.3 Level 2 data quality and description document). In the same web site (http://mls.jpl.nasa.gov/) it is also possible to obtain the a priori profiles needed for the calculation.

The results of the convolution of MARSCHALS profiles with MLS AK are shown in Fig. 93 and 94. In each panel are reported MARSCHALS retrieved profiles in blue, MLS profiles in red and MARSCHALS profiles after the convolution with MLS AK in cyan for temperature, H_2O, HNO_3, O_3.MARSCHALS results for temperature, H_2O, HNO_3, O_3 for scan 6 are shown in Fig. 93, while in Fig. 94 are shown results for temperature, H_2O, HNO_3, O_3 for scan 57, CO from MARSCHALS scan 56 and N_2O from scan 55. The errors associated to the convoluted MARSCHALS profiles are obtained from the interpolation of the original errors on the MLS pressure grid and are reported only in order to give an estimate of the size of MARSCHALS errors.

All the results presented in Fig. 93 and Fig. 94 show how the convolution with the MLS AK smoothes the MARSCHALS profiles (e.g. see O_3 profile around 100 hPa).

In general a good agreement is obtained when the MLS AK are applied to MARSCHALS results and the use of MLS AK improves the quality of the comparison. On the other hand this exercise also show that the AURA/MLS satellite data can not completely resolve the finer vertical structures seen by the MARSCHALS instrument.

7.1.8 Examples of comparison of MARSCHALS and in-situ data using MARSCHALS Averaging Kernel

In this section we show some examples of comparison between MARSCHALS results and in-situ profiles when the MARSCHALS AK are applied to the in-situ profiles for Flight 1. The profiles that MARSCHALS would observe are calculated using equation 1 used for the convolution of models data with MARSCHALS AK. In case of in-situ data we interpolate the in-situ profiles over the 500 m altitude grid used for the models. Data above the highest and below the lowest cwaltitudes of the in-situ data were set equal to the data obtained by the CLAMS model.

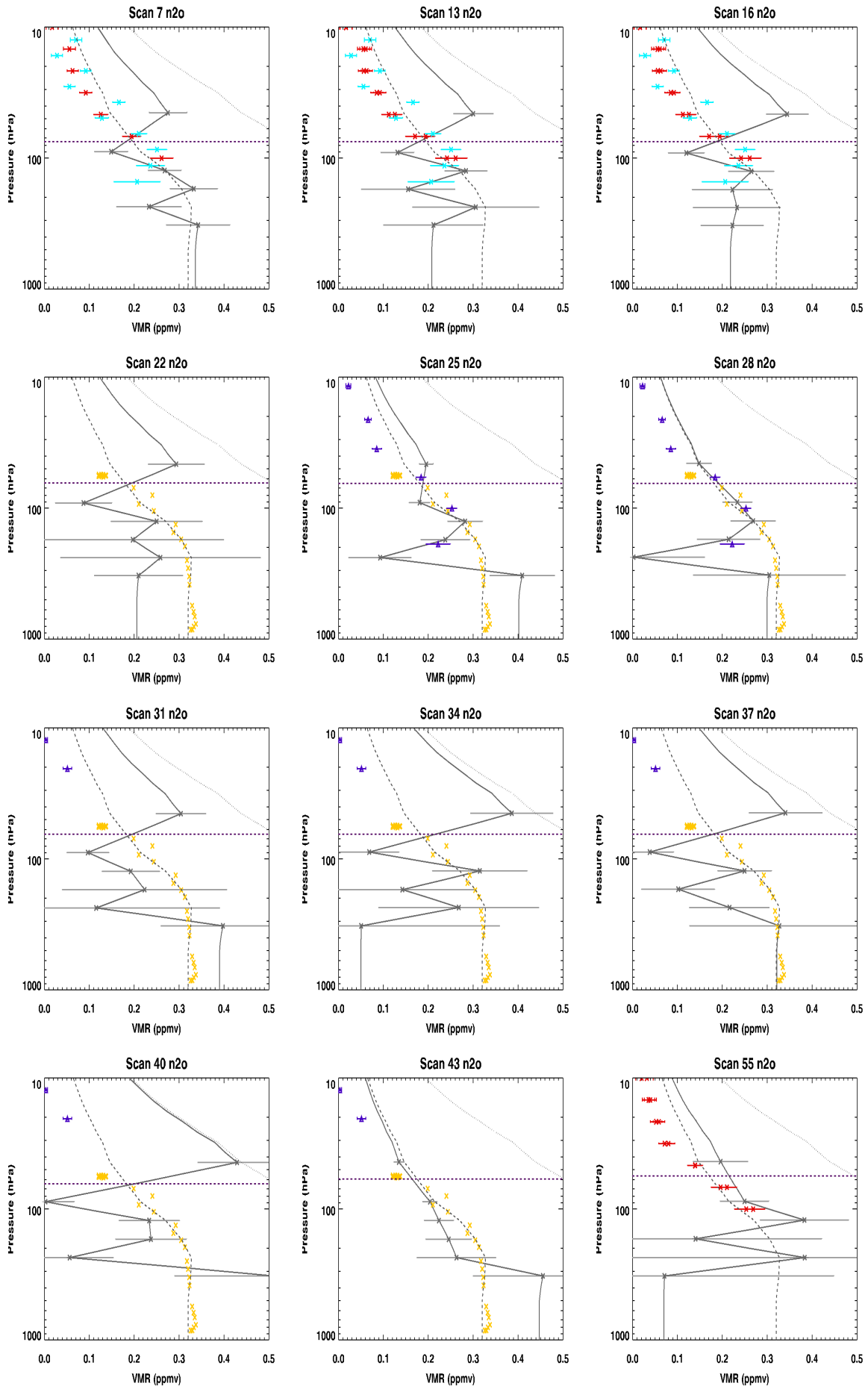

Fig. 91: MARSCHALS N_2O profiles for scan 7, 13, 16, 22, 22, 25, 28, 31, 34, 37, 40, 43, 55 (in grey) together with initial guess profile (dashed) and correlative measurements: MLS in red, MIPAS in blue, SMR in cyan and in in situ data (HAGAR) in yellow. Dashed purple line indicates the flight altitude level

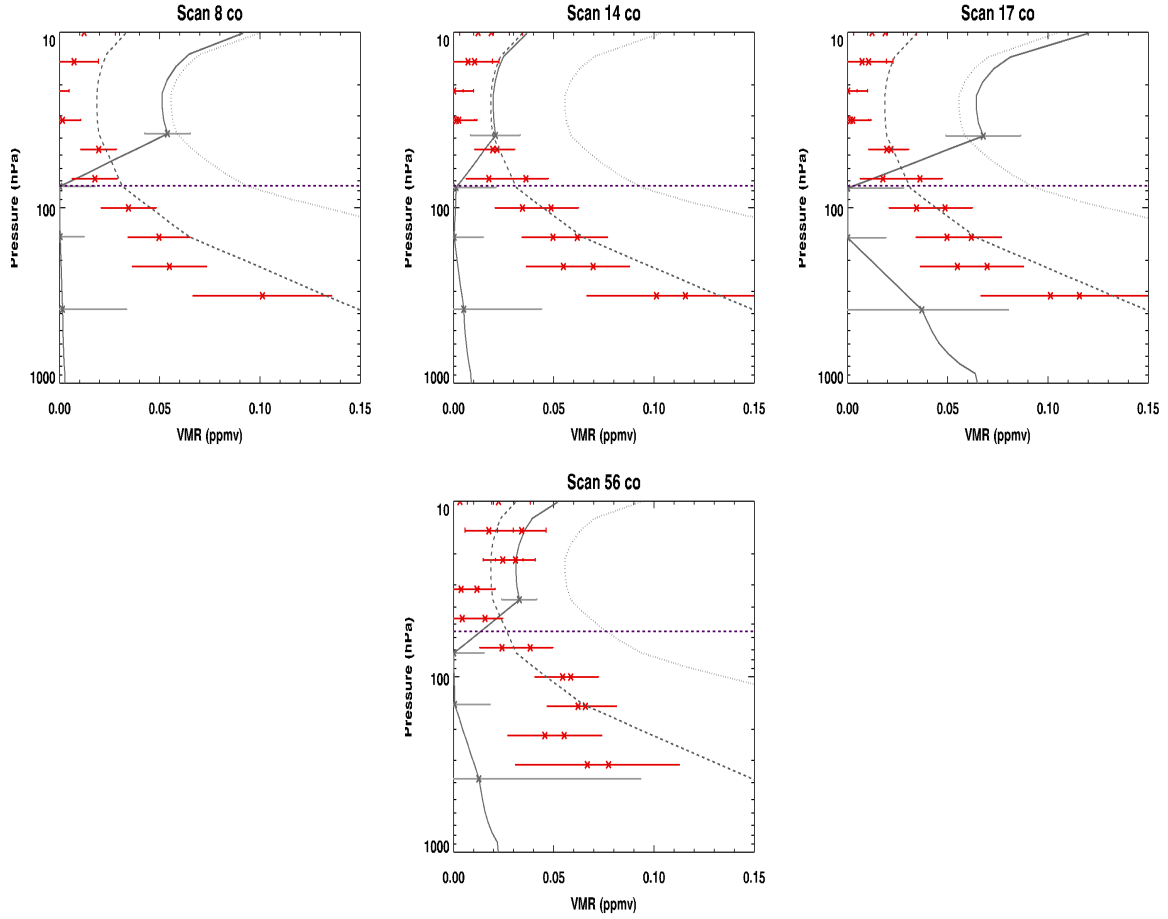

Fig. 92: MARSCHALS CO profiles for scan 8, 14, 17, 56 (in grey) together with initial guess profile (dashed) and correlative measurements: MLS in red. Dashed purple line indicates the flight altitude level

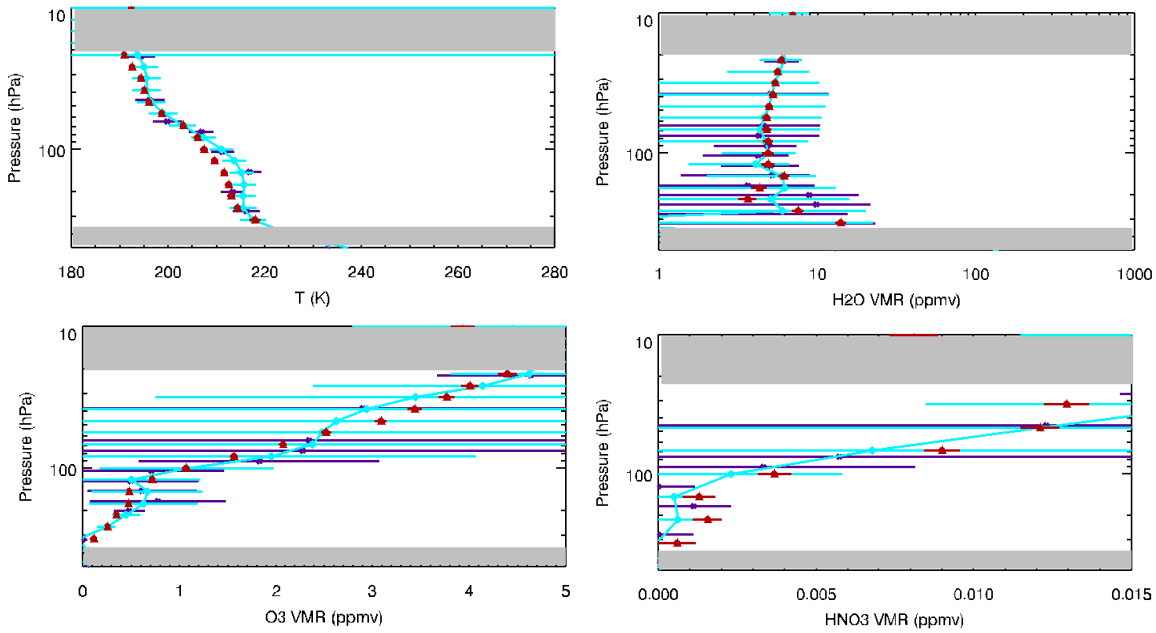

Fig. 93: MARSCHALS temperature, H_2O , O_3 , HNO_3 for scan 6 (in blue) together with MLS profile (red) and MARSCHALS profiles after the convolution with MLS AK (in cyan).

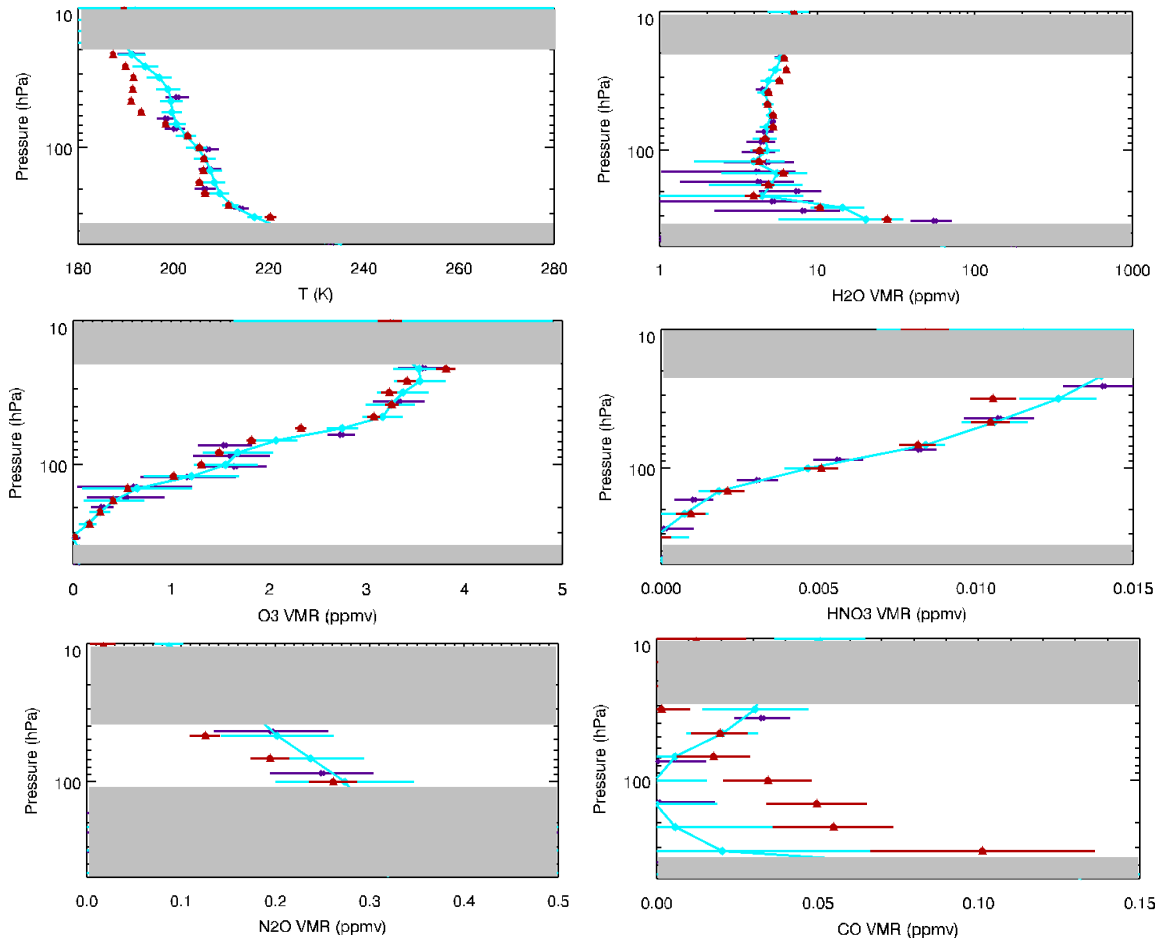

Fig. 94: MARSCHALS temperature, H_2O , O_3 , HNO_3 for scan 57, N_2O scan 55, CO from scan 56 (in blue) together with MLS profile (red) and MARSCHALS profiles after the convolution with MLS AK (in cyan).

The comparison of MARSCHALS results with convoluted in-situ profiles is then performed only in the altitude region covered by the in-situ data. In Figs. 95 and 96 are reported the comparison between MARSCHALS retrieved profiles for $H_2O$and $N_2O$and in-situ profiles obtained from FISH and HAGAR convoluted with MARSCHALS AK (in blue) togheter with FISH and HAGAR profiles mesured during descent. The comparison has been performed for MARSCHALS scans 27, 30, 33, 36, 39, 42 for $H_2O$and 22, 25, 28, 31, 34, 37, 40, 43 for N_2O.

In figure 97 we report, as an example, the results of the comparison of MARSCHALS temperature profile obtained from scan 33, 42 and 45 and the profile obtained from the Sodankyla station at 12 (in green) togheter with the same profile convoluted with MARSCHALS AK. It can be noticed that in these cases the profiles convoluted with MARSCHALS AK are in good agreement with the MARSCHALS one (even if an oscillations are present in MARSCHALS scan 42).

In general, for Flight 1, the conclusions obtained comparing MARSCHALS results with in-situ data can be extended to the comparison of MARSCHALS results with in-situ data convoluted with MARSCHALS AK.

7.1.9 Flight 1 validation: Conclusions

The validation of MARSCHALS retrieved profiles for Flight 1 can be performed using data from AURA/MLS, ODIN/SMR and ENVISAT/MIPAS satellites. Furthermore data for H_2O (FISH) and N_2O (HAGAR) are available during ascent and descent from in-situ instruments on board the M55 Geophysica. Radiosoundings are available from the Bodo and Sodankyla, Sundsvall and Orland stations for the validation of temperature and H_2O profiles.

Temperature retrieved by MARSCHALS provide good results except for some spikes in some profiles in comparison with satellite data, radiosoundings and radiosoundings convoluted with MARSCHALS AK.

MARSCHALS profiles for H_2O show a general quite good agreement with the correlative measurements (satellite data, radiosoundings and in-situ) even if the quality of the retrieved profiles varies from scan to scan due to the different measurements coverage.

Also O_3 profiles are in good agreement with all the satellite data. As for water, the quality of the retrieved profiles varies from scan to scan.

In case of HNO_3 retrievals a quite good agreement is found with satellite data, some scans in band C shows lower values with respect to AURA/MLS and ENVISAT/MIPAS data.

N_2O retrieved profiles show strong oscillations especially for those scans with reduced information content values. In general N_2O profiles are in good agreement with the AURA/MLS below flight altitude even if MLS measurements covers only a reduced altitude range with respect to MARSCHALS. A negative bias is present above flight altitude. The agreement is good also with ODIN/SMR (comparison performed on three scans) and ENVISAT/MIPAS (comparison available for two scans). However MARSCHALS N_2O profiles show a slightly worse agreement in comparison with in-situ data at lower altitudes (this is true also in the case in which HAGAR data are convoluted with MARSCHALS AK).

Comparison between MARSCHALS CO profiles and AURA/MLS profiles show that MARSCHALS profiles are always lower below flight altitude with respect to the MLS ones and comparable above. Since MLS CO values are of the same order of magnitude of our CO initial guess profiles, and, as we have seen in section 5.2.4, the IG2 polar winter profile is at the limit of the MARSCHALS sensitivity to CO we can conclude that with the current instrument configuration and auxiliary data MARSCHALS cannot measure CO below flight altitude with satisfactory results.

In general quite good results are obtained for Flight 1 despite of the fact that the pointing problems encountered during the flight prevent the nominal vertical coverage of the measurements to be achieved.

7.2 Validation of the Flight 2 measurements

For the satellite instruments ODIN/SMR, ENVISAT/MIPAS and AURA/MLS we have found correlative measurements for all of them. On the 16^{th} of December 2011, ENVISAT/MIPAS sounded the atmosphere near Kiruna with two orbits 51229 (recorded at 10:44 UTC around -4 deg. longitude) and 51235, (recorded at 20:33 UTC at about 25 deg. longitude). Selected scans from these orbits were used for the validation of MARSCHALS scans in the middle of the flight (scans 10-13) and at the end of the flight (scans 30-32).

On the 16 December 2011 MLS measurements in the region sampled by the Geophysica flight were performed at 11:43 UTC. These data can be used for the validation of MARSCHALS scans at the beginning and in the middle of the flight, from scan 8 to 27. The SMR instrument sounded the atmosphere near Kiruna at 16:50 UTC and 18:24 UTC around 25 and 2 longitude degrees. We used these data for the validation of MARSCHALS scans in the middle (scans 10-13 and 18) and at the end (scans 30-33) of the flight.

The coincidence between MLS (in red), MIPAS/ENVISAT (in blue), SMR (in cyan) and MARSCHALS (grey) measurements is presented in Figure 98, while in figure 99 are shown the coincidences with radiosondes stations.

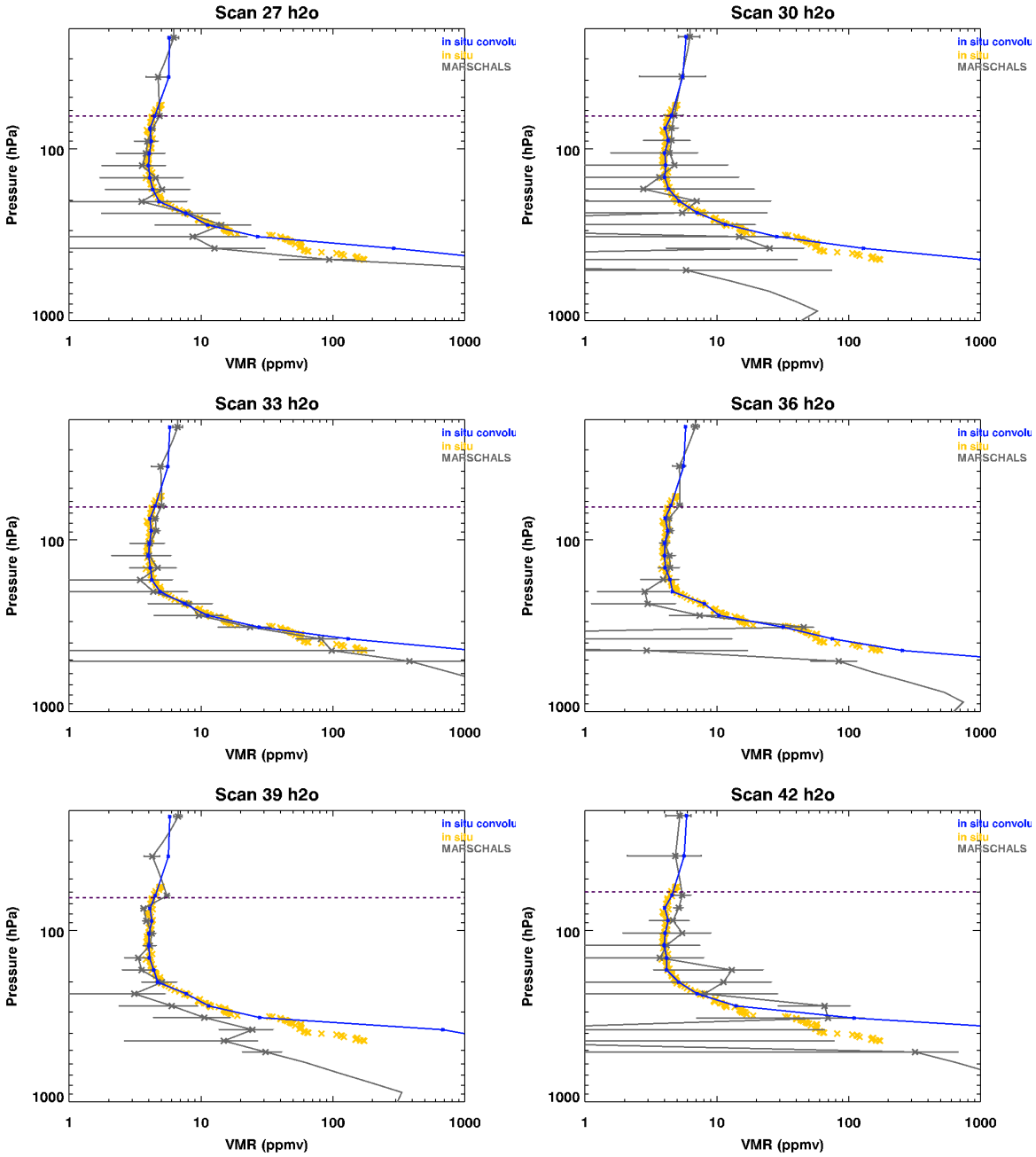

Fig. 95: MARSCHALS H_2O for scans 27, 30, 33, 36, 39, 42 together with FISH profiles (yellow) and FISH profiles after the convolution with MARSCHALS AK (in blue).

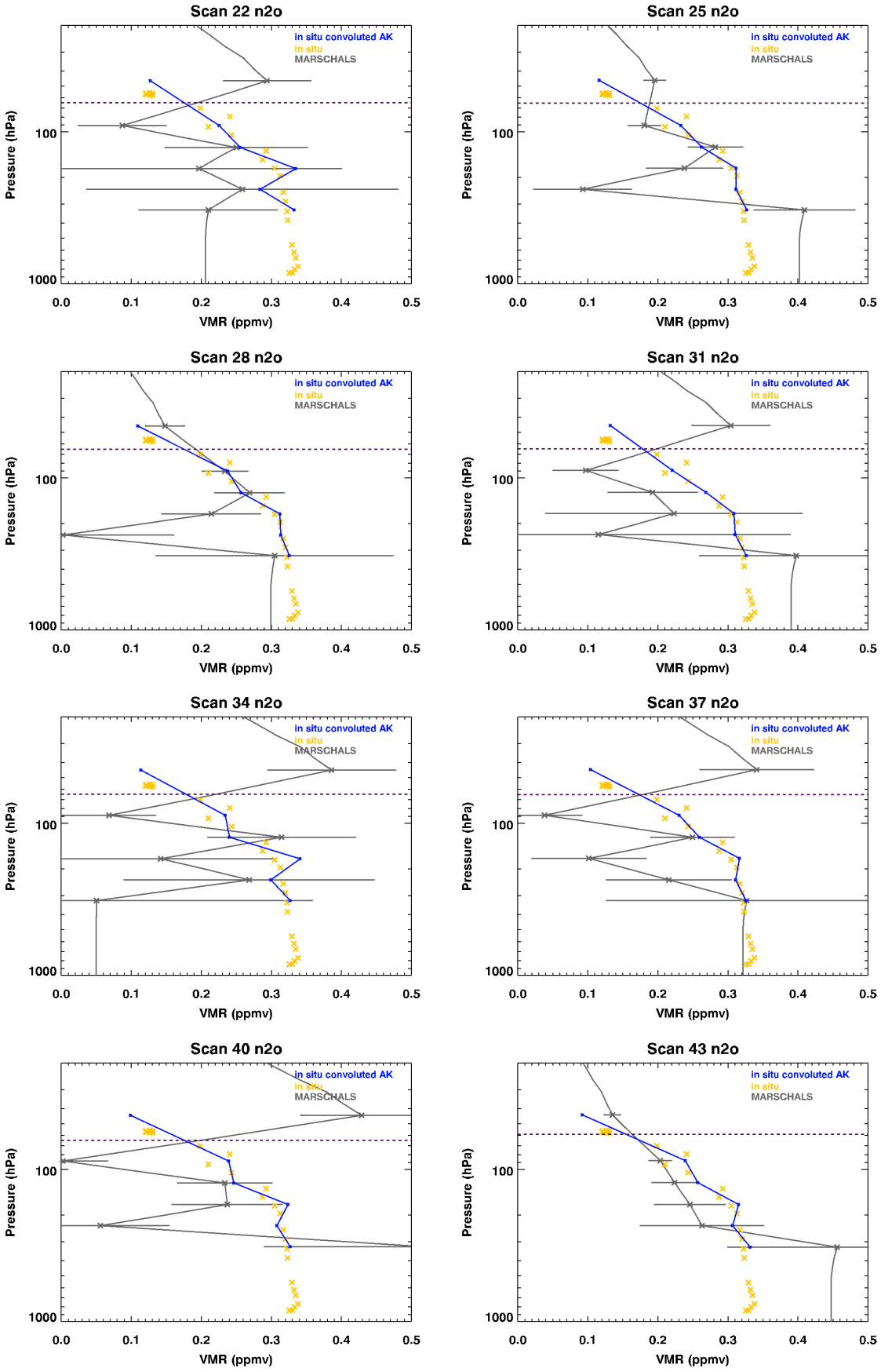

Fig. 96: MARSCHALS N_2O for scans 22, 25, 28, 31, 34, 37, 40, 43 together with HAGAR (N_2Odata) profiles (yellow) and HAGAR profiles after the convolution with MARSCHALS AK (in blue).

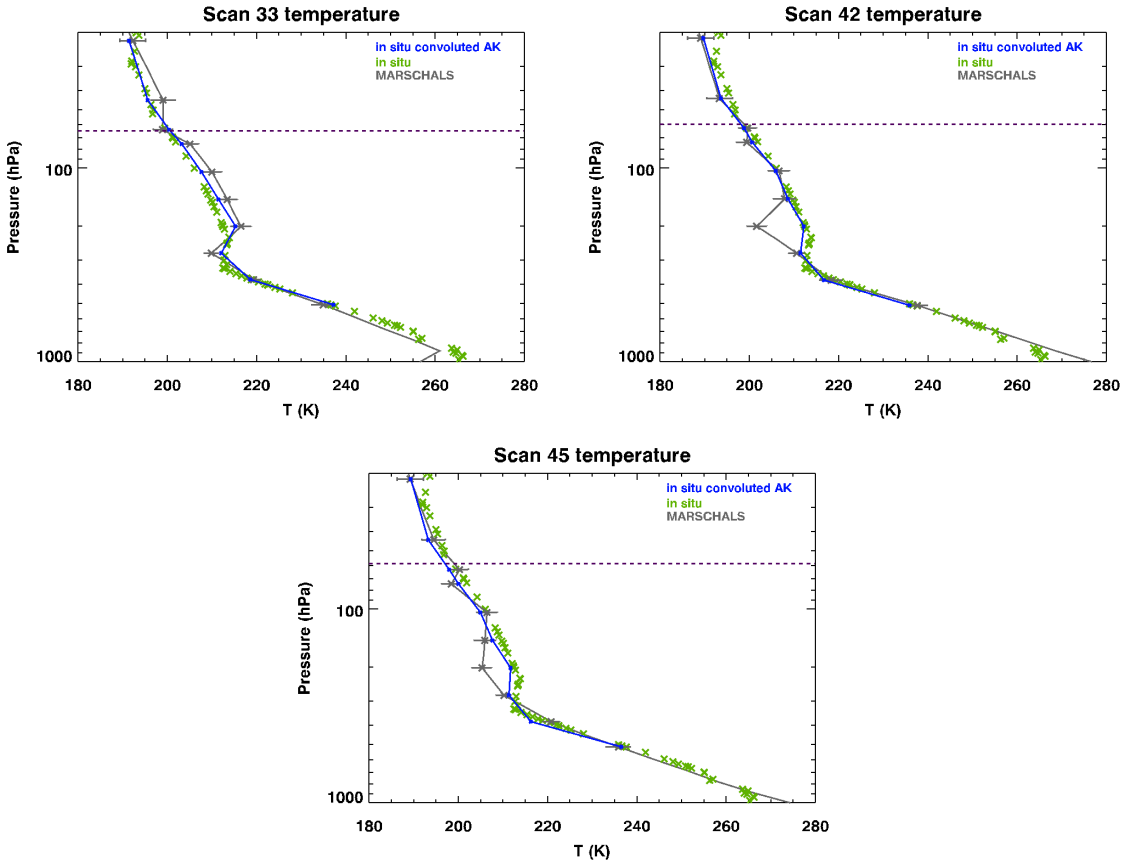

Fig. 97: MARSCHALS temperature for scan 33, 42, 45 together with Sodankyla profiles (green) and the same profiles after the convolution with MARSCHALS AK (in blue).

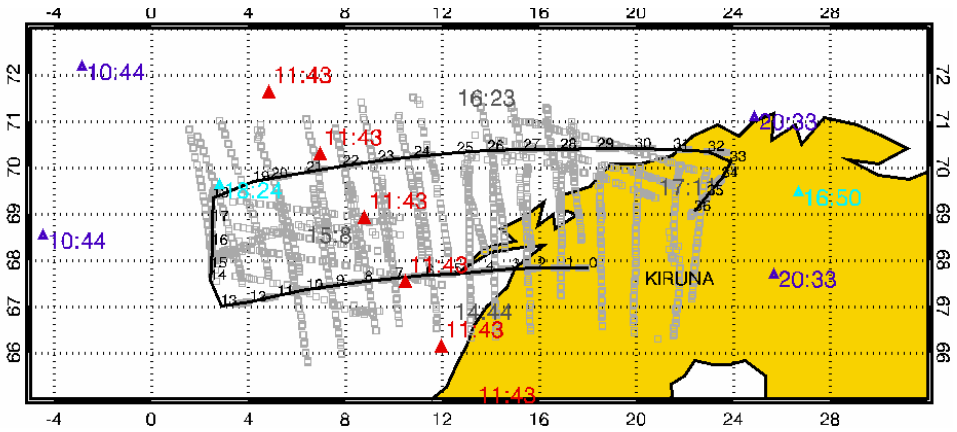

Fig. 98: MARSCHALS flight pattern and tangent points Geo-location (grey) and SMR (cyan), MLS (red) and MIPAS (blue) data Geo-locations.

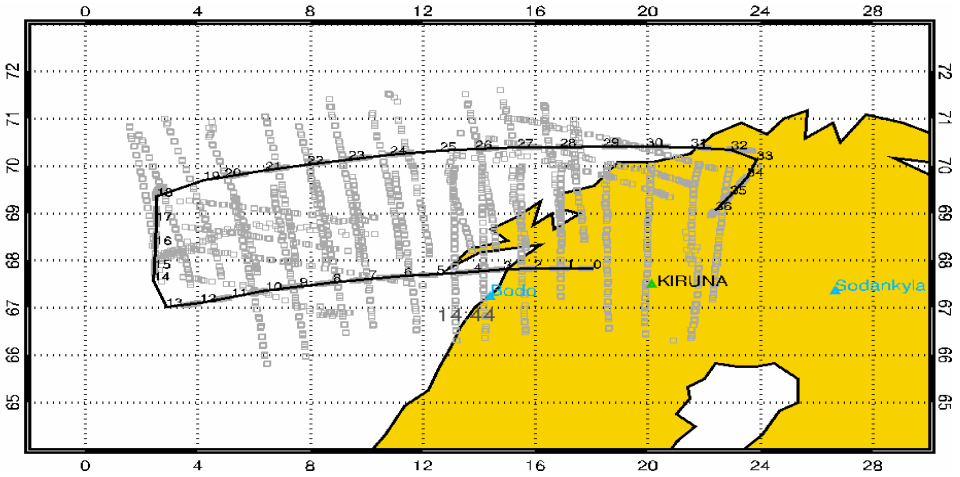

Fig. 99: MARSCHALS flight pattern and tangent points Geo-location (grey) and Radiosondes data geo-locations.

The time delay between ENVISAT/MIPAS and MARSCHALS for scans number 10-13 is about 4 hours, while for scans 30-33 is about 3 hours and 20 minutes. In the case of AURA/MLS and MARSCHALS the time displacement is about 3 hours and for scans 6-18 and about 3 hours and 30 minutes for scans 20-27. Because of the representation of AURA/MLS data in terms of atmospheric pressure, all the figures used for the validation exercise report MARSCHALS targets as a function of pressure. In the case of ODIN/SMR and MARSCHALS the time displacement is about 20 minutes for scans 30-33 and 3 hours and 30 minutes for scans 10-18. In general a quite good temporal and spatial coincidence is achieved for AURA/MLS and MARSCHALS data and a quite good coincidence for ENVISAT/MIPAS and ODIN/SMR data.

As already said and as can be noticed from Figure 39 during the flight the M55 Geophysica did not perform any dive. For this reason the possibility of retrieving informations about vertical profiles of atmospheric constituents using in situ sensors on board the aircraft is limited to the ascending and descending part of the flight at Kiruna.

For Flight 2 is also possible to cross-validate the MARSCHALS results since the tangent points of some scans crosses exactly the same air masses with close time coincidence. This is the case of scans 8-22, 9-21, 10-20 (see Fig. 100) that have a maximum time difference of 1h and 07 minutes. Scan 10 (in band B) and scan 20 (in band D) are in close time coincidence however the results of scan 20 are not so good (see very low gain value in Fig. 53) and for this reason the result of the comparison is not so good. Scan 9 and scan 21, in close time coincidence (58 min.) are both in band C and for this reason T, H_2O, O_3, HNO_3 profiles can be compared. The results of this comparison are shown in Fig. 101 with results for scan 9 in red and for scan 22 in blue. As can be noticed an very good agreement is found particularly for O_3 and $HNO_3\dot{O}_3$ profiles for Scan 8 (in band D) and scan 22 (in band B) are compared in Fig. 102 with results for scan 8 in red and for scan 22 in blue. also in this case a very good agreement is found (e.g. peak at 14 km).

7.2.1 Temperature validation

Temperature profiles obtained from MARSCHALS measurements can be validated using both satellite data (ENVISAT/MIPAS, AURA/MLS, ODIN/SMR), radiosondes (from Bodo and Sodankyla) and UCSE temperature data obtained during the M55 Geophysica ascent and descent.

In Fig. 103 are reported the temperature profiles retrieved from MARSCHALS measurements for scans 3, 6, 9, 12, 21, 24, 27, 30 (in grey) together with the a priori profile (dashed grey) and correlative measurements. Data from the Bodo (used for the coincidence with scans 3 to 27) and Sodankyla (used for the coincidence with scan 30) stations are reported in green, temperature profile from UCSE data during the descent are reported in yellow. Satellite data are reported as follows: AURA/MLS in red, ENVISAT/MIPAS in blue, ODIN/SMR in cyan. Apart from scan 24 a general good agreement can be found between MARSCHALS temperature profiles and all the correlative measurements (note that MLS profiles are very similar to our initial guess profile from ECMWF).

7.2.2 H_2O validation

H_2O profiles retrieved from MARSCHALS data can be validated using radiosounding data, in-situ data from FISH during ascent and descent and using satellite data from all the three instruments we have selected for the comparison.

Retrieved H_2O profiles are reported in Fig. 104 together with correlative measurements.

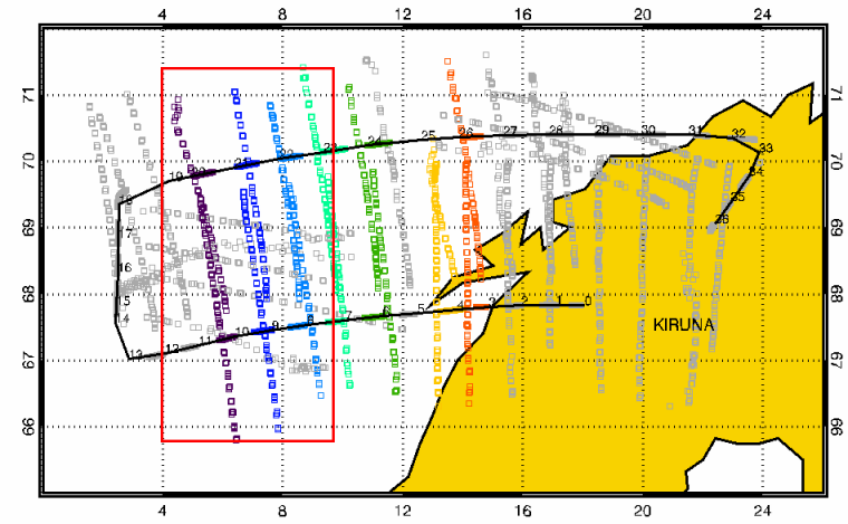

Fig. 100: MARSCHALS flight pattern and tangent points Geo-location for scans 8-22 (purple), 9-21 (blue) and 10-20 (light blue).

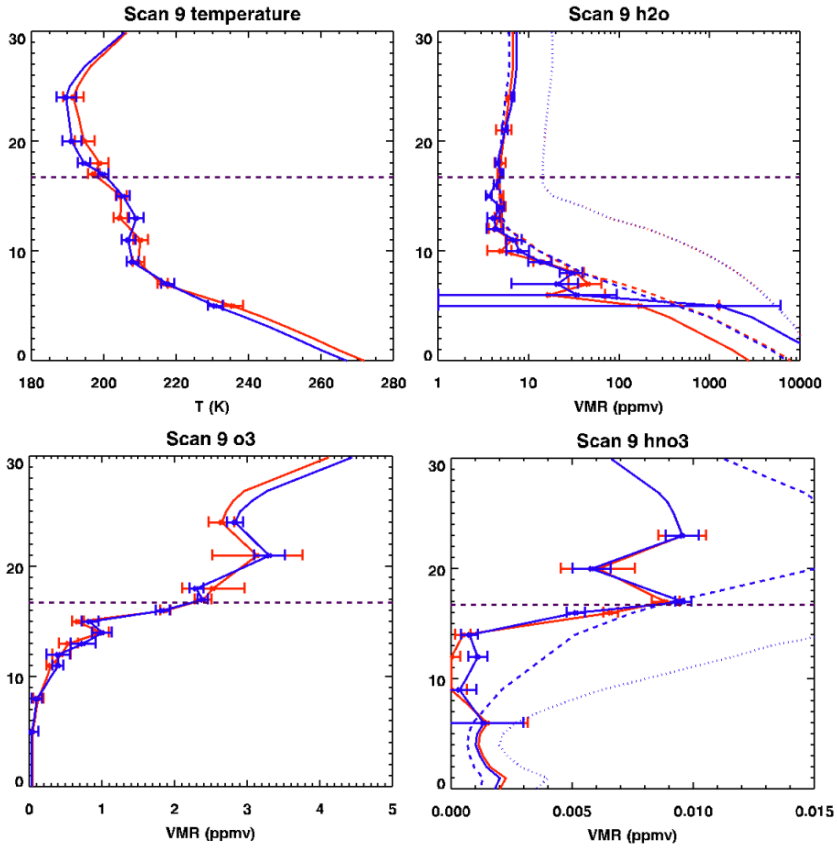

Fig. 101: Temperature, H_2O, O_3, HNO_3 profiles for scan 9 in red and 21 in blue.

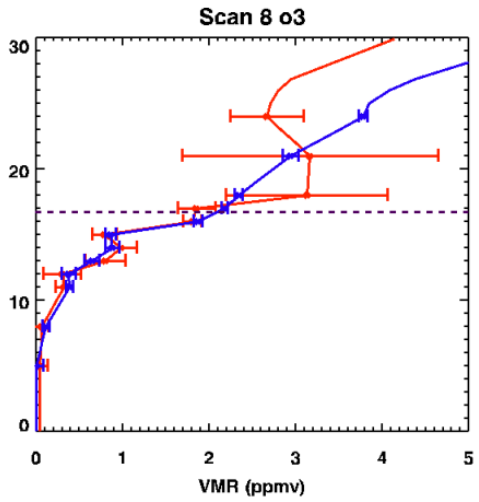

Fig. 102: O_3 profiles for scan 8 in red and 22 in blue.

Data from radiosounding stations becomes constant above about 400 hPa and can be used to infer the H_2O profile at low altitude levels. The agreement between the data from Bodo station (used for the coincidence with scans 3 to 27) and from Sodankyla station (coincidence with scan 30) are quite good apart from scans 3, 24 and 27 where the MARSCHALS profiles oscillates at low altitudes. In general, MARSCHALS H_2O profiles agree very well with AURA/MLS data, with VMR values lower than the initial guess ones for pressure levels higher than 100 hPa (see for example scans 21 and 24). Furthermore the agreement with ENVISAT/MIPAS data is quite good, even if for scan 12 the altitude range covered by the MIPAS profile is limited. The comparison with in-situ data from FISH (scan 3-12 compared with FISH data acquired during the M55 Geophysica ascent, scan 27-30 compared with FISH data acquired during the descent) show good agreement.

7.2.3 O_3 validation

O_3 profiles retrieved from MARSCHALS data can be validated using only satellite data from all the three instruments we have selected for the comparisons.

Retrieved O_3 profiles are reported in Fig. 105 (band B), Fig. 106 (band C) and Fig. 107 (band D) together with satellite data. In some cases the results from the satellite do not agree very well (see for example ODIN/SMR data in scan 10, 11, 12 in comparison with AURA/MLS and ENVISAT/MIPAS data). Possibly this is due to the quite large time discrepancy between the satellites (ODIN/SMR measurements are performed at 18:24, AURA/MLS and ENVISAT/MIPAS at 11:43 and 10:44 respectively). MARSCHALS O_3 profiles agrees very well with AURA/MLS data in almost all scans and in the whole altitude range down to 8 km. The same conclusion can be driven for the comparison with ENVISAT/MIPAS profiles towards the end of the flight. Slightly worst results are obtained from the comparison with ODIN/SMR O_3 profiles even if, as mentioned before, the O_3 ODIN/SMR profiles are not consistent also with the O_3 profiles from others satellite (possibly due to time displacement between Odin/SMR and other satellite measurements). Similar conclusions can be applied to the recursive analysis shown in Fig. 108 for band C scans.

7.2.4 HNO_3 validation

As in the case of O_3 the validation of HNO_3 MARSCHALS profiles can be achieved only using data from instruments on-board the satellites.

Comparisons of MARSCHALS HNO_3 profiles with satellite data are shown in Fig. 109 for scans in band C and in Fig. 110 for scans in band D.

In case of HNO_3 the data from the three satellite are in quite good agreement also in the altitude region above the M55 Geophysica flight altitude. For all the scans in band C the agreement with satellite data is good below flight altitude, above flight altitude the satellite data show denitrification at about 30 hPa. The same structure is present in MARSCHALS profiles (scan from 9 to 21) even if this values are acquired above flight altitude and thus with very low vertical resolution. HNO_3 profiles from band D scans show very good agreement with satellite data especially below flight altitude.

The same considerations can be applied to the results obtained from band B scans during the recursive retrieval procedure , with particularly good results for the comparison of scan 10 and 22 and satellite data (see Fig. 111).

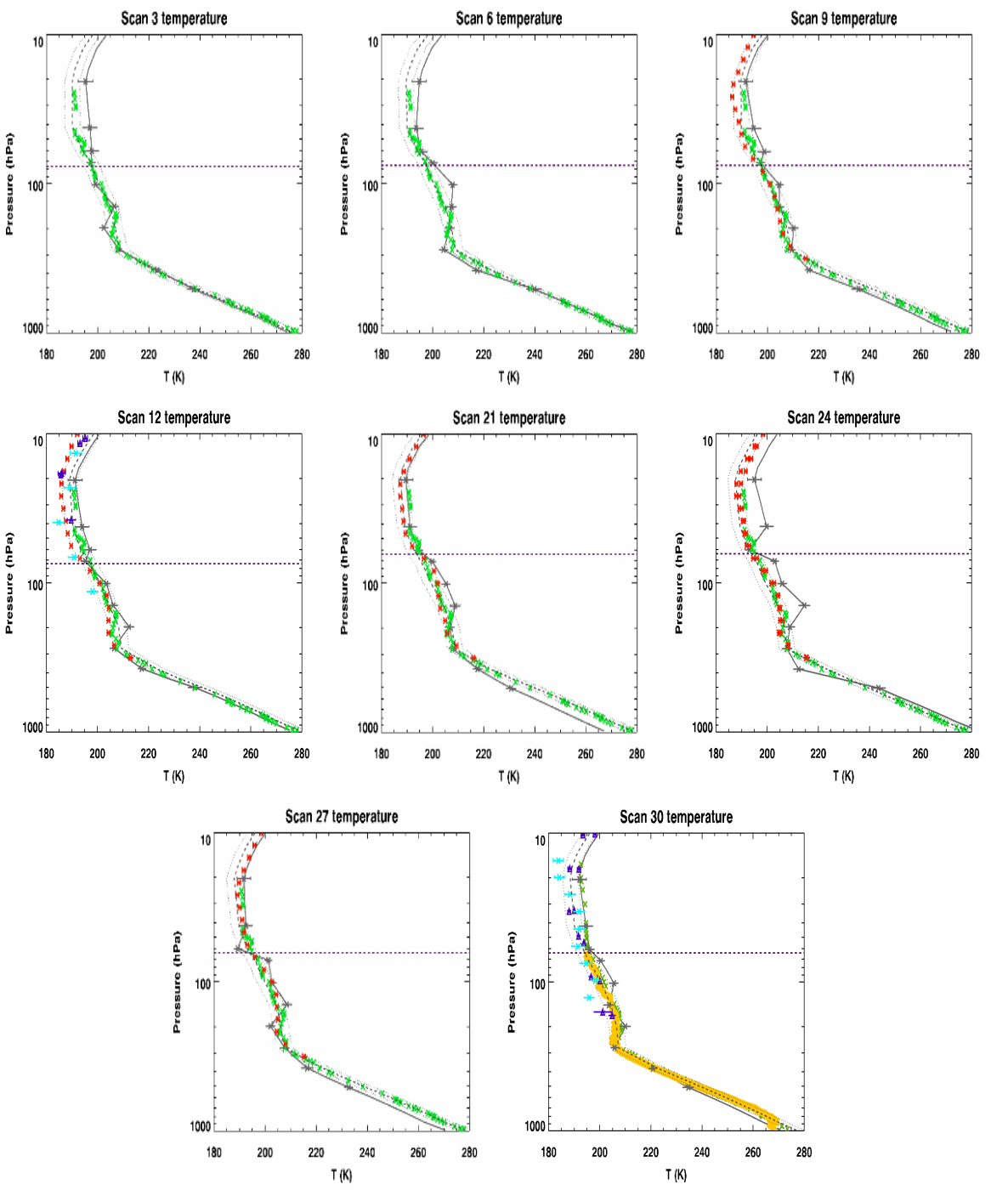

Fig. 103: MARSCHALS temperature profiles for scan 3, 6, 9, 12, 21, 24, 27, 30 (in grey) together with initial guess profile (dashed) and correlative measurements: MLS in red, MIPAS in blue, SMR in cyan, radiosonde in green and in in situ data (UCSE) in yellow. Dashed purple line indicates the flight altitude level

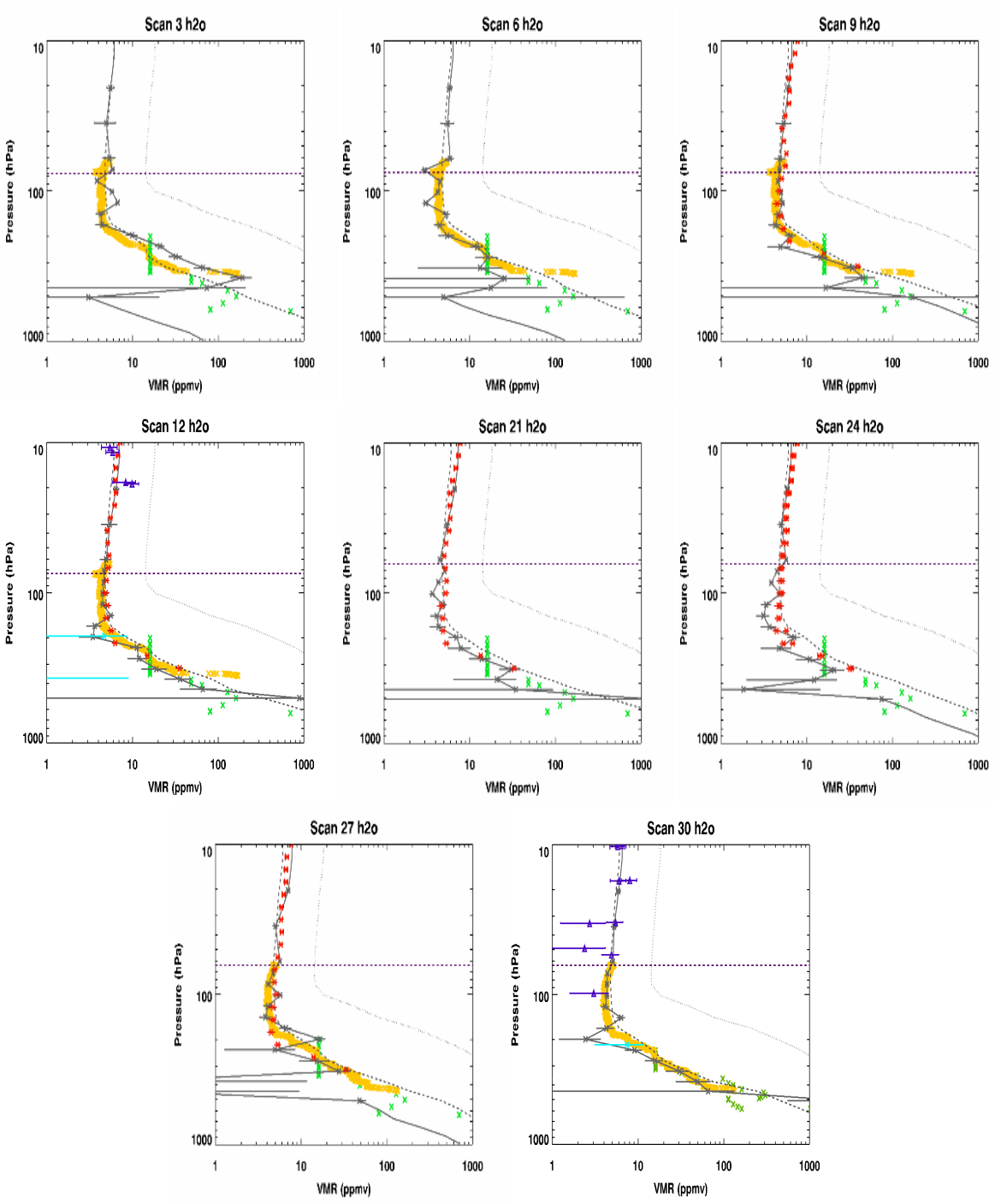

Fig. 104: MARSCHALS H_2O profiles for scan 3, 6, 9, 12, 21, 24, 27, 30 (in grey) together with initial guess profile (dashed) and correlative measurements: MLS in red, MIPAS in blue, SMR in cyan, radiosonde in green and in in situ data (FISH) in yellow. Dashed purple line indicates the flight altitude level

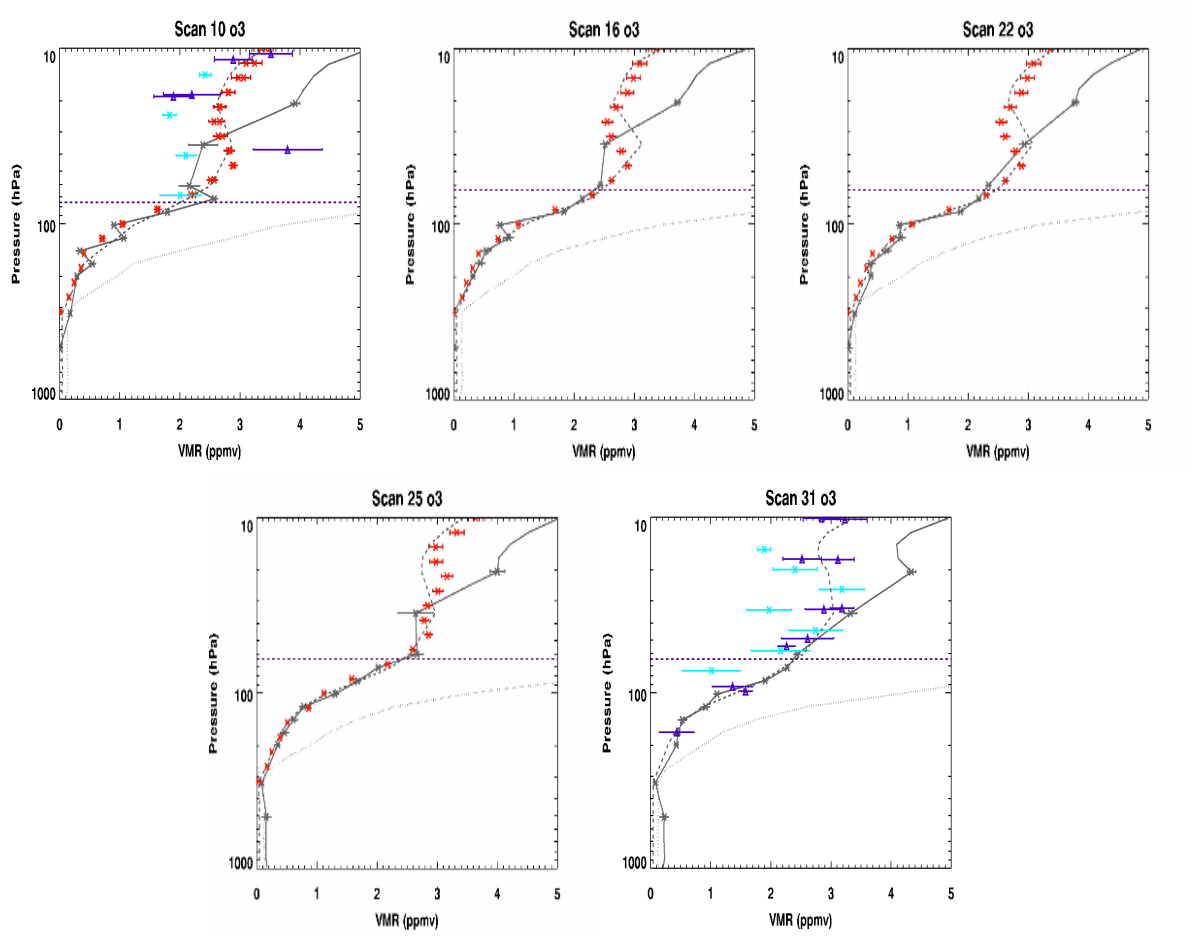

Fig. 105: MARSCHALS O_3 profiles for scan 10, 16, 22, 25, 31 (in grey) together with initial guess profile (dashed) and correlative measurements: MLS in red, MIPAS in blue, SMR in cyan. Dashed purple line indicates the flight altitude level

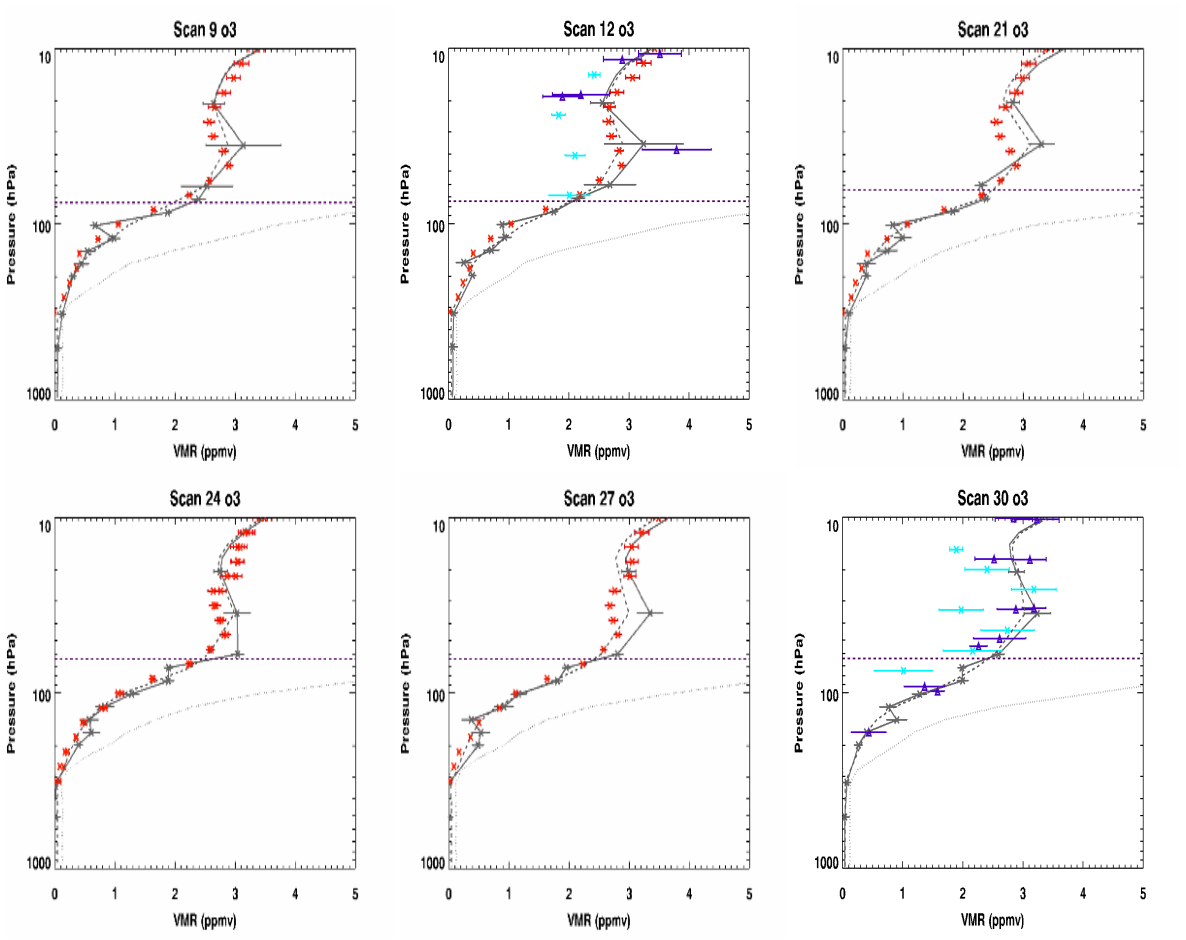

Fig. 106: MARSCHALS O_3 profiles for scan 9, 12, 21, 24, 27, 30 (in grey) together with initial guess profile (dashed) and correlative measurements: MLS in red, MIPAS in blue, SMR in cyan. Dashed purple line indicates the flight altitude level

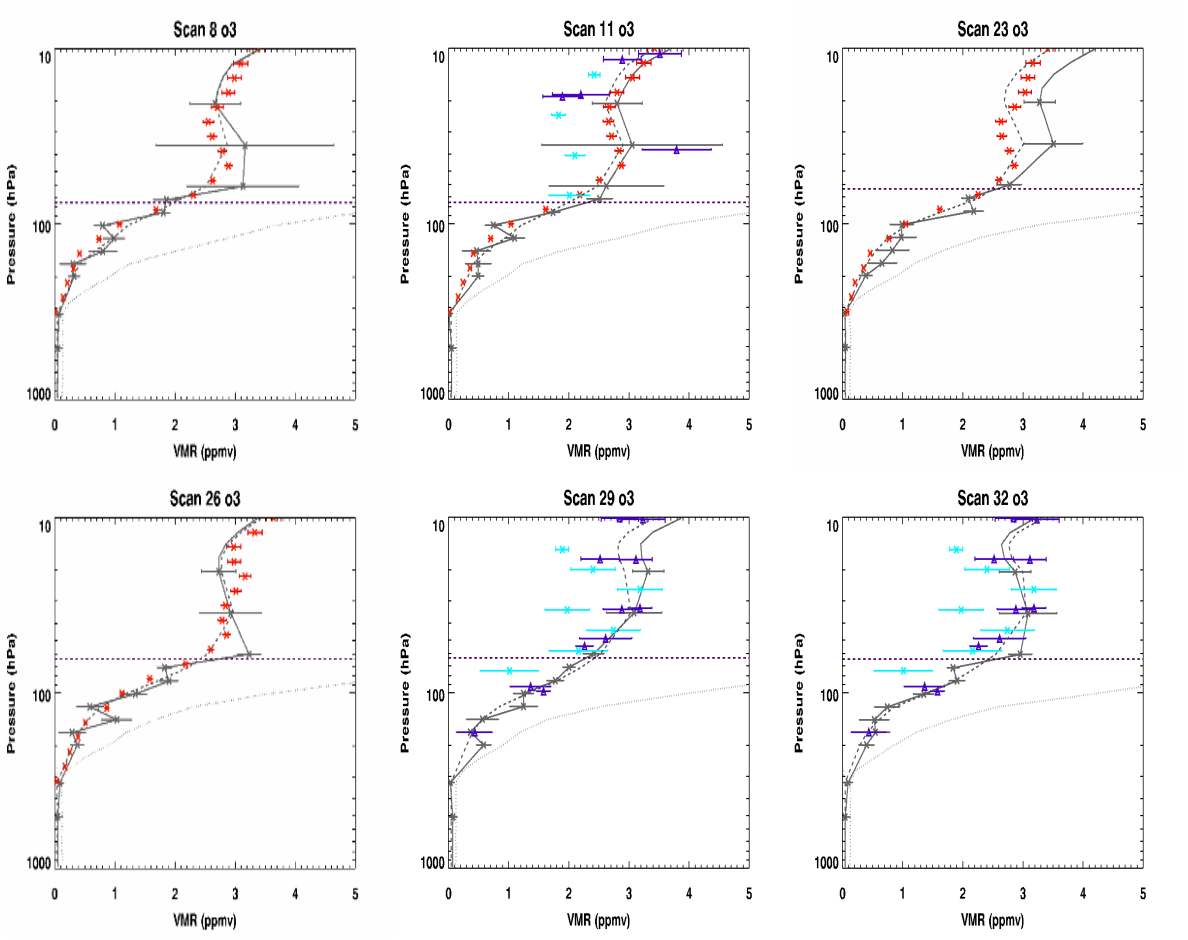

Fig. 107: MARSCHALS O_3 profiles for scan 8, 11, 23, 26, 29, 32 (in grey) together with initial guess profile (dashed) and correlative measurements: MLS in red, MIPAS in blue, SMR in cyan. Dashed purple line indicates the flight altitude level

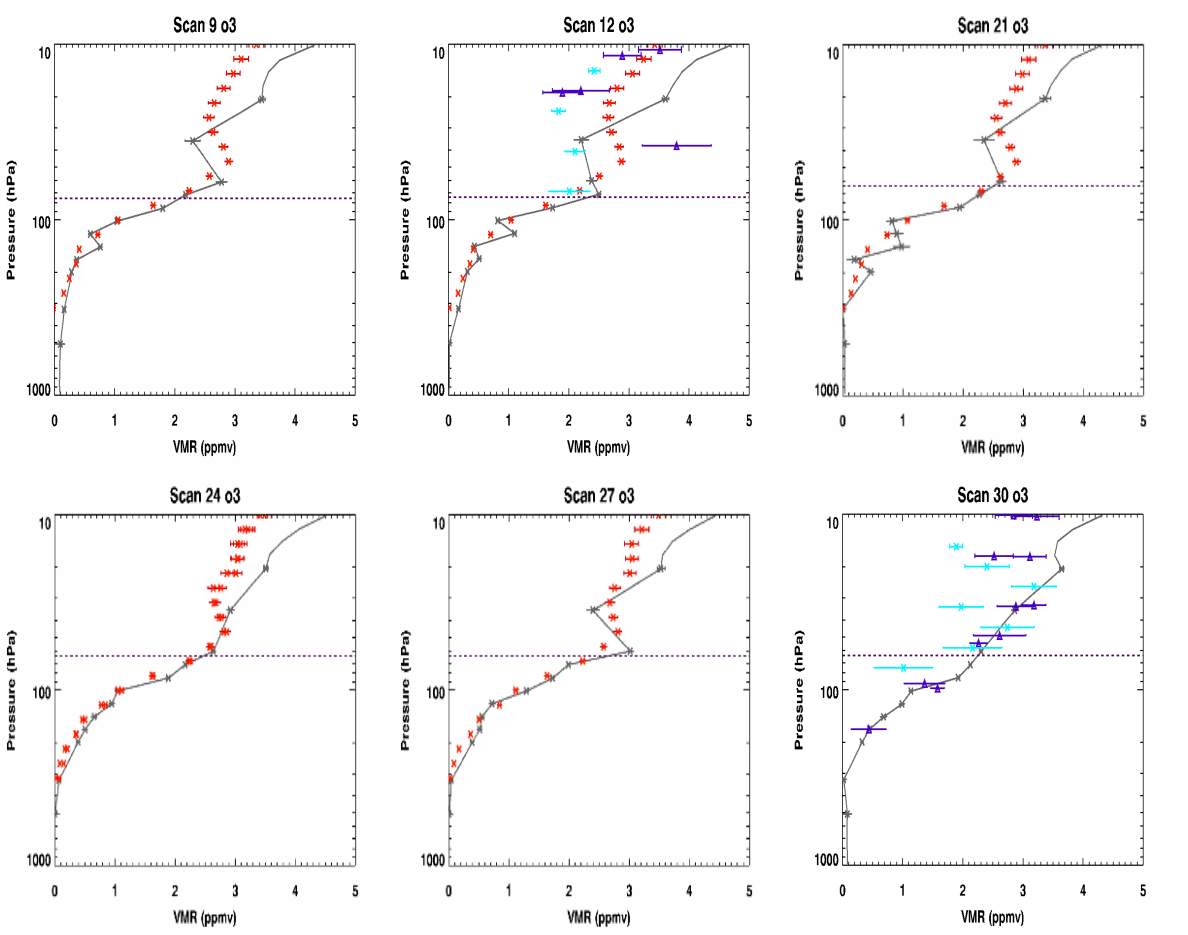

Fig. 108: MARSCHALS O_3 profiles for scan 9, 12, 21, 24, 27, 30 from recursive retrievals analysis (in grey) together with initial guess profile (dashed) and correlative measurements: MLS in red, MIPAS in blue, SMR in cyan. Dashed purple line indicates the flight altitude level

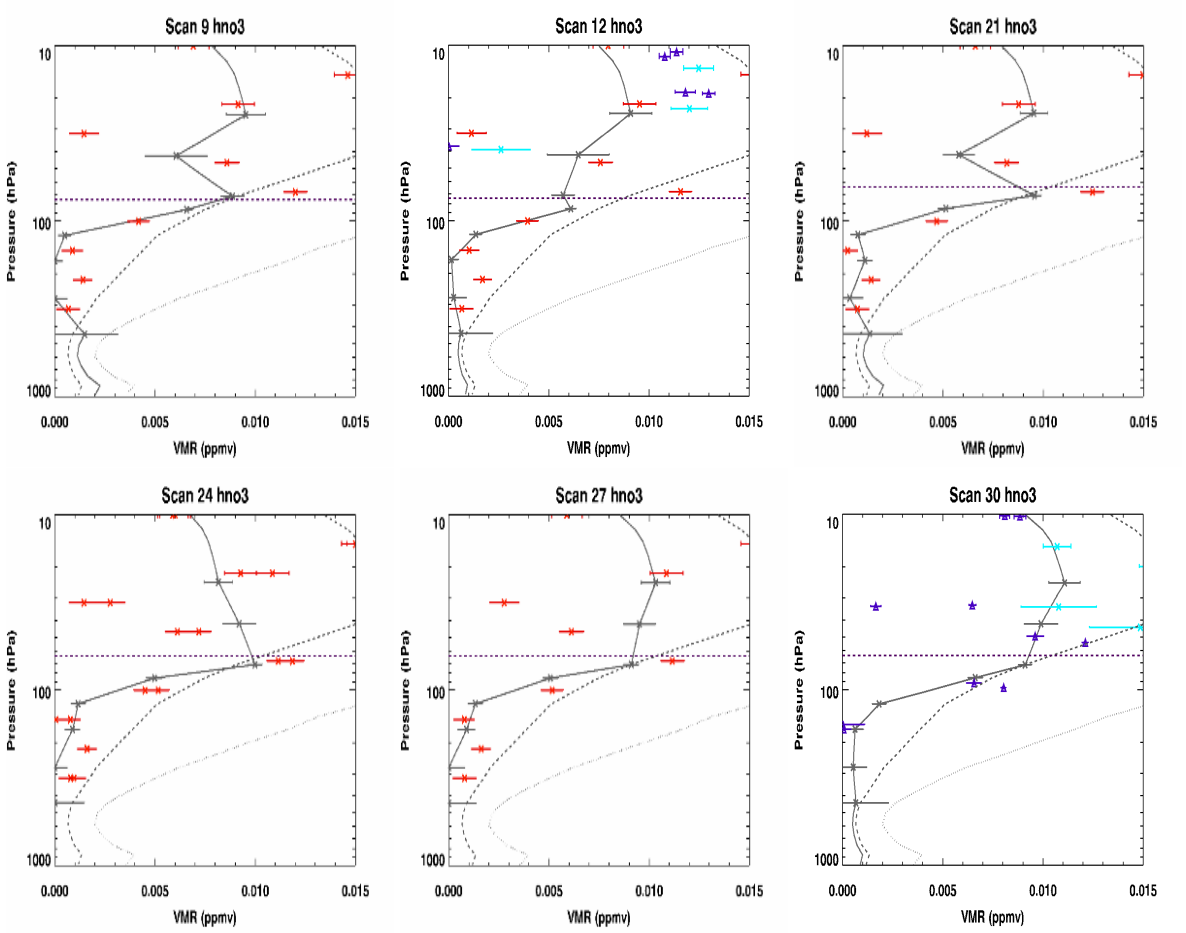

Fig. 109: MARSCHALS HNO_3 profiles for scan 9, 12, 21, 24, 27, 30 (in grey) together with initial guess profile (dashed) and correlative measurements: MLS in red, MIPAS in blue, SMR in cyan. Dashed purple line indicates the flight altitude level

In case of HNO_3 validation it is worth mentioning that the retrieved profiles differs a lot from the provided initial guess profiles.

7.2.5 N_2O validation

N_2O profiles retrieved from MARSCHALS data can be validated using in-situ data from HAGAR during ascent and descent and using satellite data from all the three instruments we have selected for the comparison.

Retrieved N_2O profiles are reported in Fig. 112 together with correlative measurements.

In general a good agreement is found between AURA/MLS and MARSCHALS N_2O profiles even if MLS profiles cover only a reduced altitude range with respect to the MARSCHALS scans. The agreement with ODIN/SMR N_2O profile is good in both scan 10 and 31, while the comparison with MIPAS data is possible only in scan 31: a quite good agreement is found in this case.

Comparing MARSCHALS results with HAGAR data during the ascent (scans 4-7-10) we found a good agreement below 100 hPa while some oscillations in MARSCHALS profiles are present near the flight altitude. The comparison with HAGAR data acquired during the M55 Geophysica descent (scan 28-31) show a good agreement for scan 28 and the part of scan 31 near the flight altitude. At higher pressure level (pressure higher than 150 hPa) the N_2O retrieved profile for scan 31 is lower with respect to the HAGAR one.

7.2.6 CO validation

MARSCHALS CO profiles can be compared only with AURA/MLS data.

The result of this comparison is shown in Fig. 113. The values above flight altitude are in good agreement with the AURA/MLS ones while below this altitude MARSCHALS CO profiles are always lower than the MLS ones even if for scan 26 the differences between the MARSCHALS and the MLS profile are reduced with respect to the

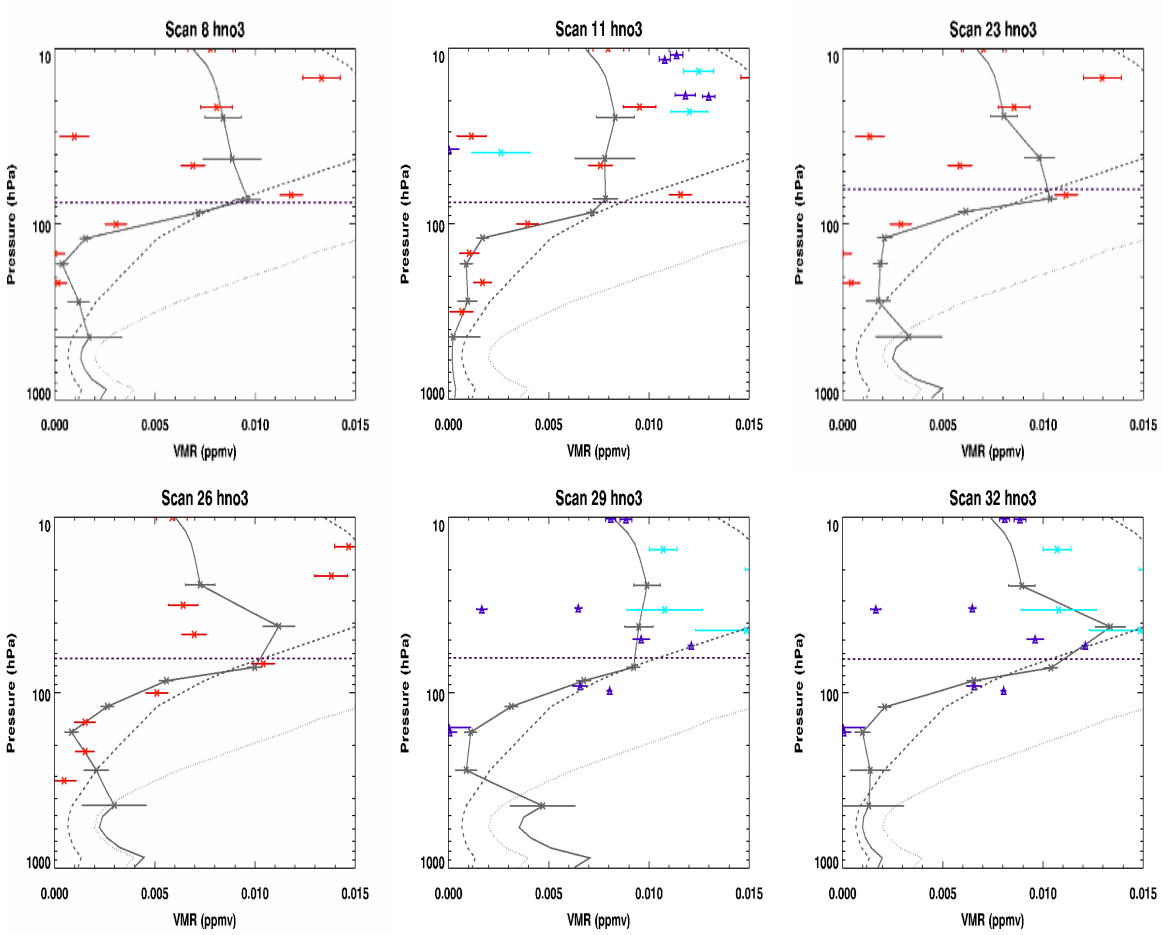

Fig. 110: MARSCHALS HNO_3 profiles for scan 8, 11, 23, 26, 29, 32 (in grey) together with initial guess profile (dashed) and correlative measurements: MLS in red, MIPAS in blue, SMR in cyan. Dashed purple line indicates the flight altitude level

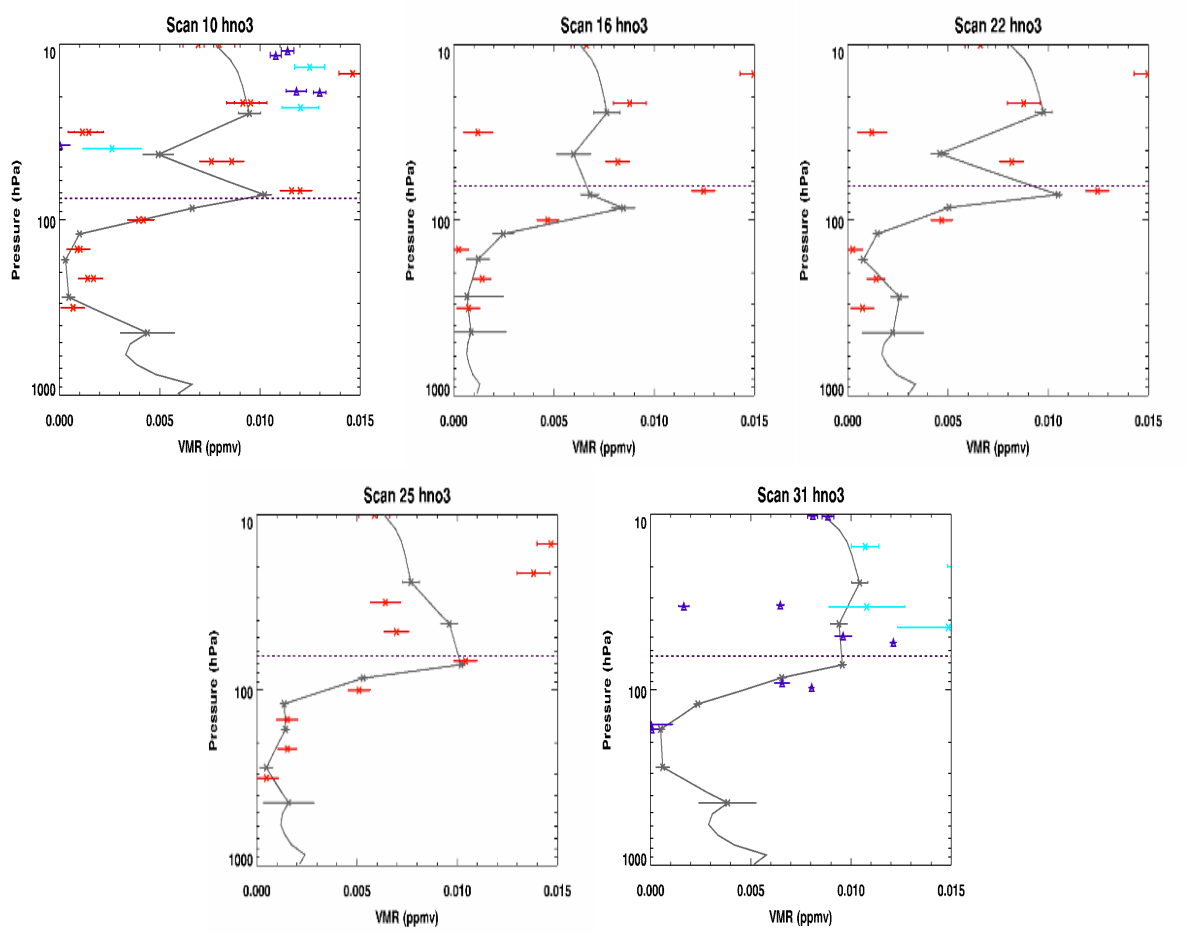

Fig. 111: MARSCHALS HNO_3 profiles for scan 10, 16, 22, 25, 31 from recursive retrievals analysis (in grey) together with initial guess profile (dashed) and correlative measurements: MLS in red, MIPAS in blue, SMR in cyan. Dashed purple line indicates the flight altitude level

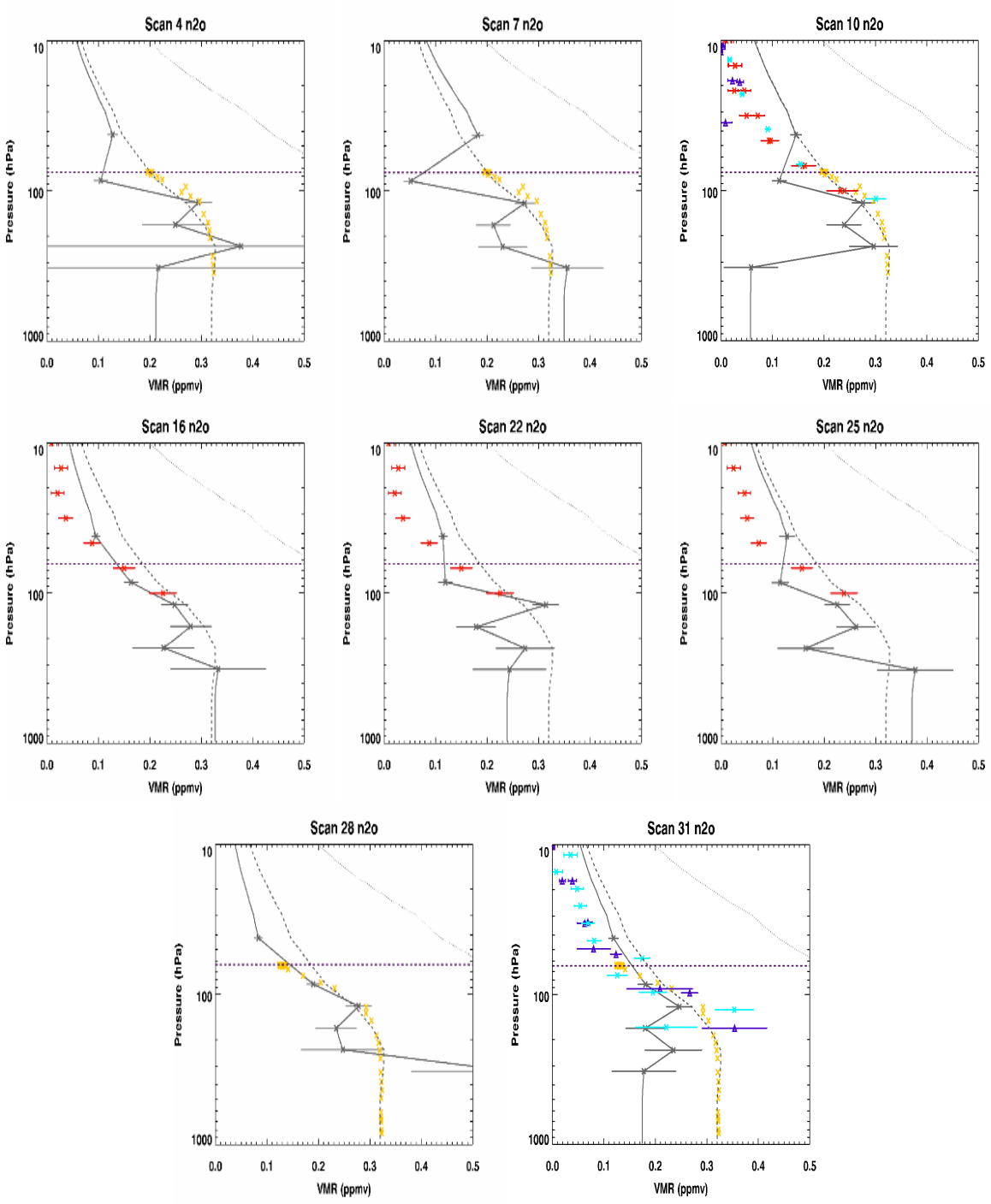

Fig. 112: MARSCHALS N_2O profiles for scan 4, 7, 10, 16, 22, 25, 28, 31 (in grey) together with initial guess profile (dashed) and correlative measurements: MLS in red, MIPAS in blue, SMR in cyan and in in situ data (HAGAR) in yellow. Dashed purple line indicates the flight altitude level

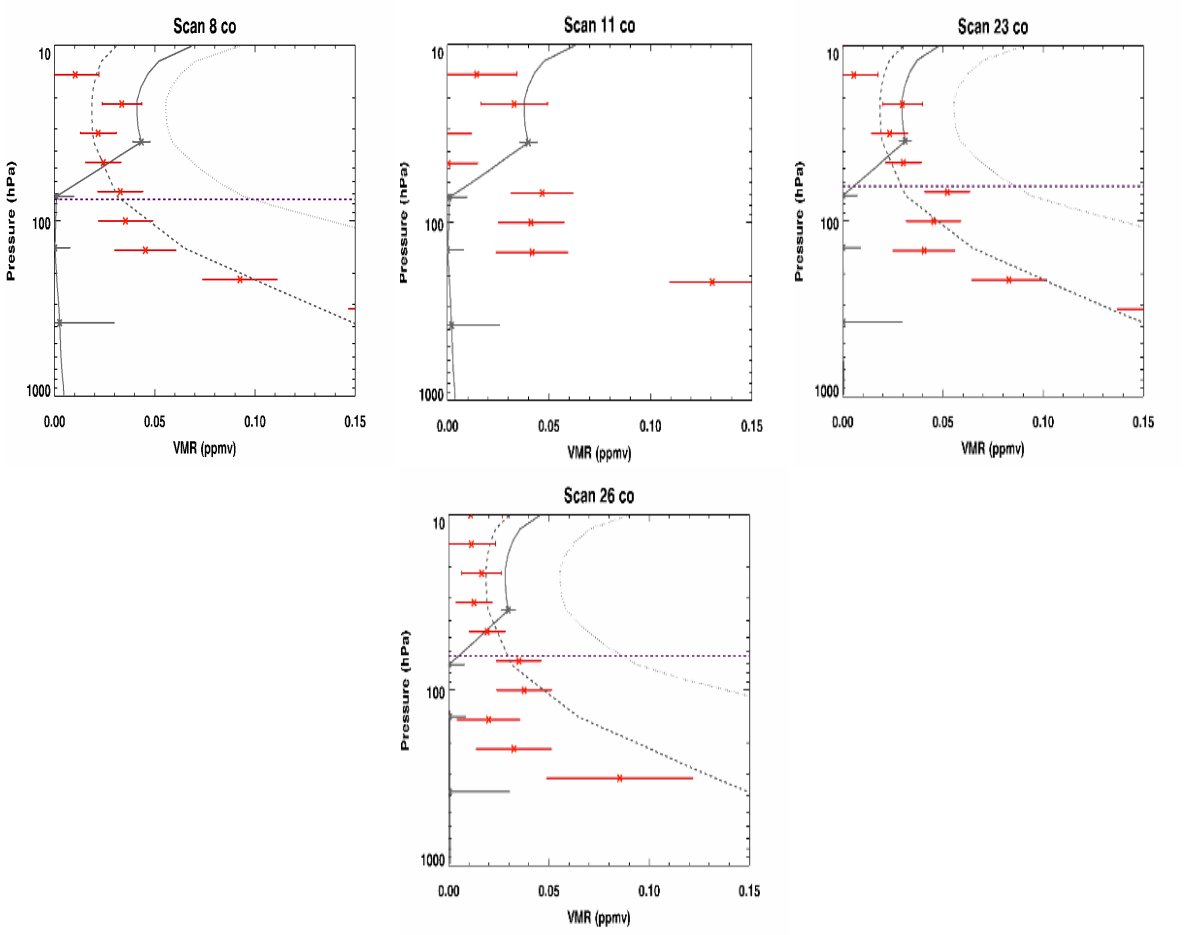

Fig. 113: MARSCHALS CO profiles for scan 8, 11, 23, 26 (in grey) together with initial guess profile (dashed) and correlative measurements: MLS in red. Dashed purple line indicates the flight altitude level

other scans. Furthermore, the Aura/MLS N_2Ovalues below flight altitude are of the order of or lower than the IG2 polar winter profile that we use as initial guess profile and that is at the limit of MARSCHALS sensitivity to CO.

7.2.7 Examples of comparison of MARSCHALS and AURA/MLS data using AURA/MLS Averaging Kernel

In this section we show some examples of comparison between MARSCHALS results and AURA/MLS profiles when the AURA/MLS AK are applied to the MARSCHALS profiles for Flight 2, following the same procedure used for Flight 1.

The results of these calculations are shown in Fig. 114. In each panel are reported MARSCHALS retrieved profiles in blue, MLS profiles in red and MARSCHALS profiles after the convolution with MLS AK in cyan for temperature, H_2O, HNO_3, O_3, retrieved from MARSCHALS scan 9, CO from MARSCHALS scan 11 and N_2O from scan 16. The errors associated to the convoluted MARSCHALS profiles are obtained from the interpolation of the original errors on the MLS pressure grid and are reported only in order to give an estimate of the size of the MARSCHALS errors.

All the results presented in Fig. 114 show how the convolution with the MLS AK smooths the MARSCHALS profiles (e.g. see O_3 profile around 100 hPa). In case of O_3, H_2O and N_2O a very good agreement is obtained when the MLS AK are applied to MARSCHALS results. For temperature a good agreement is obtained at pressure levels higher than 80 hPa. In case of HNO_3 some differences are found above flight altitudes. In general the use of MLS AK improves the quality of the comparison. It also highlights the fact that small high resolution oscillations in the profiles can not be resolved by the AURA/MLS instrument.

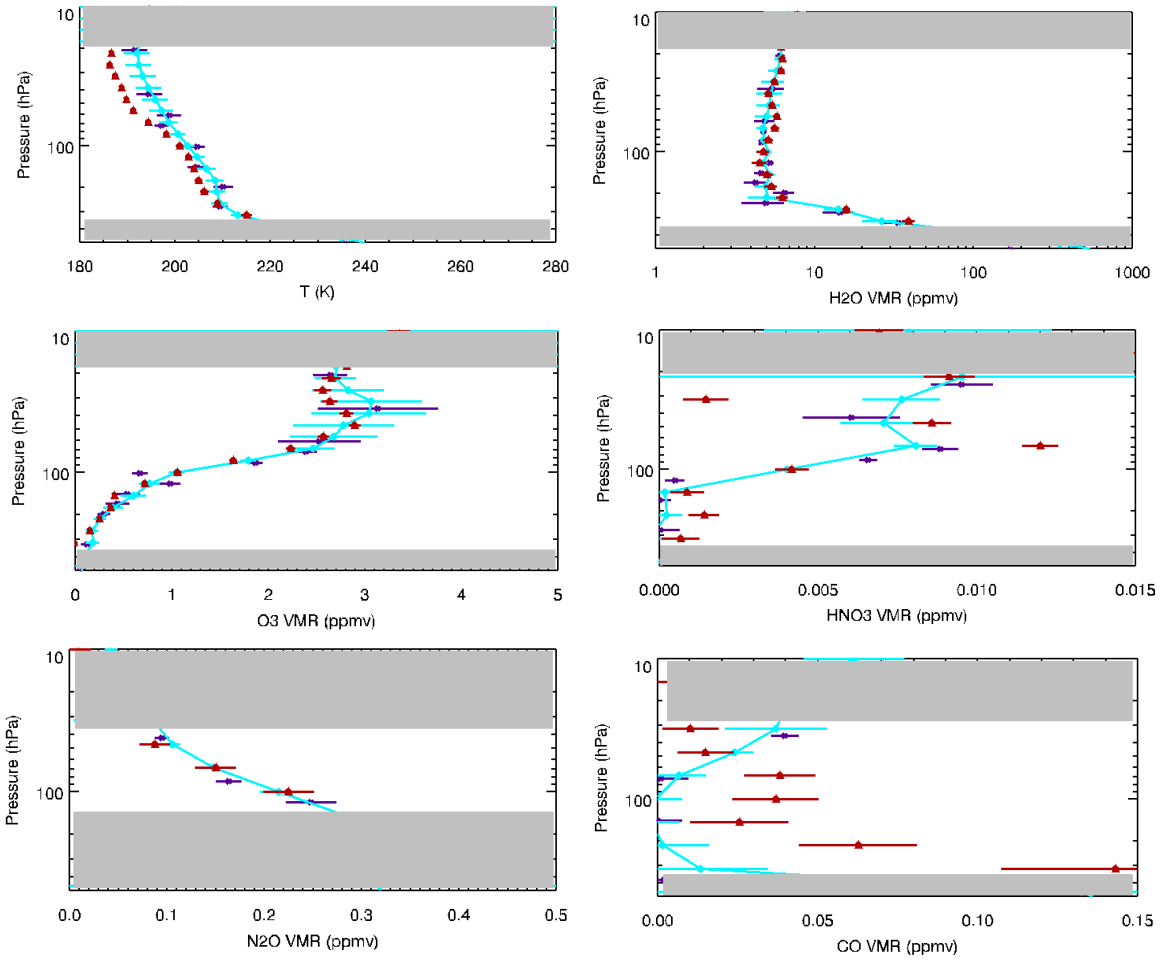

Fig. 114: MARSCHALS temperature, H_2O , O_3 , HNO_3 for scan 9, N_2O scan 16, CO from scan 11 (in blue) together with MLS profile (red) and MARSCHALS profiles after the convolution with MLS AK (in cyan).

7.2.8 Examples of comparison of MARSCHALS and in-situ data using MARSCHALS Averaging Kernel

In this section we show the results of of comparison between MARSCHALS results and in-situ profiles when the MARSCHALS AK are applied to the in-situ profiles for Flight 2. The profiles that MARSCHALS would observe are calculated using the formula (1) used for the convolution of models data with MARSCHALS AK as done for Flight 1. In case of in-situ data we interpolate the in-situ profiles over the 0.5 km altitude grids used for the models convolution. Data above the highest point in the in-situ profiles and below the lowest point in in situ data are set equal to the data obtained from the CLAMS model. The comparison of MARSCHALS results with convoluted in-situ profiles is then meaningful only in the altitude region covered by the in-situ data.

In Figs. 115 and 116 are reported the comparison between MARSCHALS retrieved profiles for temperature, $H_2O$and N_2O(in grey) and in-situ profiles obtained from Ucse, FISH and HAGAR (in yellow) together with in situ data convoluted with MARSCHALS AK (in blue) for scans 3,6,9,12,27,30 (for H_2O), scans 4,7,28,31 (for N_2O) and scan 30 for temperature.

In general the results of the comparison between MARSCHALS and in-situ products obtained using the convoluted in-situ profiles are very similar to the ones obtained using the original in-situ profiles. In few cases, (e.g. N_2Oretrieval at low from scan 4 in Fig. 116) the convolution with AK produce results more similar to the MARSCHALS ones.

7.2.9 First comparisons with preliminary MIPAS-STR results

MIPAS-STR was present on board the M55 Geophysica during the ESSEnCe Campaign. In this section we present the results of the inter comparison between MARSCHALS and MIPAS-STR preliminary results for the Flight 2. The comparisons can be performed for temperature, H_2O , O_3 , HNO_3 in the altitude range from the aircraft to about 10-9 km since MIPAS-STR detected some clouds below this altitude during the flight. The results of the comparison are reported in Fig.s 117, 118, 119, 120 for scan 3, 4, 5, 6 (these are the same scan used for the comparison with the GLORIA instrument in the next section) and in Fig. 121, 122, 123, 124, 125 for scan 9, 12, 21, 27 and 30.

¿From these plots a general good agreement can be found for all the targets even if for some scan the HNO_3 values retrieved by MARSCHALS below 14 km are lower than the MIPAS ones. In general, the MIPAS-STR preliminary profiles are smoother than the MARSCHALS ones (probably because of different regularization strategy adopted in the two analysis). Furthermore the MIPAS-STR altitude retrieval range is reduced with respect to the MARSCHALS one. This is due to the fact that cloud with CTH from 8 to 10 km were present during the flight as can be inferred from MIPAS-STR CI (not shown) and highlights the MARSCHALS capability of retrieving the atmospheric composition also in presence of clouds.

7.2.10 First comparisons with GLORIA

GLORIA is a is a prototype of an imaging Fourier Transform Spectrometer for a candidate Earth Explorer mission by ESA. The instrument was flying on board the M55 Geophysica during the Flight 2. In this section we briefly present the results of first inter comparisons between MARSCHALS and GLORIA retrieval results. The GLORIA dataset allow the comparison for few MARSCHALS scans at the very beginning of the flight, namely MARSCHALS scans 3,4,5,6. These scans corresponds to about 40 GLORIA profiles. The comparison can be performed for the following species: T, H_2O, O_3, HNO_3 and the GLORIA data for this part of the flight are valid in the altitude range from about 11 to 17 km, possibly because of cloud presence below 10 km at the beginning of the flight. The results of the comparison are reported in Fig.s 126, 127, 128 and 129. MARSCHALS results are reported in blue while corresponding profiles from GLORIA are reported in yellow. In red is highlighted the GLORIA profile retrieved from the measurement acquired when the GLORIA instrument was in the nearest position (and so at the nearest time) of the mean position of the MARSCHALS instrument during the scan acquisition.

Even if it is a preliminary comparison and only the first scans at the beginning of the flight were available, in general a very good agreement is found between MARSCHALS and GLORIA data for all the analysed targets. As in case of the comparison with MIPAS-STR data we can notice the MARSCHALS capability of retrieving data also at altitude levels where the infrared instruments are blinded by the clouds.

7.2.11 Flight 2 validation: Conclusions

The validation of MARSCHALS retrieved profiles for Flight 2 can be achieved using data from AURA/MLS, ODIN/SMR and ENVISAT/MIPAS satellites. Furthermore data for Temperature (UCSE), H_2O (FISH) and N_2O (HAGAR) are available during ascent and descent from in-situ instruments on board the M55 Geophysica. Radiosoundings are available from the Bodo and Sodankyla stations for the validation of temperature and H_2O profiles.

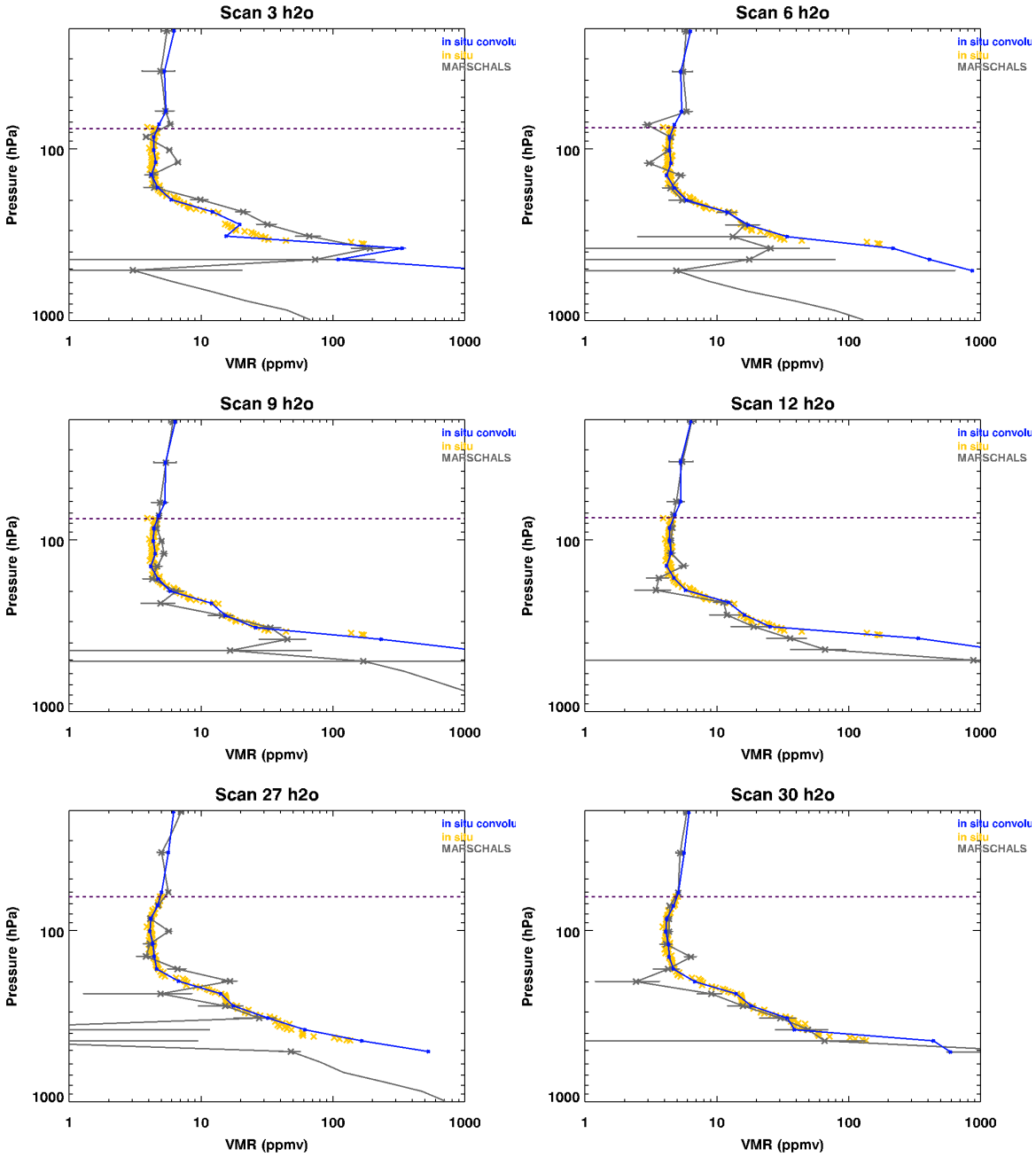

Fig. 115: MARSCHALS H_2O for scans 3, 6, 9, 12, 27, 30, together with FISH profiles (yellow) and FISH profiles after the convolution with MARSCHALS AK (in blue).

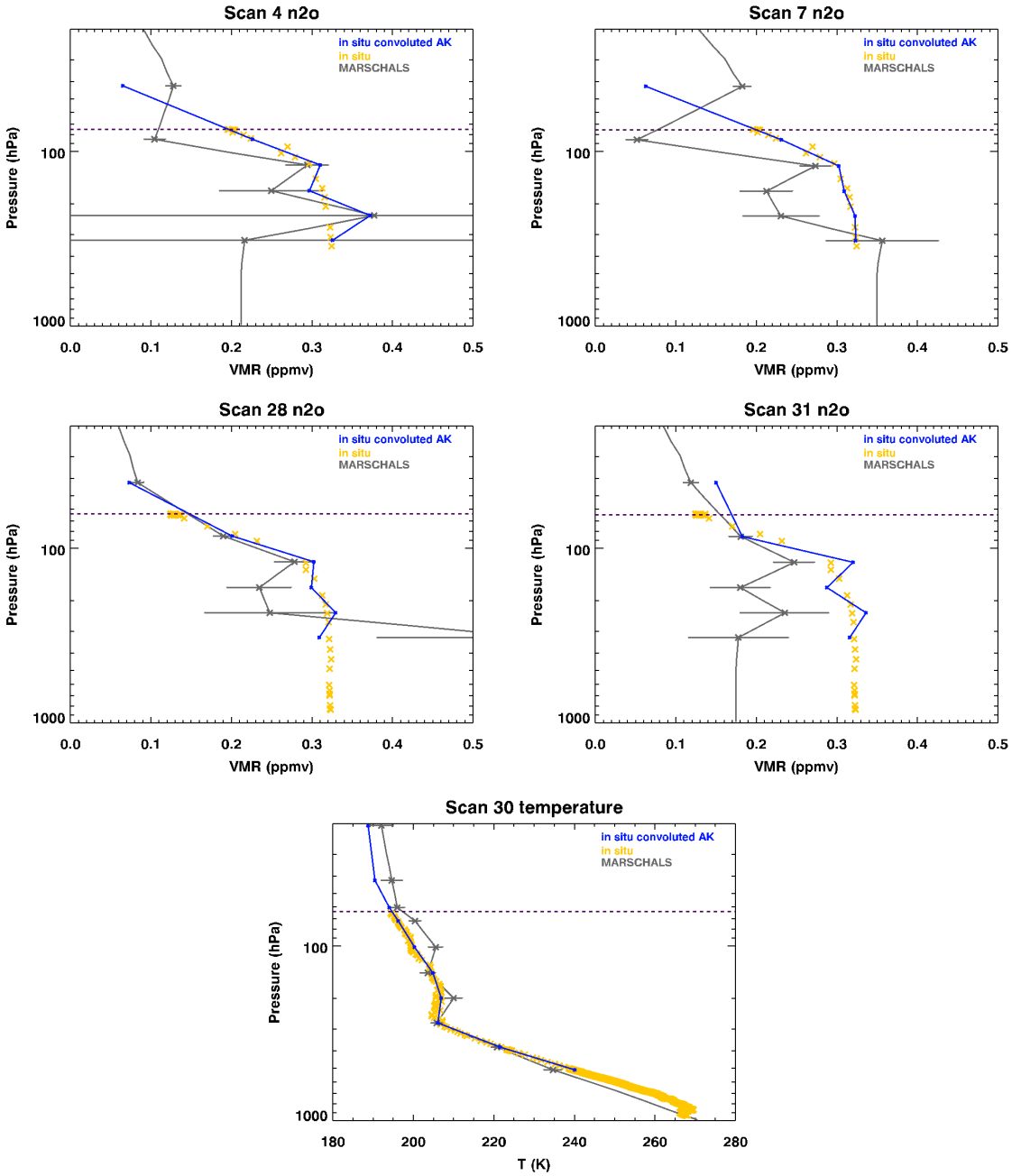

Fig. 116: MARSCHALS N_2O for scans 4, 7, 28, 31 and MARSCHALS temperature from scan 30 together with HAGAR (N_2Odata) and UCSE (temperature) profiles (yellow) and HAGAR and UCSE profiles after the convolution with MARSCHALS AK (in blue).

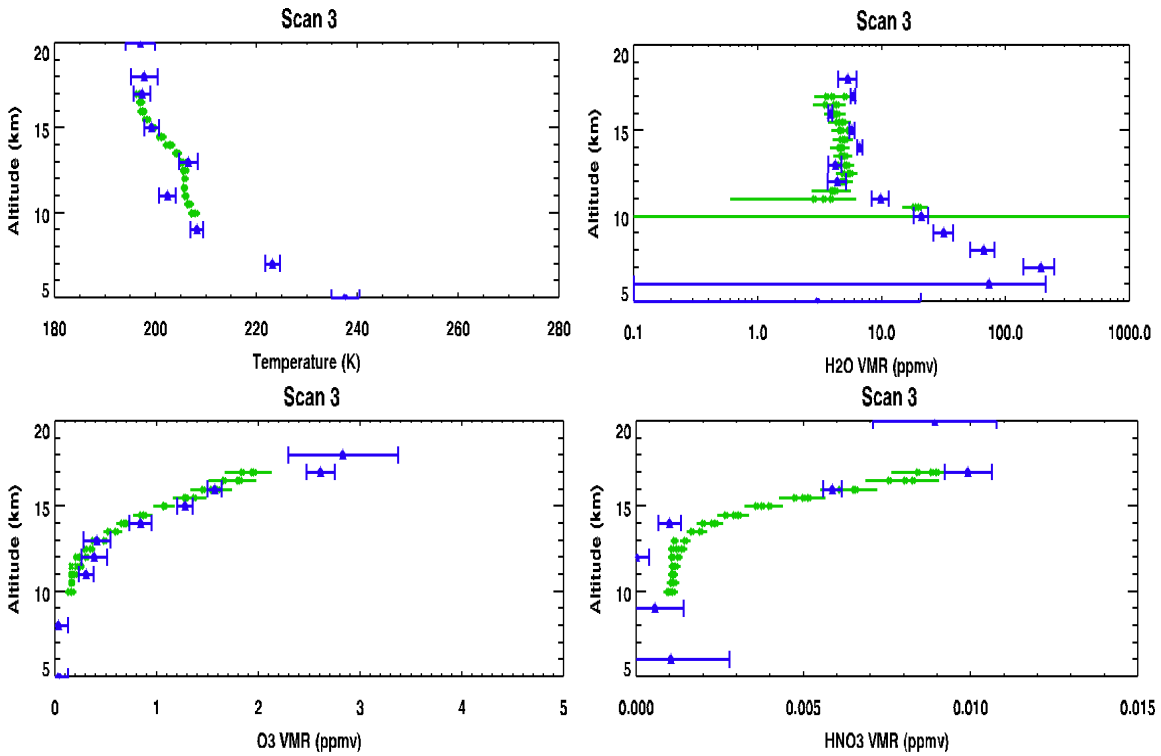

Fig. 117: MARSCHALS retrieved profiles for temperature, H_2O, O_3, $HNO_3$for scan 3 in blue versus the corresponding MIPAS-STR profiles in green

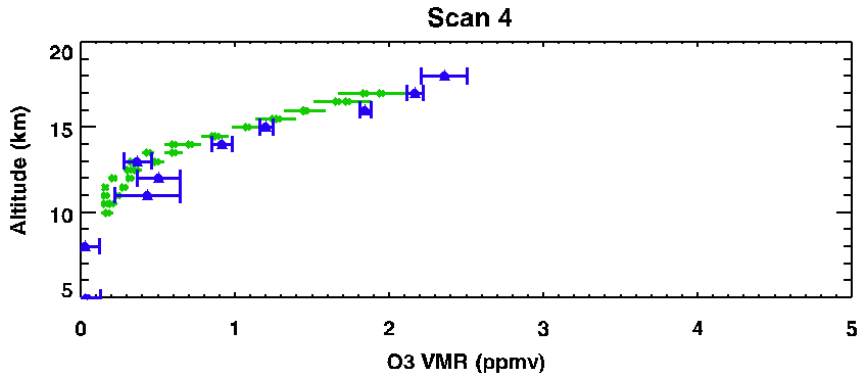

Fig. 118: MARSCHALS retrieved profiles for O_3 scan 4 in blue versus the corresponding MIPAS-STR profiles in green

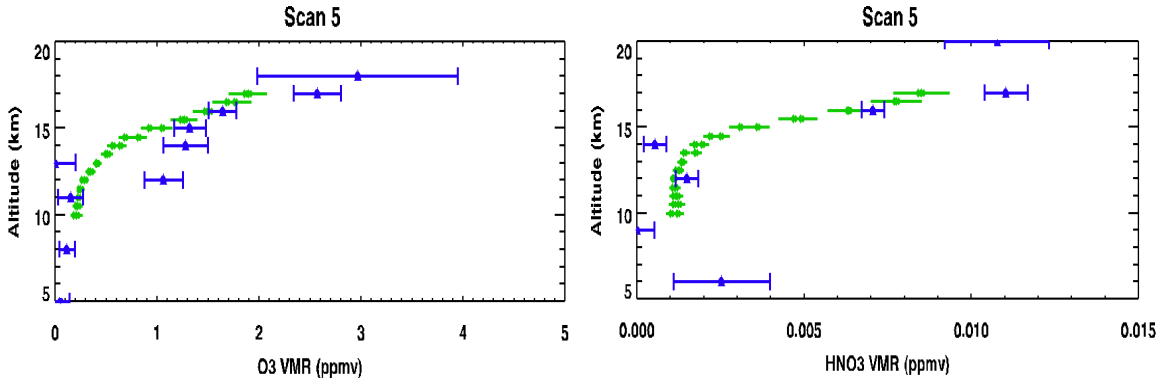

Fig. 119: MARSCHALS retrieved profiles for O_3, HNO_3 for scan 5 in blue versus the corresponding MIPAS-STR profiles in green.

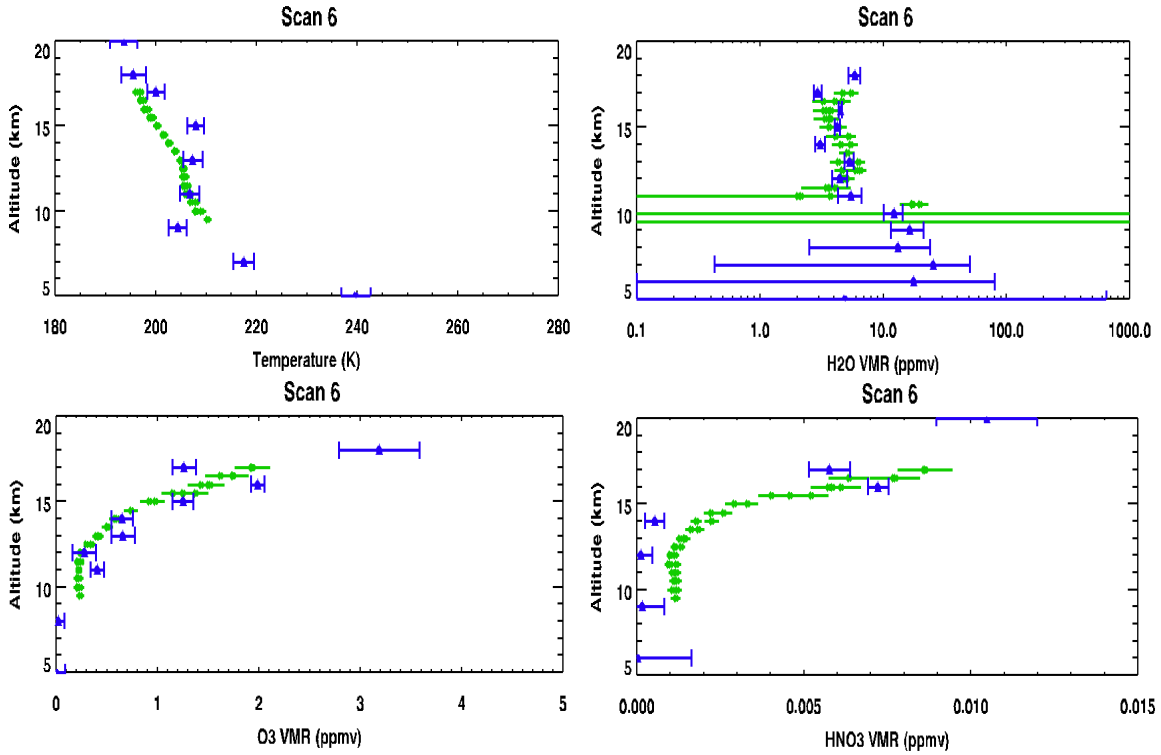

Fig. 120: MARSCHALS retrieved profiles for temperature, H_2O, O_3, HNO_3 for scan 6 in blue versus the corresponding MIPAS-STR profiles in green.

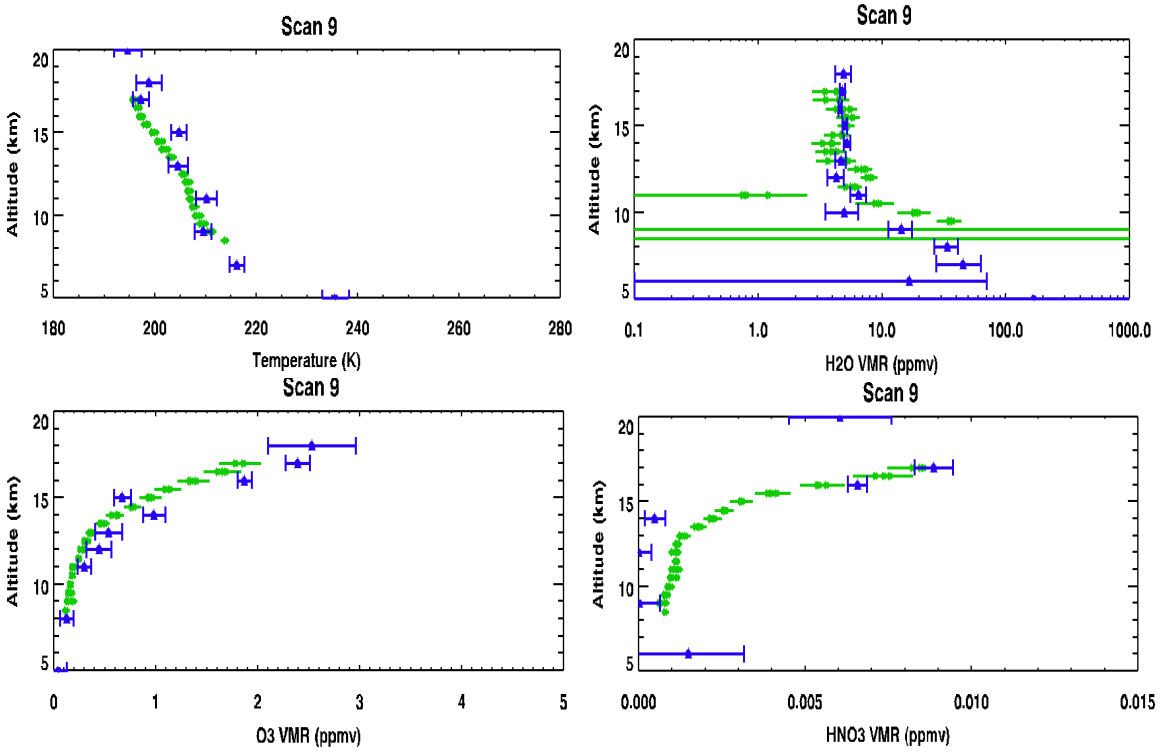

Fig. 121: MARSCHALS retrieved profiles for temperature, H_2O, O_3, HNO_3 for scan 9 in blue versus the corresponding MIPAS-STR profiles in green.

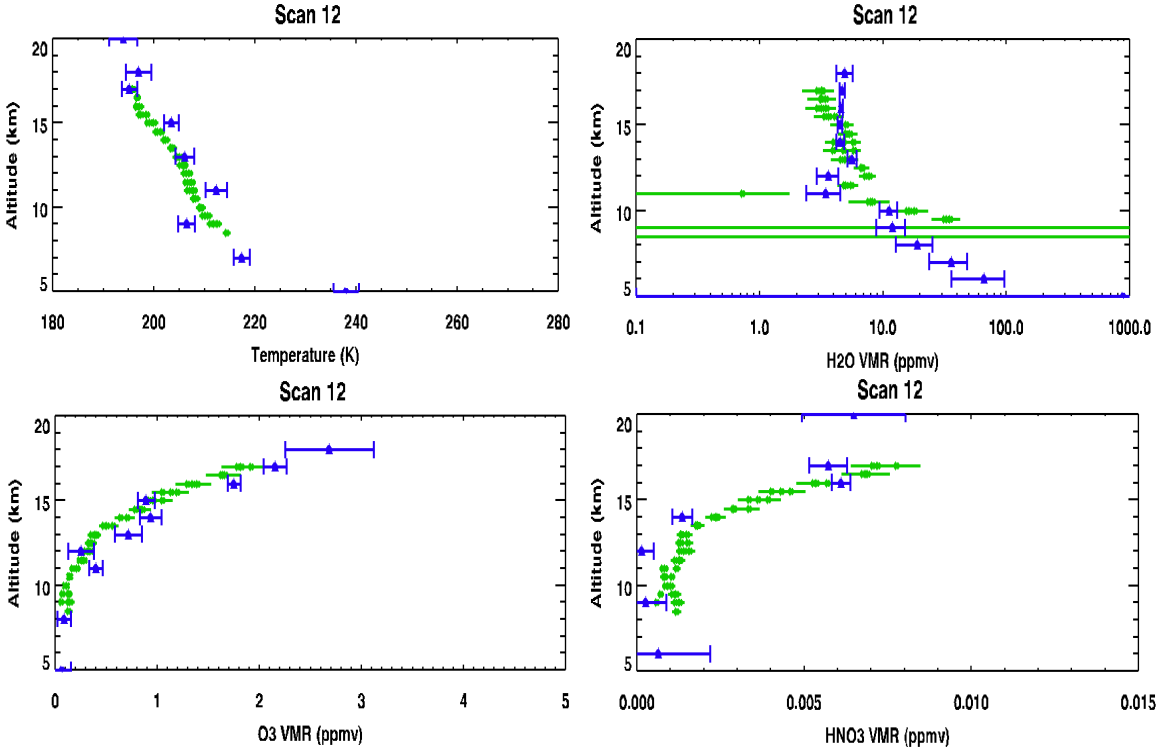

Fig. 122: MARSCHALS retrieved profiles for temperature, H_2O, O_3, HNO_3 for scan 12 in blue versus the corresponding MIPAS-STR profiles in green.

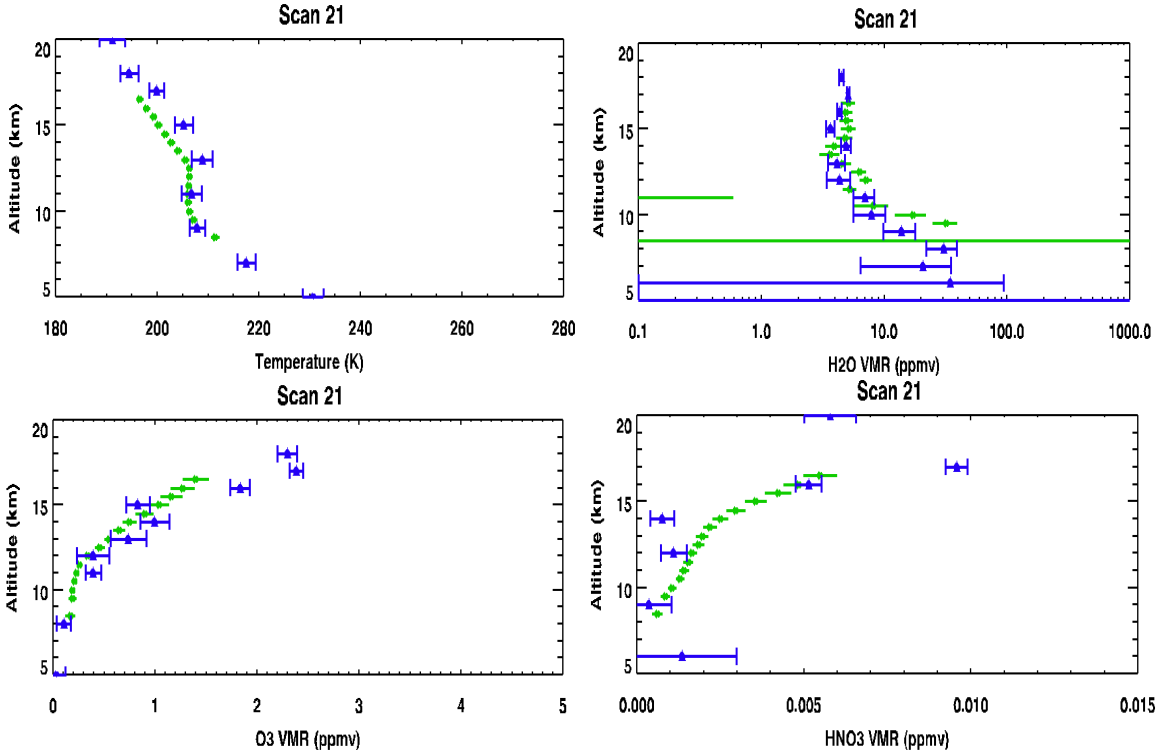

Fig. 123: MARSCHALS retrieved profiles for temperature, H_2O, O_3, HNO_3 for scan 21 in blue versus the corresponding MIPAS-STR profiles in green.

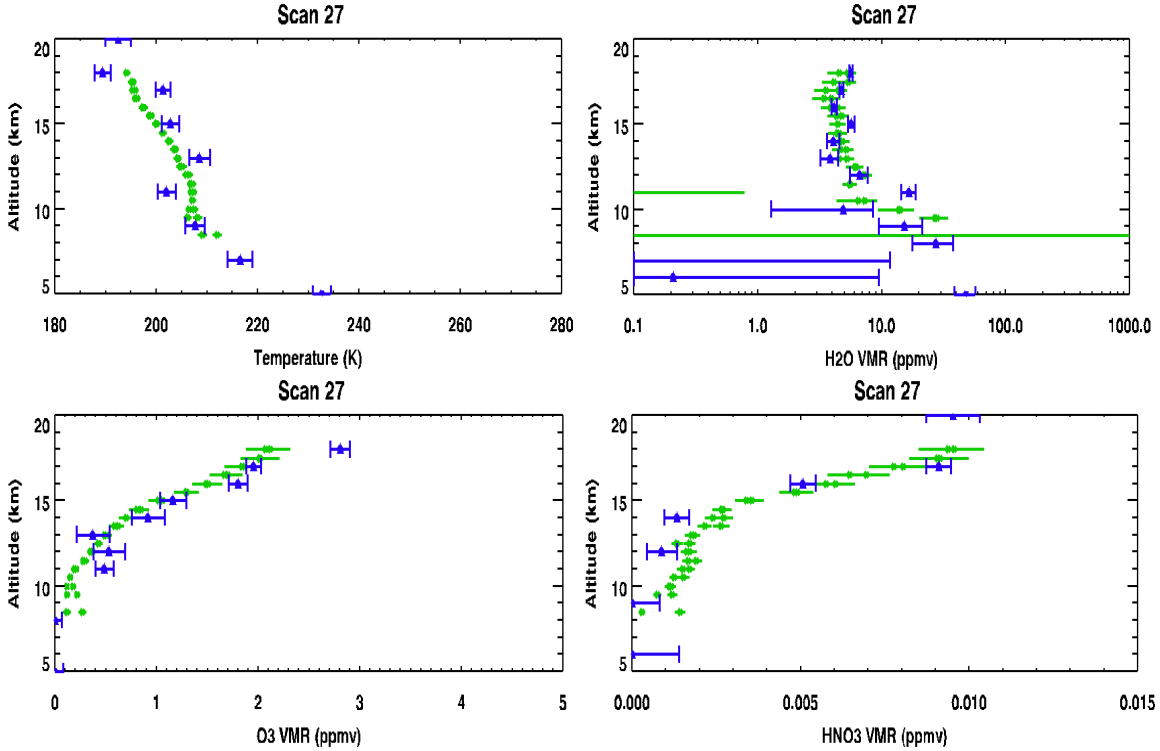

Fig. 124: MARSCHALS retrieved profiles for temperature, H_2O, O_3, HNO_3 for scan 27 in blue versus the corresponding MIPAS-STR profiles in green.

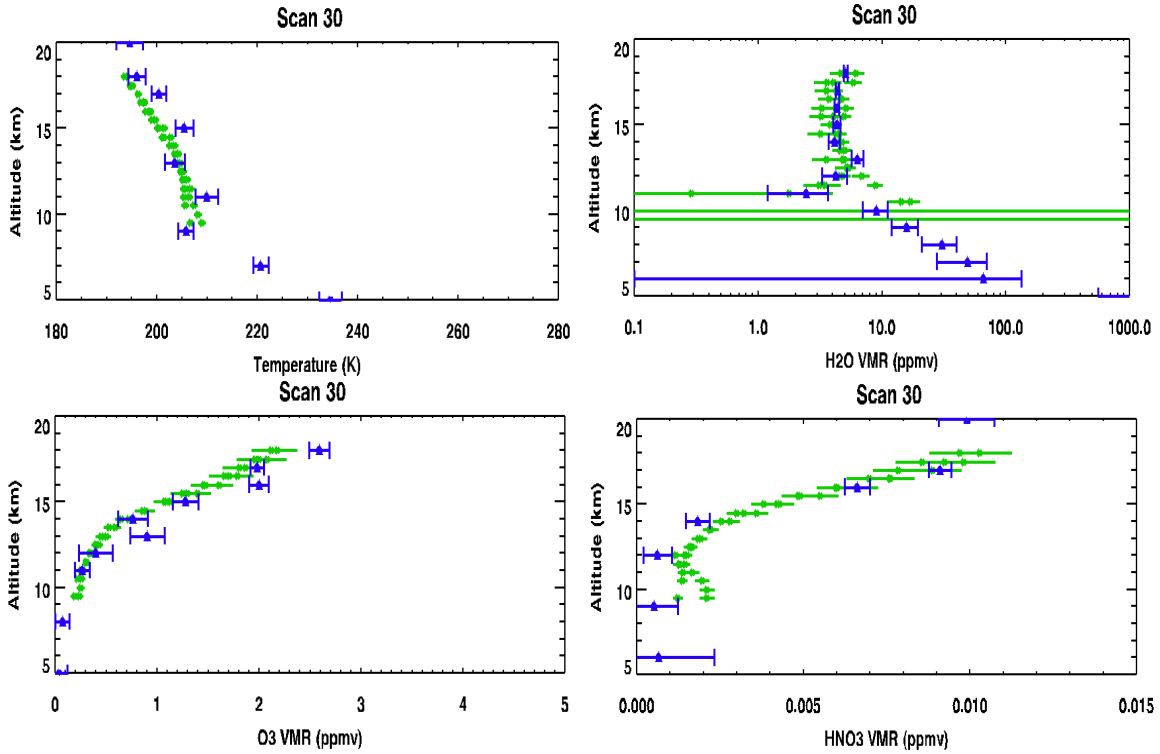

Fig. 125: MARSCHALS retrieved profiles for temperature, H_2O, O_3, HNO_3 for scan 30 in blue versus the corresponding MIPAS-STR profiles in green.

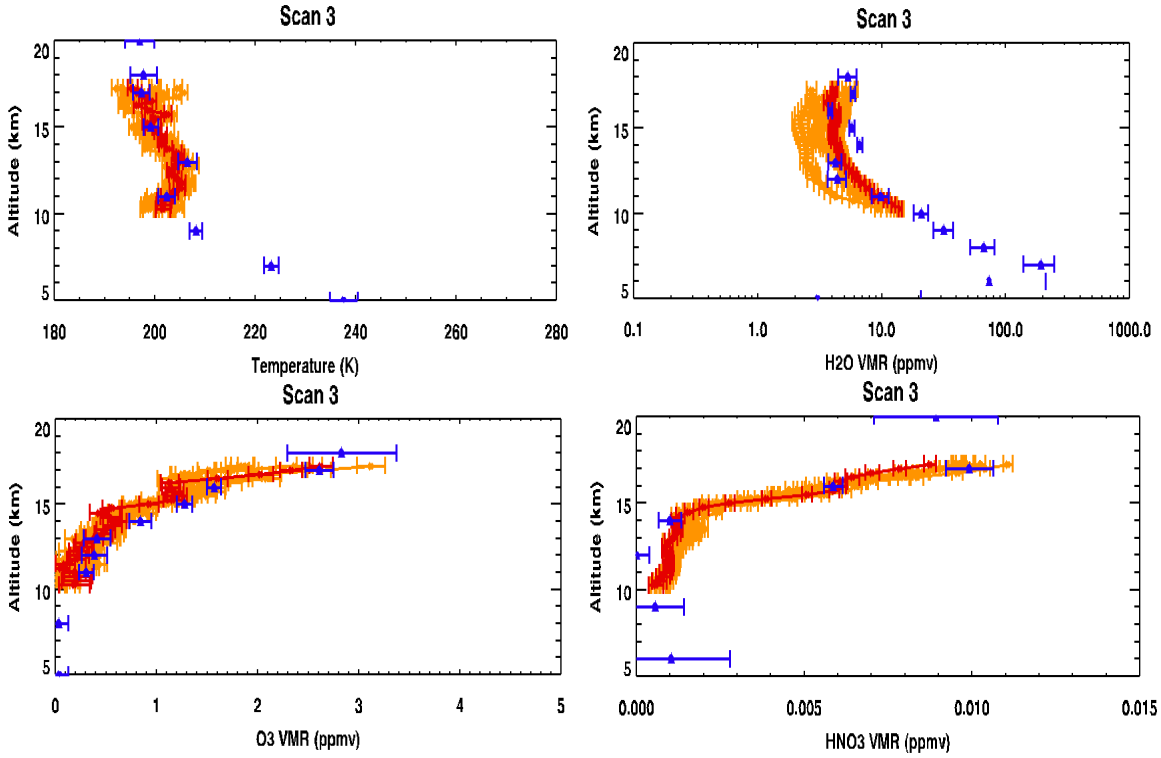

Fig. 126: MARSCHALS retrieved profiles for temperature, H_2O, O_3, HNO_3 for scan 3 in blue versus the corresponding GLORIA profiles in yellow. See text for further details.

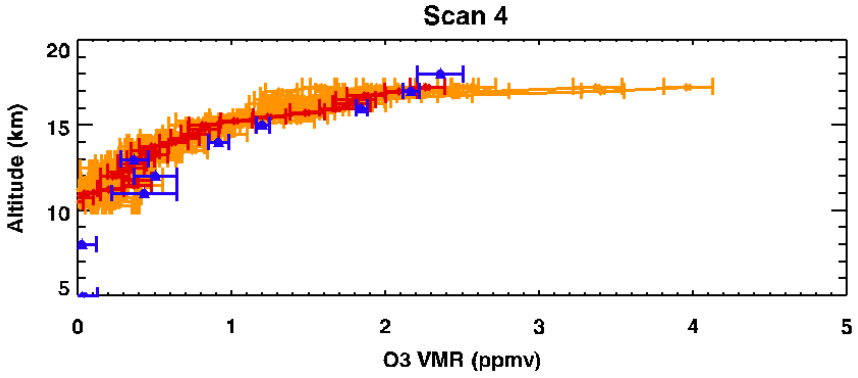

Fig. 127: MARSCHALS retrieved profiles for O_3 scan 4 in blue versus the corresponding GLORIA profiles in yellow. See text for further details.

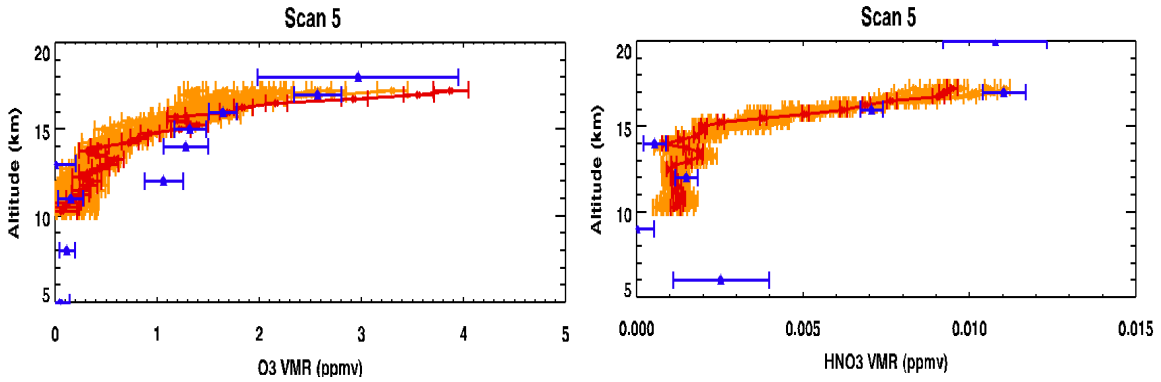

Fig. 128: MARSCHALS retrieved profiles for O_3, HNO_3 for scan 5 in blue versus the corresponding GLORIA profiles in yellow. See text for further details.

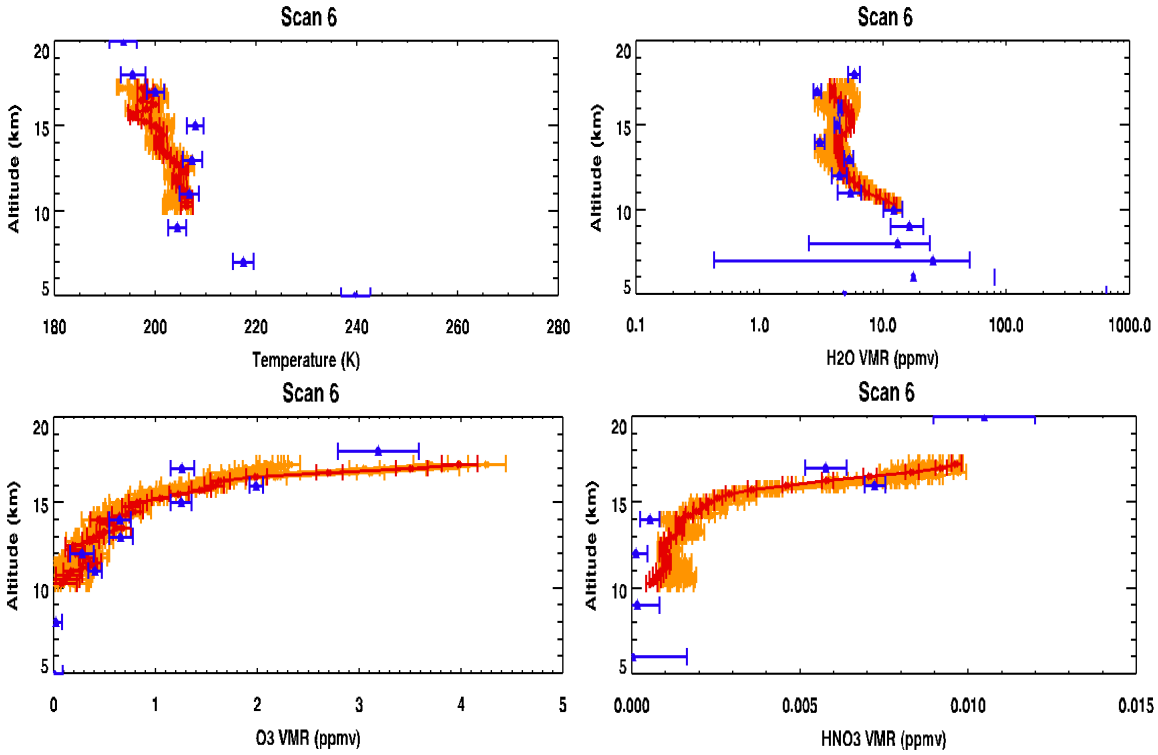

Fig. 129: MARSCHALS retrieved profiles for temperature, H_2O, O_3, HNO_3 for scan 6 in blue versus the corresponding GLORIA profiles in yellow. See text for further details.

In addition, comparisons of MARSCHALS profiles for scans that crosses the same air masses were performed showing a quite good agreement.

Temperature retrieved by MARSCHALS provide quite good results (except for scan 24) in comparison with satellite data, radiosonde and in-situ data.

MARSCHALS profiles for H_2Oshow a general very good agreement with all the correlative measurements (satellite data, radiosonde and in-situ).

Also O_3profiles are in good agreement with satellite data.

In case of HNO_3retrievals a very good agreement is found with satellite data also above flight altitude with hint of denitrification found in both satellite and MARSCHALS data from some scans.

N_2O retrieved profiles are in good agreement with the AURA/MLS ones even if MLS measurements covers only a reduced altitude range with respect to MARSCHALS. The agreement is good also with ODIN/SMR (comparison available for 2 scan) and quite good with MIPAS (comparison available for only one scan). However MARSCHALS N_2O profiles show a slightly worse agreement in comparison with in-situ data especially for scan 31 at low altitudes(lower values at low altitudes).

Comparison between MARSCHALS CO profiles and AURA/MLS profiles show that MARSCHALS profiles are always lower below flight altitude with respect to the MLS ones and comparable above even if for one scan the differences between the MARSCHALS and the MLS profile are not so large. Furthermore, the AURA/MLS profiles are of the order of the IG2 polar winter profile used as initial guess that is at the limit of MARSCHALS sensitivity to CO. Again we can conclude that with the current instrument configuration and auxiliary data provided by the level 1 team, CO cannot be satisfactorily measured below flight altitude.

An example of the effect of the application of AURA/MLS AK to MARSCHALS profiles show that when the MLS AK are applied the resulting MARSCHALS smoothed profiles and in good agreement with the MLS ones. This also highlights that the Aura/MLS instrument cannot resolve high resolution vertical oscillations.

A first comparison with GLORIA results for temperature, H_2O , O_3 , HNO_3 highlights good agreement between the two limb sounding instruments at the beginning of the flight. The comparison with preliminary MIPAS-STR profiles for the same targets along the flight show a general good agreement as well. The comparison with both infrared instruments on board the Geophysica also highlights the capability of MARSCHALS of obtaining informations on the atmosphere where the infrared instruments are blinded by clouds.

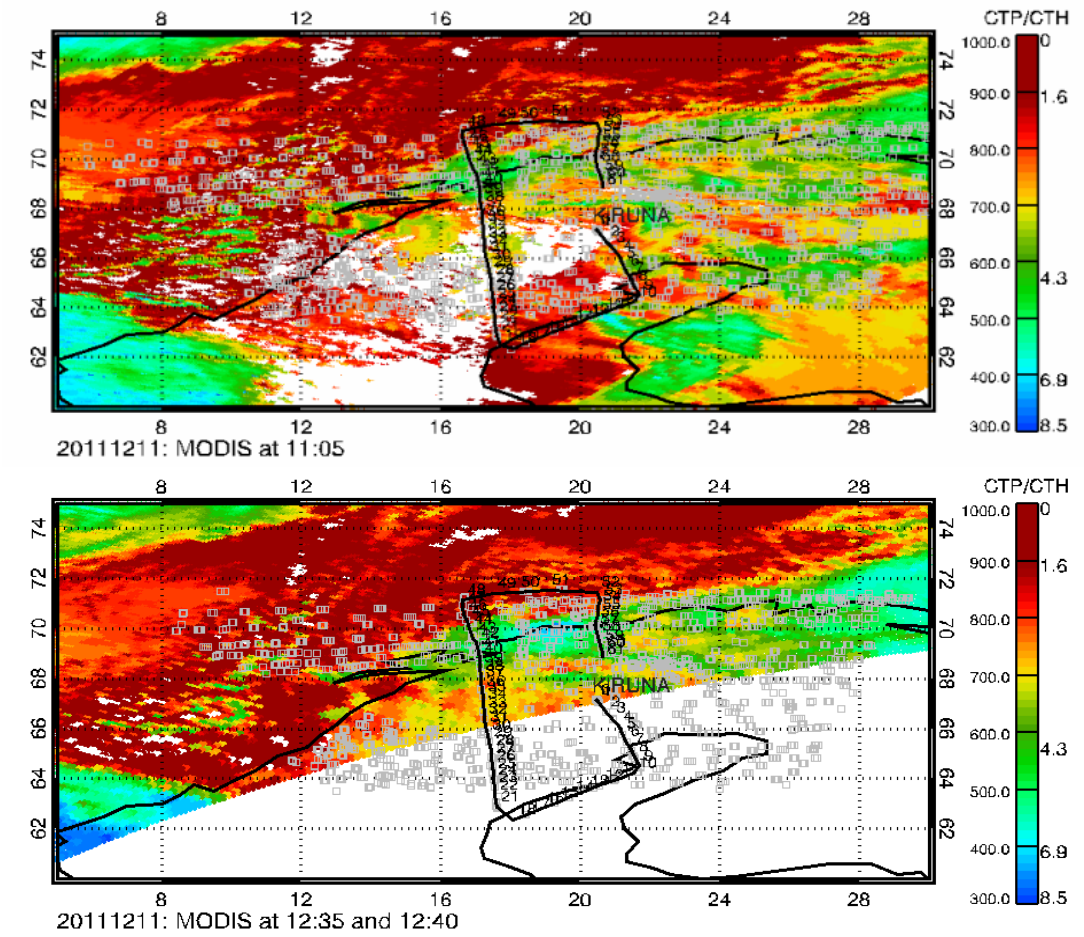

Fig. 130: Upper panel: MARSCHALS tangent points geo-location and MODIS CTP at 11:05 UTC. Lower panel: MARSCHALS tangent points Geo-location and MODIS CTP at 12:40 UTC

8 MARSCHALS cloud products

8.1 Flight 1 - Cloud detection

The retrieved external continuum for MARSCHALS Flight 1 is shown in Fig. 32. The figure highlights that no opaque cloud was present during this flight. Possibly some clouds can be present near the end of the flight (scan 54,55). However, as shown in Fig. 73 the individual information gain during this flight was particularly low below 15 km and especially for these scan the value of the individual information gain is very low (below 1 and near to 0) at these altitudes, thus suggesting very low sensitivity to cloud presence below this altitude. We can conclude that no opaque cloud is detected by MARSCHALS during Flight 1.

8.2 Flight 1 - Validation of the cloud detection

The OCM module collected some data in the first part of the flight. However, as reported in the ”MARSCHALS Compact data acquisition Report” no cloud was visible because of the low contrast due to low-light condition and to the fact that the aircraft was rolling a lot also during the straight flight legs. If available the Cloud Index values from MIPAS-STR instrument can be used for validate our results. however, an overall picture of cloud coverage during the flight can be obtained using correlative satellite data as data from MODIS and CALIPSO.

MODIS Cloud Top Pressure (CTP) retrieved at 11:05 UTC and at 12:40 UTC (in very good time coincidence with the flight) are reported in Figure 130, while in Figure 131 are reported the values of the CTP for cloud layer at 10:30 - 11:24 UTC and the CTP for aerosol layer (PSC, Polar Stratospheric Cloud) at the same time.

¿From MODIS and CALIPSO data we can see that no or very low clouds were present in almost the whole flight with some higher clouds towards the end of the flight (CTH approximately at 7-8 km as seen in bottom panel of Fig. 130). This is in agreement with the results of MARSCHALS external continuum retrieval.

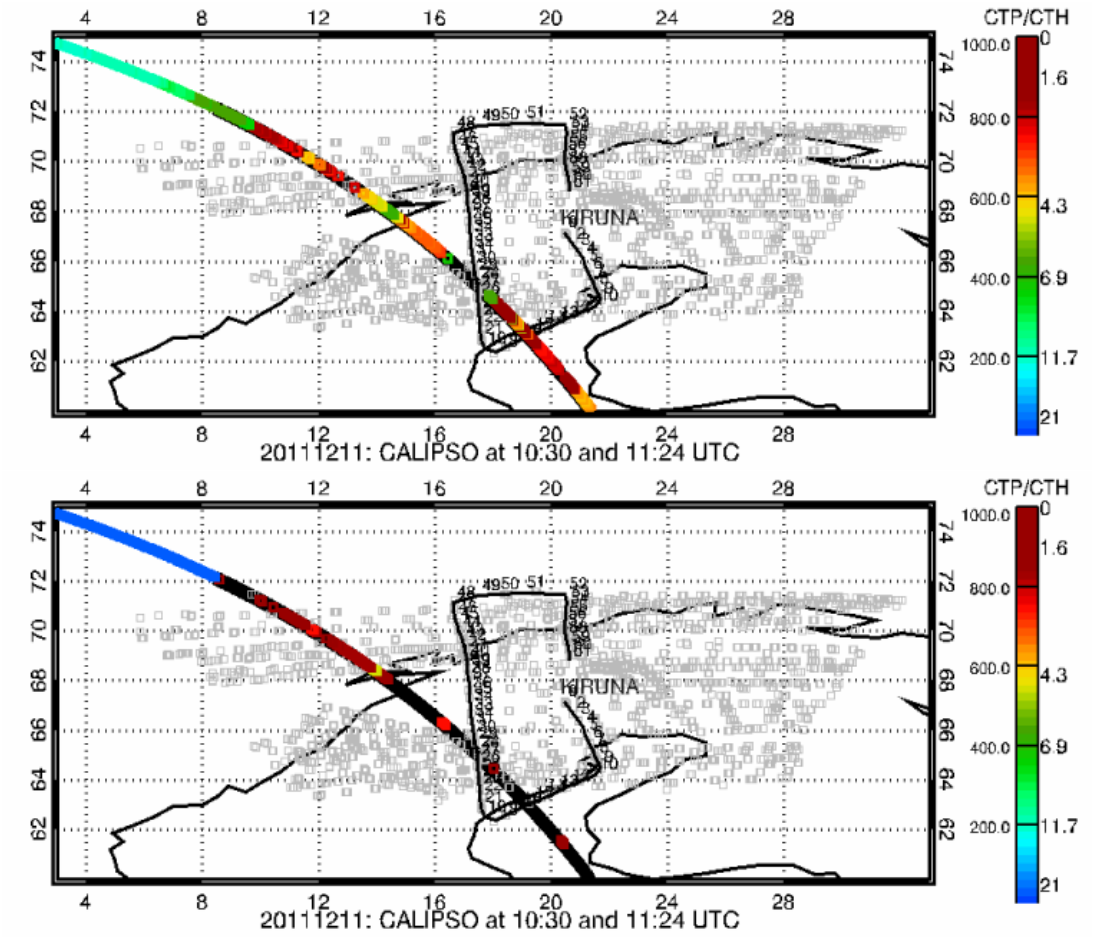

Fig. 131: Upper panel: MARSCHALS tangent points geo-location and CALIPSO Cloud CTP at 10:30 - 11:24 UTC. Lower panel: MARSCHALS tangent points geo-location and CALIPSO areosol CTP at 10:30 - 11:24 UTC.

8.3 Flight 2 - Cloud detection

The retrieved external continuum for MARSCHALS Flight 2 is shown in Fig. 72. As already discussed no evidence of opaque clouds is evident from this figure. Possibly some thin clouds can be present at the beginning of the flight at 10 km (scan 4) and near the end of the flight (scan 27) at the same altitude. However, as shown in Fig. 73 the individual information gain for these scan at this altitude is very low (below 1 and near to 0). In conclusion, no opaque cloud is detected by MARSCHALS above 10 km during this flight.

8.4 Flight 2 - Validation of the cloud detection

An overall picture of cloud coverage during the flight can be obtained using correlative satellite data since as reported in the "MARSCHALS Compact data acquisition Report" no OCM data were available for this flight due to the dark conditions. For our validation exercise we have chosen to use the data measured by MODIS and CALIPSO. MODIS Cloud Top Pressure (CTP) retrieved at 12:55 UTC (about 1 hour and half before the flight) and at 17:45 UTC (about 30 minutes after the flight) and at 19:25 UTC are reported in Figure 132, while in Figure 133 are reported the values of the CTP for cloud layer at 10:50 UTC and the CTP for aerosol layer (PSC, Polar Stratospheric Cloud) at 10:50 UTC and at 2:34 UTC of the 17 December 2011.

Even if the coincidence between MARSCHALS and MODIS/CALIPSO data is not so good, the fact that the two MODIS images (see Fig. 132) at 12:55 and 19:25 shows very similar cloud coverage can in first approximation allow an estimate of the cloud coverage at the time of the M55 Geophysica flight. ¿From these images we can infer that some scattered high clouds (CTH at about 8-9 km) were present in the first part of the flight (MARSCHALS scans from 7 to 23, the same considerations comes from CALIPSO data in Fig. 133), while low clouds were present during the second part of the flight (MARSCHALS scans 24-35). Preliminary CI MIPAS-STR data obtained during the flight indicates cloud presence with CTH near 9-10 km for almost all the flight. At the moment this preliminary results is the best estimate of the cloud coverage that we can obtain. Furthermore this is in agreement with MARSCHALS cloud assessment that reveal that no opaque clouds was present during the flight with CTH above 10 km (the external continuum information gain is extremely low (almost 0) below 10 km). The presence of PSC clouds is highlighted by the CALIPSO instrument.

9 Comparison between MARSCHALS retrieval products and CLaMS/EMAC model data

9.1 Introduction and strategy

In this section, we show the results of the comparison between MARSCHALS retrieval products, as reported in section 4 and 5, with the state of the atmosphere simulated using CLaMS and EMAC atmospheric chemical transport models. A brief overview of the main features of the two models is given in section 9.2 and 9.3. The rationale for the choice of these atmospheric transport models and more details on the synergy between their complementary capabilities are given in section 9.4. The targets of the comparison are the VMR vertical profiles of the following atmospheric constituents: H_2O, O_3, HNO_3, N_2O, and CO. The Temperature profile is not a product of the models (it is provided by ERA-Interim) and it is not object of this comparison.
Here below, we summarize the basic steps of the strategy adopted for the comparison:

- The IFAC team provided to the atmospheric modelers (FZJ team for CLaMS and KIT team for EMAC) the spatial (longitude, latitude, altitude) and temporal coordinates of a vertical grid from 0 km to 26 km, in steps of 0.5 km (hereafter indicated as the Vertical Grid of the Comparison or VGC) associated to each limb scan of MARSCHALS;
- For each altitude level of the VGC in the range between the lowest and highest MARSCHALS tangent points, we used the interpolated time, latitude and longitude of the tangent points immediately above and below the selected altitude;
- For each altitude level of the VGC above the highest MARSCHALS tangent point, we used the time, latitude and longitude values of the highest MARSCHALS tangent point;
- For each altitude level of the VGC below the lowest MARSCHALS tangent point, we used the time, latitude and longitude values of the lowest MARSCHALS tangent point.
- The atmospheric modelers provided to the IFAC team the H_2O, O_3, HNO_3, N_2O, and CO VMR vertical profiles simulated by CLaMS and by EMAC, along with additional information as the Temperature and Pressure profiles.

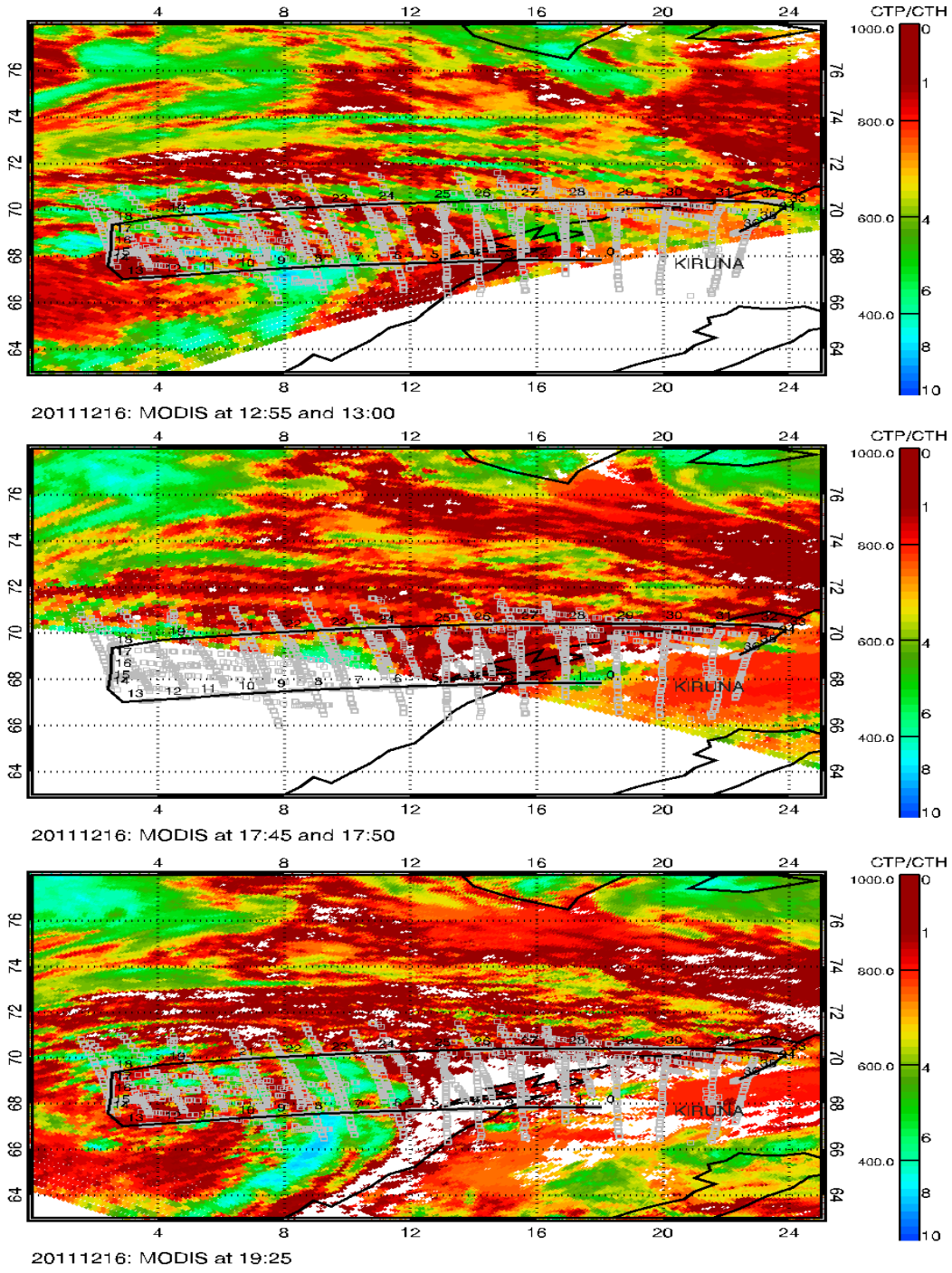

Fig. 132: Upper panel: MARSCHALS tangent points Geo-location and MODIS CTP at 12:55 UTC. Middle panel:MARSCHALS tangent points Geo-location and MODIS CTP at 17:45 UTC. Lower panel: MARSCHALS tangent points geo-location and MODIS CTP at 19:25 UTC

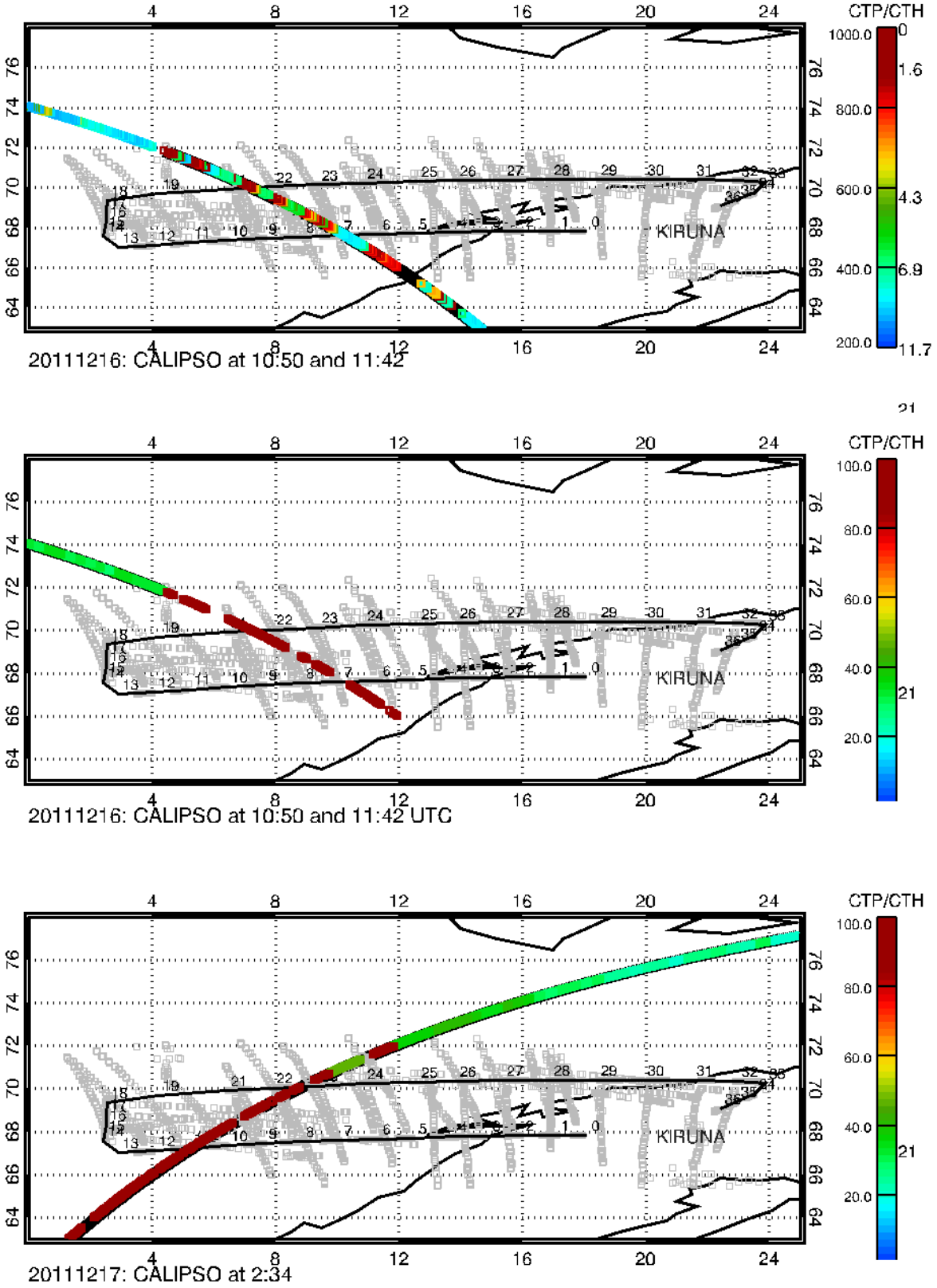

Fig. 133: Upper panel: MARSCHALS tangent points geo-location and CALIPSO Cloud CTP at 10:42 UTC. Middle panel:MARSCHALS tangent points geo-location and CALIPSO areosol CTP at 10:50 UTC. Lower panel: MARSCHALS tangent points geo-location and CALIPSO aerosol CTP on the 17 December 2011 at 02:34 UTC.

- In order to compare the target vertical profiles provided by the models on a high resolution altitude grid with the retrieved vertical profiles on the optimized vertical grid, we need to take into account the smoothing introduced by the retrieval procedure due of the information content of the MARSCHALS measurements. Ceccherini (2012) [5] demonstrated how to take into account the retrieval effect on the model profiles, when the vertical grid is the same. From the results of Ceccherini we can obtain the expression in the case of high resolution vertical grid:

$$\mathbf{x}_{model} = \mathbf{AK}_h * \mathbf{x}_{model,h} + (\mathbf{I} - \mathbf{AK}) * \mathbf{x}_a + \mathbf{AK} * \hat{\mathbf{x}} - \mathbf{AK}_h * \hat{\mathbf{x}_h} \quad (1)$$

  where $\mathbf{x}_{model}$ is the vertical profile obtained by the models and reported on the vertical grid of the retrieval, $\mathbf{x}_{model,h}$ is the vertical profile provided by the models on the high resolution altitude grid, $\hat{\mathbf{x}}$ is the retrieved profile on the vertical grid of the retrieval, $\hat{\mathbf{x}_h}$ is the retrieved profile interpolated on the high resolution altitude grid, $\mathbf{x}_a$ is the vertical a priori information used in the retrieval procedure, $\mathbf{AK}$ is the square Averaging Kernel matrix, $\mathbf{AK}_h$ is the rectangular high resolution Averaging Kernel matrix.

- After the convolution, MARC retrieved profiles and the convoluted model profiles are compared on the same vertical grid.

The results of the comparison are reported in section 9.6 for ESSenCe Flight 1 and Flight 2.

9.2 EMAC model description

The ECHAM/MESSy Atmospheric Chemistry (EMAC) model is a numerical chemistry and climate simulation system that includes sub-models describing tropospheric and middle atmosphere processes and their interaction with oceans, land and human influences [31]. It uses the first version of the Modular Earth Submodel System (MESSy1) [30] to link multi-institutional computer codes. The core atmospheric model is the 5^{th} generation European Centre Hamburg general circulation model (ECHAM5) [55].

The applied model setup of EMAC (ECHAM5 version 5.3.01, MESSy version 1.10) comprised the submodels MECCA1 for the gas-phase chemistry [57], JVAL for the calculation of photolysis rates [33], the microphysical submodel PSC for the simulation of polar stratospheric clouds [23], SEDI for the sedimentation of aerosol particles [18], SCAV for the scavenging and liquid phase chemistry in cloud and precipitation [62], CLOUD for calculating the cloud cover as well as cloud microphysics including precipitation [64], DRYDEP for dry deposition of trace gases and aerosols [18], LNOX for the source of NOx produced by lightning [65], CONVECT for the parameterization of convection [63], CVTRANS for convective tracer transport [66], OFFLEM for offline emissions of trace gases and aerosols [19], TNUDGE for tracer nudging [19], PTRAC for additional prognostic tracers [32], TROPOP for diagnosing the tropopause and boundary layer height, H_2O validation for stratospheric water vapor, RAD4ALL for the radiation calculation, and HETCHEM for calculating reaction coefficients of heterogeneous reactions on aerosols (see [31], and references therein).

For the inter-comparison with the MARSCHALS data we used EMAC in the T42L90MA-resolution, i.e. with a spherical truncation of T42 (corresponding to a quadratic Gaussian grid of approx. 2.8 by 2.8 degrees in latitude and longitude) with 90 vertical hybrid pressure levels up to 0.01 hPa (about 80 km) resulting in a vertical resolution of about 500-600 m between 5 and 20 km. The model time step was 10 min.

The simulation was initialized on January 1^{st} 2011 with data from a T42L39 model run started in January 2008. A Newtonian relaxation technique of the prognostic variables temperature, vorticity, divergence above the boundary layer and below 1 hPa and the surface pressure towards the ERA-Interim meteorological data has been applied, in order to allow a direct comparison with the observations. Sensitivity studies with different EMAC runs have shown that nudging up to the upper stratosphere is important to reproduce the observed stratospheric temperature distribution which governs the formation of PSC and therefore the amount of active chlorine [74].

The simulation included a comprehensive chemistry setup from the troposphere to the lower mesosphere with 98 gas phase species, 178 gas phase reactions, 60 photolysis reactions, and 10 heterogeneous reactions on liquid aerosols, NAT- and ice particles. Boundary conditions for greenhouse gases are taken from the IPCC-A1B scenario [29] and adapted to observations from the AGAGE database [49]. Halogenated hydrocarbons are included according to the WMO Ab scenario [75]. The calculation of the photolysis rates is based on the fast on-line scheme by [33], which accounts for spherical geometry by employing an air mass factor correction with an extrapolation of the calculated photolysis rates for solar zenith angles between 88 and 94.5 degrees. Rate constants of gas-phase reactions are mainly taken from the compilation of [56], absorption cross sections from the recommendation of [58]. The parameterization of NAT is based on the efficient growth and sedimentation of NAT particles as described in [23]. Therein, the NAT formation takes place below the NAT existence temperature (TNAT) with the assumption

Tab. 3: Summary of EMAC simulation used in WP4000 and WP4100

Model Setup	Information
Model Version	EMAC (ECHAM5 version 5.3.01, MESSy version 1.10)
Horizontal Resolution	T42 (2.8 ° x 2.8 °)
Vertical Resolution	90 hybrid layers from surface up to 1 Pa (∼80 km)
Initialization	January 1^{st} 2011 from EMAC T42L39 simulation started in January 2008
Time Step	10 minutes
Meteorology	Nudging of ERA-Interim meteorological data
	(temperature, vorticity, divergence, and surface pressure) up to 1 hPa
QBO	Nudging of zonal wind observations
Chemistry	Stratospheric and tropospheric chemistry up to isoprene (without iodine reactions)
Solar Variability	Medium solar flux (no solar cycle)
Volcanic Aerosols	Background conditions 1999 for H_2SO_4 (SAGE)
Boundary Conditions	IPCC-Scenario A1B [29]: CO_2, N_2O, CH_4
	WMO-Scenario Ab [75]: CFCs and Halons
	EDGAR3.2FT2000 database [48]: VOC (repeat of year 2000)
Bry (VSLS)	Additional 5 pptv to CH_3Br
Output Frequency	600 s for 11^{th} and 16^{th} of December 2011

of a necessary super cooling of 3 K. The STS formation is based on [2] and takes place through uptake of HNO_3 by liquid sulphuric acid aerosols. During cooling of STS the fraction of HNO_3 increases in the particles.

The EMAC setup is summarised in table 3. The complete EMAC model output data were saved every 10 min for the ESSenCe campaign flights at 11^{th} and 16^{th} of December 2011, respectively. The model output for the targets Temperature, H_2O, O_3, HNO_3, N_2O, and CO has been interpolated in time and space to the Vertical Grid of the Comparison (VGC) and also to the geo-location and time of the MARSCHALS flight altitude, both data sets provided by IFAC.

9.3 CLaMS model description

The Chemical Lagrangian Model of the Stratosphere (CLaMS) was originally developed for the stratosphere ([42], [43], [24]) and was extended to the troposphere ([25], [26]). CLaMS is based on a Lagrangian formulation of the tracer transport and, unlike Eulerian CTMs, considers an ensemble of air parcels on a time-dependent irregular grid that is transported by use of the 3d-trajectories. The irreversible part of transport, i.e. mixing, is controlled by the local horizontal strain and vertical shear rates with mixing parameters deduced from observations. The CLaMS model is well known for representing transport and mixing processes in the upper troposphere and lower stratosphere (UTLS) quite realistically. In particular, CLaMS is very well suited to describe gradients of atmospheric tracers in regions where transport barriers exist like the polar vortex, the subtropical jet, and the tropopause region. This has been shown by numerous comparisons of models results with measurements in the tropics and extra-tropics and for various seasons (e.g. [14], [15], [70]). For the inter-comparison with the MARSCHALS data we performed a CLaMS simulations for the Arctic winter 2011. The global CLaMS simulation covers an altitude range from the surface up to the 900 K potential temperature (∼ 5 hPa pressure) with a horizontal resolution of approximately 100 km. The vertical resolution at the tropical tropopause is adapted via an aspect ratio of 250 [16] expressing the ratio between horizontal and vertical scales [25]. This results in a vertical resolution of about 400 m around the tropopause. The horizontal winds were taken from the ERA-Interim reanalysis data provided from the European Centre for Medium-Range Weather Forecasts (ECMWF). The vertical velocity above an altitude of about 300 hPa is deduced from the ERA-Interim total diabatic heating rate, including the effects of all-sky radiative heating, latent heat release and diffusive heating as described in [46]. Below this altitude, the vertical model coordinate smoothly transforms into an orography-following σ-coordinate [36]. In CLaMS, an initial distribution of the air parcels is transported according to trajectories with subsequent mixing. The mixing procedure inserts or removes air parcels into the irregular grid, where the distances between next neighbors are larger or lower than a critical deformation parameter y_c (for details see [24]). Here, we use a critical Lyaponov exponent λ_c of 1.5 per day ($y_c = \lambda_c \times \Delta t; \Delta t = 24h$) as mixing parameter.

The simulation was initialized on November 1^{st}, 2011 with data from MLS satellite measurements (e.g., [37]), tracer tracer correlations to MLS N_2O following [13], and results of a multi-annual CLaMS simulation started in October 1^{st}, 2001 [26]. The same data sets are also used as upper boundary conditions (900 K potential temperature) for the model simulation. At the lower boundary (surface) ozone is set equal to zero,which means that no tropospheric source of O_3 is included in the simulation. The boundary condition for CO in the free troposphere are

deduced from MOPITT satellite measurements as described in [47]. Water vapor values in the lower troposphere are prescribed by ERA-Interim. Above, freeze drying of water vapor (dehydration) is calculated based on a simplified cirrus treatment. Freeze drying occurs as soon as the relative humidity exceeds 100%. Ice sedimentation is included in the dehydration scheme, based on the fall velocity of (spherical) ice particles [71]. The simulation for the Arctic winter 2011 include stratosheric chemistry and heterogeneous chemistry on water ice, nitric acid trihydrate (NAT), and liquid $H_2O/HNO_3/H_2OSO_4$ ternary solution (STS) particles. The four particle types may coexist in the steady state (for more details, see [43]). Sedimentation of NAT particles was calculated as by [12]. For this work package we have provided CLAMS results for water vapor, ozone, HNO_3, N_2O, and CO for the Vertical Grid of the Comparison (VGC), for the MARSCHALS Tangent Altitude (TA) and for MARSCHALS FLIGHT Altitude (FLY). All three data sets are provided by IFAC.

9.4 Synergistic use of the capabilities of CLaMS and EMAC models in the comparison with MARSCHALS data

In this section, we briefly discuss the complementary capabilities and features of the CLaMS and EMAC models and their potential synergy in the application to the comparison with MARSCHALS retrieval products. Although the main focus of the scientific studies performed in the past with CLaMS and EMAC, respectively, differ as CLaMS has been used for chemistry-transport-simulations investigating atmospheric processes in high resolution studies whereas EMAC has been mainly designed as chemistry climate-model to investigate the past and future development of the atmosphere and its composition both models are well suited for the comparions with the MARSCHALS data and complements each other. This complementarity is mainly due to differences in model architecture / transport scheme, treatment of tropospheric processes, model resolution as well as initialisation which allows to identify shortcomings in the data sets.

With respect to the model architecture / transport scheme ClaMS uses a Lagrangian approach, one considers an ensemble of air parcels (APs) following the fluid and, consequently, forming a time-dependent irregular grid moving with the fluid elements; by contrast, with a Eulerian approach (EMAC), one considers a fixed spatial grid through which fluid elements move. In ClaMS, the irreversible part of transport, i.e. mixing, is controlled by the local horizontal strain and vertical shear rates and thus by physical principles. An advantage of ClaMS transport scheme is to preserve tracer gradients or filaments in a much more realistic manner than alternative simulations with chemistry transport models (CTMs) employing Eulerian transport schemes.

Tropospheric processes are included in different ways, also. Whereas the tropospheric chemistry and microphysic is treated in a simplified approach in CLaMS, EMAC uses a detailed tropospheric chemistry scheme (including Non Methane HydroCarbons (NMHCs) up to isoprene) to simulate the atmospheric oxidation of VOCs into CO and at least to CO_2 in a realistic manner. In order to allow in this study a direct comparison with the measurements and with CLaMS, also, EMAC is used in a so-called nudged mode (see Section 9.2). However, due to the finer horizontal resolution of CLaMS and the re-initialisation of CLaMS with satellite data 6 weeks prior to the MARSCHALS measurements, the simulation results of CLaMS respresent more or less the short term capabilities of high-resolution CTM simulations whereas the EMAC results highlights on a more long-term CTM view.

9.5 CLaMS/EMAC model data and effect of the convolution

In this section we report the results of the CLaMS and EMAC models. In figures 134 and 135 we report the maps with the state of the atmosphere for Flight 1 and Flight 2 simulated by CLaMS and EMAC models.

Both simulations performed with EMAC and CLaMS, respectively, show that Flight 1 occurred at the edge of the Arctic polar vortex (see Figures 136 and 137).

Measurements inside and outside the polar vortex yield differences in measured O_3, HNO_3, and N_2O profiles in altitudes between 10 km until 18 km. The simulated HNO_3 profiles at 450 K potential temperature show a strong reduction of HNO_3 due to denitrification, the permanent removal of nitrogen compounds through sedimentation of HNO_3-containing PSC particles. Below this layer (375 K or 380 K), evidence for an enhancement of HNO_3 is found caused by renitrification in both model simulations. Moreover, both model simulations show a transport induced structure of enhanced HNO_3, O_3 and reduced N_2O in the later part of Flight 1 at about 15 km that is also well reproduced by the MARSCHALS observations (see Figures 150 and 154, sequences from 40 to 45). In contrast to Flight 1, the simulations show that Flight 2 occurred inside the Arctic polar vortex. Also here denitrification and renitrification signals were found in both model simulations.

In order to compare the target vertical profiles provided by the models on a high resolution altitude grid with the retrieved vertical profiles on the optimized vertical grid, we need to take into account (as described in equation 1) the smoothing introduced by the retrieval procedure due to the information content of MARSCHALS measurements, and the a priori information used in optimal estimation approach used in MARC.

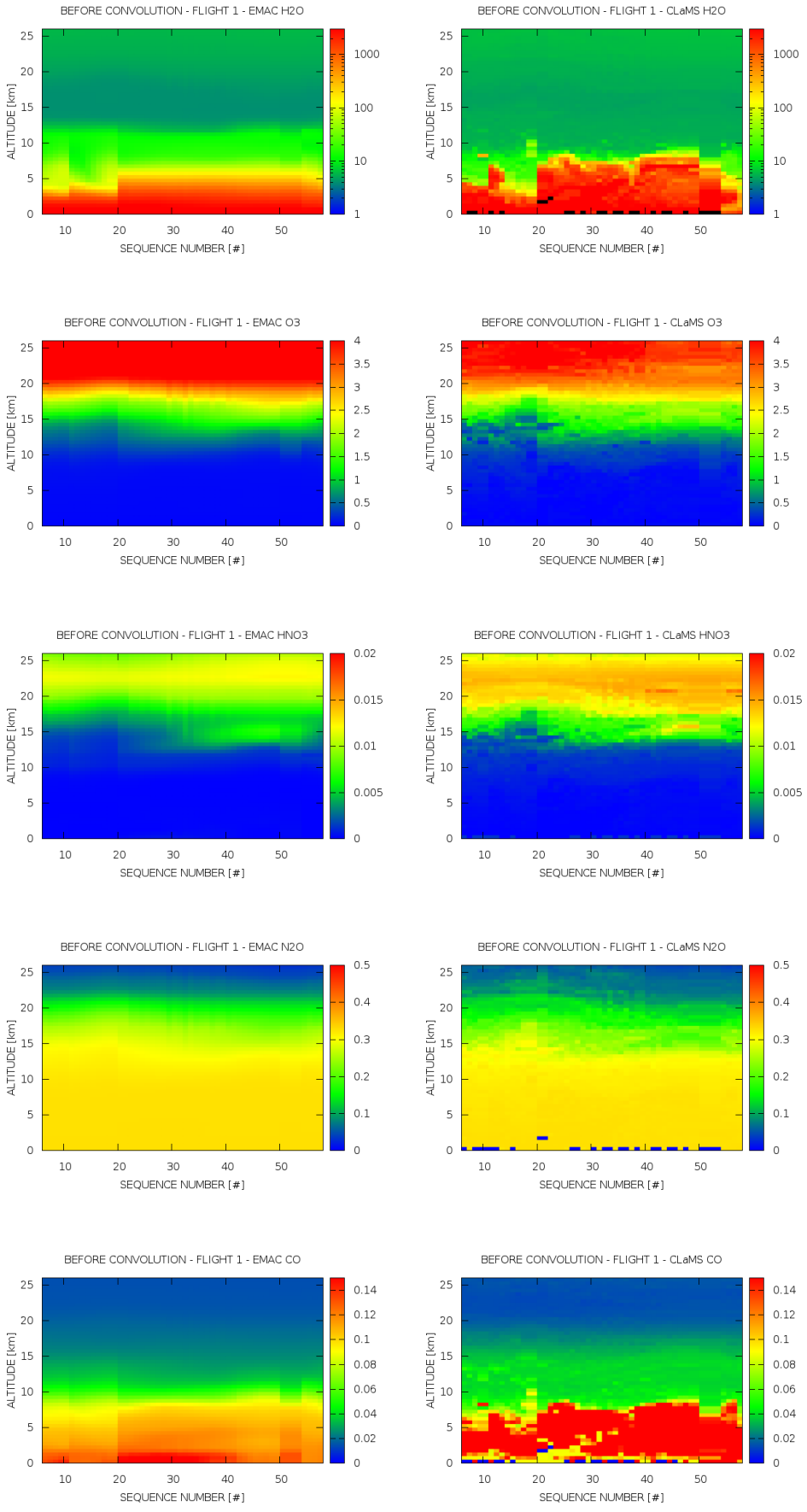

Fig. 134: Maps containing the state of the atmosphere for Flight 1 simulated by CLaMS and EMAC models.

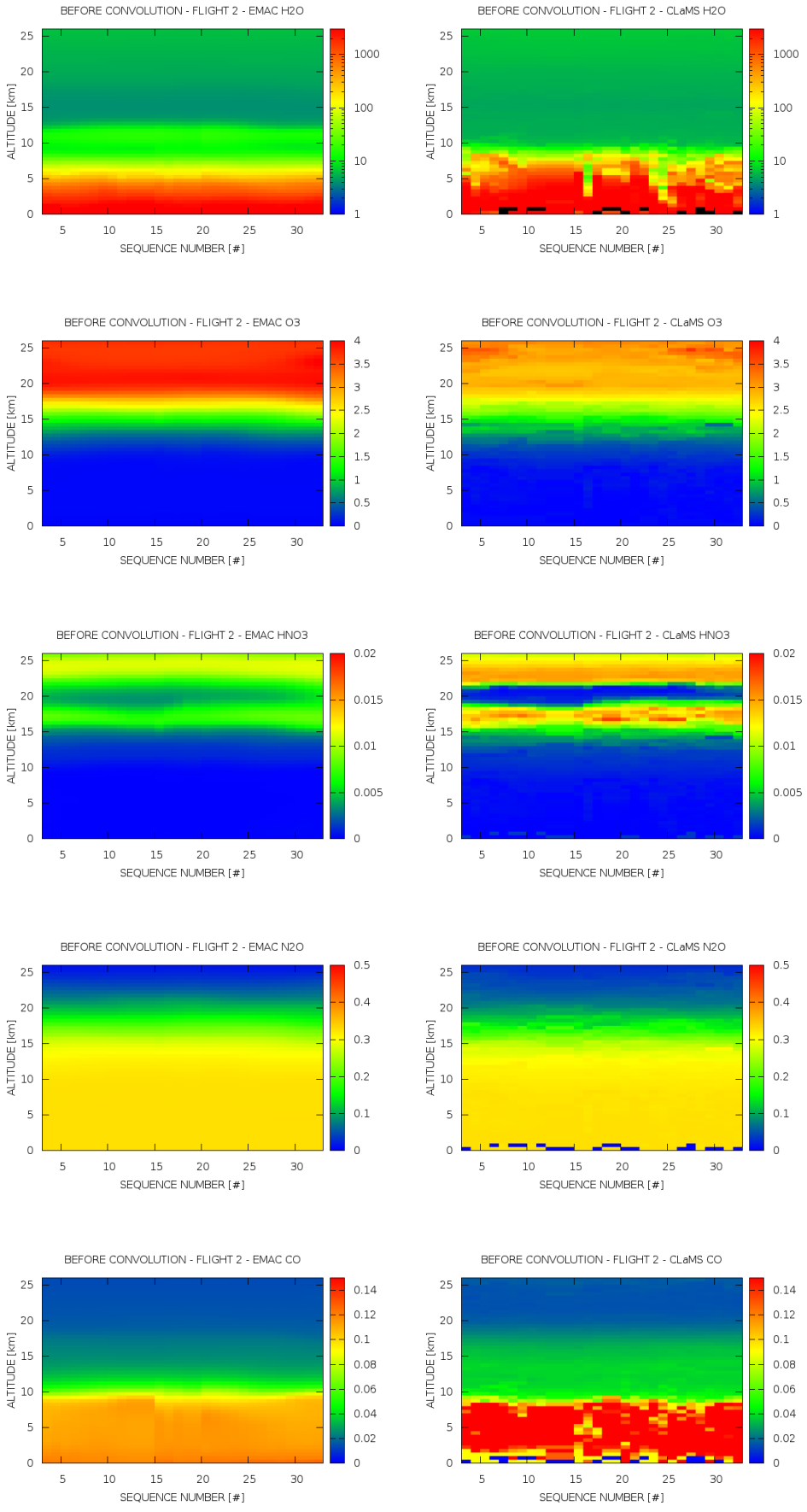

Fig. 135: Maps containing the state of the atmosphere for Flight 2 simulated by CLaMS and EMAC models.

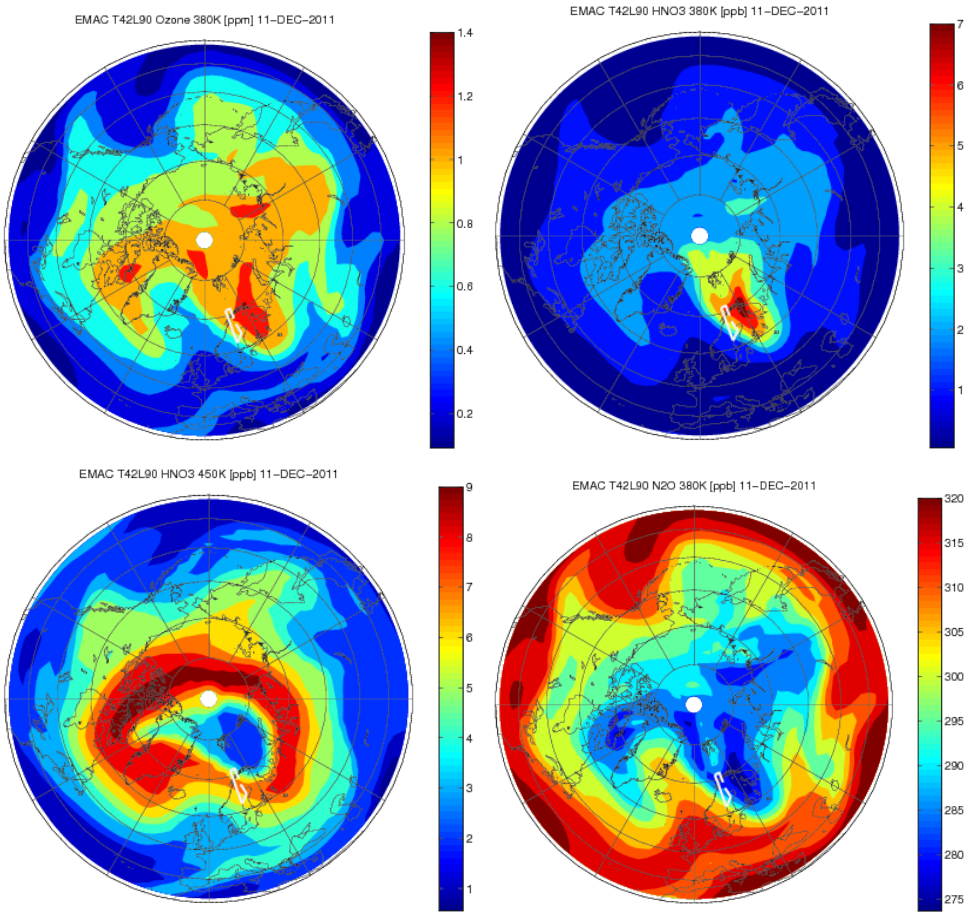

Fig. 136: EMAC model calculations for 11 December 2011 (Flight 1), interpolated to isentropic levels of 450 K (about 18 km) and 380 K (about 14 km). a) O_3 at 380 K, b) HNO_3 at 380 K, c) HNO_3 at 450 K and d) N_2O at 380 K. Observations (flight path shown as white line) were taken at the edge of the polar vortex, e.g. as evident by the large gradient in N_2O. HNO_3 profiles at 450 K show a strong reduction of HNO_3 due to denitrification, with enhanced levels of HNO_3 at 380 K.

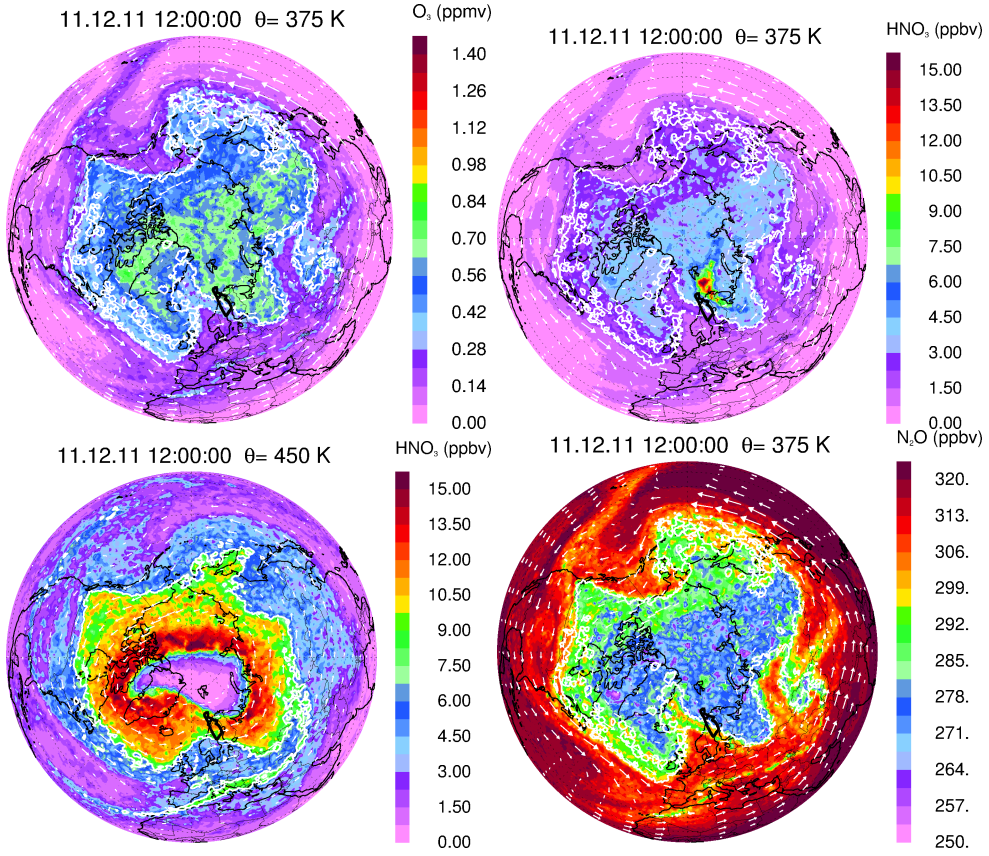

Fig. 137: The horizontal distribution of O_3, N_2O, and HNO_3 at 375 K potential temperature on 11 December 2011 (12.00 UT) obtained by CLaMS model. The vortex edge [45] is marked by white contour lines. The horizontal winds are indicated by white arrows. The flight path is marked in black.

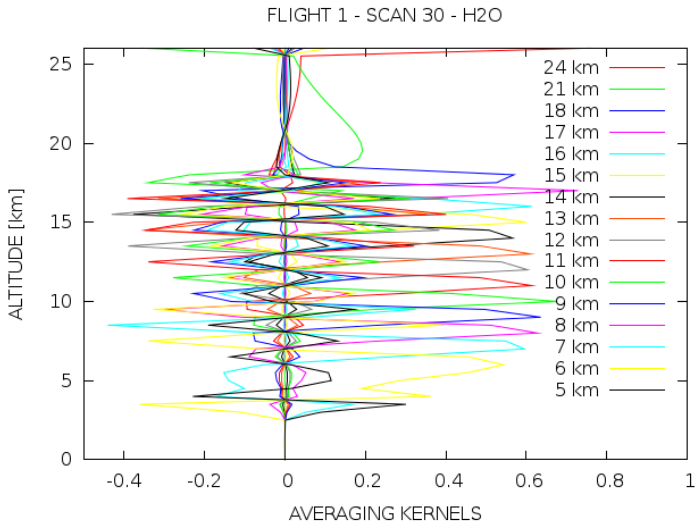

Fig. 138: High resolution Averaging Kernel matrix calculated for H_2O (Scan 30 of the Flight 1).

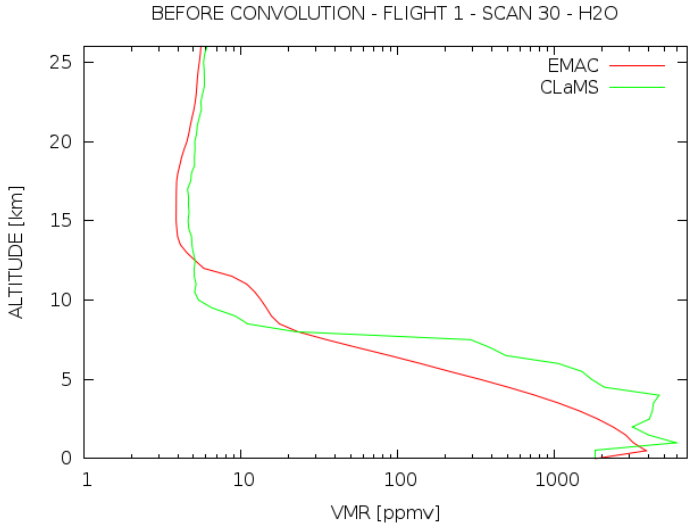

Fig. 139: High resolution profiles calculated for H_2O by EMAC and CLaMS model (Scan 30 of the Flight 1).

To provide a physical meaning of equation 1 for the convolution of the high resolved model profiles we point up that $\mathbf{x}_{model}$ is the profile which the retrieval process (based on the MARC processor) would obtain if the true profile was $\mathbf{x}_{model,h}$. The first two terms represent the classical convolution, as described by equation 15 in [5]; the last two terms are a correction which takes into account the difference between the MARC vertical retrieval grid and the vertical grid of the model (this difference is negligible in our case, being less than 0.05%).

If we consider that the VGC is in steps of 500 m (much finer than the vertical resolution of the optimal retrieval grid of MARSCHALS measurements) and that the a priori information adopted to constraint the inversion process of MARSCHALS data is relatively week (a priori uncertainty of 200%), the sensitivity of MARSCHALS measurements even if combined with the a priori information might be insufficient to retrieve the profile on the retrieval vertical grid. This is clearly highlighted by the oscillations of MARSCHALS AKs calculated on the fine vertical grid in steps of 500 m wrt the lower altitudes as shouwn in Figure 138. When the oscillating averaging kernels are convoluted with the profile simulated by the models, which can also be characterirized by very strong gradients as for example to water vapor profiles simulated by CLaMS model (see Figure 139), the resulting convoluted profile shows strong gradients that might also lead to negative values (see Figure 140).

In figures 141 and 142 we report the maps with the state of the atmosphere for Flight 1 and Flight 2 by CLaMS and EMAC models and convoluted taking into account the MARSCHALS AKs as described in equation 1. We can note that the resulting water vapor convoluted profile obtained for CLaMS model data shows strong gradients that lead to negative values of the VMR.

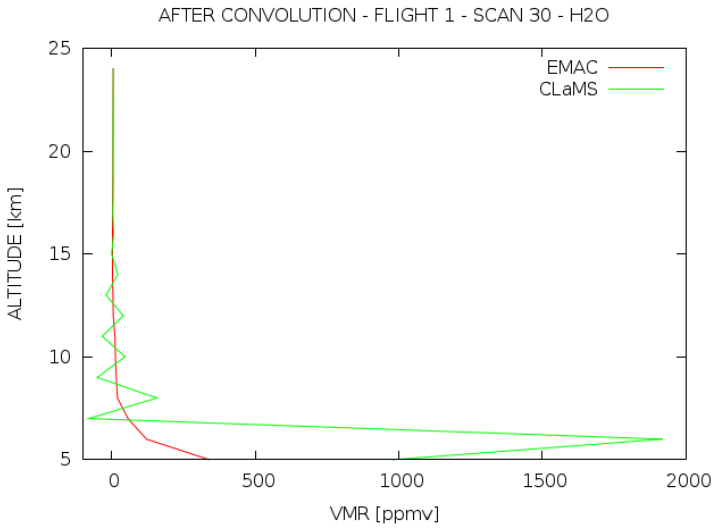

Fig. 140: Convoluted H_2O profiles (Scan 30 of the Flight 1).

In order to improve the H_2O profiles comparison and in particular avoid the negative value, we performed some tests to evaluate the effect of the high resolution Averaging Kernel matrix in the convolution. In fact the AKs are evaluated on the state of the atmosphere at the last iteration of the MARC procedure, and in the case of the H_2O the state of the atmosphere is orders of magnidute different from the CLaMS simulations. For this reason, we implemented in MARC the feature to export the AKs evaluated on the H_2O profiles obtained by CLaMS simulations, and we applied them to EMAC and CLaMS high resolved profiles. The results of these tests for CLaMS are reported in Figure 143 and show that a better evaluation of the AKs reduces the convolution instability that can be occur when the information contains in the measurements is weak. On the base of this tests, we report in the following sections the results we obtained using the AKs evaluated on the H_2O profiles obtained by CLaMS simulations limited to CLaMS convoluted profiles for H_2O comparison.

9.6 Comparison of MARSCHALS retrieval products with model data for the ESSenCe Flight 1 and Flight 2

In this section, we report the results of the comparison of MARSCHALS retrieval products for ESSenCe Flight 1 and Flight 2 with CLaMS and EMAC models data. The comparison was performed on H_2O, O_3, HNO_3, N_2O, and CO VMR profiles retrieved from the sequences of Flight 1 and Flight 2 of MARSCHALS, as reported in sections 4.1 and 4.1. MARSCHALS retrieval setup is described in sections 4.2.2 and 5.3.1, and the comparison is shown, for each profile of the targets of the comparison, on the bands identified in sections 4.3 and 5.5. In particular, we show the H_2O on band C, the O_3 on all bands, the HNO_3 on band C and D, the N_2O on band B, and CO on band D.

The results are organized in plot panels related to each target and to each band of the analysis and map panels containing the profiles of the targets along flight path. The results are shown for Flight 1 and Flight 2. For each plot panel we report the results of the comparison between the profiles obtained by MARC (blue line), and the convoluted model profiles on the retrieval vertical grid as described in equation 1 (EMAC results: red line, CLaMS results: green line). Each plot is labelled with the corresponding scan number. For each map panel we report the results of the models before the convolution (first row), after the convolution (second row), and the results of the MARC retrieval procedure (third row).

A noteworthy feature of enhanced HNO_3 and enhanced O_3 is observed towards the end of Flight 1 at about 15 km altitude. Both models consistently reproduce these transport induced features (see also Figures in Section 9.4). Renitrification (i.e. sedimentation of HNO_3 containing particles) may have contributed to the enhanced HNO_3, but is not the only cause, as both models (and the MARSCHALS observations) show also a simultaneous enhancement of O_3 and a reduction of N_2O.

9.6.1 Water vapor comparison results

In figures 144, 145, and 146 we report the comparison for the H_2O on band C. The comparison shows that the models are in a quite good agreement above 12 km, while below 12 km CLaMS results are systematically larger.

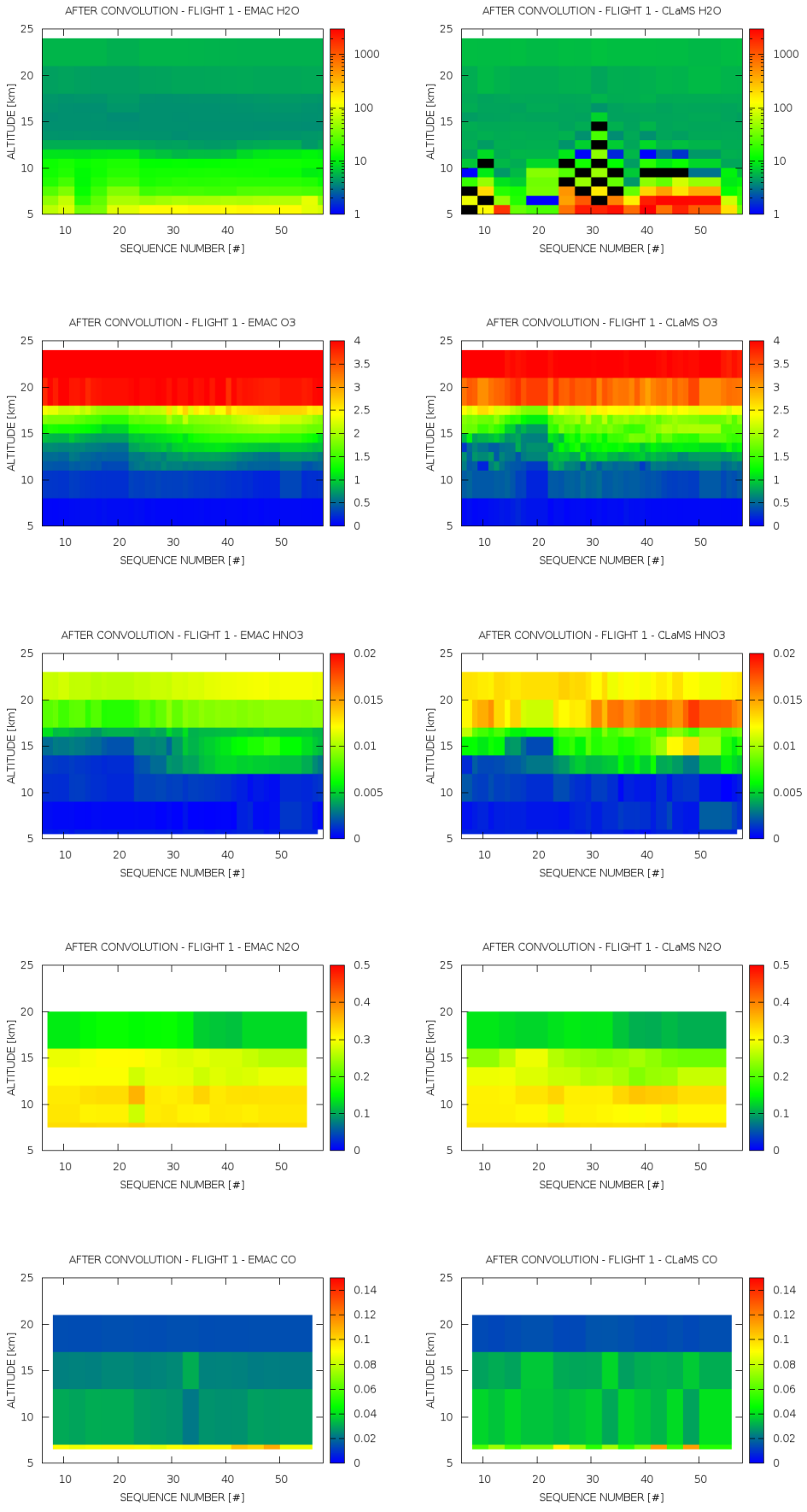

Fig. 141: Maps containing the state of the atmosphere for Flight 1 simulated by CLaMS and EMAC models and convoluted with the MARSCHALS AKs.

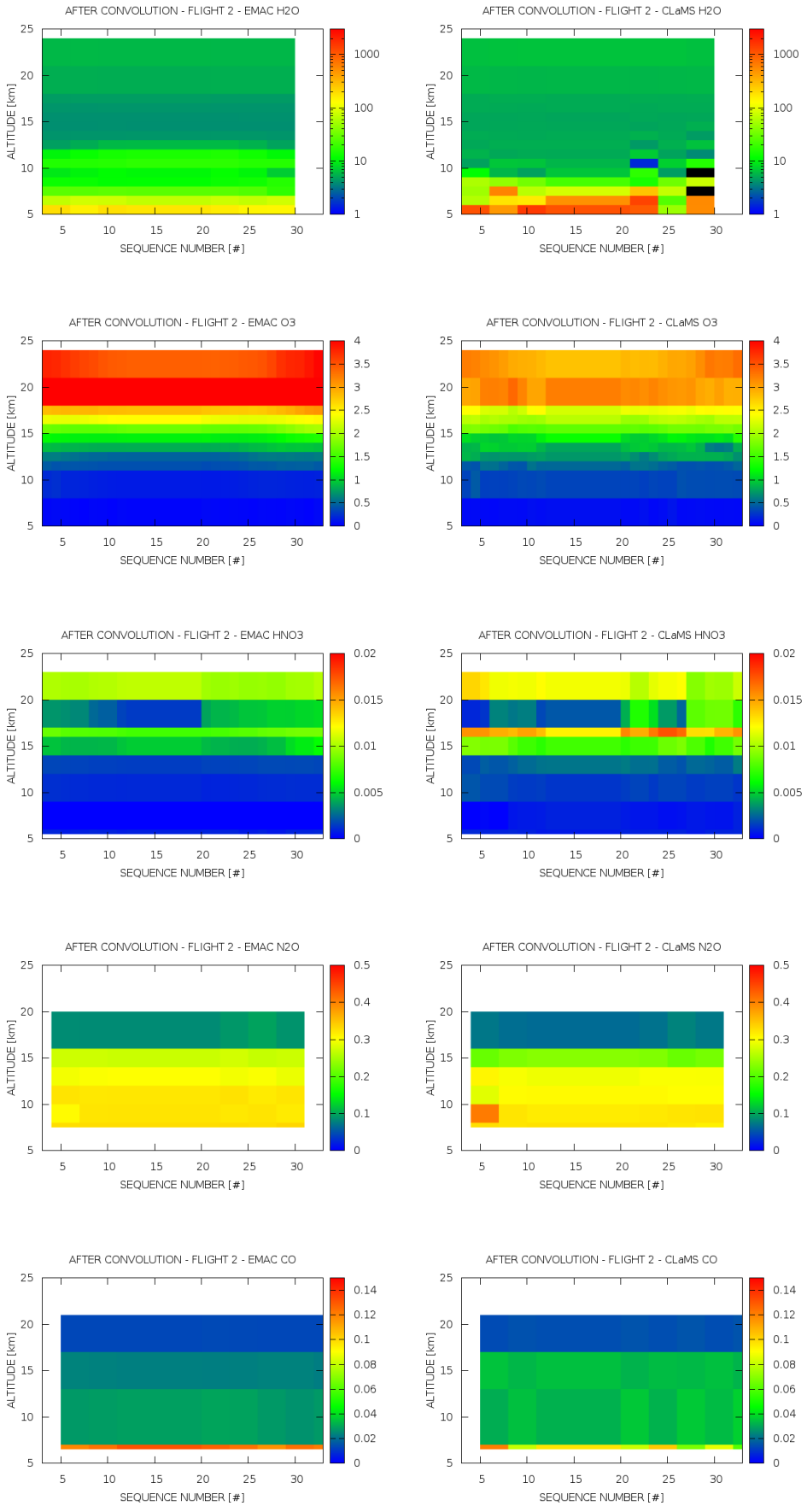

Fig. 142: Maps containing the state of the atmosphere for Flight 2 simulated by CLaMS and EMAC models and convoluted with the MARSCHALS AKs.

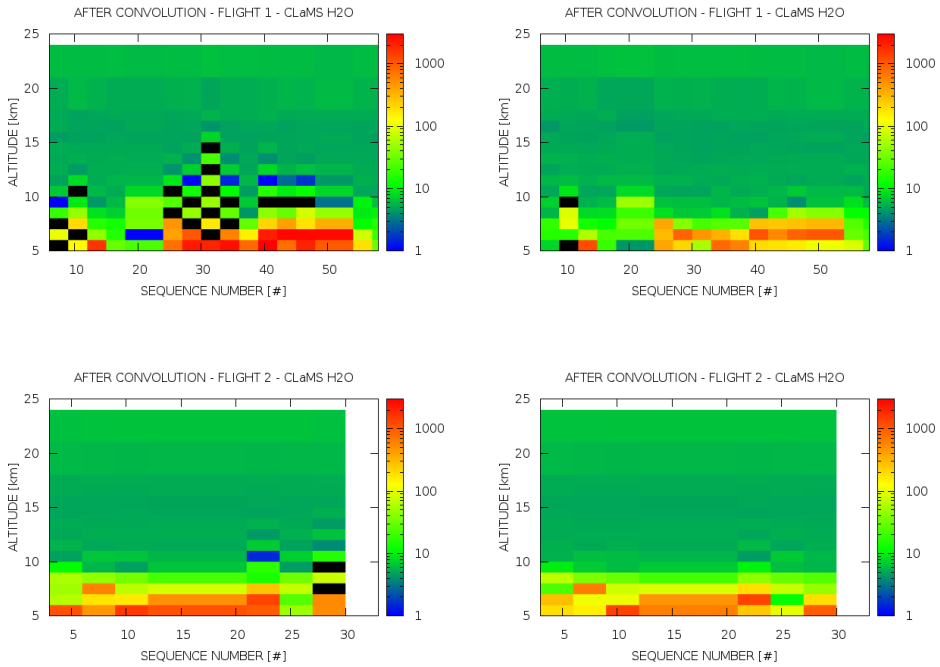

Fig. 143: Maps containing the H_2O for Flight 1 and 2 simulated by CLaMS and EMAC models and convoluted with the MARSCHALS AKs: On the left side we show the results obtained using the AKs evaluated on the MARSCHALS products; On the right side we show the results obtained using the AKs evaluated on the CLaMS simulations.

At lower altitudes, the differences with CLaMS are larger, and a better agreement is found between MARSCHALS profiles and EMAC data.

As pointed out in the model description (see section 9.3) CLaMS H_2O is calculated using a simplified cirrus treatment. This could explain that below 10 km ClaMS H_2O mixing ratios are higher than EMAC and MARSCHALS data.

Very good agreement between the models above (about) 12 km. Below 12 km some differences in the profile shapes are obvious which could be explained by the simplified cirrus treatment in CLaMS.

9.6.2 Ozone comparison results

In figures 147, 148, 149, 150, and 151 we report the results of the comparison for O_3 on band B, C and D. The comparison shows that the models are in a quite good agreement below 17 km, while above 17 km EMAC results are systematically larger. The agreement between models data and MARSCHALS measurements is quite good. Generally, the MARC products are between the model profiles (larger values are found with respect to CLaMS lower values with respect to EMAC). Below 15 km the differences are always less than five times the MARC error. Above 15 km MARC results appear to be in a better agreement with CLaMS profiles.

Previous studies show that ClaMS O_3 mixing ratios in the polar vortex region are in good agreement with measurements [13, 69].

Above 18 km, EMAC ozone values are higher than the CLaMS data, which agree well with the MARC data. Overestimation of polar O_3 VMRs above $\sim$18 km is a known feature for the chemistry-climate-model EMAC during the course of the Arctic winter, but unfortunately the reason for this overestimation is still unknown. One reason for the good agreement of the CLaMS O_3 VMR with the MARC data could be found in the initialisation with MLS data on November 1^{st}, 2011. Please note, that EMAC has been initialised on January 1^{st}, 2011, with model data only. Due to these differences in the chemical initialisation differences in the modelled polar O_3 VMRs between CLaMS and EMAC can be expected.

9.6.3 Nitric acid comparison results

In figures 152, 153, 154, and 155 we report the results of the comparison for HNO_3 on band C and D. The comparison shows that the models are in a quite good agreement below 15 km, while above 15 km CLAMS results are systematically larger. As for the O_3 the agreement between the models data and MARSCHALS measurements

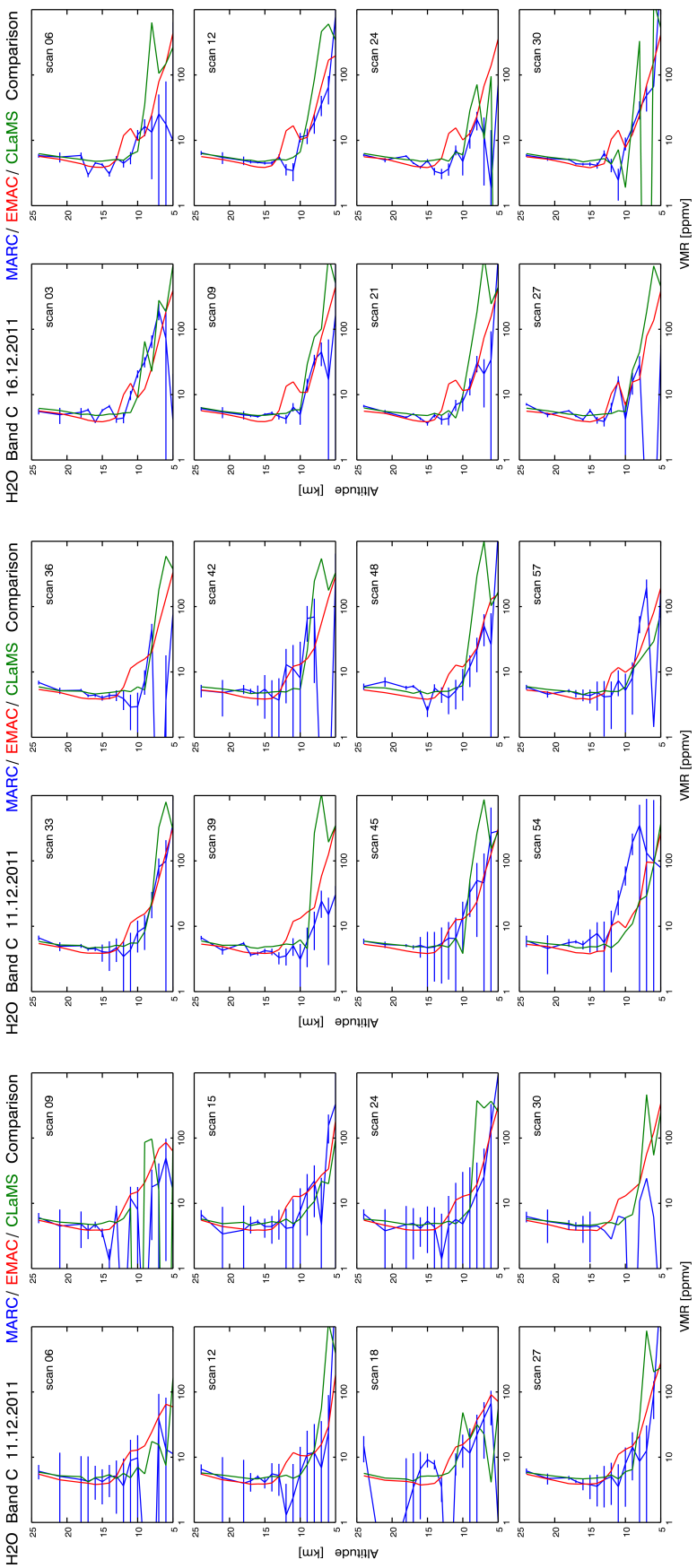

Fig. 144: Plot panels: H_2O comparison between MARSCHALS products obtained from Flight 1 and Flight 2, and CLaMS/EMAC model data on band C.

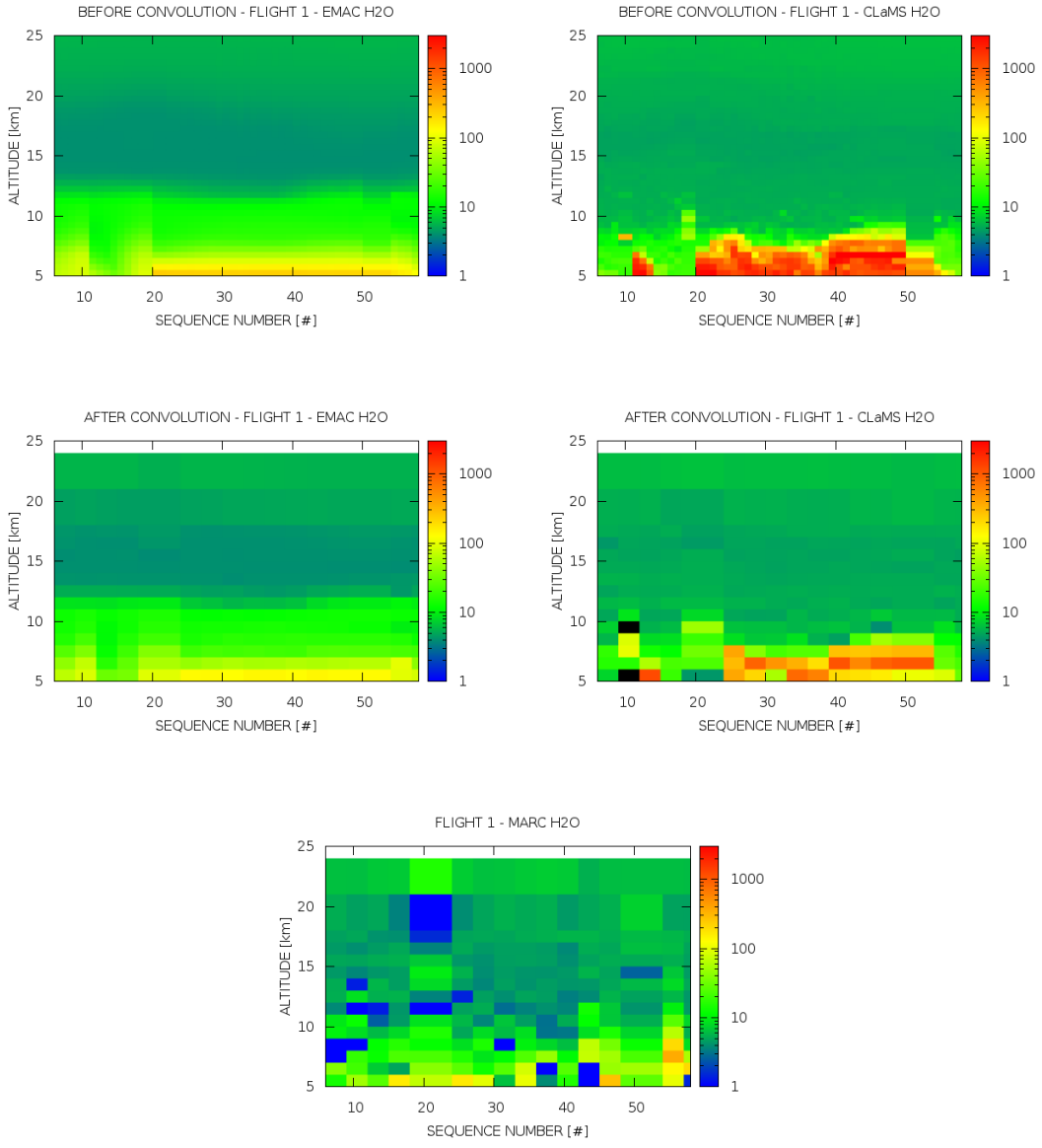

Fig. 145: Map panels: H_2O comparison between MARSCHALS products obtained from Flight 1 and CLaMS/EMAC model data.

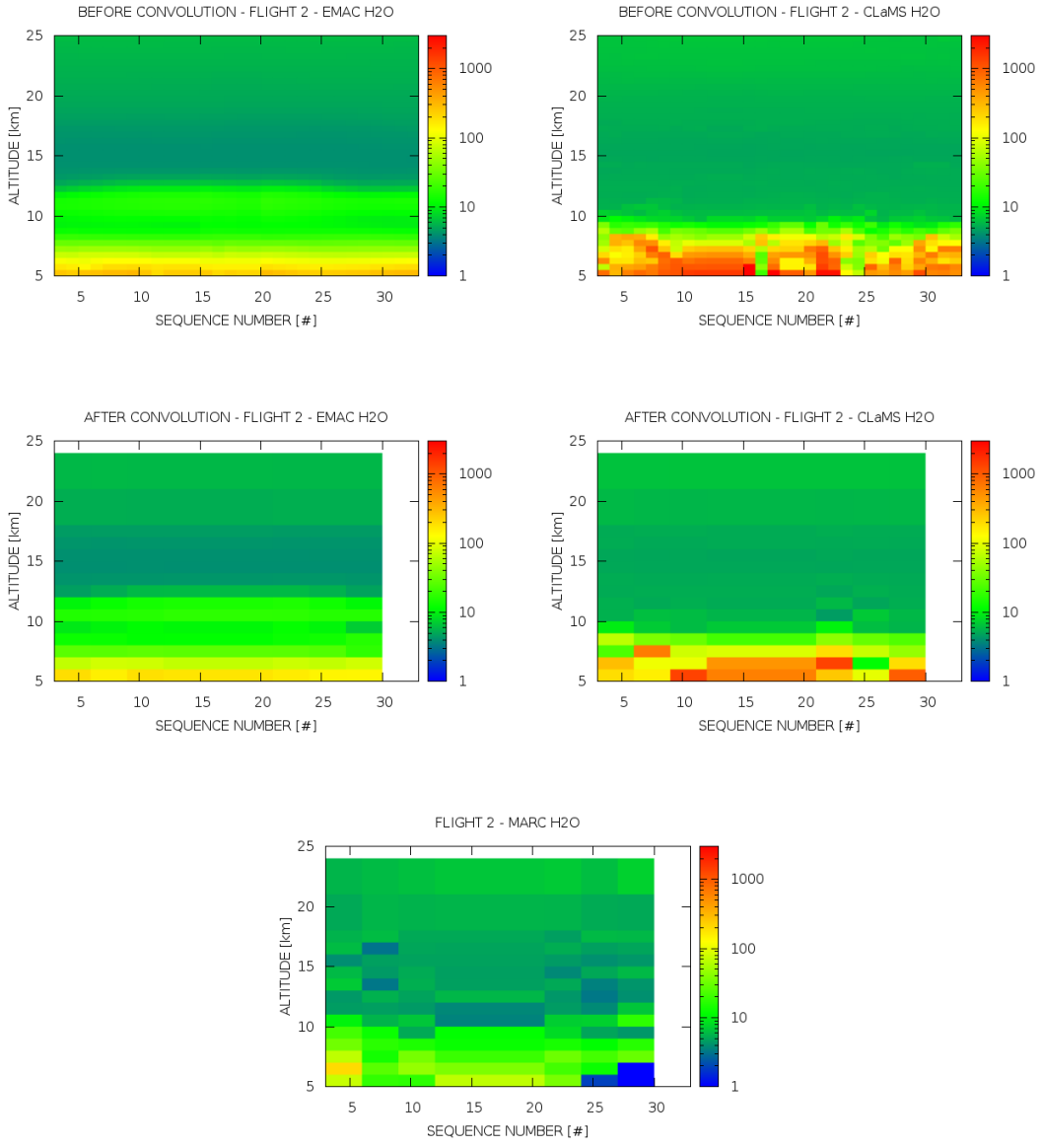

Fig. 146: Map panels: H_2O comparison between MARSCHALS products obtained from Flight 2 and CLaMS/EMAC model data.

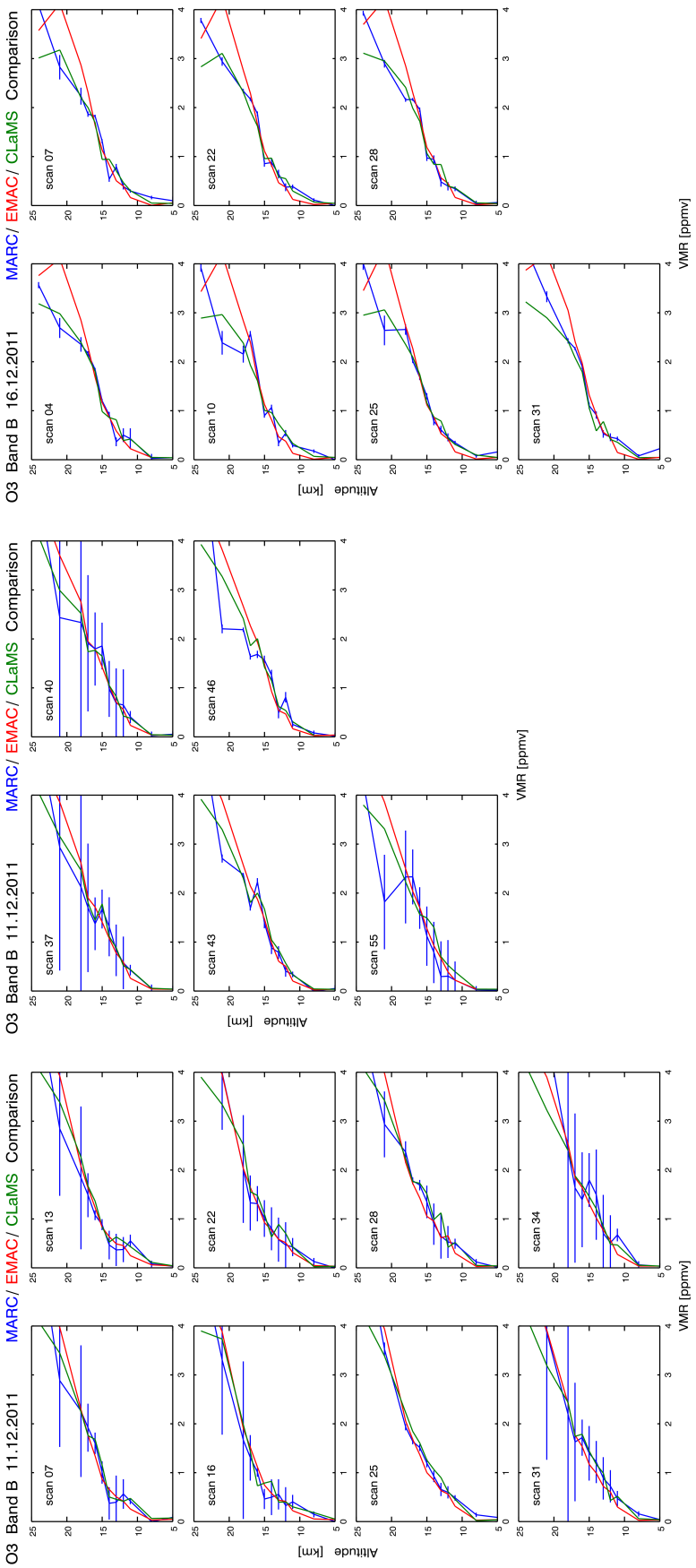

Fig. 147: Plot panels: O_3 comparison between MARSCHALS products obtained from Flight 1 and Flight 2, and CLaMS/EMAC model data on band B.

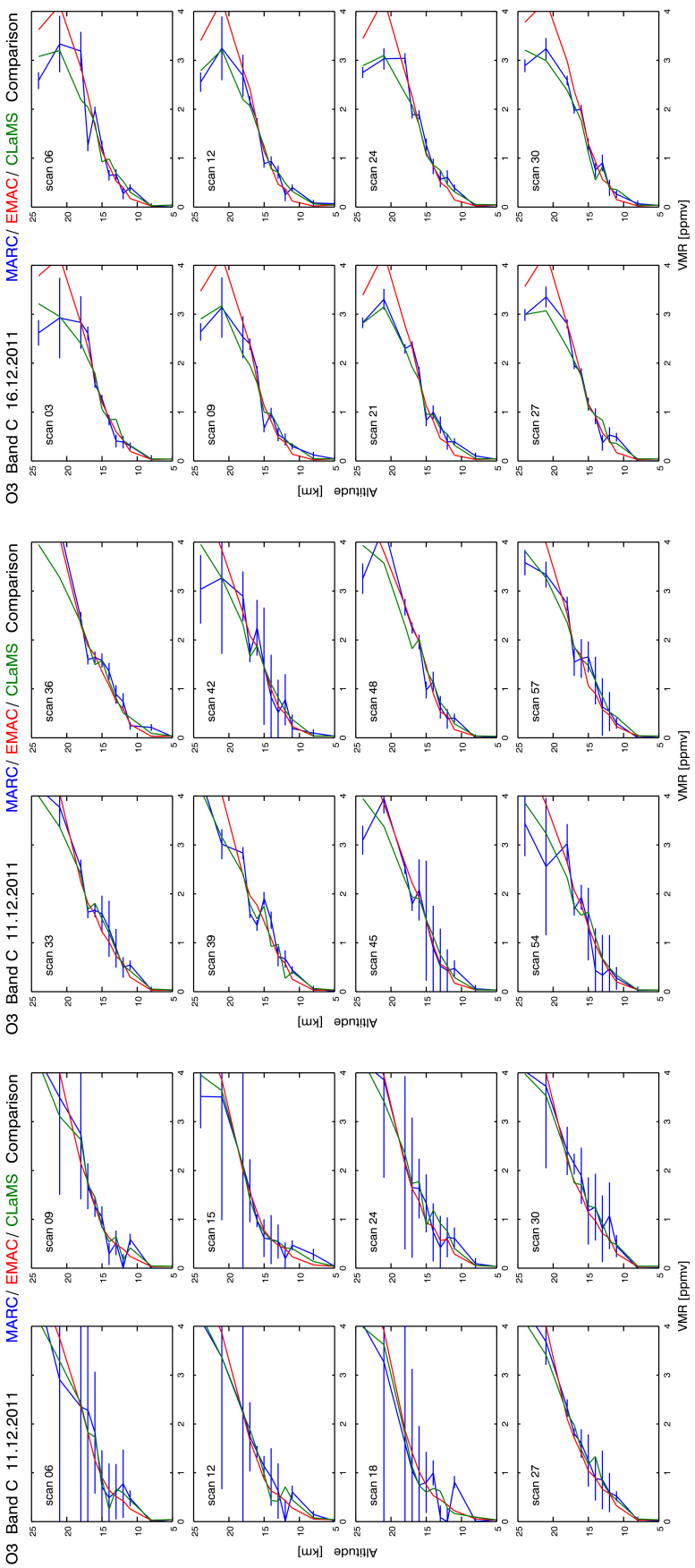

Fig. 148: Plot panels: O_3 comparison between MARSCHALS products obtained from Flight 1 and Flight 2, and CLaMS/EMAC model data on band C.

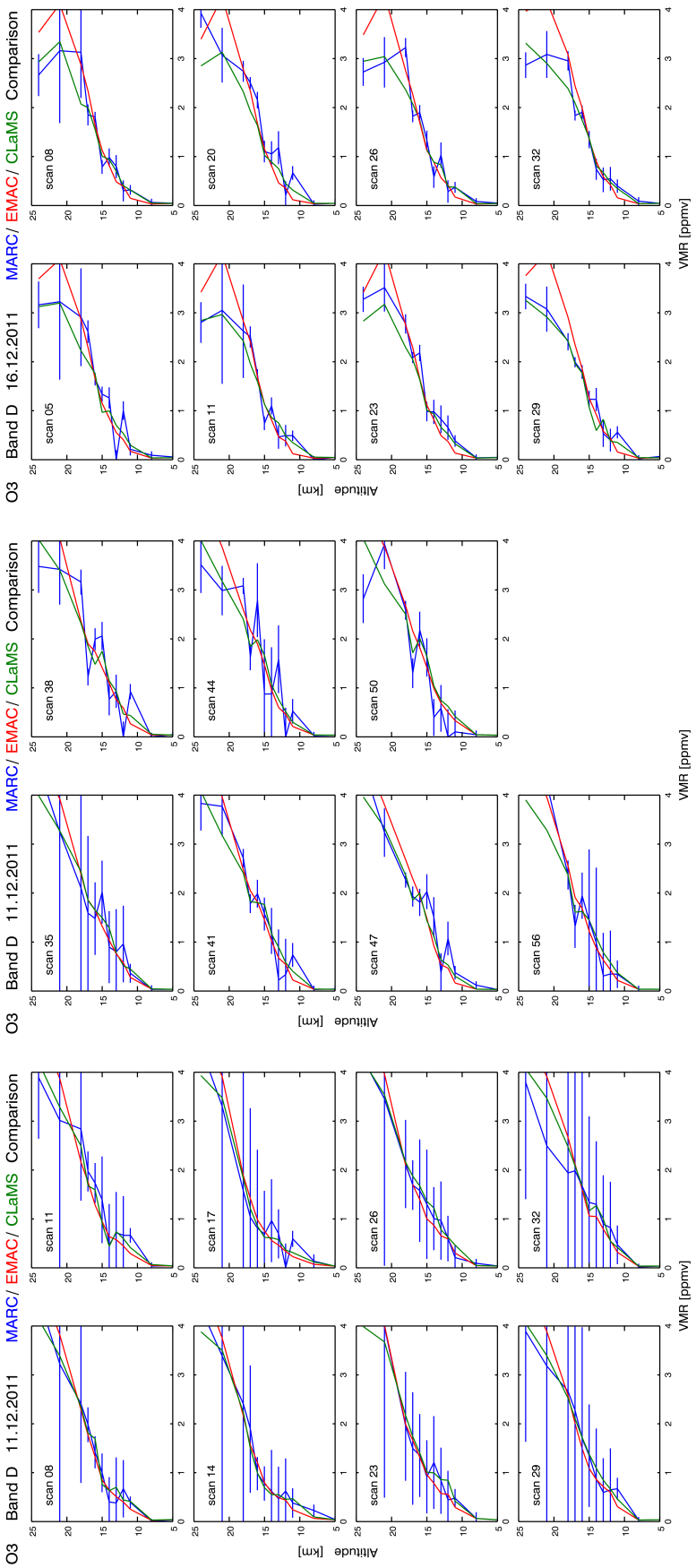

Fig. 149: Plot panels: O_3 comparison between MARSCHALS products obtained from Flight 1 and Flight 2, and CLaMS/EMAC model data on band D.

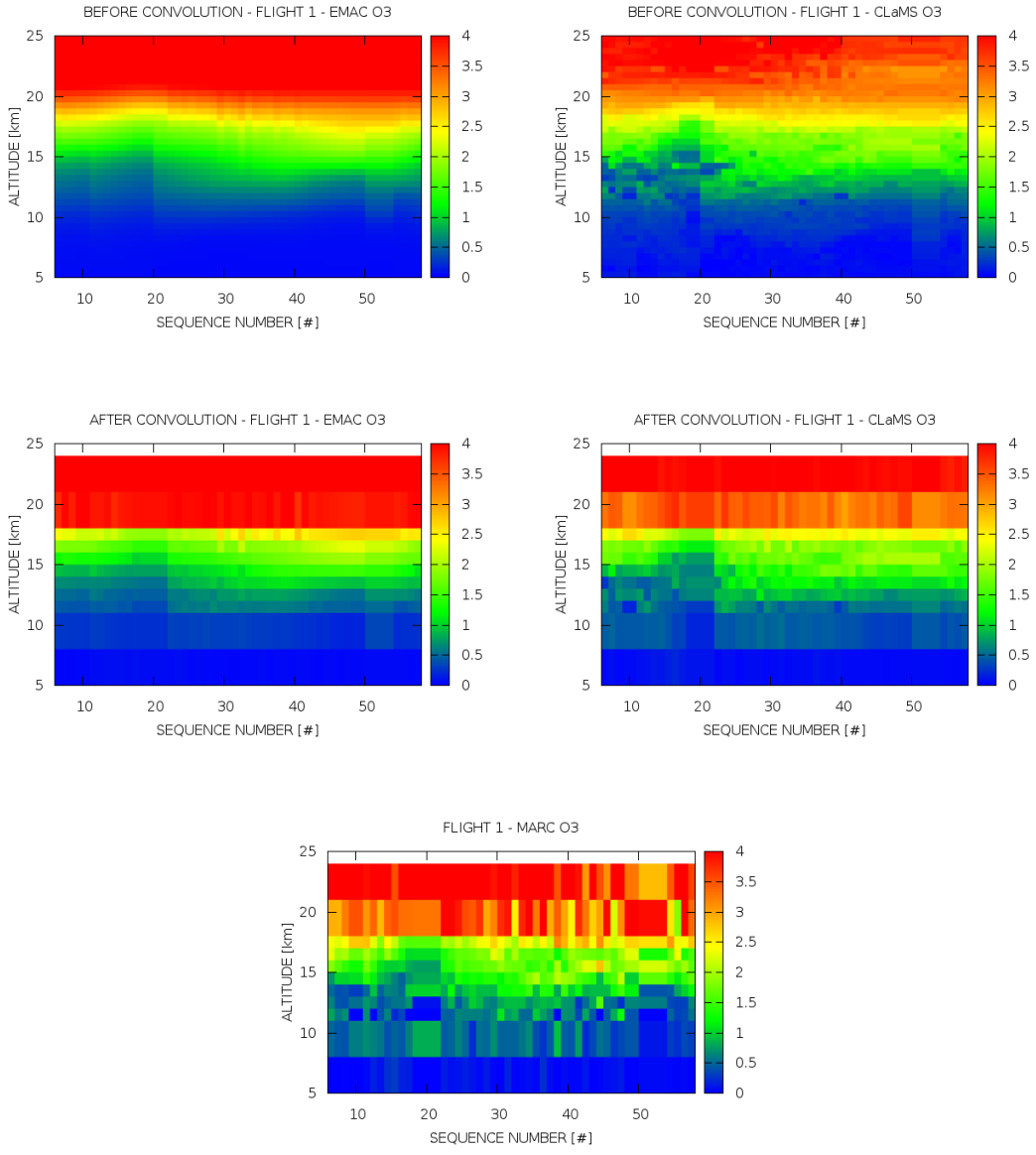

Fig. 150: Map panels: O_3 comparison between MARSCHALS products obtained from Flight 1 and CLaMS/EMAC model data.

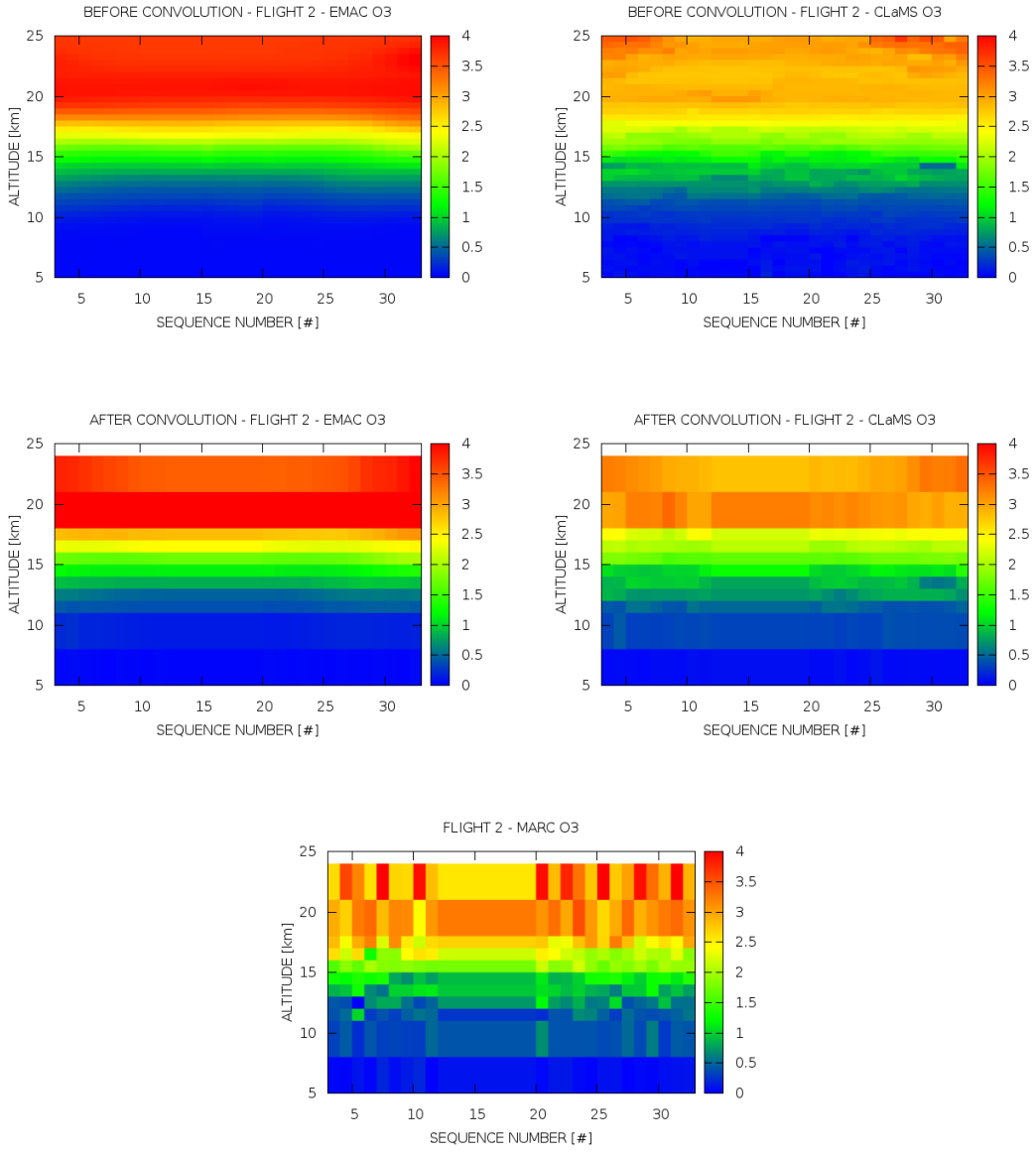

Fig. 151: Map panels: O_3 comparison between MARSCHALS products obtained from Flight 2 and CLaMS/EMAC model data.

is quite good below 15 km. Above 15 km the differences are larger than five times the MARC error and also the model profiles do not agree, even if the shapes of the three curves consistently show a HNO_3 reduction at 20 km.

The HNO_3 profiles around 20 km show a strong reduction of HNO_3 due to denitrification, the permanent removal of nitrogen compounds through sedimentation of HNO_3-containing PSC particles. Below this layer, an enhancement of HNO_3 is found caused by renitrification. In CLaMS, sedimentation of NAT particles is calculated with a global nucleation rate for NAT particles [12]. This could yield an overestimation of both denitrification and renitrification.

9.6.4 Nitrous oxide comparison results

In figures 156, 157, and 158 we report the comparison for N_2O on band B. The comparison shows that the models are in a quite good agreement. MARC results are systematically less than the models below the flight altitude and the differences below 15 km are less than tree times the MARC error.

Above 15 km the EMAC N_2O are larger than those of CLaMS. This could be also due to the intialisation of CLaMS N_2O with MLS data on November 1^{st}.

9.6.5 Carbon monoxide comparison results

In figures 159, 160, and 161 we report the comparison for CO on band D. The comparisons shows that both models agree quite well in the stratosphere above 10 km but show substantial differences in troposphere caused by the different treatment of tropospheric CO in the two models. While EMAC calculates CO interactively from prescribed emissions, CLaMS uses tropospheric CO from MOPITT observations.

CO from MARSCHALS retrievals shows much lower values (in fact below detection limit in most cases) below flight altitude and higher CO than the models above flight altitude. This is consistent with the comparisons between MARSCHALS CO profiles and Aura/MLS satellite data shown in the section of the validations of MARSCHALS measurements.

9.7 Conclusions

In this section, we present a summary of the results obtained from the comparison of MARSCHALS retrieval products with the state of the atmosphere simulated using CLaMS and EMAC atmospheric chemical transport models.

The EMAC model is a numerical chemistry and climate simulation system that includes sub-models describing tropospheric and middle atmosphere processes and their interaction with oceans, land and human influences while CLaMS model was originally developed for the stratosphere and was extended to the troposphere. Although the main focus of the scientific studies performed in the past with CLaMS and EMAC, respectively, differ as CLaMS has been used for chemistry-transport-simulations investigating atmospheric processes in high resolution studies whereas EMAC has been mainly designed as chemistry climate-model to investigate the past and future development of the atmosphere and its composition both models are well suited for the comparions with the MARSCHALS data and complements each other. This complementarity is mainly due to differences in model architecture / transport scheme, treatment of tropospheric processes, model resolution as well as initialisation which allows to identify shortcomings in the data sets.

As target of the comparison, we hconsidered the VMR vertical profiles of the following atmospheric constituents: H_2O, O_3, HNO_3, N_2O, and CO. In order to compare the target vertical profiles provided by the models on a high resolution altitude grid (from 26 km to 0 km in steps of 0.5 km) with the retrieved vertical profiles on the optimized vertical grid, we took into account the smoothing introduced by the retrieval procedure due of the information content of the MARSCHALS measurements using equation 1.

Both simulations performed with EMAC and CLaMS, respectively, show that Flight 1 occurred at the edge of the Arctic polar vortex. Measurements inside and outside the polar vortex yield differences in measured O_3, HNO_3, and N_2O profiles in altitudes between 10 km until 18 km. The simulated HNO_3 profiles at 450 K potential temperature show a strong reduction of HNO_3 due to denitrification, the permanent removal of nitrogen compounds through sedimentation of HNO_3-containing PSC particles. Below this layer (375 K or 380 K), evidence for an enhancement of HNO_3 is found caused by renitrification in both model simulations. Moreover, both model simulations show a transport induced structure of enhanced HNO_3, O_3 and reduced N_2O in the later part of Flight 1 at about 15 km. In contrast to Flight 1, the simulations show that Flight 2 occurred inside the Arctic polar vortex. Also here denitrification and renitrification signals were found in both model simulations.

The H_2O comparison shows that the models are in a quite good agreement above $\sim$12 km, while below 12 km CLaMS results are systematically larger. At lower altitudes, the differences between MARSCHALS and CLaMS are larger, and a better agreement is found with EMAC data. The fact that CLaMS H_2O is calculated using a

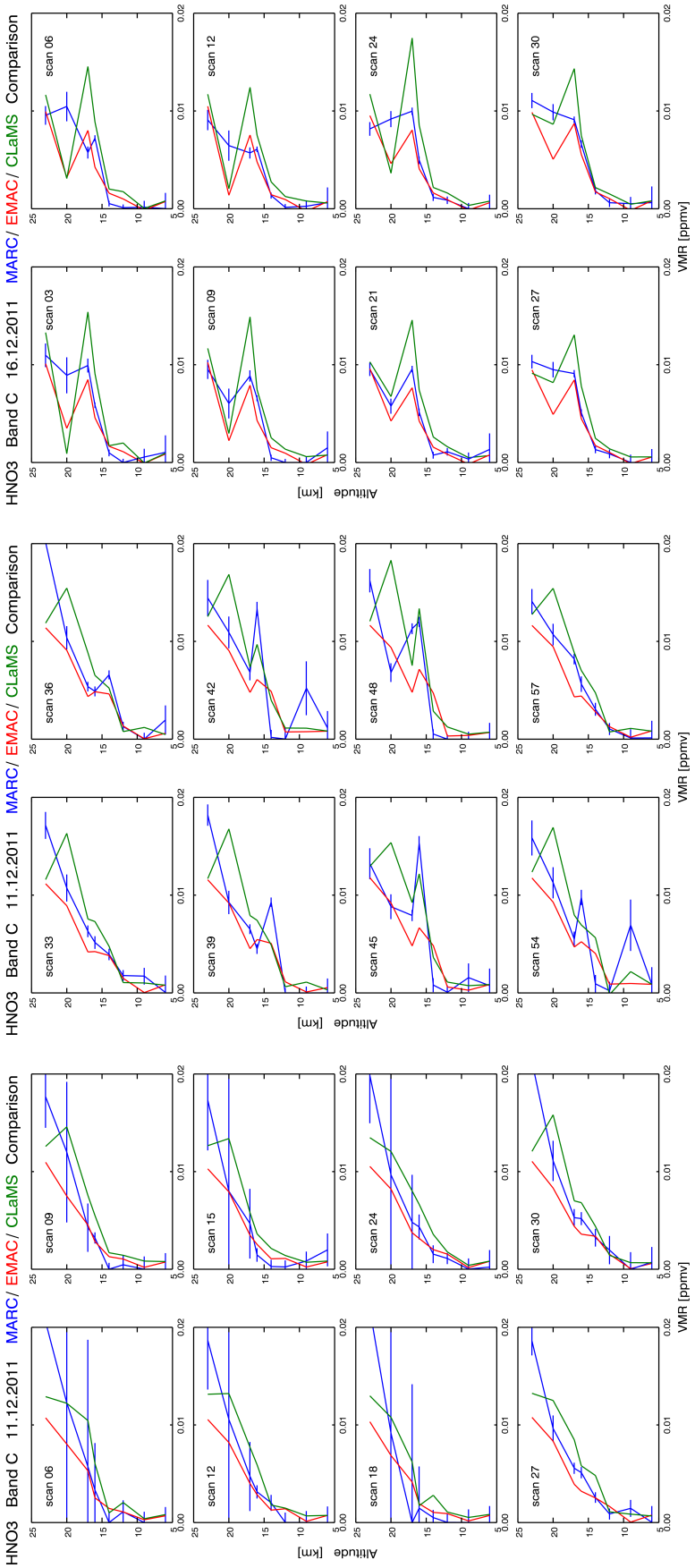

Fig. 152: Plot panels: HNO_3 comparison between MARSCHALS products obtained from Flight 1 and Flight 2, and CLaMS/EMAC model data on band C.

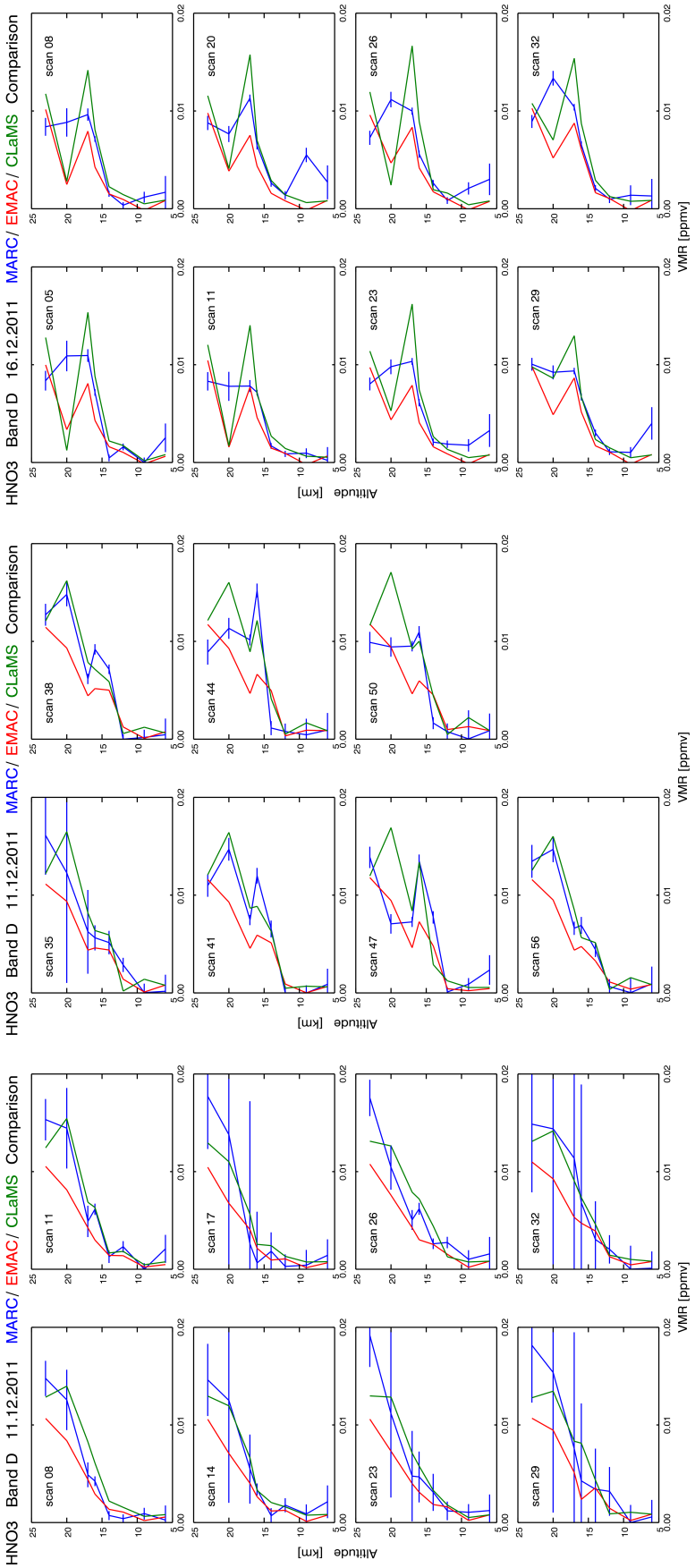

Fig. 153: Plot panels: HNO_3 comparison between MARSCHALS products obtained from Flight 1 and Flight 2, and CLaMS/EMAC model data on band D.

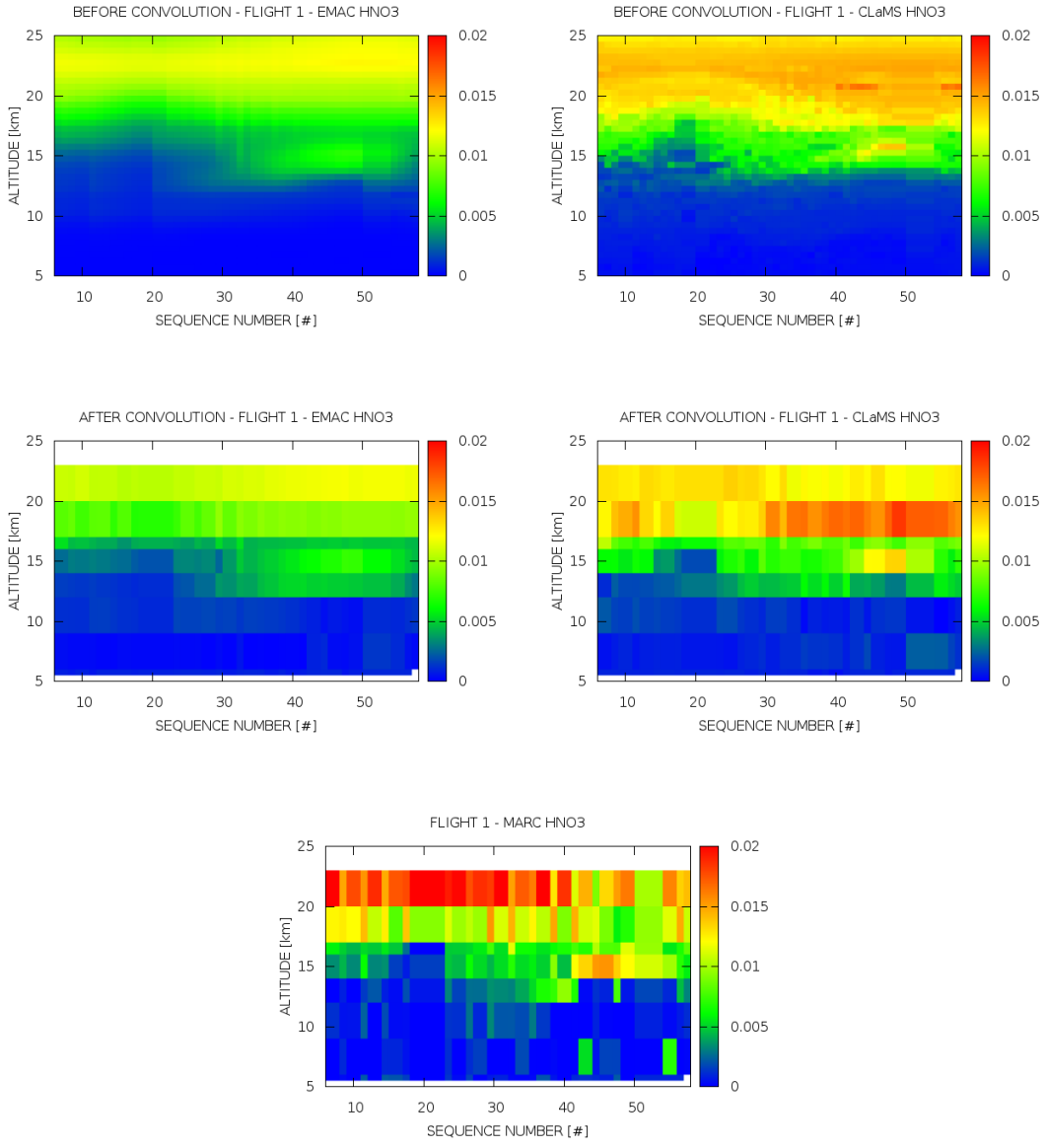

Fig. 154: Map panels: HNO_3 comparison between MARSCHALS products obtained from Flight 1 and CLaMS/EMAC model data.

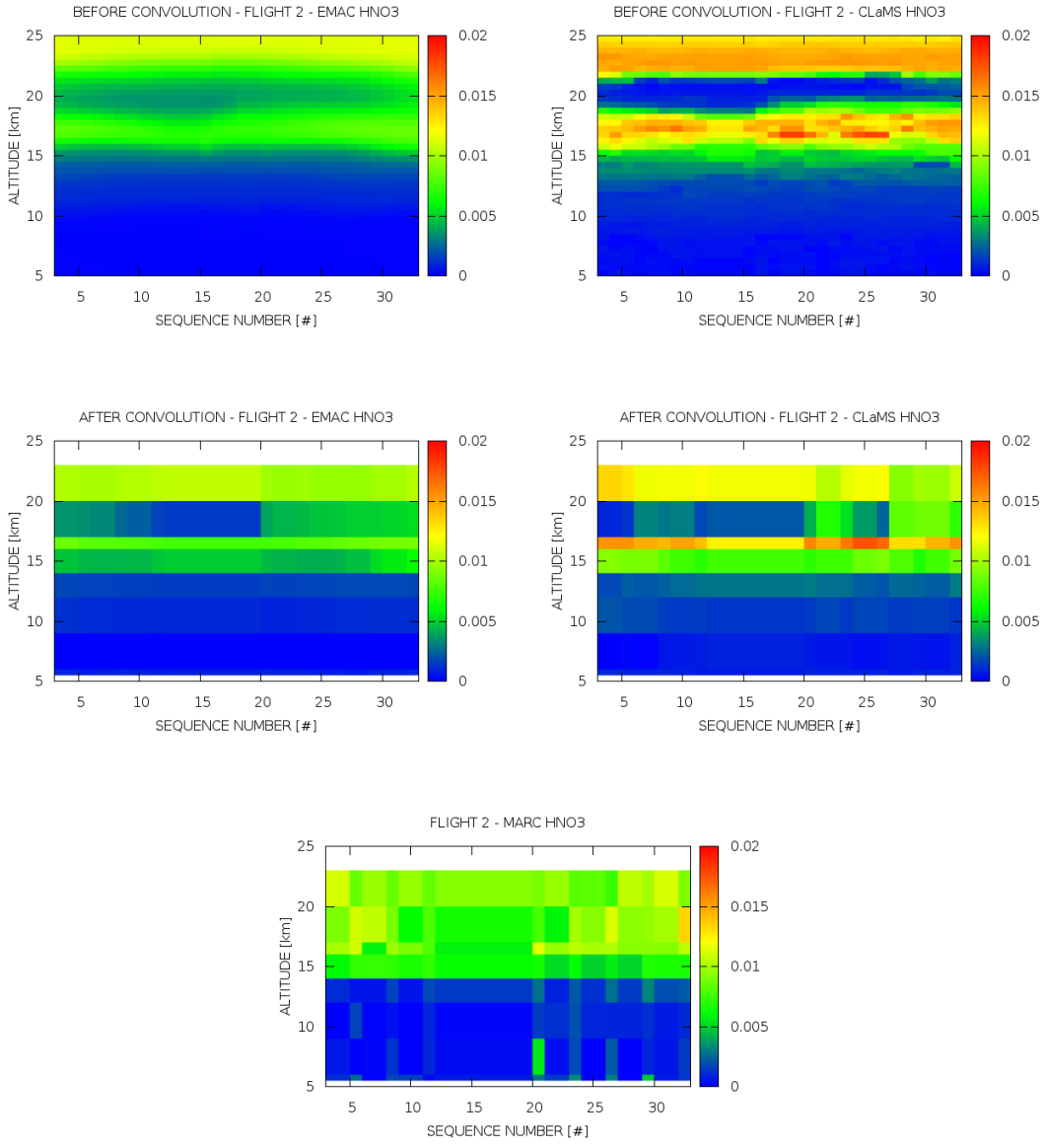

Fig. 155: Map panels: HNO_3 comparison between MARSCHALS products obtained from Flight 2 and CLaMS/EMAC model data.

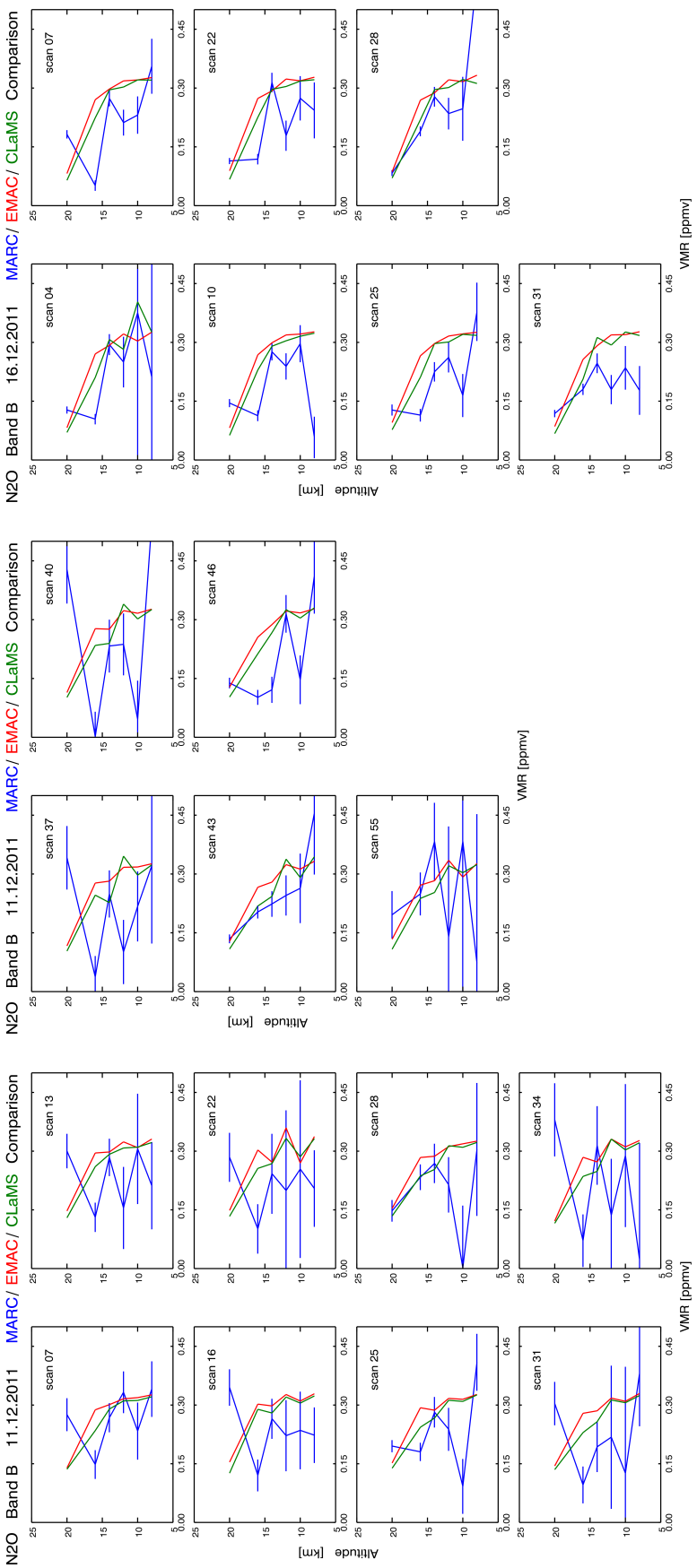

Fig. 156: Plot panels: N_2O comparison between MARSCHALS products obtained from Flight 1 and Flight 2, and CLaMS/EMAC model data on band B.

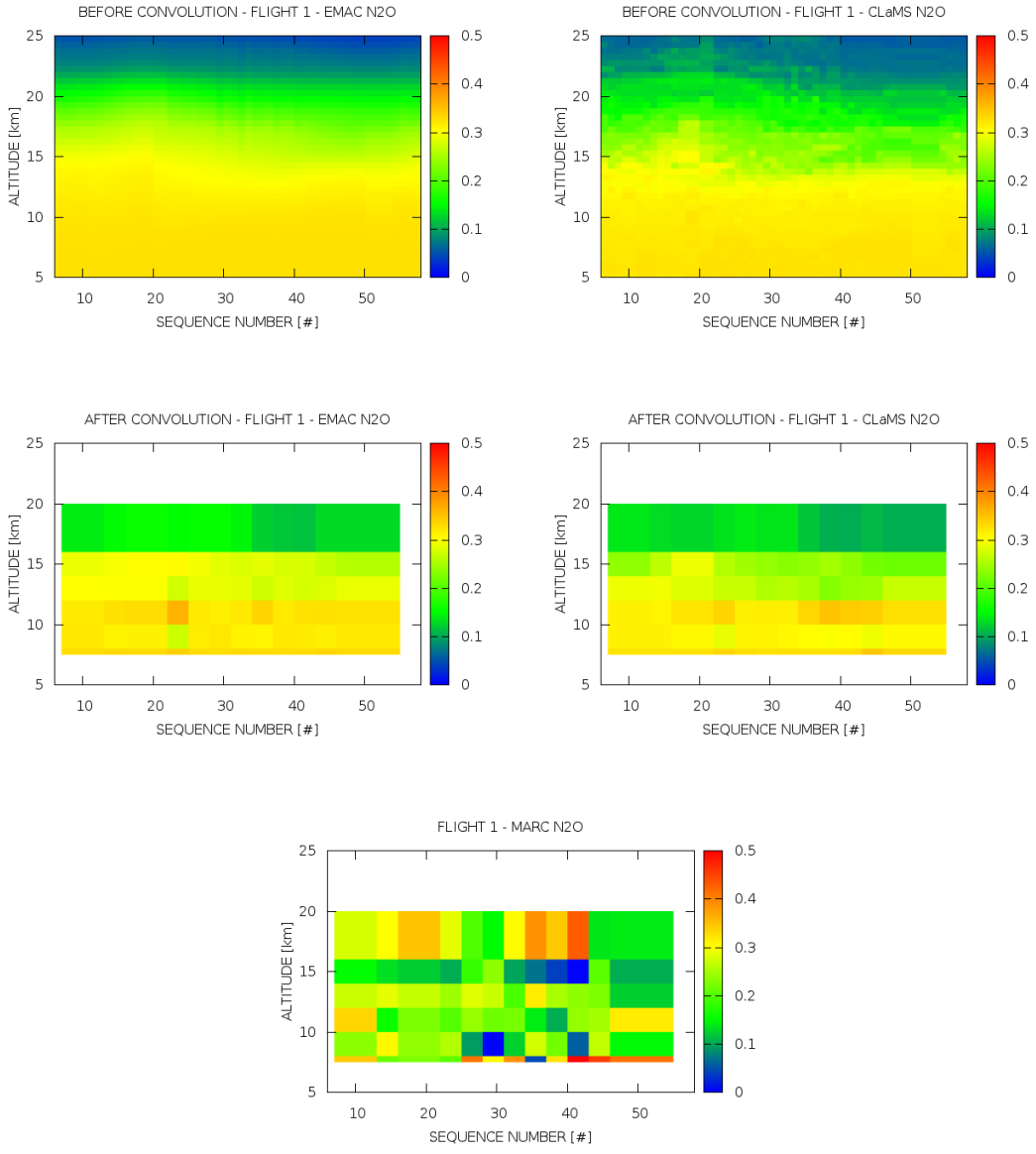

Fig. 157: Map panels: N_2O comparison between MARSCHALS products obtained from Flight 1 and CLaMS/EMAC model data.

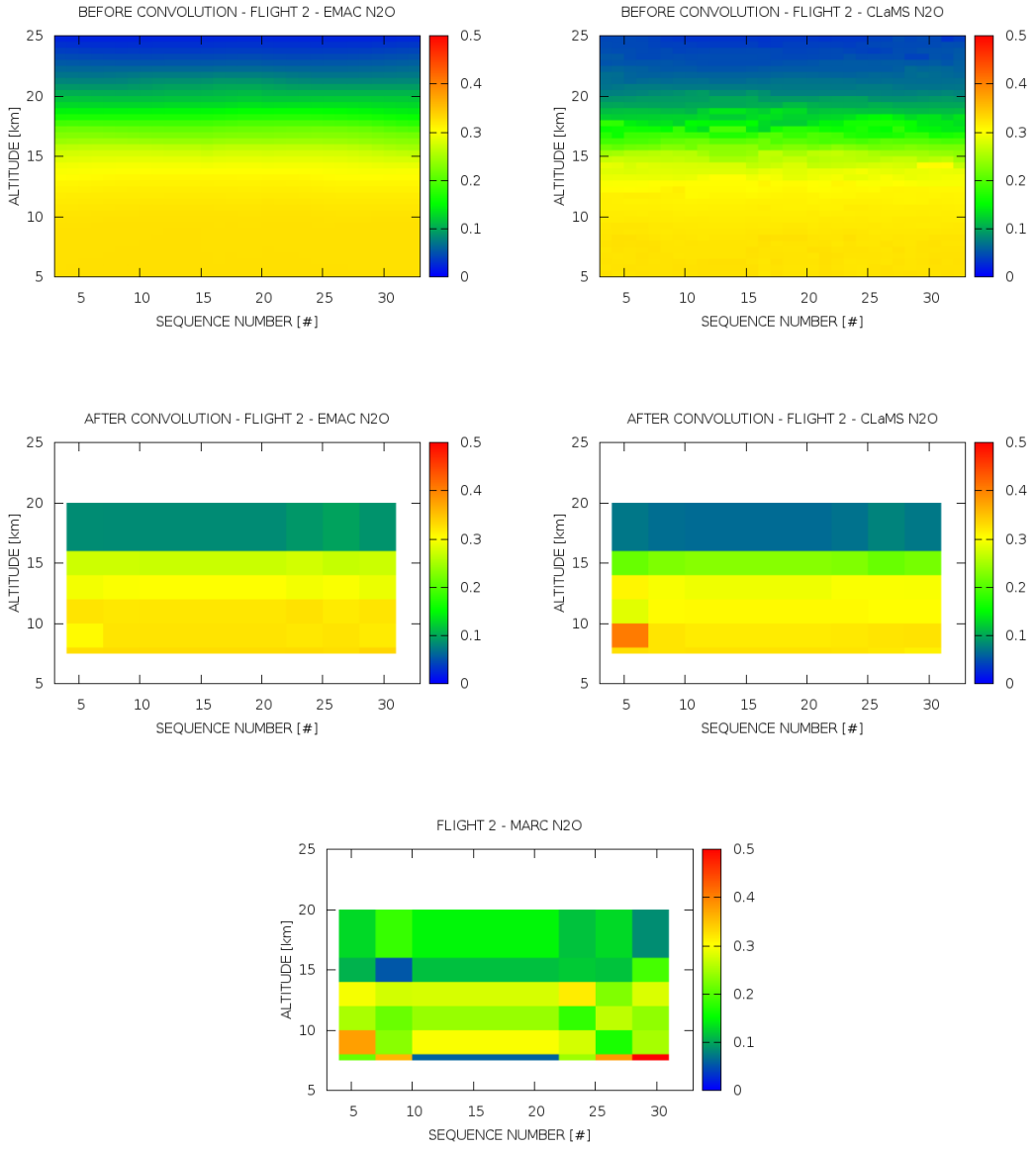

Fig. 158: Map panels: N_2O comparison between MARSCHALS products obtained from Flight 2 and CLaMS/EMAC model data.

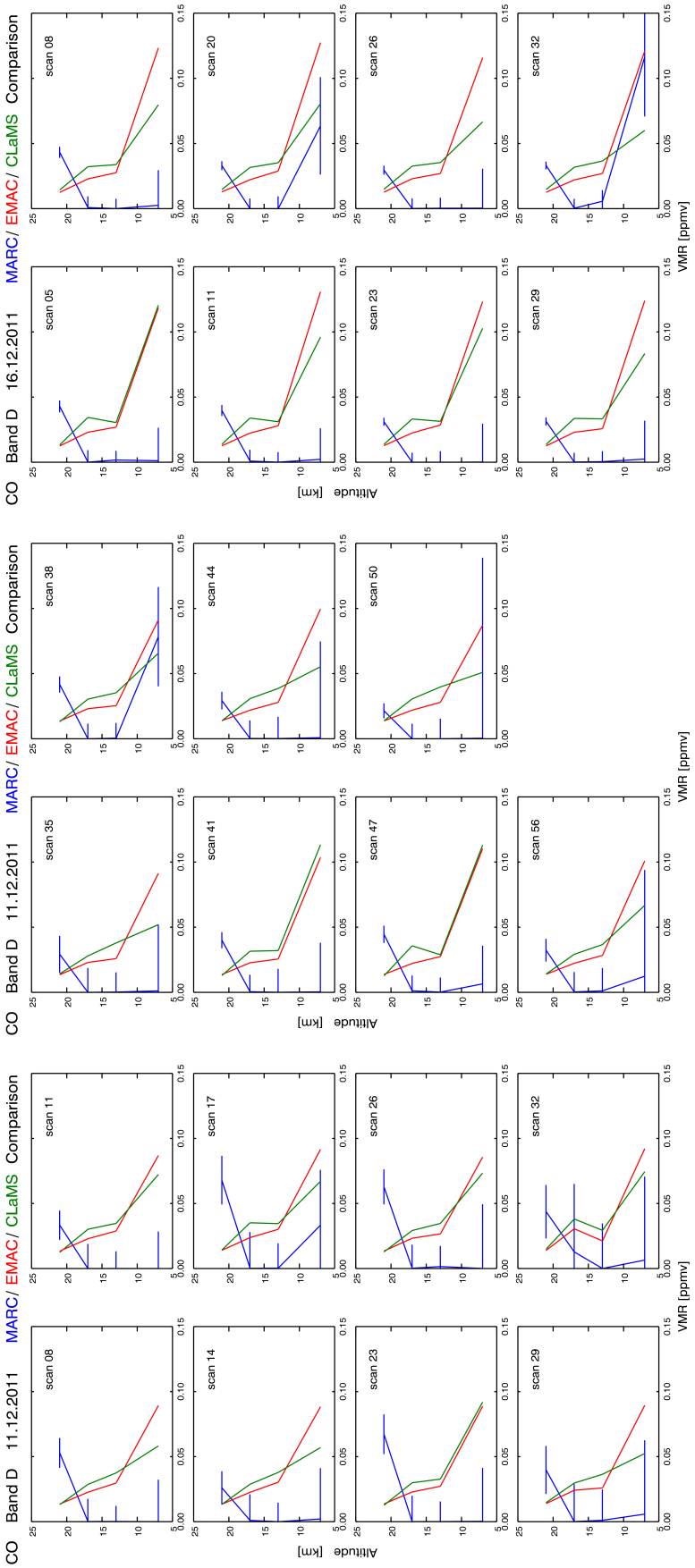

Fig. 159: Plot panels: CO comparison between MARSCHALS products obtained from Flight 1 and Flight 2, and CLaMS/EMAC model data on band D.

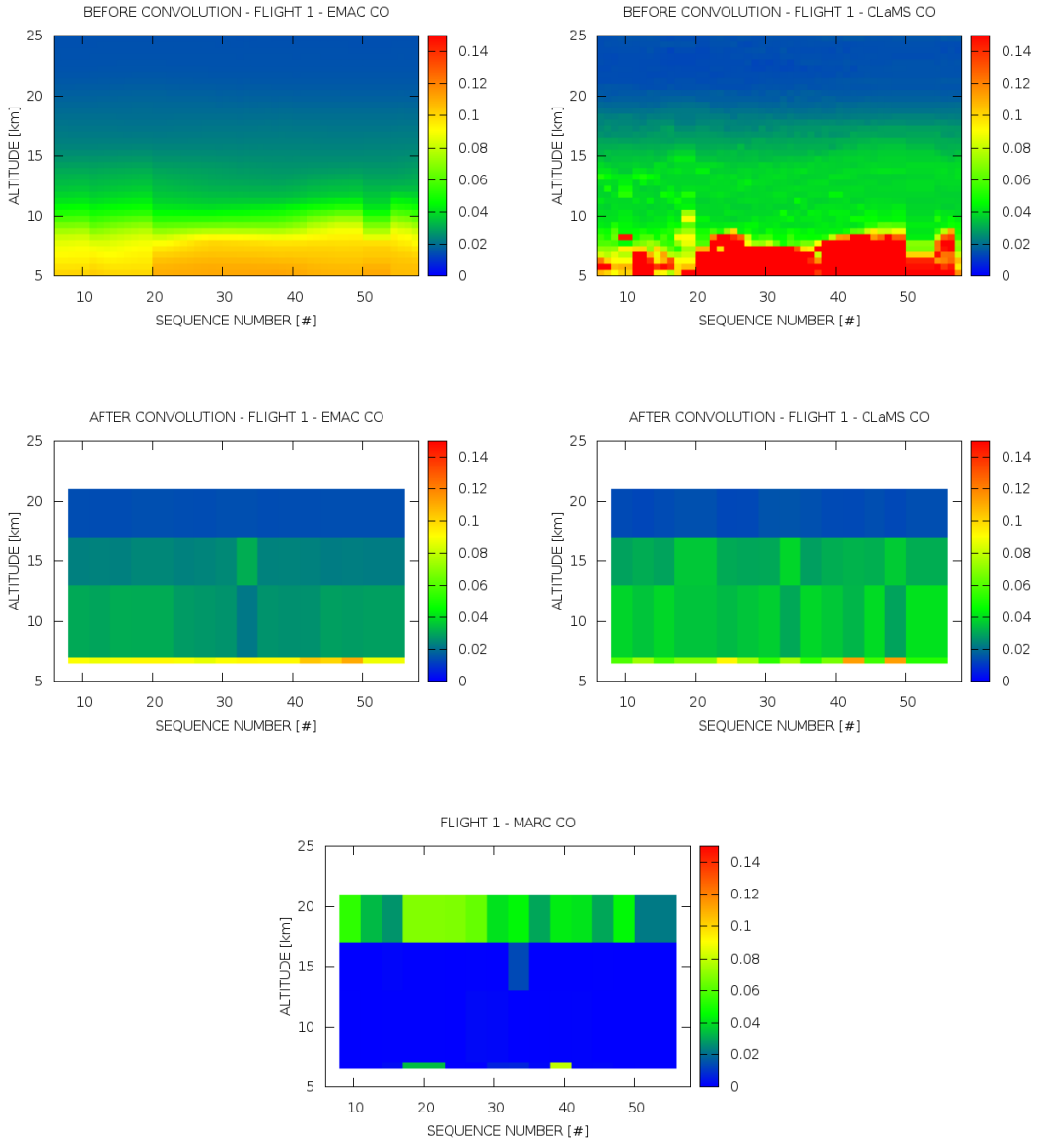

Fig. 160: Map panels: CO comparison between MARSCHALS products obtained from Flight 1 and CLaMS/EMAC model data.

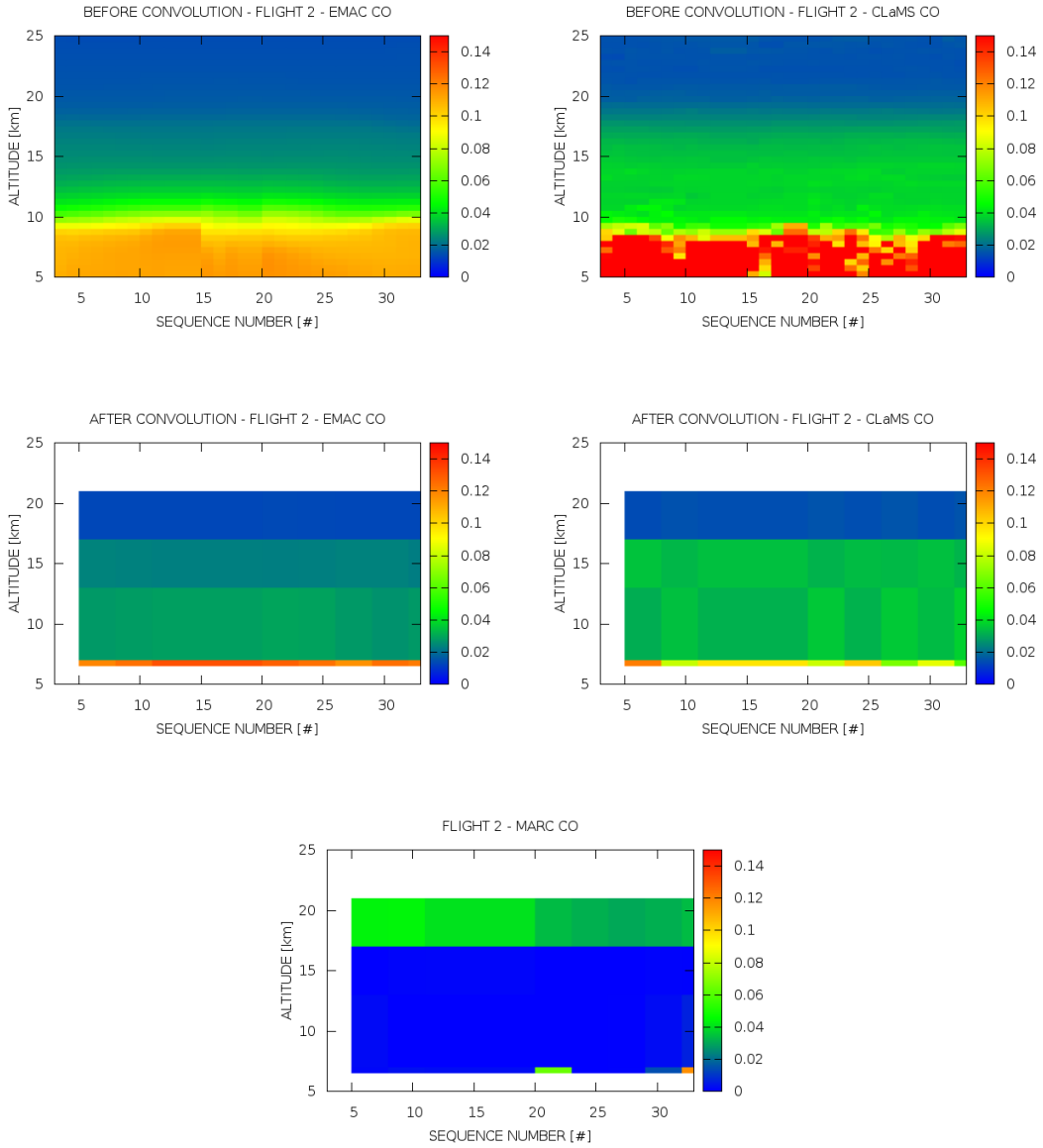

Fig. 161: Map panels: CO comparison between MARSCHALS products obtained from Flight 2 and CLaMS/EMAC model data.

simplified cirrus treatment could explain that below 10 km ClaMS H_2O mixing ratios are higher than EMAC and MARSCHALS data.

The O_3 comparison shows that the models are in a quite good agreement below 17 km, while above 17 km EMAC results are systematically larger. The agreement between models data and MARSCHALS measurements is quite good. Above 15 km MARC results appear to be in a better agreement with CLaMS profiles. Previous studies show that ClaMS O_3 mixing ratios in the polar vortex region are in good agreement with measurements. Above 18 km, EMAC ozone values are higher than the CLaMS data which agree well with the MARC data. Overestimation of polar O_3 VMRs above $\sim$18 km is a known feature for the chemistry-climate-model EMAC during the course of the Arctic winter, but unfortunately the reason for this overestimation is still unknown. One reason for the good agreement of the CLaMS O_3 VMR with the MARC data could be found in the initialisation with MLS data on November 1^{st}, 2011. Please note, that EMAC has been initialised on January 1^{st}, 2011, with model data only. Due to these differences in the chemical initialisation differences in the modelled polar O_3 VMRs between CLaMS and EMAC can be expected.

The HNO_3 comparison shows that the models are in a quite good agreement below 15 km, while above 15 km CLaMS results are systematically larger. As for the O_3 the agreement between the models data and MARSCHALS measurements is resonably good below 15 km. Above 15 km the differences are larger also the model profiles do not agree, even if the shapes of the three curves consistently show a HNO_3 reduction at 20 km. The HNO_3 profiles around 20 km show a strong reduction of HNO_3 due to denitrification, the permanent removal of nitrogen compounds through sedimentation of HNO_3-containing PSC particles. Below this layer, an enhancement of HNO_3 is found caused by renitrification. In CLaMS, sedimentation of NAT particles is calculated with a global nucleation rate for NAT particles. This could yield an overestimation of both denitrification and renitrification.

The N_2O comparison shows that the models are in a quite good agreement. MARC results are systematically less than the models below the flight altitude. Above 15 km the EMAC N_2O are larger than those of CLaMS. This could be also due to the intialisation of CLaMS N_2O with MLS data on November 1^{st}.

The CO comparison shows that both models agree quite well in the stratosphere above 10 km, but show substantial differences in troposphere caused by the different treatment of tropospheric CO in the two models. While EMAC calculates CO interactively from prescribed emissions, CLaMS uses tropospheric CO from MOPITT observations. CO from MARSCHALS retrievals shows much lower values (in fact below detection limit in most cases) below flight altitude and higher CO than the models above flight altitude. This is consistent with the comparisons between MARSCHALS CO profiles and Aura/MLS satellite data shown in the section of the validations of MARSCHALS measurements.

A noteworthy feature of enhanced HNO_3 and enhanced O_3 is observed towards the end of Flight 1 at about 15 km altitude. Both models consistently reproduce these transport induced features. Renitrification (i.e. sedimentation of HNO_3 containing particles) may have contributed to the enhanced HNO_3, but is not the only cause, as both models and the MARSCHALS observations also show a simultaneous enhancement of O_3 and a reduction of N_2O.

10 Acknowledgements

We acknowledge ECMWF for having granted direct access to their archives of atmospheric data. CALIOP data were obtained from the NASA Langley Research Center Atmospheric Science Data Center. The MLS data used in this effort were acquired as part of the activities of NASA's Science Mission Directorate, and are archived and distributed by the Goddard Earth Sciences (GES) Data and Information Services Center (DISC).The MODIS data are obtained from GSFC/NASA LAADS. We acknowledge the Odin/SMR science team for SMR data.

11 Reference Documents

RD1:
MARSCHALS Level 2 Architectural Design Document, study: The Scientific Analysis of Limb Sounding Observations of the Upper Troposphere.

RD2:
MARSCHALS Level 2 Software User and Reference Manual, study: The Scientific Analysis of Limb Sounding Observations of the Upper Troposphere.

RD3:

MARSCHALS Level 2 Report on data analysis of SCOUT O3 MARSCHALS flight campaign, study: The Scientific Analysis of Limb Sounding Observations of the Upper Troposphere.

References

[1] www.ecmwf.int/research/ifsdocs/DYNAMICS/Chap2_Discretization4.html

[2] Carslaw, K. S., Luo, B., and Peter, T.: An analytic expression for the composition of aqueous HNO3-H2SO4 stratospheric aerosols including gas phase removal of HNO3, Geophys. Res. Lett., 22(14), 1877-1880, 1995.

[3] Castelli E., S. Del Bianco, B. M. Dinelli, A. Dudhia, M. Gai, and L, Santurri, MARSCHALS Level 2 Report on data analysis of SCOUT O3 MARSCHALS flight campaign. Technical note of the study: The Scientific Analysis of Limb Sounding Observation of the Upper Troposphere, ESA-ESTEC contract N. 16530/02/NL/MM, 2007.

[4] Ceccherini, S., P. Raspollini and B. Carli, Optimal use of the information provided by indirect measurements of atmospheric vertical profiles, Optics Express, 17, 7, 4944-4958, 2009.

[5] Ceccherini, S., A generalization of optimal estimation for the retrieval of atmospheric vertical profiles, Journal of Quantitative Spectroscopy and Radiative Transfer, 113, 1437-1440, (2012).

[6] Cortesi U, Del Bianco S, Gai M., Dinelli B.M, Castelli E, Gerber D., Oelhaf H., Woiwode W., 'PREMIER Analysis of Campaign Data, ESA-ESTEC Contract 4000101374/NL/10/CT', IFAC Technical, Sceintific and Research Reports, 4, 79-239, 2012.

[7] Del Bianco S., B. Carli, Ceccherini S., B. Carli, U. Cortesi, S. Del Bianco, P. Raspollini, Retrieval of the vertical column of an atmospheric constituent from data fusion of remote sensing measurements, Journal of Quantitative Spectroscopy and Radiative Transfer, 111, 507-514, 2010.

[8] Del Bianco S., B. Carli, C. Cecchi Pestellini, B. M. Dinelli, M. Gai and L. Santurri, Retrieval of minor constituents in a cloudy atmosphere with remote sensing millimetre wave measurements, Quarterly Journal of the Royal Metereological Society , 133: (S2), pp. 163-170, 2007.

[9] Dinelli, B. M., Castelli, E., Carli, B., Del Bianco, S., Gai, M., Santurri, L., Moyna, B. P., Oldfield, M., Siddans, R., Gerber, D., Reburn, W. J., Kerridge, B. J., and Keim, C.: Technical Note: Measurement of the tropical UTLS composition in presence of clouds using millimetre-wave heterodyne spectroscopy, Atmos. Chem. Phys., 9, 1191–1207, 2009.

[10] Dinelli, B.M. et al. Theoretical retrieval study, Report of the study: The Scientific Analysis of Limb Sounding Observations of the Upper Troposphere.

[11] B. M. Dinelli, E. Arnone, G. Brizzi, M. Carlotti, E. Castelli, L. Magnani, E. Papandrea, M. Prevedelli, and M. Ridolfi: The MIPAS2D database of MIPAS/ENVISAT measurements retrieved with a multi-target 2-dimensional tomographic approach, Atmos. Meas. Tech., 3, 355–374, 2010.

[12] Grooß, JU; Gunther, G; Müller, R; et al., Simulation of denitrification and ozone loss for the Arctic winter 2002/2003, ATMOSPHERIC CHEMISTRY AND PHYSICS, 5, 1437-1448, 2005.

[13] Grooß, J.U., and R. Müller, Simulation of ozone loss in Arctic winter 2004/2005, Geophys. Res. Lett., 34, L05804, doi:10.1029/2006GL028901, 2007.

[14] Grooß, J.-U., R. Müller, P. Konopka, H.-M. Steinhorst, A. Engel, T. Möbius, and C. M. Volk, The impact of transport across the polar vortex edge on Match ozone loss estimates, Atmos. Chem. Phys., 8, 565-578, 2008.

[15] Günther, G., R. Müller, M. von Hobe, F. Stroh, P. Konopka, and C. M. Volk, Quantifcation of transport across the boundary of the lower stratospheric vortex during Arctic winter 2002/2003, Atmospheric Chemistry and Physics, 8, 3655 - 3670, 2008.

[16] Haynes, P., and J. Anglade, The vertical scale cascade in atmospheric tracers due to large-scale differential advection, J. Atmos. Sci., 54, 1121-1136, 1997.

[17] Keim, C., Entwicklung und Verifikation der Sichtlinienstabilisierung fr MIPAS auf dem hochfliegenden Forschungsflugzeug M-55 Geophysica, Dissertation, University of Karlsruhe and Research Centre Karlsruhe, Wissenschaftliche Berichte FZKA 6729, 2003.

[18] Kerkweg, A., Buchholz, J., Ganzeveld, L., Pozzer, A., Tost, H., and Jöckel, P.: Technical Note: An implementation of the dry removal processes DRY DEPosition and SEDImentation in the Modular Earth Submodel System (MESSy), Atmospheric Chemistry and Physics, 6, 4617-4632, 2006a.

[19] Kerkweg, A., Sander, R., Tost, H., and Jöckel, P.: Technical note: Implementation of prescribed (OFFLEM), calculated (ONLEM), and pseudo-emissions (TNUDGE) of chemical species in the Modular Earth Submodel System (MESSy), Atmospheric Chemistry and Physics, 6, 3603-3609, 2006b.

[20] Kerridge, B.J., R Siddans, J Reburn, et al. (2001), Definition of Mission Objectives and Observational Requirements for an Atmospheric Chemistry Explorer Mission, ESTEC Contract no. 13048/98/NL/GD Final report, 2001.

[21] Kerridge, B.J., R Siddans, J Reburn, et al., Definition of Mission Objectives and Observational Requirements for an Atmospheric Chemistry Explorer Mission, ESA Contract No:13048/98/NL/GD Study Extension: Contract Change Notice No.3 Final Report. Jan. 2002.

[22] Kerridge, B.J., R Siddans, J Reburn, et al., Consideration of mission studying chemistry of the UTLS, Final Report August 2004, ESA Contract 15457/01/NL/MM. 2004.

[23] Kirner, O., Ruhnke, R., Buchholz-Dietsch, J., Jöckel, P., Brhl, C., and Steil, B.: Simulation of polar stratospheric clouds in the chemistry-climate-model EMAC via the submodel PSC, Geoscientific Model Development, 4, 169-182, 2011.

[24] Konopka, P., Steinhorst, H.-M., Grooß, J.-U., Günther, G., Müller, R., Elkins, J W., Jost, H.-J., Richard, E., Schmidt, U., Toon, G., and McKenna, D S., Mixing and ozone loss in the 1999-2000 Arctic vortex: Simulations with the 3-dimensional Chemical Lagrangian Model of the Stratosphere (CLaMS), J. Geophys. Res., 109. D02315,doi:10.1029/2003JD003792. 2004.

[25] Konopka, P., Günther, G., Müller, R., dos Santos, F. H. S., Schiller, C., Ravegnani, F., Ulanovsky, A., Schlager, H., Volk, C. M., Viciani, S., Pan, L. L., McKenna, D.-S., and Riese, M., Contribution of mixing to upward transport across the tropical tropopause layer (TTL), Atmos. Chem. Phys., 7, 3285-3308, 2007.

[26] Konopka, P., J.-U. Grooß, G. Günther, F. Ploeger, R. Pommrich, R. Müller, and N. Livesey, Annual cycle of ouone at and above the tropical tropopause: observations versus simulations with the chemical model of the stratosphere (CLaMS), Atmos. Chem. Phys., 10, 121-132. 2010.

[27] T. Kuhn et al., Characterization of Millimetre-Wave Spectroscopic Signatures, ESTEC contract No. 16377/02/NL/FF.

[28] Fischera J., R. R. Gamache, A.Goldmanb, L. S. Rothmanc and A. Perrin, Total internal partition sums for molecular species in the 2000 edition of the HITRAN database, Journal of Quantitative Spectroscopy and Radiative Transfer, 82, 401-412, 2003.

[29] IPCC (Intergovernmental Panel on Climate Change): Climate Change 2001: Synthesis Report. A Contribution of Working Groups I, II and III to the Third Assessment Report of the Intergovernmental Panel on Climate Change, edited by: Watson, R. T. and the Core Writing Team, Cambridge University Press, Cambridge, UK, and New York, USA, 2001.

[30] Jöckel, P., Sander, R., Kerkweg, A., Tost, H., and Lelieveld, J.: Technical Note: The Modular Earth Submodel System (MESSy) - a new approach towards Earth System Modeling, Atmospheric Chemistry and Physics, 5, 433-444, 2005.

[31] Jöckel, P., Tost, H., Pozzer, A., Brhl, C., Buchholz, J., Ganzeveld, L., Hoor, P., Kerkweg, A., Lawrence, M. G., Sander, R., Steil, B., Stiller, G., Tanarhte, M., Taraborrelli, D., van Aardenne, J., and Lelieveld, J., The atmospheric chemistry general circulation model ECHAM5/MESSy1: consistent simulation of ozone from the surface to the mesosphere, Atmos. Chem. Phys., 6, 5067-5104, 2006.

[32] Jöckel, P., Kerkweg, A., Buchholz-Dietsch, J., Tost, H., Sander, R., and Pozzer, A.: Technical Note: Coupling of chemical processes with the Modular Earth Submodel System (MESSy) submodel TRACER, Atmospheric Chemistry and Physics, 8, 1677-1687, 2008.

[33] Landgraf, J. and P.J. Crutzen: An efficient method for online calculations of photolysis and heating rates. J. Atmos. Sci., 55, 863-878., 1998.

[34] N. J. Livesey, W. G. Read, L. Froidevaux, A. Lambert, G. L. Manney, H. C. Pumphrey, M. L. Santee, M. J. Schwartz, S. Wang, R. E. Cofield, D. T. Cuddy, R. A Fuller, R. F. Jarnot, J. H. Jiang, B. W. Knosp, P. C. Stek, P. A. Wagner, and D. L. Wu.: Aura Microwave Limb Sounder Version 3.3 Level 2 data quality and description document.JPL D -33509. Version 3.3x-10, 18 January, 2011

[35] Livesey, N. J., et al. (2008), Validation of Aura Microwave Limb Sounder O_3 and CO observations in the upper troposphere and lower stratosphere, J. Geophys. Res., 113, D15S02, doi:10.1029/2007JD008805.

[36] Mahowald, N. M., R. A. Plumb, P. J. Rasch, J. del Corral, and F. Sassi, Stratospheric transport in a three-dimensional isentropic coordinate model, J. Geophys. Res., 107, D15, 4254, doi:10.1029/2001JD001313, 2002.

[37] Manney, G. L., M. L. Santee, L. Froidevaux, K. Hoppel, N. J. Livesey, and J. W. Waters, EOS MLS observations of ozone loss in the 2004 2005 Arctic winter, Geophys. Res. Lett., 33, L04802, doi:10.1029/2005GL024494, 2006.

[38] MARSCHALS Level 2 Architectural Design Document, study: The Scientific Analysis of Limb Sounding Observations of the Upper Troposphere.

[39] MARSCHALS Level 2 Software User and Reference Manual, study: The Scientific Analysis of Limb Sounding Observations of the Upper Troposphere.

[40] MARSCHALS Level 2 Report on data analysis of SCOUT O3 MARSCHALS flight campaign, study: The Scientific Analysis of Limb Sounding Observations of the Upper Troposphere.

[41] Maucher, G., Das Sternreferenzsystem von MIPAS-B2: Sichtlinien-Bestimmung fr ein ballongetragenes Spektrometer zur Fernerkundung atmosphrischer Spurengase, Dissertation, University of Karlsruhe and Research Centre Karlsruhe, Wissenschaftliche Berichte FZKA 6227, 1999.

[42] McKenna, D. S., Konopka, P, Grooß, J.-U., Günther, G., Müller, R., Spang, R., Offermann, D., Orsolini, Y., A new Chemical Lagrangian Model of the Stratosphere (ClaMS): Part I Formulation of Advection and Mixing, J. Geophys. Res.,Vol. 107, D16,10.1029/2000JD000114 , 2002.

[43] McKenna, D. S., J.-U. Grooß, G. Günther, P. Konopka, R. Müller, G. Carver, and Y. Sasano, A new Chemical Lagrangian Model of the Stratosphere (CLaMS): 2. Formulation of chemistry scheme and initialization, J. Geophys. Res., 107, D15, 4256, doi:10.1029/2000JD000113, 2002.

[44] MDB., High-altitude M-55 Geophysica aircraft: Investigators Handbook, 3rd Edition, Myasishchev Design Bureau, 1996.

[45] Nash, E. R., Newman, P. A., Rosenfield, J. E., et al., An objective determination of the polar vortex using Ertel's potential vorticity, JOURNAL OF GEOPHYSICAL RESEARCH-ATMOSPHERES, 101, D5, 9471-9478, DOI:10.1029/96JD00066, 1996.

[46] Ploeger, F., P. Konopka, G. Günther, J.-U. Grooß, and R. Müller, Impact of the vertical velocity scheme on modeling transport in the tropical tropopause layer, J. Geophys. Res., 115, D03301, doi:10.1029/2009JD012023, 2010.

[47] Pommrich, R., Müller, R., Grooß, J.-U., Konopka, P., Günther, G., Pumphrey, H.-C., Viciani, S., D'Amato, F., and Riese, M.: Carbon monoxide as a tracer for tropical troposphere to stratosphere transport in the Chemical Lagrangian Model of the Stratosphere (CLaMS), Geosci. Model Dev. Discuss., 4, 1185-1211, doi:10.5194/gmdd-4-1185-2011, 2011.

[48] Olivier, J.G.J., Van Aardenne, J.A., Dentener, F., Pagliari, V., Ganzeveld, L.N. and J.A.H.W. Peters: Recent trends in global greenhouse gas emissions: regional trends 1970-2000 and spatial distribution of key sources in 2000. Env. Sc., 2 (2-3), 81-99, 2005.

[49] Prinn, R. G., Huang, J., Weiss, R. F., Cunnold, D. M., Fraser, P. J., Simmonds P. G., McCulloch, A., Harth, C., Salameh, P., O-Doherty, S., Wang, R. H. J., Porter, L., and Miller, B. R.: Evidence for substantial variations of atmospheric hydroxyl radicals in the past two decades, Science, 292, 1882-1888, 2001.

[50] Pumphrey H. C., M. J. Filipiak, N. J. Livesey, M. J. Schwartz, C. Boone, K. A. Walker, P. Bernath, P. Ricaud, B. Barret, C. Clerbaux, R. F. Jarnot, G. L. Manney, and J. W. Waters, Validation of middle-atmosphere carbon monoxide retrievals from the MicroWave Limb Sounder on Aura, j. Geophys. res., 112, D24S38, doi:10.1029/2007JD008723, 2007.

[51] Remedios, J. J., Leigh, R. J., Waterfall, A. M., Moore, D. P., Sembhi, H., Parkes, I., Greenhough, J., Chipperfield, M.P., and Hauglustaine, D.: MIPAS reference atmospheres and comparisons to V4.61/V4.62 MIPAS level 2 geophysical data sets, Atmos. Chem. Phys. Discuss., 7, 9973–10017, 2007.

[52] P. Ricaud, D. Alexandre, B. Barret, E. Le Flochmoën, E. Motte, G. Berthet, F. Lefevre, D. Murtagh: Measurements of mid-stratospheric formaldehyde from the Odin/SMR instrument, Journal of Quantitative Spectroscopy and Radiative Transfer 107, 91-104, 2007.

[53] M. Ridolfi and L. Sgheri: A self-adapting and altitude-dependent regularization method for atmospheric profile retrievals, Atmos. Chem. Phys., 9, 18831897, 2009.

[54] Rodgers, C., Inverse Methods for Atmospheric Sounding: Theory and Practice, Vol. 2 of Series on Atmospheric, Oceanic and Planetary Physics, World Scientific., Singapore, 194, 2000.

[55] Roeckner, E., Brokopf, R., Esch, M., Giorgetta, M., Hagemann, S., Kornblueh, L., Manzini, E., Schlese, U., and Schulzweida, U.: Sensitivity of simulated climate to horizontal and vertical resolution in the ECHAM5 atmosphere model, J. Climate, 19, 3771-3791, 2006.

[56] Sander, S. P., Friedl, R. R., Golden, D. M., Kurylo, M. J., Huie, R. E., Orkin, V. L., Moortgat, G. K., Ravishankara, A. R., Kolb, C. E., Molina, M. J., and Finlayson-Pitts, B. J.: Chemical kinetics and photochemical data for use in atmospheric studies, Evaluation no. 14, JPL Publ. 02-25, Jet Propulsion Laboratory, Pasadena, CA, USA, 2003.

[57] Sander, R., Kerkweg, A., Jöckel, P., and Lelieveld, J.: Technical note: The new comprehensive atmospheric chemistry module MECCA, Atmospheric Chemistry and Physics, 5, 445-450, 2005.

[58] Sander, S. P., Friedl, R. R., Barker, J. R., Golden, D. M., Kurylo, M. J., Wine, P. H., Abbatt, J., Burkholder, J. B., Kolb, C. E., Moortgat, G. K., Huie, R. E., and Orkin, V. L.: Chemical kinetics and photochemical data for use in atmospheric studies Evaluation no. 17, JPL Publ. 10-6, Jet Propulsion Laboratory, Pasadena, CA, USA, 2011.

[59] Santee, M. L., et al., Validation of the Aura Microwave Limb Sounder HNO_3 measurements, j. Geophys. res., 112, D24S40, doi:10.1029/2007JD008721, 2007.

[60] Spang, R. et al., Colour indices for the detection and differentiation of cloud types in infra-red limb emission spectra, Advances in Space Research, 33, 1041-1047, 2004.

[61] Stiller, G.P. et al., The Karlsruhe Optimized and Precise Radiative transfer Algorithm (KOPRA), Wissenschaftliche Berichte FZKA 6487, Forschungszentrum Karlsruhe, 2004.

[62] Tost, H., Jöckel, P., Kerkweg, A., Sander, R., and Lelieveld, J.: Technical note: A new comprehensive SCAVenging submodel for global atmospheric chemistry modelling, Atmospheric Chemistry and Physics, 6, 565-574, 2006a.

[63] Tost, H., Jöckel, P., and Lelieveld, J.: Influence of different convection parameterisations in a GCM, Atmospheric Chemistry and Physics, 6, 5475-5493, 2006b.

[64] Tost, H., Jöckel, P., Kerkweg, A., Pozzer, A., Sander, R., and Lelieveld, J.: Global cloud and precipitation chemistry and wet deposition: tropospheric model simulations with ECHAM5/MESSy1, Atmospheric Chemistry and Physics, 7, 2733-2757, 2007a.

[65] Tost, H., Jöckel, P., and Lelieveld, J.: Lightning and convection parameterisations - uncertainties in global modelling, Atmospheric Chemistry and Physics, 7, 4553-4568, 2007b.

[66] Tost, H., Lawrence, M. G., Brhl, C., Jöckel, P., The GABRIEL Team, and The SCOUT-O3-DARWIN/ACTIVE Team: Uncertainties in atmospheric chemistry modelling due to convection parameterisations and subsequent scavenging, Atmospheric Chemistry and Physics, 10, 1931-1951, 2010.

[67] Urban, J., D. Gerber, VINNOVA funded simulation study of the Swedish STEAM Science Reference group, 2010.

[68] Verdes, J.L., et al., A sensitivity study on spectroscopic parameter accuracies for a mm/sub-mm limb sounder instrument, Journal of Molecular Spectroscopy 229 266-275, 2010.

[69] Vogel, B.; Konopka, P.; Grooß, J. U.; Müller, R.; Funke, M.; Lopez-Puertas, M.; Reddmann, T.; Stiller, G.*; von Clarmann, T.; Riese, M. Model simulations of stratospheric ozone loss caused by enhanced mesospheric NOx during Arctic Winter 2003/2004 Atmospheric Chemistry and Physics, 8 (2008), 5279 - 5293

[70] Vogel, B., L. L. Pan, P. Konopka, G. Günther, R. Müller, T. Campos, W. Hall, I. Pollack, A. Weinheimer, J. Wei, E. L. Atlas, and K. P. Bowman, Transport pathways and signatures of mixing in the extratropical tropopause region derived from Lagrangian model simulations, J. Geophys. Res., 116,D05,306, doi:10.1029/2010JD01487, 2011.

[71] Von Hobe, M., J.-U. Grooß, G. Günther, P. Konopka, I. Gensch, M. Krämer, N. Spelten, A. Afchine, C. Schiller, A. Ulanovsky, N. Sitnikov, G. Shur, V. Yushkov, F. Ravegnani, F. Cairo, A. Roiger, C. Voigt, H. Schlager, R.Weigel, W. Frey, S. Borrmann, R.Müller and F. Stroh, Evidence for heterogeneous chlorine activation in the tropical UTLS (2011), Atmos. Chem. Phys., 11, 241-256.

[72] Von Clarmann, T., Zur Fernerkundung der Erdatmosphre mittels Infrarotspektrometrie: Rekonstruktionstheorie und Anwendung, Wissenschaftliche Berichte FZKA 6928, Forschungszentrum Karlsruhe, 2010.

[73] Wenger, Ch., J.P. Champion, and V. Boudon, The partition sum of methane at high temperature, Journal of Quantitative Spectroscopy and Radiative Transfer, 109, 16, 2697-2706, 2008.

[74] Wetzel, G., Oelhaf, H., Kirner, O., Friedl-Vallon, F., Ruhnke, R., Ebersoldt, A., Kleinert, A., Maucher, G., Nordmeyer, H., and Orphal, J.: Diurnal variations of reactive chlorine and nitrogen oxides observed by MIPAS-B inside the January 2010 Arctic vortex, Atmos. Chem. Phys., 12, 6581-6592, 2012.

[75] WMO (World Meteorological Organization): Scientific Assessment of Ozone Depletion: 2006, Global Ozone Research and Monitoring Project - Report No. 50, 572 pp., Geneva, Switzerland, 2007.

Definitions and Acronyms

ACAP	Azimuthally Collapsed Antenna Pattern
AGAGE	Advanced Global Atmospheric Gases Experiment
AK	Averaging Kernel
ADD	Architectural Detailed Design
ATBD	MARSCHALS Level 2 Algorithm Theoretical Baseline Document
BTSN	Brightness Temperature Spectral Noise
CALIPSO	Cloud-Aerosol Lidar and Infrared Pathfinder Satellite Observations
DOF	Degrees Of Freedom
CKD	Clough, Kneizys and Davies (model)
CCP	Cloud Combination Probe
CIP	Cloud Imaging Probe
CRISTA-NF	Cryogenic Infrared Spectrometers and Telescopes for the Atmosphere . New Frontiers (CRISTA-NF)
CTH	Cloud Top Height
CTP	Cloud Top Pressure
CLaMS	Chemical Lagrangian Model of the Stratosphere
DOF	Degree of Freedom
ECHAM5	European Centre Hamburg general circulation model
ECMWF	European Center for Medium range Weather Forecasting
EMAC	ECHAM/MESSy Atmospheric Chemistry
ENVISAT	ENVinronment SATellite
ESD	Estimated Standard Deviation
ESSenCe	ESA Sounder Campaign 2011
FISH	Fast In situ Stratospheric Hygrometer
FLASH	FLuorescent Advanced Stratospheric Hygrometer
FM2D	Forward Model 2D
FOV	Field Of View
FSSP	Forward Scattering Spectrometer Probe
FOZAN	Fast OZone ANalyzer
FWHM	Full Width Half Maximum
GLORIA	Gimballed Limb Radiance Imager of the Atmosphere
GMTR	Geofit Multi Target Retrieval
GNS	Global Navigation System
GPS	Global Positioning System
HAGAR	High Altitude Gas Atmospheric Research
HITRAN	HIgh resolution TRANsmission
IG2	Initial Guess level 2
ILS	Instrumental Line Shape
IR	InfraRed
GI	Gain of Information
FOV	Field Of View
L1, L1B, L2	Level 1,Level 1B, Level 2
LOS	Lines Of Sight
MARC	Millimetre-wave Atmospheric-Retrieval Code
MARS	Meteorological Archival and Retrieval System
MARSCHALS	Millimetre wave Airborne Receivers for Spectroscopic CHaracterization of Atmospheric Limb Sounding
MIPAS-STR	Michelson Interferometer for Passive Atmospheric Sounding - STRatospheric aircraft
MESSy1	Modular Earth Submodel System
MLS	Microwave Limb Sounder
MMR	Mass Mixing Ratio
MODIS	Moderate Resolution Imaging Spectroradiometer
MOPITT	Measurements Of Pollution In The Troposphere
MSS	Measurement Space Solution
MSSF	Mie Scattering Source Function

MTR	Multi Target Retrieval
NAT	Nitric Acid Trihydrate
OCM	Optical Cloud Monitoring
OSIRIS	Optical Spectrograph and Infrared Imaging System
PACD	Premier Analysis of Campaign Data
PREMIER	PRocess Exploration through Measurements of Infrared and millimetre-wave Emitted Radiation
PSC	Polar Stratospheric Clouds
QBO	Quasi Biennial Oscillation
RMS	Root Mean Square
SAMM	Supervising Analyzer of MARSCHALS Measurements
SCOUT O3	Stratospheric-Climate links with emphasis On the Upper Troposphere and lower stratosphere
SMR	Sub-Millimeter Radiometer
SOW	Statement Of Work
STS	Supercooled Ternary Solution
TC9	Test Campaign 2009
TDC	Thermo Dynamic Complex
TRS	Theoretical Retrieval Study
UCSE	Unit for Connection with Scientific Equipment
UTC	Universal Time Coordinate
VCM	Variance Covariance Matrix
VGC	Vertical Grid of the Comparison
VMR	Volume Mixing Ratio
VVW	Van Vleck Weisskopf
WMO	World Meteorological Organization

Table of Contents